Debris flows in New Zealand Alpine Catchments

Patrick Kailey

A thesis submitted in partial

fulfillment of the requirement for the award of the

Degree of Doctor of Philosophy

UNIVERSITY of Canterbury

February 2013

I hereby declare that this thesis entitled "Debris flows in New Zealand Alpine Catchments" is the result of my own research except as cited in the references. This thesis has not been accepted for any degree and is not concurrently submitted in candidature of any other degree.

Signature :
Student : Patrick Kailey
Date : February19, 2013

Supervisor : Elisabeth Bowman

Co-Supervisor: Tim Davies
Co-Supervisor: Chris Massey

"The gaps are the thing. The gaps are the spirit's one home, the altitudes and latitudes so dazzlingly spare and clean that the spirit can discover itself like a once-blind man unbound. The gaps are the clefts in the rock where you cower to see the back parts of God; they are fissures between mountains and cells the wind lances through, the icy narrowing fiords splitting the cliffs of mystery. Go up into the gaps. If you can find them; they shift and vanish too. Stalk the gaps." -Annie Dillard, Pilgrim at Tinker Creek

Acknowledgments

Many people have made this work possible. First, thank you to my main supervisor, Lis Bowman, for her patience, knowledge, encouragement, and leadership. Her intellectual curiosity, both for debris flows and the world in general, never wavered, even when mine did. Also thanks to Chris Massey for his expertise and initial instruction in the black art of debris flow investigation. Tim Davies' experience and vast knowledge of all things geomorphological was also a huge help. How he advises so many students and still manages to always be available to discuss a problem or proof a chapter cannot be explained by science.

I also owe a huge debt of gratitude to those who helped me in the field. Thanks to Sam McColl, Susan Neuner, Angus Newsam, and Warren McKenzie. I could not have asked for better company. It was sometimes tough going, but I'm happy to report that no field assistants were hurt in the making of this dissertation.

Thanks go to members of the geotechnical group at ETH, Zurich, for their patience and generosity – in particular, Jan Laue, Sarah Springman, Heinz Buschor, Bernd Imre, Ralf Herzog, Marco Sperl, and Anita Meyer. Thank you to the centrifuge wizard, Markus Iten, who was indispensable and irreplaceable both before, during and after the experiments.

The research was also made possible by a New Zealand Earthquake Commission Biennial Grant, the University of Canterbury Doctoral Scholarship, and a New Zealand Postgraduate Study Abroad Award. Also thanks the staff of the University of Canterbury Civil Engineering department for their support, especially Elizabeth Ackermann, Siale Faitotonu, and Alan Jolliffe.

I'm thankful for my New Zealand family—the people that have kept me mostly sane over the last five years. The people that were always keen for adventure and did not let me forget what is important. Thanks to Sam McColl, Julia Valigore, and Charlotte Brown. Also thanks to my engineering compatriots Kim Rait, Kelly (and Todd) Robinson, Merrick Taylor,

and Mauricio Arias. I also could not forget the Crossfit ChCh team (Pete, Sara, Chris, and Johanna), Team 199 (Sophie and Bruce) , or my friends Adam, Jesse, Suz, Joncie, Marga, Elizabeth, Jo, Matt, and Lotus.

Finally and foremost, thanks to my parents, Jan and John. Without their unconditional love and support I would not have been able to survive over these last few years so far from home. I owe them my sense of wonder, my persistence, and everything else required to get this far. This thesis is dedicated to you.

Patrick Kailey, Christchurch, New Zealand

Abstract

This research aims to improve our knowledge of debris flow occurrence and behaviour in New Zealand. Detailed field data collected in four debris flow prone areas in New Zealand are presented and compared. The travel distance of these events is then modelled with an empirical-statistical model, UBCDflow, and an analytical, "equivalent fluid" continuum model DAN-W. While field studies are useful, they are often not linked to the underlying mechanics of debris flow motion or compared with the behavior of small scale flows due to the inherent complexity and unknown boundary conditions in field scale flows. Physical modelling simplifies the situation and allows boundary conditions to be controlled. The second part of this research uses physical modelling, including a series of novel debris flow tests in a geotechnical centrifuge, to compare and contrast flow behaviour and mechanics of laboratory and field scale flows.

The debris flows events investigated in the field were categorized into hillslope, torrent, or intermediate-type events. Hillslope events were less channelized and progressively deposited on high slope angles. Consequently, high friction coefficients were needed to model their mobility. Torrent flows entrained more material than hillslope flows and deposited on lower angle slopes in response to unconfinement on the debris flow fan. Friction coefficients back-calculated for torrent events were lower than for the hillslope flows, but still larger than most of the friction coefficients given for large, channelized, debris flow events in the literature. Intermediate events were similar to hillslope events in terms of deposition angle and best-fit friction coefficients, but were very confined. Both UBCDflow and DAN-W were found to be useful decision support tools, but the capability of each model was limited. Greater modelling capability was gained by using the volume change behaviour predicted by UBCDflow in DAN-W, as DAN-W simulates flow heights and velocities, but does not predict the depth of erosion.

In the second part of the research, a geotechnical centrifuge is used to model debris flow processes in a larger acceleration field than earth's gravity. While centrifuges have been

used to model a variety of processes in other geotechnical problems, debris flows are a relatively new phenomenon to be tested on a centrifuge. The centrifuge was successful in increasing the frictional properties of flow, but viscous forces were still the dominant form of shear stress with the materials used. Markedly different flow behaviour of tests using different pore-fluid rheologies suggested that the dominant mechanism of shear resistance may have changed between confined, downslope movement and unconfined runout. The results also showed that in geotechnical centrifuge testing, the viscosity of the pore fluid scales with the g-level, N. This research is an important step in developing centrifuge testing as an accepted method of modelling debris flow processes.

Finally, a brief comparison of friction slopes between small-scale 1-g flume tests and field scale flows suggests that 1-g flume experiments are able to model the mobility of field scale flows if the soil used is well-graded and the pore-fluid is not too viscous. This research shows that the the ability of laboratory scale flows to model large scale processes may not be as limited as previously suggested by some investigators.

Contents

List of Figures

List of Tables

List of Appendices

1. Introduction and aims

Debris flows are defined by Hungr (2005) as "rapid to extremely rapid flows of saturated non-plastic debris in a steep channel". Iverson (1997) describes them as "masses of poorly sorted sediment, agitated and saturated with water that surge down slopes in response to gravitational attraction".

These definitions emphasize three fundamental elements required for debris flow formation; a source of well-graded material (debris), a source of water to saturate that material, and a source of potential energy (slope). Debris flows occur wherever these three ingredients are found; a condition met in any alpine area in the world. Indeed, debris flows are extremely important agents of geomorphic change in alpine environments (Stock and Dietrich, 2003, 2006; Brummer and Montgomery, 2003).

From a natural hazards perspective, these same three ingredients, and how their properties change as a flow travels down its path, determine the potential danger from the flow. The severity of a debris flow can be assessed by its peak velocity, total volume of debris, inundated area, impact pressures generated, or distance travelled.

In order for a debris flow to be dangerous, however, a fourth ingredient is required; people or infrastructure along its path. As populations in both developed and developing countries continue to push into mountainous terrain, the risk from debris flows is likely to increase. Other factors such as global warming and changes in land use may exacerbate the frequency and magnitude of landslides and debris flows (Wieczorek and Glade, 2005; Petley, 2012). From 2004 to 2010, the International Landslide Center has recorded 80,058 deaths due to various types of landslides, many of which were due to debris flows (Petley, 2012).

New Zealand's position in the mid-latitudes of the Pacific Ocean results in periods of high-intensity rainfall – leading to high rates of physical weathering. Combined with extremely high rates of uplift and highly indurated, fractured bedrock, these factors result in a particularly

high temporal occurrence of debris flows. Despite the danger they pose, the public recognition of the losses wrought by debris flows is relatively low in New Zealand. This is largely a result of the country's low population density, especially in regions most prone to debris flows. This situation is gradually changing as hilly and mountainous terrain, once thought marginal, is developed.

Recent debris flow disasters in Matata (Bay of Plenty), the Rees Valley (Otago), and the Wellington region evince their destructive potential. The May 18th 2005 debris flow event in Matata, resulted in the destruction of 27 houses and damage to 87 further dwellings (McSaveney et al., 2005). While this debris flow was comparatively large, many smaller debris flows leading to lesser economic losses also occur each year. As well as generating economic losses, a number of debris flows have claimed lives both historically and in recent years, including the Waihi events in 1846 and 1910, near Lake Taupo, which resulted in a combined loss of 66 lives; the Klondyke corner, Arthur's Pass debris flow of 1979 which claimed 4 lives; the Thames, Te Aroha event of 1985 which killed 3 people and the Rees Valley, West Otago, tragedy of 2002 in which one died (McSaveney and Glassey, 2002; McSaveney and Davies, 2005).

Earth scientists and engineers charged with mitigating debris flow hazards face many challenges. First, they must understand the sometimes confusing terminology and classification schemes which debris flows fall under, as well as the differences between different types of flows. Second, they must understand where a debris flow might initiate. Third, they must understand the basic mechanics of movement. Using this knowledge, they must then choose a method to model a potential flow in an attempt to predict its severity.

In this process, researchers must work in parallel with practitioners to collect new field data, create new empirical and numerical models useful in hazard evaluation. Research must also advance the understanding of debris flow physics through field, laboratory, and numerical observation and experimentation.

1.1. Aims

In comparison to North America and Europe, very little debris flow research has been conducted in New Zealand. In other parts of the world, debris flow paths within a locality have been extensively surveyed to understand flow behaviour and to develop tools and techniques for risk evaluation. Physical models have also been used to elucidate the mechanics of debris flow movement. However, it has been questioned whether or not small scale physical models are able to adequately represent important debris flow processes.

The aims of this project were:

1. To document characteristic debris flow events in New Zealand at a variety of scales and classify them according to debris flow type.
2. To compare the events documented with others in the debris flow literature.
3. To model the travel distance of these events with common empirical and dynamic models and therefore suggest empirical values and methods which could be used by practitioners.
4. To increase mechanical understanding of debris flow behaviour using physical modelling in a geotechnical centrifuge, and in particular to address the role of flow quantity, moisture condition, and pore fluid rheology in determining downslope velocity and runout.
5. To question whether or not small-scale experiments are able to adequately model the mobility of larger scale flows.

1.2. Dissertation organization

Chapter 2 defines the basic vocabulary which is used in debris flows science. It also briefly summarizes background relevant to physical, empirical, and analytical debris flow modelling. The rest of the dissertation is split between two major lines of inquiry; field observation of alpine debris flows in New Zealand and modelling debris flow travel distance and runout. The basic outline is:

- Chapter 2 covers the basic terminology used in debris flow science and a brief review of debris flow modelling.
- Field data
  - Chapter 3, 4, and 5 are devoted to the field methods, data, and analysis, respectively.
- Modelling of field data
  - Chapter 6 uses the field data to calibrate two commonly used models for debris flow travel distance.
- Physical modelling
  - Chapter 7 discusses the experimental setup, data, analysis, and scaling of a series of small-scale debris flow experiments conducted in a geotechnical centrifuge.

- Synthesis
  - Chapter 8 discusses the concept of friction slope with reference to both physical models and field scale flows.
  - Chapter 9 summarizes the dissertation outputs and suggests future research directions.

2. Literature review

This chapter briefly defines common debris flow types and describes the morphology of a debris flow surge and path. The terminology covered provides the basis for the discussion of field methods and observations. Background information specific to the field methodology, field areas studied, and physical modelling instrumentation are covered later in the dissertation at the beginning of Chapters 3, 4, and 5, respectively.

The chapter next summarizes the basic models used to predict and explain debris flow behaviour, as well as some of the scaling laws and limitations applicable to debris flow modelling. This provides the background to Chapters 6 through 8.

2.1. Debris flow classification

Debris flow behaviour depends on the material properties, interactions, and proportions of the solid and fluid phases of the flow. Accordingly, many classifications of debris flows focus on the dominant mechanism in the flow, ie. whether solid-solid collisions or solid-fluid interactions are considered the most important (Bagnold, 1954; Bardou et al., 2003). Other classifications combine mechanisms with measurable parameters such as sediment concentration and fines content (Coussot and Meunier, 1996; Davies, 1988). Figure 2.1 shows the classification scheme of Schatzmann (2005), which classifies landslide types according to solids concentration and fines content. The following sections use Schatzmann (2005) classification scheme to discuss the different types debris flows.

2.1.1. Granular or bouldery debris flows

Granular flows are debris flows composed of water, coarse sediment, and a small amount of fine material. Figure 2.1 classifies debris flows by volumetric sediment concentration (C_v) and fines content (Schatzmann, 2005). Granular flows plot on the the far left side of the diagram, with very high solid concentrations and low fines contents (Zone A). Granular flows are most often treated as two phases; a fluid phase and a solid phase. Inter-particle collision and friction between grain contacts are the dominant mechanism of energy loss in granular debris flows. Segregation and the migration of coarser grains to the front of the flow is a major control on flow behaviour (Iverson, 2005a,b).

2.1.2. Viscous debris flows

In a viscous debris flow (zone B in Figure 2.1), the entire flow behaves as a homogenous viscous fluid. The sediment concentration of the flow is still very high, but the fines content is larger than 10% of the flow by weight. The larger particles are surrounded by a mixture of viscous fluid and fine material which dampens the collisions between coarse particles (Schatzmann, 2005).

2.1.3. Mudflows

If the fines concentration is increased still further, a mudflow is produced (Zone C in Figure 2.1). In a mudflow, the fluid and fines make up a fluid phase which is indistinguishable from the coarser fraction. The importance of inter-granular collisions and friction decreases, while the importance of intermolecular attractions and cohesive strength increases.

In reality, these processes occur on a spectrum from very coarse flows with almost no fines (e.g. Okano et al. 2011) to mudflow or earthflow with material over 80% sand or finer (Coussot and Meunier, 1996; Hungr et al., 2001). For example, a viscous-granular debris flow is a transitional flow between the granular and viscous type (Takahashi, 2007).

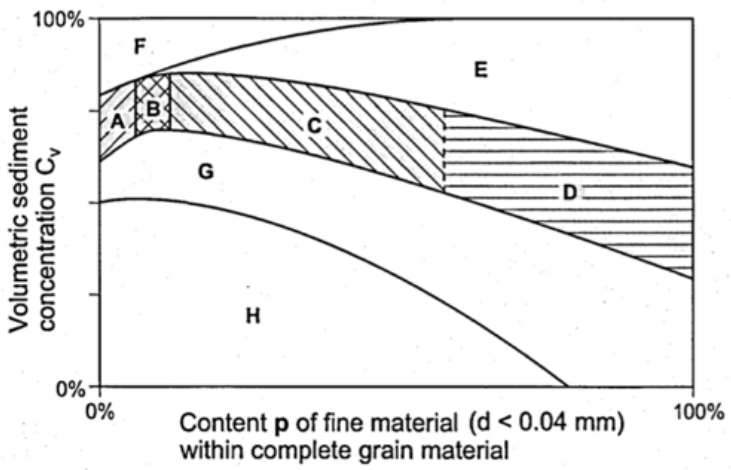

Figure 2.1.: Classifications of debris flow types according to Schatzmann (2005) who adapted the diagram from Coussot and Meunier (1996). A-granular debris flow; B-viscous-granular debris flow; C-viscous debris flow, D-mud flow; E-block type landslide; F-rock fall/avalanche; G-hyper-concentrated flow; H-bed load transport.

2.1.4. Hyper-concentrated flow

At low solids concentrations, a hyper-concentrated flow is produced (zone G in Figure 2.1). In this type of flow, particle settling, particle collision and turbulence become more important (Schatzmann, 2005). Pierson (2005) emphasizes the role of fines, which give the hyper-concentrated flows a weak yield strength that enable the flow to transport coarse particles in suspension (i.e. gravel). These coarser particles, however, will be selectively deposited as the flow velocity decreases, unlike in a debris flow.

From a hazard perspective, the inability to carry cobble and boulder sized clasts in suspension makes hyper-concentrated flows much less dangerous than debris flows. It should be emphasized, however, that hyper-concentrated flows exist along a continuum from flood flow to debris flow processes (Pierson, 2005). Hyper-concentrated flows and flood flow usually always accompany debris flow surges. Specific morphological features common in hyper-concentrated flow deposits are discussed in Section 3.3.

2.2. Debris flow morphology

2.2.1. Surge morphology

The characteristics of debris flow material, the extent of saturation, and the nature of flow will often change as the flow proceeds downslope. Often debris flow events will be made up of a series of discrete surges of coarse material separated by watery inter-surge flow (Hungr, 2005). These surges are not homogenous. Coarse particles tend to rise to the surface through a kinetic sieving process Iverson (1997). These large particles move toward the flow front, creating a bouldery accumulation at the head of the flow (as represented in Figure 2.2). Behind the flow front, flow height, average clast size and solids concentration decrease over time until the arrival of the next surge.

In granular type debris flows, the frictional properties of the bouldery front will largely control flow velocity and deposition (Iverson, 1997, 2005b). Consolidation is controlled by the smaller particle sizes in the debris flow material. Consolidation, along with the normal stress, controls pore fluid pressure. The permeability at the bouldery front, therefore, is often too high to develop any basal fluid pressure, while the finer flow interior may support pressures up to or over the total normal stress. In the body and tail of the flow, these pore pressures decrease the effective normal stress and hence intergranular friction. This process increases flow mobility (Iverson, 2005b; Major, 2000). It also causes the bouldery front to act as a moving dam which is driven by the flow interior. The flow stops when the grain contact and basal friction at the flow margins overcomes the driving force of the liquefied material behind the front.

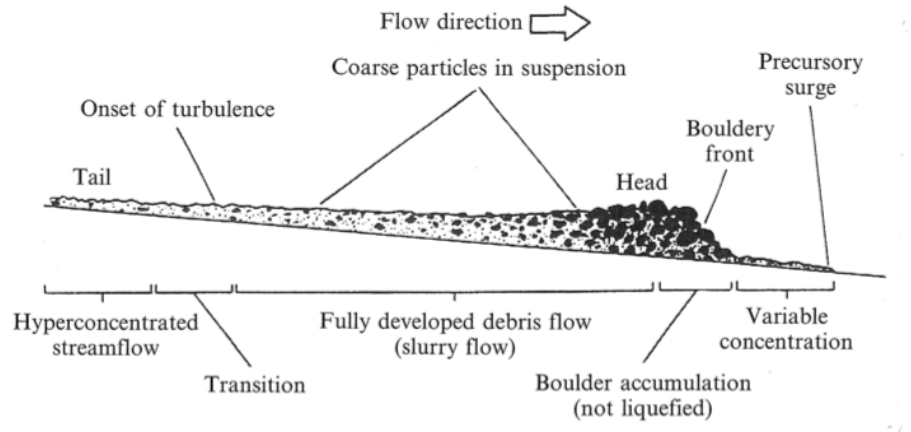

Figure 2.2.: Sketch of a debris flow surge (Pierson, 1986). Coarser material accumulates near the front of the flow due to segregation processes.

2.2.2. Path morphology

Figure 2.3 shows an archetypal debris flow path divided into a source area, a transport zone, and deposition zone. The source area (which is also sometimes referred to as the initiation or starting zone) is where the initial failure occurs. The initial failure is often a shallow, translational failure in a headwall, gully sideslope, or in the stream channel. In other debris flow channels, the debris flow will initiate through progressive bulking of sediment by stream flow (Berti and Simoni, 2005). Initiation can occur on any slope with sufficient inclination (usually 20° to 45°) and enough soil or colluvial accumulation to generate a slide. In general, slopes steeper than 45° will not sustain deep enough soils to be prone to failure (Iverson et al., 1997). However, these slopes may often supply debris to lower angle talus or colluvial foot-slopes which serve as source areas for slope failures.

Once initiated, shallow translational slides often mobilize into debris flows due to static liquefaction and begin to flow downslope (Sassa and Hui, 2005; Iverson et al., 1997). This flow often enters an established gully or stream channel and proceeds down-slope. Through the transport zone, the flow may both erode or deposit material, but in general the flow will not gain or lose significant amounts of volume. This transport zone is characterized by intermediate slope angles of approximately 15° to 25° (Fannin and Wise, 2001) depending on whether the flow is moving down a channel or an open slope. Finally, the debris flow will come to a halt in response to a decrease in slope and a reduction in confinement in a terminal zone of deposition. This is often on a debris flow fan built up from subsequent debris flows, although not always. This zone is also sometimes referred to as the runout zone.

In reality, zones of erosion, transport, and deposition are gradational. Their length and location will vary from event to event. For example, very large debris flows may erode a significant amount of material through what is usually a transport zone and even incise a channel through the debris flow fan. Further, the finer tail portion of the flow and subsequent flood flow will often erode and rework the main deposit in the runout zone.

Whether a debris flow will erode will also depend on how much sediment is stored in the channel at the time of the event. If the channel has an ample and continuous supply of sediment, the limiting factor in debris flow occurrence will be a hydrologic event large enough to mobilize this material. This is the "transport limited" concept proposed by Bovis and Jakob (1999). In contrast, the sediment supply in some debris flow channels may be limited. A triggering event will not produce another debris flow until the channel has "recharged" with sediment. This situation is termed "supply limited" (Bovis and Jakob, 1999).

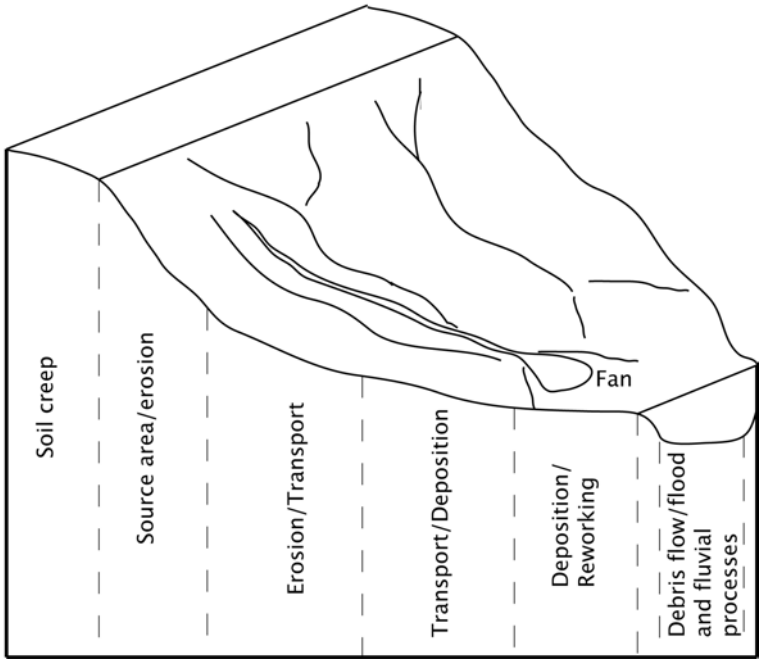

Figure 2.3.: Sketch of a debris flow path showing the initiation, transport, and deposition zones.

2.3. Modelling entrainment, travel distance and runout

In order to mitigate the hazard posed by debris flows, scientists and engineers would like to know where a flow may occur, when will it occur, and its severity. In order to predict landslide occurrence, empirical thresholds of the rainfall needed to trigger shallow landslides have been developed for many areas throughout the world (Chien-Yuan et al., 2005; Crosta, 1998; Crosta and Frattini, 2008; Wilson and Wieczorek, 1995) These thresholds can also be linked to slope-stability models to predict the storm event needed to initiate failure (Berti and Simoni, 2005; Brooks et al., 2004; Crosta, 1998). These studies show that the intensity and duration of a triggering storm can be predicted if one knows the mechanism of failure, the limiting permeability of the hydrologic system, and the depth of saturated material.

The severity of a flow is largely controlled by event volume. Larger flows travel further, attain higher velocities, and entrain more material than smaller flows (Corominas, 1996; Rickenmann, 1999, 2005). Unfortunately, the volume of a debris flow can be extremely hard to predict. Sometimes the volume of the flow is determined by the initiating event, but far more often it is controlled by how much sediment the flow entrains or deposits as it proceeds

down-slope (Bovis and Jakob, 1999; Hungr et al.). Consequently, the more a flow entrains, the more destructive it is likely to be. Thus, the success of debris flow hazard analysis hinges on approximating the volume change of a flow as it travels down its path.

The material composition and sediment concentration of the flow are also important. For two flows of the same volume and channel morphology, differences in these parameters will control differences in velocity and peak discharge. These parameters will also affect how far the debris flow travels down its path and spreads onto the debris flow fan.

Estimates of event volume or velocity must be coupled with a model for travel distance or runout to be useful in hazard mapping. *Travel distance* is defined as the length of debris flow travel from the head of the failure to the toe of the debris. *Runout* usually refers to the distance travelled in the final, terminal zone of deposition (Rickenmann, 2005; Corominas, 1996).

2.3.1. Empirical approaches

The mechanics of debris flow motion are extremely complex. Measuring debris flow parameters required by analytical equations for debris flow motion (Iverson, 1997, 2005b) such as solids concentration, unit weight, and viscosity at the field scale is both difficult and dangerous. Consequently, most models for debris flow entrainment, travel distance, and runout are empirical or at least semi-empirical. The three most common empirical-statistical approaches to estimate travel distance are the limiting criteria, angle of reach, or volume-change rate.

2.3.1.1. Limiting criteria

Some debris flow models rely on a set of empirical limiting criteria to estimate debris flow travel distance. For example, Benda and Cundy (1990) found that channelized debris flows in the Pacific Northwest usually stop when the channel gradient drops below 0.06 or the flow encounters a tributary junction which produces a bend of more than 70°. However, while various limiting criteria have been proposed as rules of thumb for the onset of debris flow deposition (see Table 2.1), none have been found to be universal. Like empirical models in general, such rules apply only in the climate and geologic setting in which they were produced.

Table 2.1.: Examples of deposition angles in the debris flow literature (taken from Hungr et al.).

Reference	Location	Deposition slope (°)	
		confined	unconfined
Ikeya (1981)	Japanese alps	not specified	10
Hungr et al. (1984)	Forested, B.C.	8-12	10-14
Wong et al. (1997)	Open slope, Hong Kong	not specified	30-40
Benda and Cundy (1990)	Forested, B.C.	not specified	3.5
Fannin and Wise (2001)	Forested, B.C.	10-22	19-24
Jordan (1994)	B.C. Interior	not specified	0.2-15
Lopez et al. (2003)	Venezuela	not specified	2
Pierson (1995)	Mt. Saint Helens	not specified	1

B.C. is British Columbia.

2.3.1.2. Angle of reach

The angle of reach or "fahrboschung" angle is defined as the angle of the line connecting the head of the landslide source to the distal extent of the landslide mass (Figure 2.4). The angle of reach is often considered a index for the efficiency of a landslide's movement (Hsu, 1975; Corominas, 1996; Iverson, 1997)

Corominas (1996) found that the angle of reach differed by landslide type and developed regression equations for each. Debris flows were found to have intermediate angles of reach between rock-fall events and fine-grained mud and earth flows. He also found that the angle of reach did not depend on flow height, and that therefore the differences were caused by the intrinsic properties of the material, landslide mass, and the mechanics of motion.

In an extension of the angle of reach concept, Prochaska et al. (2008a) developed a model which predicted the runout distance of the flow based on the angle connecting the fanhead and the elevation half-way between this point and the drainage divide of the basin. This angle was considered a proxy for the average slope of the channel. The model was tested and worked well for a variety of unobstructed, moderate sized, non-volcanic debris flows in western North America.

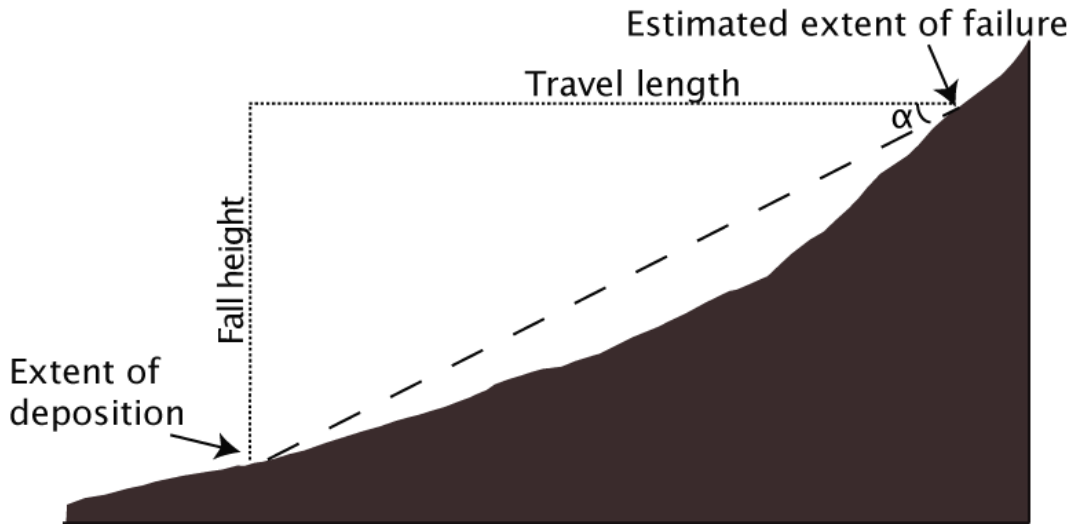

Figure 2.4.: The angle of reach or "fahrboschung" angle of a landslide (α). The angle is the slope of a line connecting the head of a landslide with distal extent of deposition.

2.3.1.3. Volume change rate

The other common empirical-statistical approach is based on volume change as the flow proceeds downslope. Rather than predict debris flow travel distance based on the geometry of the path (i.e. travel angle), the volume-change approach predicts when the flow will run out of material using a set of rules for deposition, entrainment, or transport. This assumes that as the debris flow travels it continuously entrains, deposits, or transports material and that the landslide stops once the volume of the flow reaches zero (Cannon and Savage, 1988; Conway et al., 2010; Fannin and Wise, 2001).

Fannin and Wise (2001) developed an empirical model called UBCDflow for debris flow travel distance and event volume based on field data from 131 debris flows in Queen Charlotte Island, BC, Canada. The key parameters that determined the amount of deposition or entrainment in each reach were channel geometry (defined as confined, unconfined, or transitional), slope angle, and whether or not the flow encountered a bend as it transitioned from one reach to another. Given an initial failure volume, changes in debris flow volume from entrainment and deposition were summed for each reach along the path until the cumulative volume equalled zero, at which point the flow stopped.

UBCDflow has generally performed well when tested outside of the Queen Charlotte Islands. When tested with two debris flow events on Vancouver Island, B.C., which has different geology but similar climate to the Queen Charlotte Islands, Fannin and Wise (2001) found

that the model predicted travel distance quite well. Busslinger (2010) applied the model to several events in the Kootenay mountains of British Columbia; a field area with both different climatic and geologic conditions to those in the Queen Charlotte islands. Despite the differences, the model predicted the travel distances of the flows well, but generally over-predicting event volume. The success of the model was attributed to similarities between the slope angle of entrainment and deposition in both field areas (Busslinger, 2010).

While these successes are encouraging, the model still needs to be tested in different geoclimatic settings before being used with confidence. UBCDflow is evaluated with New Zealand data in Chapter 6.

2.3.2. Dynamic approaches

Dynamic models estimate the runout distance, velocity, and momentum of the debris flow based on the gravitational driving force and a constitutive law which governs the frictional resistance to movement. Dynamic models can be split into four major groups; lumped mass models, momentum models which consider pressure from discharge upslope (i.e. the Takahashi/Hungr momentum equation), continuum models, and distinct element models.

2.3.2.1. Lumped-mass models for travel distance

Lumped mass models model the moving debris flow mass as a single point with some mass. This simplification ignores internal deformation or the motion of the debris flow front, which is often considered the most important aspect of a debris flow hazard. It also ignores variables such as channel shape and entrainment.

Lumped mass models include the sliding block model of Sassa (1989), a modified version of this model (Wang and Sassa, 2003), and the sliding consolidation model (Hutchinson, 1986). The most basic sliding block model assumes that all energy loss during movement is due to friction at the bed surface. This is referred to as the equivalent or average coefficient of friction by Hsu (1975) and Scheidegger (1973). This coefficient is a catch-all for all the various factors increasing flow resistance which may include viscosity, channel roughness, path tortuousity and obstacles in the path.

The sliding block model was improved by considering effects of pore pressure at the sliding plane in separate models by Wang and Sassa (2003) and Hutchinson (1986). The model of Wang and Sassa (2003) incorporates a user defined pore pressure which has the effect of lowering the effective friction angle. The method requires pore pressures and dynamic friction

parameters to be found in laboratory tests. Hutchinson's (1986) model assumes pore pressures at the base of the flow dissipate according to one-dimensional consolidation theory. As the flow moves downslope, pore pressures dissipate and frictional resistance at the base increases.

2.3.2.2. Takahashi/Hungr momentum equation and the concept of friction slope

The Takashi/Hungr momentum model focuses solely on runout on the fan. It is similar to the lumped mass models, except that the pressure from upstream discharge is considered and the runout length calculated is to the extent of the deposition, not the center of mass.

The equation was originally developed by Takahashi (1978) in Japanese, then summarized in English by Takahashi (1991) and used by Hungr et al. (1984). The equation calculates the runout of an inertial, stony debris flow based on the conservation of momentum over an abrupt change in channel slope (Figure 2.5) . Takahashi (1991) assumes the change in momentum as the surge makes the transition must be the sum of the force due to gravity, the momentum of the surge that is upstream of the transition, the hydrostatic and earth pressure terms, less the friction at the base of the surge. By neglecting the small terms and assuming a constant flow height and width before and after the transition, Takahashi (1991) derives the following equation:

$$X_L = V^2/G \tag{2.1}$$

$$V = v_u cos(\theta_u - \theta_d)\left[1 + \frac{\{(\sigma - \rho_m)\, c_s \kappa_a + \rho_m\}\, cos\theta_u)}{2\,\{(\sigma - \rho_m)\, c_s + \rho_m\}} \frac{g h_u}{v_u^2}\right] \tag{2.2}$$

$$G = \frac{(\sigma - \rho_m)\, g c_s cos\theta_d tan\alpha}{(\sigma - \rho_m)\, c_s + \rho_m} - g sin\theta_d \tag{2.3}$$

where v_u is the velocity at the transition point, h_u is flow height at the transition point, θ_u is the slope angle of the upstream reach, θ_d is the slope angle of the downstream reach, ρ_m is density of the intergranular fluid, σ is the density of the solid, c_s is the solids concentration, α is the dynamic friction angle, and κ_a is the active earth pressure coefficient.

Hungr et al. (1984) introduces the term "friction slope", S_f, by defining:

$$S_f = \frac{(\sigma - \rho_m)\, c_s}{(\sigma - \rho_m)\, c_s + \rho_m} tan\alpha \tag{2.4}$$

Thus, the original physical meaning of S_f, according to Hungr et al. (1984) and Takahashi (1991), is related to the solids concentration of the flow (c_s) and the dynamic friction

angle between the particles (α). In Equation, 2.1 the S_f is assumed to be constant along the runout path.

While, in theory, the S_f could be determined for field scale events from the solids concentration and dynamic friction angle, in practice this is extremely difficult because both parameters are difficult to measure and may be variable in space and time. Therefore, S_f is most often treated as an empirical, lumped parameter which is determined by back-calculation with observed travel distances.

The model is very dependent on the value chosen for S_f. If the fan-slope (θ_d) is equal to S_f then the runout will be infinite. The fan is built up by previous debris flows, therefore, the fan slope is often very close to the equilibrium slope on which debris flows come to rest. In practice, this means that the S_f is always slightly higher than the deposition slope. For this reason, S_f is often empirically related to the θ_d by the equation $S_f = f\,tan\theta_d$, where f is an empirical coefficient (Rickenmann, 2005).

Hungr et al. (1984) reported good agreement between calculated simulations using a S_f of tan10° and observed runout distances for five flows in western Canada. However, the best back-calculated friction slope varies from flow to flow and locality to locality (Rickenmann, 2005). For debris flows in the Southern Alps of Japan, f was found to be 1.12 (Okuda and Suwa, 1984). For 12 debris flow events in the Swiss Alps, f=1.08 yielded more realistic values of X_L (Rickenmann, 2005).

In practice, S_f reflects both properties of the flowing mass and parameters such as channel roughness, angularity, obstacles, and confinement. This will be discussed further in Chapter 8.

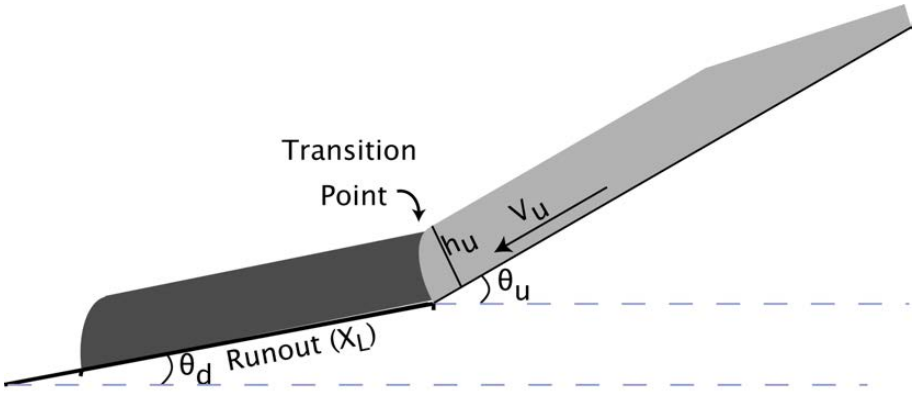

Figure 2.5.: Process of stoppage of inertial, stony debris flow front transitioning from steep slope to gentler runout (modified from Takahashi, 1991). The subscripts u and d stand for upstream and downstream of transition.

2.3.2.3. Continuum models

Continuum models apply the conservation equations of mass, momentum, and energy and a rheological model to describe the material behaviour. They also, unlike lumped mass models or the Takahashi/Hungr momentum equation, account for internal deformation of the flowing mass. Some runout models are extensions of the sliding block model concept; they allow the block (or sets of blocks) to deform and interact with each other as they move down the slope (Hungr, 1995). Other models use a deforming mesh and a hydrograph input rather than a starting block or series of blocks which deform as they move downslope (Christen et al., 2010).

Whatever model is chosen, the choice of rheology (constitutive law) used to model resistive forces in the flow is one of most important elements of the modelling exercise. Some models use a single rheology, while others allow the user to choose from a list (e.g. DAN-W). The basic rheologies used in debris flow modelling are discussed below. These rheologies have been used by various investigators to back-calculate basic debris flow parameters and explain debris flow morphology (Johnson, 1970; Takahashi, 1978; Hungr et al., 1984; Bagnold, 1954; Ancey and Evesque, 2000; among others). Continuum models, with emphasis on DAN-W (Hungr, 1995), are discussed further in Section 6.1.1.

2.3.2.4. Discontinuum models

Rather than model the flow as one continuously deforming material, discontinuum models treat the problem as an assemblage of distinct, interacting particles. This approach is collectively called the discrete-element method. Discrete element methods are currently being developed for dry granular flows such as sand and rock avalanches (Tommasi et al., 2008; Stead et al., 2006). While this approach could be used to model debris flows, it at present requires much more development to deal with the problem of coupling solid and fluid behaviour. Even once the codes are developed, they will have to be compared and calibrated against physical models and mapped flows (Poisel et al., 2008).

2.3.3. Basic rheological models

If a continuum approach is used, the rheology governing material deformation and flow resistance must be specified. In laminar fluid flow, stress is due to internal viscous deformation, while in turbulent fluid flow, stress is dominantly controlled by roughness at flow boundaries (Munson et al., 1998). All of these rheologies essentially assume that the debris flows are laminar. It is generally accepted that within a debris flow, the flow will be laminar as a result of

the high concentration of particles and small particle size (Hungr et al., 1984; Iverson, 2005a). Three of the most basic rheologies are discussed below. The Voellmy rheology is discussed in Section 6.1.1.

2.3.3.1. Newtonian or viscous

The one-dimensional flow law for Newtonian fluid is:

$$\tau = \mu \frac{du}{dz} \tag{2.5}$$

where τ is the shear stress, dz is the elevation above the datum, du is the velocity du/dz is the shear rate, and μ is viscosity.

For one-dimensional flow, the shear stress on a plane, parallel to the surface of flow with a slope angle of θ can be calculated by equation:

$$\tau = \rho g h sin\theta \tag{2.6}$$

If z in Equation 2.5 is replaced by the flow height and equations 2.5 and 2.6 are combined, the result can be integrated to give a velocity with depth (Jordan, 1994). However, it should be noted that using the Newtonian or viscous rheology to model debris flows is not mechanically correct. Only dilute dispersions of fine-grained sediment in water, where the particles do not interact substantially, will be Newtonian. This applies to normal flood flow, but not to hyper-concentrated flows or debris flows (Jordan, 1994).

2.3.3.2. Bingham or viscoplastic

Fine debris flows, earth flows, or mudflows are often modelled using a Bingham rheology for viscoplastic flow. The one-dimensional flow law for a Bingham fluid is:

$$\tau = k + \mu \frac{du}{dz} \tag{2.7}$$

where k is the yield strength of the material. In the Bingham model, the fluid only deforms after a specified yield strength has been exceeded. The yield strength concept was first applied by Johnson (1970) to explain the "freezing" of debris flow levees and lobes. The yield strength may be caused by flocculation of clay particles or an undrained shear strength in the fine material. More recent numerical models for fine grained flows which use this rheology include that of Laigle and Coussot (1997), who have applied the model to mudflows, and

Fraccarollo and Papa (2000), who used it to model debris flows with a high fines concentration in the Dolomites, Italy.

2.3.3.3. Granular or dilatant

At higher velocities, lower fines concentrations, and for flows consisting of generally larger particles, it has been suggested that inertial forces dominate over viscous forces within saturated granular flows. In experiments with buoyant, uniform particles in a Couette shear cell, Bagnold (1954) found that at higher shear rates, the shear stress was found to be proportional to the square of the shear rate.

In this situation, the momentum from a grain collision is not transferred to the pore-fluid, but rather is transferred to the next intergranular collision. These particle collisions are considered to create a dispersive grain stress. This situation is referred to as the inertial regime (Takahashi, 1978; Bagnold, 1954). The one-dimensional flow law for a granular material (inertial flow) is:

$$\tau = \mu(\frac{du}{dz})^2 \tag{2.8}$$

While some bouldery debris flows may be in the inertial regime, flows with higher fines contents and higher viscosities are in the macro-viscous regime (Davies, 1986). Additionally, the relevance of the inertial regime for flows under high normal stresses has been questioned (Savage and Hutter, 1989). Open channel experiments by Hungr and Morgenstern (1984), which used flows of geological materials at high normal stresses, showed that they could be described by frictional Mohr-Coulomb behavior. Savage and Hutter (1989) consequently proposed a non-dimensional parameter, N_S (Equation 7.2, discussed later in Section 7.13.3) to characterize the ratio between inertial and frictional stresses.

2.4. Physical modelling background

While field studies of past debris flow events are critical, the best debris flow data comes from real-time measurements of field events. However, even if one is able to observe a debris flow event in the field, the boundary conditions and key parameters influencing flow behaviour may be difficult or even impossible to measure. Using physical modelling we can simplify these processes and control the boundary conditions in the laboratory, without preconditioning the outcome. This has made small-scale flume studies of debris flows an indispensable tool in

elucidating some key aspects of debris flow mechanics.

2.4.1. Small scale flume experiments

Many authors have used small scale flume studies to elucidate the controlling factors and mechanics of debris flow behaviour (Ancey and Evesque, 2000; Bowman and Sanvitale, 2009; Carrol et al., 2007; D'Agostino et al., 2010; Savage and Lun, 1988; Takahashi and Yoshida, 1979; Takahashi, 1981, 2007). Some experimenters have used novel experimental apparatus to model debris flow behaviour. For example, Davies (1988) used a conveyer belt flume to observe the development of debris flow fronts over a longer duration than possible in small-scale flume studies. He found that the front behaviour was mainly controlled by larger grains. The maximum height of the front was determined by the velocity profile within the flow and the total volume of material used . The sediment concentration used in the test controlled the length of the more fluid body and tail (Davies, 1988). Other types of physical modelling studies have used large, rotating drums (Hsu et al., 2011; Kaitna et al., 2011) . The advantage of the rotating drum, like the conveyer belt flume, is that it allows observation of the flow over a longer time duration and makes a steady state possible. Hsu et al. (2011) found that increased particle size and angularity, as well as increased solids concentration, increased the boundary shear stress. Kaitna et al. (2011) showed that the rotating drum could model the unsaturated front of debris flows and study effects of fluid viscosity and flow velocity.

Unfortunately, the extrapolation of small-scale behaviour to field scale processes may not always be appropriate. Larger scale debris flows may be fundamentally different than idealized, small-scale models because small scale flows may not reflect the dominance of Coulomb stresses and decreasing importance of viscous stresses in field scale flows (Iverson and Denlinger, 2001). In a scaling analysis of debris flows, Iverson and Denlinger (2001) define the Quasi-Reynolds number (N_{qR}) and Pore Pressure number (N_P) as the key parameters influencing flow behaviour. N_{qR} and N_P are defined as follows.

$$N_{qR} = \frac{\rho H \sqrt{gL}}{v\mu} \tag{2.9}$$

$$N_P = \frac{D\sqrt{L/g}}{H^2} \tag{2.10}$$

where ρ is the density, H is the flow height, g is the gravitational acceleration, L is the length of the flow, v is the flow velocity, μ is the viscosity of the pore fluid, and D is the char-

acteristic grain diameter. According to Iverson and Denlinger (2001), N_{qR} represents the ratio between inertial and viscous forces; large quasi-Reynolds numbers suggest that the dominant mechanism of energy dissipation is due to inertial forces, while small numbers represent losses due to viscous forces.

N_P represents the time scale for downslope movement divided by the time scale for consolidation, which in turn reflects the extent to which pore-pressures are able to mediate frictional resistance. While H is in the numerator of Equation 2.9, it is in the denominator of Equation 2.10. Thus, as the scale of the flow is increased, the Quasi-Reynolds number will be systematically higher and the pore pressure number systematically lower. Thus, according to Iverson and Denlinger (2001) miniature flows of grain water mixtures cannot emulate the conditions of in field scale debris flows.

2.4.2. Large scale flume tests

The obvious solution to the scaling limitation inherent in small-scale modelling is to increase the scale of the model. This is precisely what has been done in experiments at the USGS debris flow site (Iverson et al., 2011; Iverson, 2005b; Denlinger and Iverson, 2001) and several other large scale flumes throughout the world. The flume is a rectangular concrete chute 95m long and 2m wide that slopes at 31°. It flattens at its base to join an unconfined runout surface that slopes at 2.5°. Approximately 10 m^3 of debris can be released from a starting gate at the head of the flume. Results of experiments using this flume are reported in Denlinger and Iverson (2001); Major (2000); Iverson (1997); Iverson and Denlinger (2001); Iverson (2005b); Iverson et al. (2011). The results of these tests show that the flume is able to model segregation behaviour and the unsaturated nature of the front, although this is possible with small scale flumes as well (as discussed in Chapter 8). Scaling analysis also show that the flows are able to simulate higher N_{qR} and lower N_P than traditional, small-scale flume tests (Iverson and Denlinger, 2001; Iverson, 1997).

2.4.3. Geotechnical centrifuge studies

As noted above, while physical modelling has proved tremendously useful in a range of applications, traditional small-scale physical modelling has difficulty recreating large stress states. This has always been a problem for geotechnical engineers, as soil behaviour is primarily a function of stress level (i.e. the weight of the overlying soil) and stress history. In almost any geotechnical problem then, the self-weight of overlying soil is a critical issue (Craig, 1995).

While large-scale physical models can mitigate this problem to some extent, there is a practical limit to the size of the model. For example, every experiment in the USGS flume requires several days of preparation by a large team of investigators. In other geotechnical problems, such as construction of piers or earth dams, a large enough physical model is simply not feasible. These large scale models also lack experimental flexibility. For example, the slope of the USGS flume is permanently set at 31°. In small scale experiments, boundary conditions such as slope and flume width can be easily changed.

As early as 1869, Edouard Phillips had realized this problem, and the potential for a centrifuge to overcome some of the scaling limitations inherent in small scale models (Craig, 1995). Centrifuges induce a radial acceleration field which can be used to simulate a high gravitational field, and therefore overcome the limitations inherent in small-scale physical modelling at earth's usual gravitational acceleration of 9.8 ms^{-2}. The initial idea languished until the early 1930's, when it was independently taken up by both American and Soviet researchers. In the 1960's, Dr. A.N. Schofield initiated a centrifuge modelling program at Cambridge (Craig, 1995). In the 1970's and 1980's Soviet expertise was married with the computational capability and more advanced instrumentation produced in the West. From this point on, the use of centrifuges in modelling geotechnical problems rapidly spread. Today, there are a number of machines operating in many countries (Craig, 1995).

Centrifuge designs are usually one of two basic configurations; rotating arms with either hinged or rigid model containers, or rotating drums where the model is set-up on the inner surface of the drum. The drum centrifuge is especially advantageous for studies of long runout landslides because the drum circumference itself can be used as the runout zone – i.e. where the flow comes to rest. In a beam centrifuge with a container on the end of a hinged arm, the experiment is confined to the length and width of the model container. This type of centrifuge can only model small runouts. With the drum configuration, the runout is only limited to the length of the inner circumference of the drum. A series of debris flow experiments conducted using a drum centrifuge are discussed in Chapter 7. A detailed discussion of the experimental apparatus is given there.

2.4.4. Scaling laws in geotechnical centrifuge testing

Scaling principles have been developed for the geotechnical centrifuge over a number of years for both static and dynamic processes including seismically induced liquefaction, rockfall behaviour, fluid flow and erosion (Chikatamarla et al., 2006; Schofield, 1980; Garnier et al., 2007; Taylor, 1995). Debris flows are a relatively new phenomenon to be tested on a centrifuge; however, it

is generally accepted that debris flows are laminar (Hungr et al., 1984; Iverson, 2005a). Since laminar flow scaling follows Darcian / conventional consolidation laws (Goodings, 1984), many principles already developed for conventional, laminar flow and Darcian flow may be applied in the context of debris flows.

2.4.4.1. Length scale

The point of physical modelling is to reduce the dimensions of a situation to a more manageable size, while still retaining similitude of relevant physical processes. In centrifuge testing, the length scale of the model is generally reduced by the same factor by which the g-level is increased (N).

Keeping track of the terminology is essential, as it becomes quite easy to confuse the model and prototype scales. The term "model scale" is the scale of the physical model. Usually the model scale is denoted in equations with the subscript m. The prototype is the hypothetical, scaled up situation the centrifuge simulates (denoted with the subscript p). The scale factor is always model:prototype (1:N). N can be thought of as "the prototype is N times bigger in every dimension than the model" or conversely, "the model is N times smaller than the prototype in every dimension". This is the basic rule from which the other scaling laws derive.

2.4.4.2. Stress and linear scale for depth

As stated above, soil behaviour is primarily a function a stress level (i.e. the weight of the overlying soil) and stress history. In almost any geotechnical problem then, the self-weight of overlying soil is a critical issue. If an acceleration N times Earth's gravity (g) is applied to a soil with material density ρ, a vertical stress, σ_v will be developed at h_m in the model. This stress in the model is given by the equation:

$$\sigma_{vm} = \rho N g h_m$$

Stress in the prototype (subscript p) is calculated by:

$$\sigma_{vp} = \rho g h_p$$

In centrifuge testing the $\sigma_{vm} = \sigma_{vp}$(this is the whole point of centrifuge testing). solving for the model height yields $h_m = h_p N^{-1}$. The scale factor for this dimension is then 1:N, the

same as for linear scale. Therefore displacements scale to 1/N as well. This also means that strains will have a scale factor of 1:1.

2.4.4.3. Consolidation and seepage

The equation for consolidation is expressed as a dimensionless number defined by:

$$T_v = \frac{c_v t}{H^2}$$

where c_v is the coefficient of consolidation (based on the particle size distribution, packing, and the shape of the particles making up the soil), t is the time, and H is the drainage path length. If the degree of consolidation is the same in both the model and the prototype, then $T_{vm} = T_{vp}$, therefore:

$$\frac{c_{vm} t_m}{H_m^2} = \frac{c_{vp} t_p}{H_p^2}$$

From the discussion of linear scaling, $H_p = NH_m$, therefore:

$$t_m = \frac{1}{N^2} \frac{c_{vp}}{c_{vm}} t_p$$

Thus, if the same soil is used in the model and the prototype then the scale factor for consolidation time is $1:N^2$. Therefore, a consolidation time that lasts 1 hour in a centrifuge running at 40g (N of 40) will be equal to an a consolidation time of 66 days in the model. As wondrous as the centrifuge may be, "it is important to recognize that this apparent speeding up of time-related processes is a result of the reduced geometric scale in the model; the centrifuge is not a time machine" (Taylor, 1995).

The discussion above becomes more intuitive if one thinks about fluid flow through through a porous medium. The increased force which the pore-fluid feels in response to the Ng equivalent radial acceleration will cause the fluid to flow faster through the medium. The fluid velocity in the model, in fact, will be N times faster than in the prototype. This is how spin dryers work; they impart a g-force which pulls moisture out of clothes, even if those clothes aren't scaled down to model (say Barbie doll) size. However, since the model is scaled down, the smaller size of the model compounds the issue. The drainage pathways encountered by the pore fluid are also N times smaller than in the prototype. The time needed for the pore fluid to escape the material (t_m) can be expressed as:

$$t_m = \frac{L_m}{v_m} = \left(\frac{L_p}{N}\right)\left(\frac{1}{Nv_p}\right) = \frac{1}{N^2}t_p$$

This is the same relationship calculated by using the equation for consolidation.

2.4.4.4. Velocity and the inertial time-scale

If it is assumed that the velocity observed in the model is equal to the velocity observed in the prototype v_m=v_p, then it can be said that:

$$\frac{x_m}{t_m} = \frac{x_p}{t_p}$$

From our discussion of linear scaling, x_m= x_p/N:

$$\left(\frac{x_p}{N}\right)\left(\frac{1}{t_m}\right) = \frac{x_p}{t_p}$$

solving for t_m reveals that the inertial time in the centrifuge model will be N times shorter than the prototype ($t_m = t_p/N$).

From the above discussion, it is clear that the inertial time in the model scales to 1/N, while the time needed for consolidation scales to $1/N^2$. This mismatch creates a problem. If we use the same soil and pore fluid in the prototype and model, and we want the model to behave like the prototype at 1/N scale, then the pore fluid in the model will drain out N times too quickly.

To resolve this inconsistency, the prototype pore fluid (assumed to be water) is usually replaced with a higher viscosity pore fluid which inhibits consolidation (Kutter, 1995). If the viscosity of the pore fluid is N times higher than water, it slows down the time for consolidation by N^2 and inertia by N in the model, resulting in the same overall time for these processes as the prototype with water. This approach also means that, in terms of consolidation, the particle size distribution used in the model is the same as the "effective" particle size distribution at the prototype scale.

2.4.4.5. Variation in g-level in the model

The earth's gravity can be considered uniform under the range of elevations encountered by a debris flow event. However, when using a centrifuge to generate high acceleration fields to

simulate field processes, acceleration varies through the model. The vertical acceleration field is $\omega^2 r$, where ω is the angular rotation speed of the centrifuge and r is the radius to any element in the soil model. When testing with a drum centrifuge, the g-level (N) commonly refers to the radial acceleration at the drum surface. For a drum centrifuge operating at N=40 and a radius of 1.1m, corresponding to a vertical acceleration at the drum surface of 392 ms^{-2}. As the height of any model element (i.e. the distance from the drum wall) increases, the angular rotation of the model stays the same, but the effective radius decreases. The effect is a decrease in the vertical acceleration field.

While this effect adds complexity, its effect can be easily calculated. For example, 30 cm away from the surface of the drum in the above scenario, the vertical acceleration will be 285.36 ms^{-2}, or a 28% reduction in the g-level.

Additionally, there is a small increase in N due to the Coriolis effect (Taylor, 1995). The maximum Coriolis acceleration is expressed by the term $2v_r\omega$, where v_r is the radial velocity of the point of interest in the model and ω is the angular velocity at that point. For example, in a centrifuge imparting a g-level where N=40, a flow traveling with a mean velocity 1.5 ms^{-1}, on a slope angle of 20° will produce a Coriolis acceleration of 19.4 ms^{-2}. This will be 5% of the vertical acceleration field. While this Coriolis 'error' is not inconsequential for models of very fast moving particles, it is quantifiable. Coriolis errors are usually ignored when they are <10% of the acceleration field (Wood, 2005).

2.5. Concluding remarks

This chapter reviewed the fundamental types of debris flows, some of the more common empirical and analytical tools used to model their travel distance, and discussed some of the scaling limitations inherent in comparing field scale flows with small laboratory flows. The geotechnical drum centrifuge was introduced as a way to overcome some of the limitations of a traditional, 1-g flume tests. Scaling laws for geotechnical centrifuge tests were then discussed.

Implicit, but not often discussed, in the debris flow literature is the primary importance observation data—whether it be from the field or laboratory. These observations form the basis of empirical models, provide a basis to calibrate and check more analytical, mechanically-based simulations. Field experience forms the basis for the engineering judgement and hazard evaluation.

From the literature review, it is also clear that scale is a critical factor in debris flow physics. The question remains whether the behaviour of large, very infrequent but catastrophic

events are fundamentally different in terms of mechanics than smaller scale field flows, and whether, in turn, these smaller flows fundamentally different than miniature flows in the laboratory.

This study aims to advance the study of debris flows by presenting both new field and experimental data. Further, by following both modes of inquiry, the data, results, and interpretations shed light on the question of scale in debris flow science.

3. Field methods

This chapter describes the methods used to collect the field dataset discussed in Chapters 4 through 6. The field methods used were based follows that developed for debris flow mapping in British Columbia Canada (Fannin and Wise, 2001; Fannin and Rollerson, 1993; Busslinger, 2010). 21 debris flow paths were traversed. The paths were split up into a series of reaches based on significant changes in slope, channel azimuth, confinement, erosion or deposition behaviour. Information on channel geometry and eroded and deposited volume were recorded for each reach. Recording upper and lower bounds of erosion helped communicate the amount of uncertainty in estimating eroded volumes.

These methods were found to be appropriate to survey small debris flow events with deposit volumes between 100 m^3 and 10,000 m^3. The limitations of inferring debris flow behaviour from a post-event survey, as well as the limitations specific to this methodology, are also discussed.

3.1. Common methods of debris flow investigation

The most appropriate way to collect data on a debris flow depends on the study objectives and resources. If the study is at a regional scale, remotely sensed data may be more advantageous than detailed field investigation. Remotely sensed data is easier to collect over a large area and if automated, it may leave out some human error associated with manual field investigation (Carrara et al., 2008; Brardinoni et al., 2003). However, it will also generate errors due to imperfect automation.

Site visits bring a higher level of detail to debris flow investigation. If the goal is primarily to observe runout and impact on infrastructure, a quantitative investigation of the fan and a qualitative survey of parts of the travel path will be sufficient. Many debris flow

case studies report this level of information, as traversing reaches uphill of the fan is often dangerous. Investigation of the fan can yield travel length and angle, runout, area inundated, type of deposition, and volume of debris deposited. However, it should not be assumed that the volume deposited on the fan is equal to the total event volume. Significant amounts of debris can be deposited upstream of the fan or final unconfined reach. Most papers are ambiguous as to whether in-channel deposition was mapped and included in the final event volume. In this study, in-channel deposition was counted as part of the total event volume.

To completely understand the flow behaviour from initiation to deposition it is necessary to map the entire debris flow travel path. Surveys of the debris flow channels are generally are of two types; predictive or forensic. Predictive site investigations estimate how much debris is available to a future debris flow. These studies typically classify sections of the path into geomorphic categories (i.e bedrock, colluvium, steep sidewalls) and estimate how much material a flow might erode based on observations from past events. Some studies also estimate an upper and a lower volume of erosion, depending on the return interval of the hypothetical, future flow (Degetto et al., 2011; D'Agostino and Marchi, 2001; Marchi and DAgostino, 2004).

Forensic studies survey a debris flow event that has already occurred in order to understand the factors that lead to initiation, entrainment, and deposition. These investigations are generally more common than predictive, geomorphic-based studies. Most forensic studies aim to identify empirical relationships between channel geometry, geology, and estimates of deposited or eroded volume. Such estimates rely heavily on the judgement and experience of the investigator.

The majority of field data in the literature comes from case-studies of a single destructive event which caused fatalities or damaged infrastructure (e.g. Jakob et al., 1997, 2000; McSaveney and Glassey, 2002; McSaveney et al., 2005). More intensive investigations of multiple flows are less common, yet more powerful since the resulting data can be used to generate empirical or analytical models to evaluate hazard or understand debris flow mechanics.

The field methodology used in this study follows that developed for debris flow mapping in British Columbia Canada, and discussed by Fannin and Wise (2001); Fannin and Rollerson (1993); Busslinger (2010). These methods were originally used to develop the Queen Charlotte Islands debris flow database, compiled by the Land Use Planning Advisory Team of the MacMillan Bloedel Forestry Company. The reach pro-forma developed for the present field investigation is a modification of the one used by the BC Ministry of Forests Landslide Profile Data Card (Busslinger, 2010). The reach pro-forma used in the second field season are shown in Section B.1.

The aim of the field investigation was to characterize the volumes eroded or deposited by the flow and the general channel morphology of the path. However, it should be noted that field investigation does not yield data on a single event or surge, but rather an entire debris flow or flood event. The observed morphology is a product of a complex series of surges and fluvial reworking. This limitation is inherent in any investigation that occurs after a debris flow event.

The appropriate method and strategy taken to characterize the debris flow will depend on the magnitude and complexity of the flow, the ease of safely traversing the path, the time and resources available for the field investigation, and the goals of the study. All of the flows in this study were relatively small in terms of magnitude and length. The investigation was carried out by a team of two, covering approximately 500 m of the travel path a day. In the author's opinion, mapping flows larger than approximately 10,000 m^3 would require more personnel and more sophisticated mapping techniques, either Light Detection And Ranging (LIDAR), Terrestial Laser Scanning (TLS), or mapping grade GPS.

The methods used here rely heavily on the judgement of the investigator for estimates of entrained and eroded volume. As the size of the flow increases, meaningful estimates of eroded and deposited volumes, as well as quantifying channel geomorphology, become more difficult. However, the method described worked well for for alpine debris flows with deposition volumes between 100 m^3 to 1000 m^3 and safely accessible paths.

3.2. Equipment requirements for basic field traversing procedure

- Essential equipment
  - Hip-chain for recording reach length if laser-rangefinder cannot be used
  - Laser-range finder for length and inclination measurements
  - Compass for recording azimuths, slopes, and strikes and dips
  - GPS (recreational grade)
  - 30 to 50m tape for length measurements
  - Folding rule or small tape-measure for short length measurements and to be used as scale in photographs
  - Digital photo camera

  - Water resistant notebook or pro-forma
  - Base map and air photos

- Optional Equipment
  - Ice-axe (useful for stability, can be used for scale, and digging to investigate old surfaces, weathering, etc, more versatile than a rock hammer)
  - Trekking poles (useful for stability and for scale in photographs)
  - Hand lens
  - Shovel if extensive sampling is planned
  - Flagging to mark reach ends

3.3. Recognizing debris flow processes in the field

As discussed in Chapter 2, debris flows are transitional processes between hyper-concentrated flows and dry grain flows. Hyper-concentrated flows and floods nearly always accompany a debris flow surge, whether in the watery tail portion of the flow or as separate, discrete surges (Hungr et al., 2001). This makes distinguishing between these processes based on field evidence sometimes difficult. Distinguishing between the two types of flow is important however, as debris flows are much more hazardous then hyper-concentrated flows.

Deposits of granular debris flow surges tend to be well graded (poorly sorted) and sometimes weakly inversely graded, with coarser clasts deposited near the flow margins. Alpine, bouldery type flows are generally clast supported, although viscous or muddy type can be matrix supported (Lowe, 1976; Hungr et al., 2001; Hungr, 2005). In contrast, deposits from hyper-concentrated flows are generally weakly graded, bedded, and may present a weak fabric. The center of the deposit is often coarser than the margins (Pierson, 2005). In plan view, deposition from hyper-concentrated flow is sometimes discontinuous in discrete lenses of deposition, rather than massive lobes of deposition typical of debris-flows. Slope angle can also be used as a rule of thumb; most bouldery debris flows will not travel on slope angles less than 10° (Takahashi, 1981; Rickenmann, 2005). For example, deposits in the last reach of mapped flow C13 (see Chapter 4) was probably deposited by hyper-concentrated flow. The deposition was featureless, lacked levee or surge deposition, and was found on a 9° slope (Figure 3.1).

At the other end of the spectrum, some fans in New Zealand are formed by dry, grain flow processes such as rock fall or snow avalanches rather than debris flows. Context is the

most important clue to distinguishing between these two types of deposition. Snow avalanches can be ruled out in field areas where there is not enough seasonal snowfall or an adequate starting zone for snow avalanche formation. However, where there is enough seasonal snowpack to allow a high recurrence interval of snow avalanches, snow-avalanche deposits are usually distinguished from debris flow deposits by detailed clast counts to characterize the particle size shape and distribution. Snow avalanches produce larger and more angular particles than debris flows (de Scally and Owens, 2005). Large clasts appear more randomly distributed in the deposit, rather than present in levee deposits or towards the margins of lobes. The only field area in this dataset where snow avalanches are likely to occur is in the Birch Hill field area (Figure 3.2) or very rarely in the Cass field area.

Figure 3.2 shows an overview of the Birch Hill catchment. Notice the large snow avalanche runout paths in the center of the frame and the sinuous debris flow paths on the left of the Figure. The former deposition area is much wider and characterized by more randomly distributed large clasts. The large starting zone in the center also suggests that the fan in the center, background of the photo is most likely formed by snow avalanche processes.

Figure 3.1.: The material in the last reach of C13 was mainly deposited by fluvial processes.

Figure 3.2.: Overview of the Birch Hill catchment. The photograph shows deposits and fans formed by both debris flow and avalanche processes.

3.4. Description of field methods

It was always useful to travel the entire length of the debris flow path before doing any formal mapping. Often, first impressions of debris flow behaviour in a single reach proved spurious once the entire flow path was traversed. On the way up the path, the objective was to understand the overall behaviour and obtain a sense of the major zones of deposition, transport, and erosion. Detailed data collection was reserved for the trip down.

During detailed data collection, the debris flow path was split up into a series of reaches. A new reach was started at any significant change in slope, channel azimuth, confinement, erosion or deposition behaviour. Each reach was classified as a source, erosion, transport, deposition, or reworked reach. Source reaches contributed material to the initial failure. Erosional reaches clearly had a negative mass balance, while depositional reaches were clearly dominated by levee or lobate deposition. Transport reaches were transitional between erosional and depositional reaches; no clear volume balance could be defined on first impression. In each reach, channel morphology, and the volume of erosion and deposition were estimated using the

methods described below.

3.4.1. Channel geometry

3.4.1.1. Chainage lengths

Chainage lengths were recorded in each reach with a laser rangefinder or hip-chain. The hip-chain was zeroed at the start of the first reach. While the hip chain could have been used to measure the distance over entire path, it was often easier to record the chainage length of each reach. The string was anchored at the start of each reach by wrapping it around a log or cobble, then the counter was zeroed for the start of the new reach. This reduced tangling and breaking.

Chainage length measurements in the second field season were made almost exclusively with a laser rangefinder. According to the manufacturer, the range of the device is 2000 m for a survey target in good atmospheric conditions, but ranges from 0 to 1000 m are typical. In practice, the reflectivity of the rock and and generally dusty conditions in debris flow channels limited maximum ranges to 300 to 500 m. The specified accuracy at the maximum range is 30 cm to high quality targets, or 1 m to low quality targets. However, the device records to a tenth of a meter. Over short distances (from 0.1 to 20 m) the laser nearly always recorded a length within 10 cm of the same length measured with a tape. Given the problems with keeping a tape both straight and flat in a debris flow channel, if the length in question was over 4-5 m, it was much more accurate to measure it with the laser rangefinder rather than a tape.

3.4.1.2. Slope angle and azimuth of reach

The average slope of each reach was recorded to the nearest tenth of a degree with an inclinometer or the laser rangefinder. The azimuth of the reach was recorded by sighting down the reach or back up the reach.

3.4.1.3. Widths

Widths were recorded with either a tape in narrower reaches (approximately $\leq$ 4m) or the laser rangefinder in larger reaches. The width of the channel, gully, trace, and erosion were recorded, as shown in Figure 3.3. The different width measurements are described below:

- The gully width was defined as the width of the largest topographic feature which could confine the flow.

- The trace width was the width of any evidence of the passing flow. For example, if there was a levee present on one side of the channel and a trim or strand-line (mud or debris left on the channel wall, vegetation, etc) on the other, the trace width was the distance from the strand-line to the outside of the levee.
- The channel width was the width of the confining channel. This is not necessarily the same as the gully width, as many channels in this dataset where cut into larger gully features. The channel may have confined all or only a part of the flow.
- The erosion width is the width of the path showing evidence of erosion.

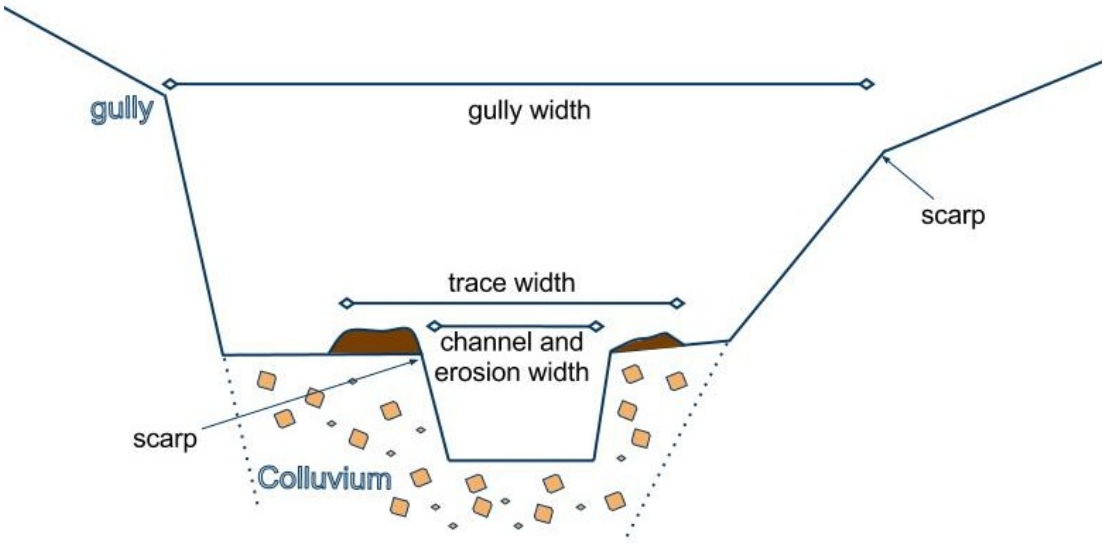

Figure 3.3.: Diagram of widths recorded in the field data. The diagram shown has a channel in gully morphology. The passing flow was partially confined in the channel.

3.4.1.4. Height

With all height measurements, the base of the current channel was used as the datum (i.e. 0). A diagram of the recorded height measurements is shown in Figure 3.4.

- The flow height was defined as the maximum height of any evidence of flow. The flow height measurement is a rough estimate. For example, if the flow leaves a strand-line, then the channel is eroded by the watery tail, the flow height will be overestimated. However, if the flow height is taken from a lateral levee, the maximum height of the flow in the center of the channel was probably higher. The levee may have also been left by a later,

smaller surge. In these cases the flow height will be underestimated. These limitations are present in any forensic investigation.

- Channel height was the average height of the confining channel (i.e. the average height of channel scarps)
- Gully height was the average height of the gully walls.
- Original surface was defined as the height of the channel bed prior to the debris flow. Evidence of the original surface after debris flow erosion often is indicated by scarps or trim lines. The trim line marks the level on the channel bank or channel wall below which there is obvious erosion and disturbance. Above this line the channel wall looks undisturbed. The trim line or height of the channel scarp may represent the original ground surface, however, this may be misleading. The debris flows investigated in this study all developed within pre-existing debris flows paths where the pre-existing channel probably had a U or V-shaped cross section. The debris flow may have only slightly widened the channel as it flowed past, rather than downcut. The original surface recorded on the reach pro-forma should therefore be considered a maximum value. Without knowing exactly what the channel looked like before the event, the height of the original surface is an educated guess. This is a limitation in every debris flow study which does not have detailed information on the channel morphology pre-event.

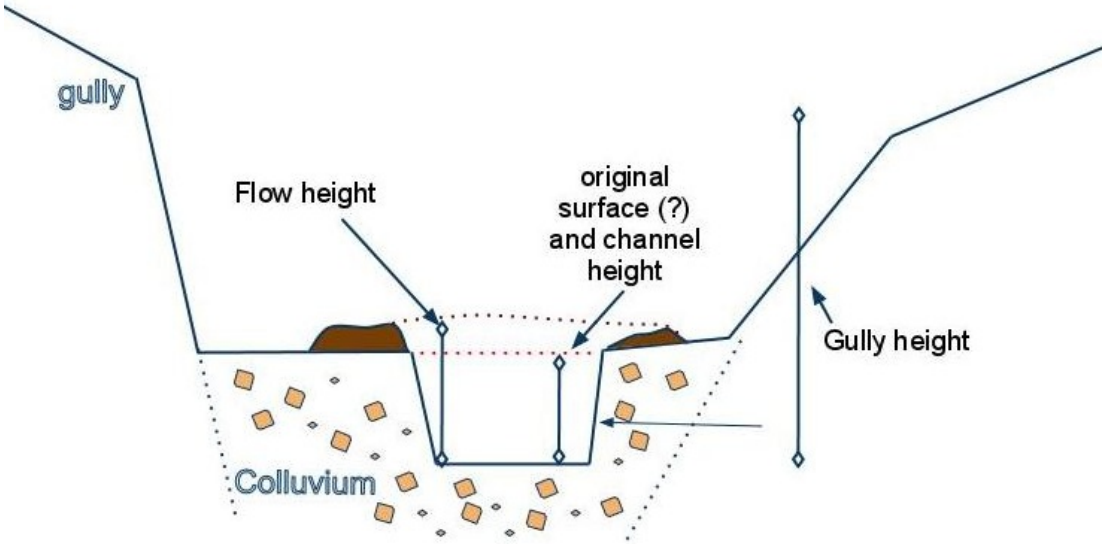

Figure 3.4.: Diagram of heights recorded in the field. The schematic reach shown has a channel in gully morphology. The passing flow was partially confined in the channel.

3.4.1.5. Sketches

At least one representative channel cross-section was sketched for each reach, which recorded the heights and widths discussed above. The chainage length at the cross-section location was also recorded. A plan view was also sketched for most reaches. Figure 3.5 shows original cross-section sketches for Reach 3 of mapped flow BH3. Widths and heights can be inferred from cross-section sketches.

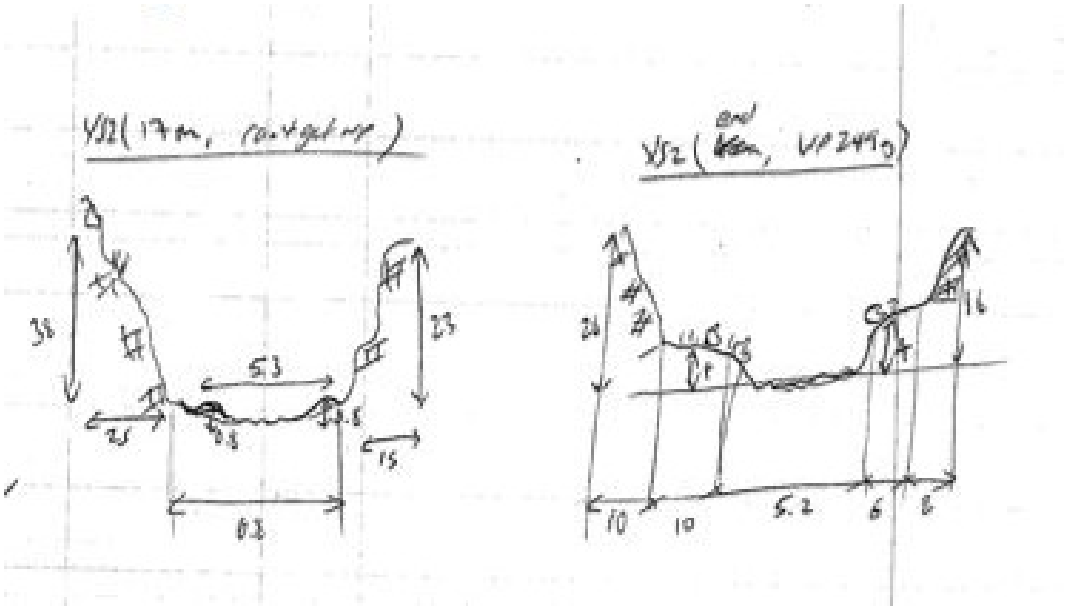

Figure 3.5.: Shows cross-section, looking down reach 3 of BH3, that was sketched in the field. Widths and heights can be inferred from cross-section sketches.

3.4.1.6. Relative confinement

The degree of debris flow confinement is determined by the size of the peak discharge relative to the size of the channel. For example, a small debris flow would be unconfined in the base or thalweg of the channel or gully. This situation was called "unconfined in gully" or "unconfined in channel" (UCIG or UCIC, Figures 3.6 and 3.7). A slightly larger flow would contact the sides of the channel (termed confined in channel or gully, CIC or CIG, Figures 3.8, 3.9, 3.10, 3.11). A larger flow would overrun the channel banks and only be partially confined by the channel (PCIC, Figures 3.12, 3.13). Over-bank deposits from this surge would then increase confinement for later surges. An even larger flow would completely overrun the banks, and if the path had a channel in gully morphology, it may be confined by the larger gully (CIG). Of course, some reaches were completely unconfined (UC). The type of situation was recorded on the reach pro-forma as "relative confinement type".

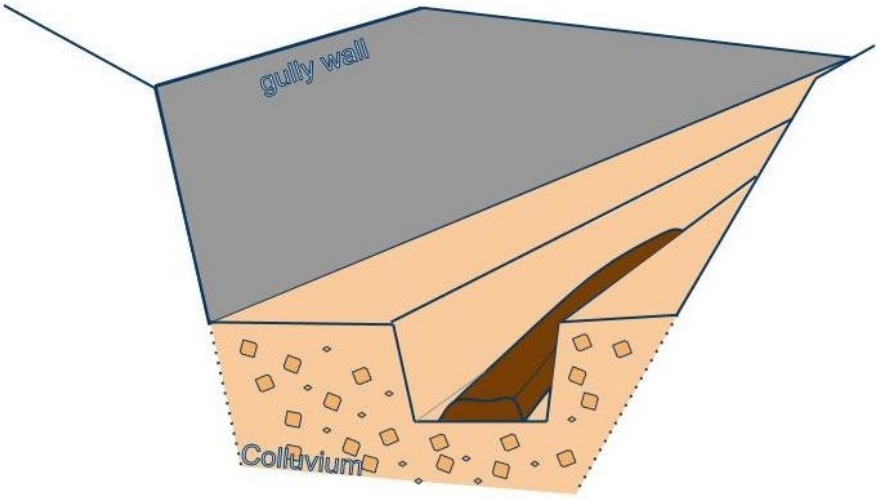

Figure 3.6.: Diagram of a typical unconfined in channel (UCIC) situation.

Figure 3.7.: An example of a lobe of debris which was unconfined in the channel (UCIC). The red circle highlights the position of a field investigator for scale.

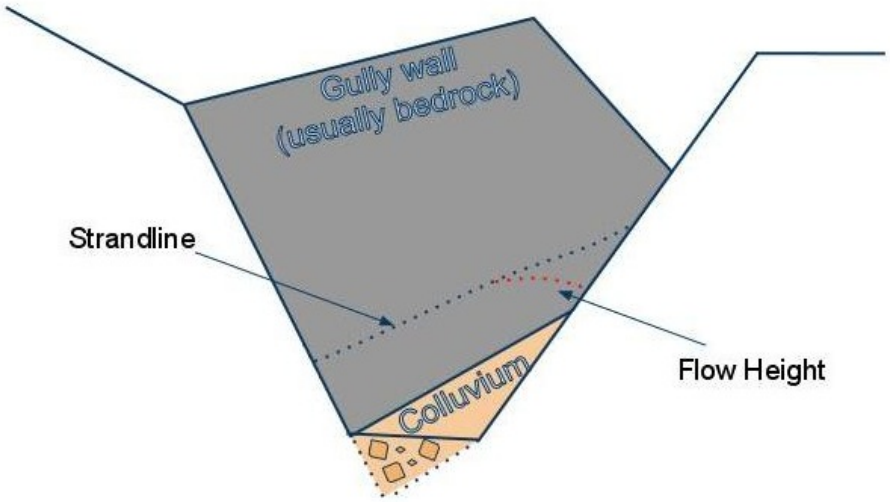

Figure 3.8.: Typical confined in gully situation (CIG).

Figure 3.9.: Example of a reach where confinement was provided by the gully (CIG). This photo was taken in Reach 4 of mapped flow FJ4.

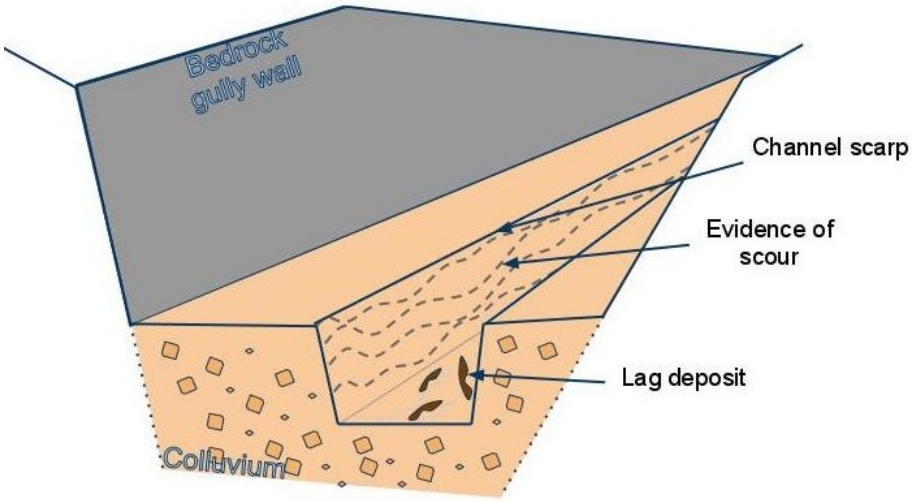

Figure 3.10.: Typical confined in channel situation (CIC).

Figure 3.11.: Example of confined in channel situation. The flow made contact with the channel walls and left a discontinuous lag deposit. Photo taken in the Orongorongo field area.

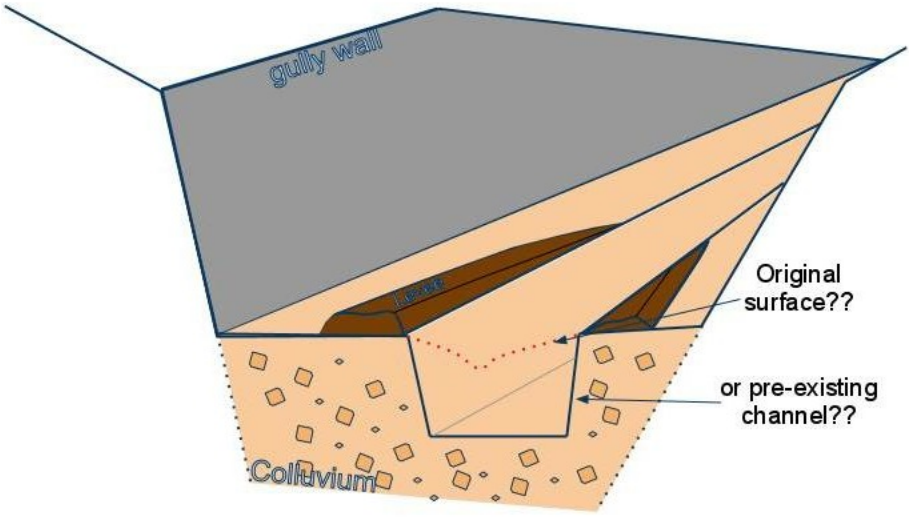

Figure 3.12.: Typical partially confined (PC) in channel situation.

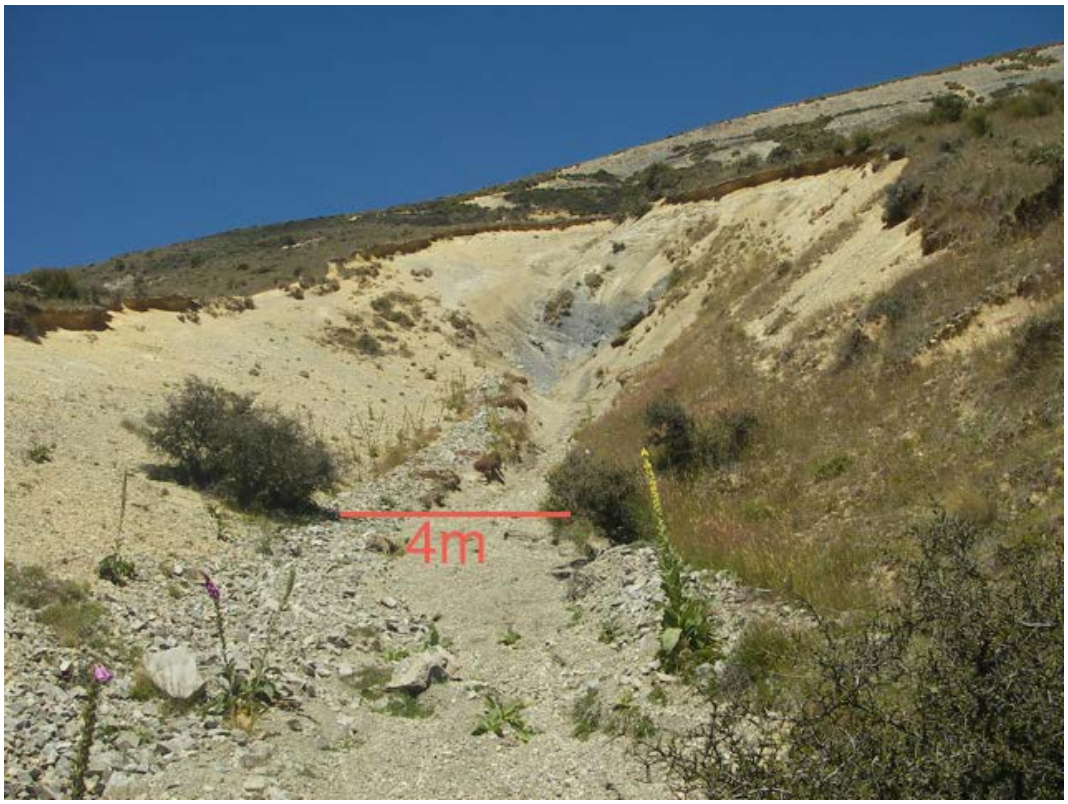

Figure 3.13.: Photo up Reach 8 of mapped flow C14. This reach was labeled as PCIC because of the levee on the true right side of the channel. There is also a small, discontinuous levee on the left side.

3.4.2. Other observations

3.4.2.1. Type of deposition

Deposition types were split into three main categories: coarse clastic material, reworked, and fluvial material. Coarse clastic material was defined as debris that was deposited by a major surge, while reworked material was defined as having been reworked and deposited by the watery-tail portion of the flow. Fluvial material had been transported and deposited by later fluvial processes. The distinction between these processes may be somewhat arbitrary. However, fluvial material generally has the characteristics of fluvial deposition described in Section 3.3.

3.4.2.2. Point sources of sediment

The location and volume of bank failures was noted on plan sketches. If the failure occurred prior to or during the debris flow event (i.e. the deposition material was missing, presumably because it was entrained by the debris flow event) the volume of these failures was incorporated into the volume balance for the reach.

3.4.2.3. Debris availability

Debris availability was recorded as either none (bedrock reach), bedrock near the surface, or unlimited if the depth to bedrock was estimated as over $\geq$ 2m.

3.4.2.4. Photographs

Photographs were taken up and down each reach. Ideally, the number of the photos should be recorded on the reach pro-forma and the location pictured on the plan view sketch. It was also helpful to photograph a short description of the last or next picture taken, so both image and description were stored together in the camera. A camera with a GPS, or a GPS point manually taken at each picture location would also be useful in future field investigations. Figure 3.14 show photos taken up down Reach 7 and up Reach 6 of mapped flow C13.

Figure 3.14.: Photos down Reach 7 and back up Reach 6 of mapped flow C13.

3.4.2.5. GPS points

GPS points were recorded at the start of each reach. This allowed the reach data to be georeferenced if it was necessary, and also provided an independent check on reach length and azimuth data. However, a satellite signal often could not be reached in very confined reaches, in which case, the GPS point was omitted.

3.5. Estimating volume of erosion and deposition

3.5.1. Erosion

Estimating erosion is difficult when the pre-existing channel morphology is unknown. As previously stated, the height of a trim-line or scarp may or may not represent the level of the channel bed prior to the event. Erosion may have occurred to the channel bank only, or the flow may have incised the channel vertically. For this reason, whenever we were not confident of the original channel morphology, we estimated an upper and lower bound of erosion in each reach to quantify the uncertainty. The upper bound represents the case where the debris flow downcut into the channel. The lower bound represents a scenario where the flow moved over an already incised, v-shaped channel, marginally widening the channel into the u-shape that has been shown to be more typical of a debris flow channel (Jordan, 1994; Johnson, 1970).

In some reaches there was discontinuous evidence of both erosion and deposition. The lower bound of erosion for these reaches was set to zero. The upper bound reflected discontinuous trim of the channel bank. Estimates of eroded volume were calculated by representing the area eroded by a simple polygon and multiplying by the average depth of erosion. For example,

a discontinuous, 1 m wide, 0.5 m deep zone of trim of the left channel bank over a 56 m long reach was calculated as 1 x 56 x 0.5 x 50% = 14 m^3.

3.5.2. Deposition

Deposition was calculated by multiplying the average depth of the deposit by its area. While estimating deposited volume in each reach was sometimes more straightforward than estimating erosion, there is still some error. The sources of error in determining debris flow volume can be split into two types; uncertainties in estimating depth and area of deposition in the field, and errors in representing these observations quantitatively during post-processing.

An accurate determination of debris depth is often difficult. Buried paleosols, if present at all, are often distinguishable on the margins of flows, but towards the mid-line they may be buried with several meters of debris and the location of the original surface (and therefore the depth) will be an educated guess. If one is lucky, erosion from fluvial reworking or later surges may cut through the main deposit, leaving a cross-section of the deposition. The surface of older events may be marked by a horizon of slightly coarser material, both because the flows are often weakly inversely graded and fines often wash out from the surface. A horizon of concentrated organic material may also represent a buried surface, as often organic debris will be washed out by the watery tail of the flow and deposited on the surface, near the edges of the fan. However, this evidence is uncommon. Both estimates of erosion and deposition have a number of potential sources of error which are difficult to quantify. These difficulties are discussed below.

3.5.3. Errors in estimating deposition

Methods of debris flow mapping rely heavily on the judgement of the investigator. Despite this, potential errors in estimating and calculating erosion and deposition are rarely discussed in the literature. Even if the volume of the coarse clastic portion of the flow is well constrained, this estimate may well leave out the volume of fine material and water which is lost as the debris flow consolidates. The finer material, if it does not wash away completely, will often collect in depressions on the edges of the fan and produce measurement inaccuracies.

3.5.4. Errors in post-processing

Errors in observation are exacerbated by errors in translating plan or cross-section sketches into quantitative data. In this study, each reach or section of the channel was approximated as

a simple rectangular, triangular, or circular area with an average depth. For example, a 20 m long, 10 m wide lobe of debris with a maximum depth of 1m would be calculated as a triangular prism having the dimensions $20 \times 10 \times 1$, yielding 100 m^3 of deposition. One could also model the same deposit as a rectangular prism of the same volume, using an average depth of 0.5m. The advantage of this method is that this can be calculated relatively easily in the field and is less time consuming for post-processing.

A potentially more accurate way of distinguishing debris flow volume would be to transfer plan view sketches to a CAD program. This method could capture more detail in plan view, although it would still rely heavily on estimates of average depth. In many debris flow data sets, the data may be mapped, entered, and analyzed by three different investigators. Simplifying the complexity of a plan sketch into a series of volumes which can be entered into a spreadsheet requires some interpretation, which may introduce some further error in the dataset.

To give an example of the potential error involved in post-processing, the volume of the largest debris flow in the dataset (OR1) was calculated twice. First, Google SketchUp™(an online drawing program) was used. The volume was calculated a year later by simplifying areas of deposition into simple polygons. Using SketchUp, the volume of the flow was calculated in January 2010 as 10867m^3. In January 2011, using the simplified method, the volume was calculated to be 9315m^3, a difference of -14% from the original calculation. The deposits of mapped flow OR1 on the debris flow fan had the largest area and were the most complex out of any flow in the dataset. This error therefore represents a likely maximum value for the data set.

3.5.5. Errors in estimating deposited volume in the field

Errors in representing the plan view of a debris flow are much less serious than errors in identifying and calculating debris depth. For small flows, approximating the average depth over the inundated area is reasonable. However, establishing an appropriate average depth over a large depositional area, especially when the surface is uneven, is difficult.

For this reason, in the second field season the depth in large, unconfined depositional reaches was inferred from transects of the debris surface conducted perpendicular to the flow path. The laser rangefinder made such transects possible. One investigator would walk out on a transect perpendicular to the flow azimuth, either stopping at breaks in slope or at specified intervals. The other investigator would shoot to their eye level on the person walking the transect, then record the vertical and horizontal distance of the shot, a description of the point,

and an estimate of the depth of debris.

Once these point elevations for the pre and post-event surface were plotted, a curve was drawn to represent each surface (Figure 3.15). The pre-event surface was based on estimates of debris depth recorded in the field. These curves were then integrated to yield two area values; one area under the inferred original surface and one area under the surface mapped. The difference between these areas multiplied by the chainage length represented by the cross-section provided an estimate of the bulk volume of deposited debris. For example, this method produced a volume of 805 m^3 was calculated for the final, unconfined reach of FJ3.

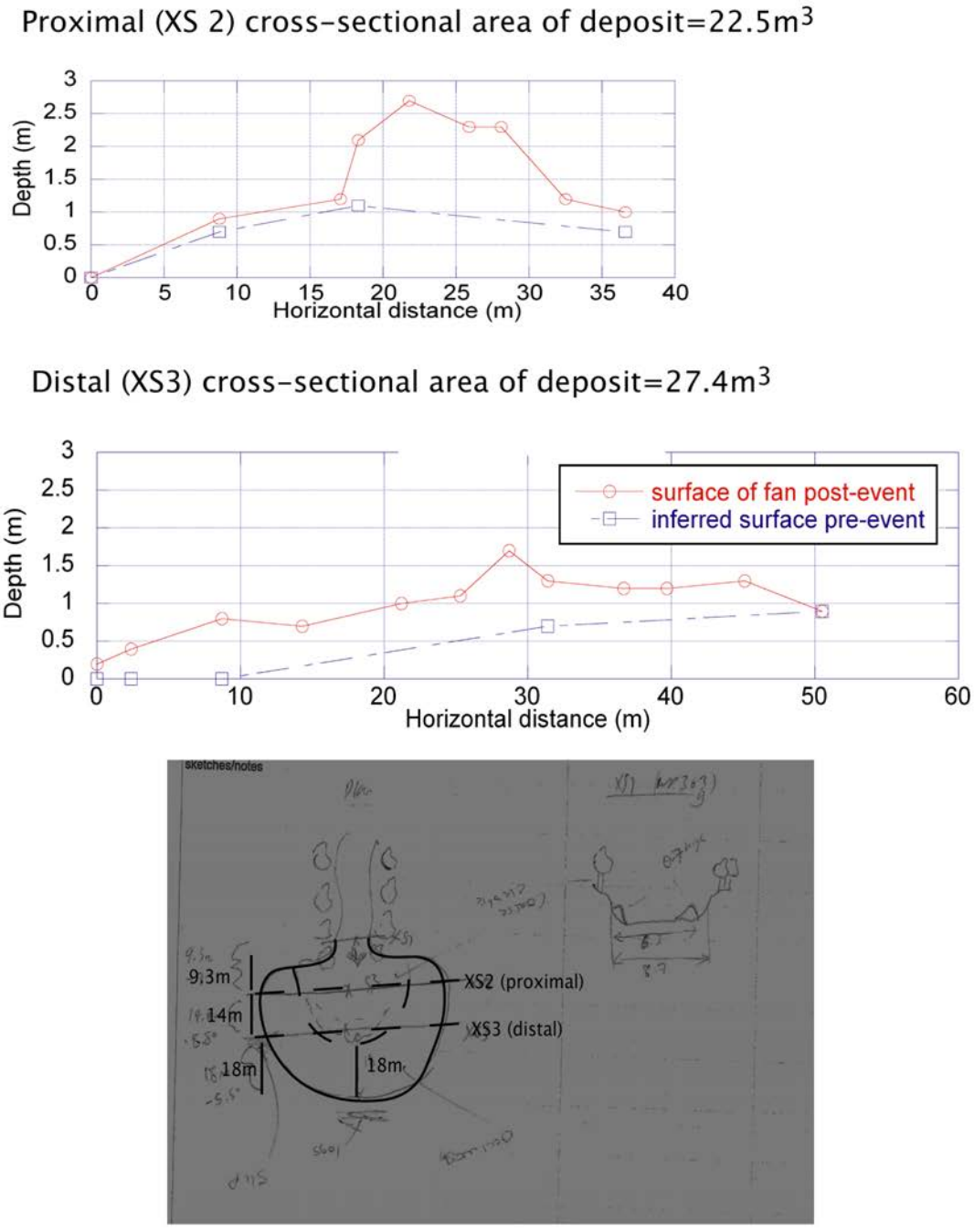

22.5m^2 x 9.3m (area under XS2)
+
24.95m^2 x 14m (average area under XS2 and XS3)
+
13.7m^2 x 18m (0.5 area under XS3 multiplied by length to edge of debris)
=805m^3

Figure 3.15.: The method used to calculate depth for larger debris flows in the second field season.

3.5.6. Comparing mapped erosion to deposition

Given the uncertainties in determining deposition, some studies have considered the volume eroded rather than the volume deposited as the main and most appropriate estimate of event volume (Gartner et al., 2008; Santi et al., 2008). This is appropriate if the morphology of the pre-event channel is known with confidence and the source area of the flow is accessible, as is often the case in anthropogenically caused or wildfire induced debris flows. In this study, because the source area was sometimes inaccessible and the shape of the pre-event channel was unknown, the measurement of deposited volume was considered more accurate than that of eroded volume.

Error values for estimating debris flow deposition are rarely reported in the literature. Those that are show a considerable amount of error. Santi et al. (2008) report that the precision of their measurements was ±23% when using a slope-profiler to exactly measure channel geometry. Using a mapping grade GPS to create a topographic surface, measuring the debris volume on the fan was precise to within -45% to +80%. CAD measurements (the method most similar to that used in the present study) showed a precision of -48% to +83%.

An indirect way of evaluating the error in volume estimates is to compare the mapped volumes of deposition with the mapped volumes of erosion. Using a very similar method to that used in this study, Brideau (2009) found the discrepancy between measurements of deposited and eroded volume for 33 open-slope flows on Vancouver Island were generally less than 100% of the volume eroded, in line with the findings of Santi et al. (2008).

In this study, the discrepancy between the mapped erosion and deposition was sometimes large, but this could usually be explained by the inability to account for erosion in the upper, source areas of some flows. The exceptions were in mapped flows FJ3 and C14. In FJ3, the mapped deposition was four times the upper bound of erosion. In C14, the lower bound of erosion was 18% more volume than the mapped volume of deposition. This flow was heavily fluvial reworked in its lower reaches. There were several, two- or three-season-old lobes of deposition on the fan which were not included in the volume balance. The lower bound of erosion mapped may represent the combined erosion from both the younger and older event.

For the remaining flows, the upper bound of erosion overestimated the event (deposit) volume by an average of +147%. The average underestimate was -38%. This supports the conclusion that there is a tendency to overestimate the amount of debris flow erosion (Peter Jordan, personal communication, 2008). It should be noted here that bulked volume (volume added by the dilation of material from erosion to deposition) was not considered. This may add as much as 10 to 20% to the volume of bedrock failures, but would be insignificant for

failures in colluvium or vertical channel incision (Davies, personal communication, 2012).

Assuming that the error of depositional volume in this study is similar to that found in prior studies (i.e. Santi et al. 2008) and that the true event volume lies somewhere between the upper and lower bounds of mapped erosion, a conservative estimate of the error in event magnitudes calculated in this study is -50% to +150%.

3.6. A few general comments on debris flow mapping in New Zealand

One of the objectives of this chapter is not only to describe the field methodology so that it can be repeated, but to provide a useful resource and some tips to future debris flow investigators in New Zealand. Towards that end, a few general and miscellaneous points which may be useful to future investigators and practitioners are summarized below.

- While the lack of population density in New Zealand spares the country many of the pains debris flows inflict in Europe or parts of Asia, it does mean that most debris flows are unreported here. Employees of the Department of Conservation and other agencies seldom know how to differentiate one type of landslide from another. A small investment in outreach by teaching employees the differences between different types of landslides (slips) would be useful. Simply alerting them that there is interest from a research perspective was helpful. It would also be useful if there was a central and open-access "landslip database" which various agencies could use to catalog the the location and type of slip.

- Site reconnaissance and gaining permission to access each site took almost as much time—and in some cases more time—than actual field investigation. While only 21 debris flows were mapped, over 36 sites were visited and 27 were partially mapped. Flows were rejected because they either had much of their deposition washed away, were too old to estimate meaningful volume balances, or were simply too dangerous to traverse over much of their length. These problems were only apparent after conducting a site visit.

- In future studies, it would be helpful to sketch the entire flow onto a contour map or air photo while in the field, in addition to field sketches on the reach pro-forma. This would aid in understanding the entire path during the mapping exercise.

- The use of a laser rangefinder is more convenient and efficient compared to a hip chain or tape. This is especially true in larger or steeper channels, where widths and heights for channel cross-sections can be recorded without negotiating steep, unstable channel banks or scarps.

- The field investigation in this study was primarily concerned with changes in debris flow volume balance, runouts, and areas inundated with deposition, rather than identifying initiation factors or in-depth analysis of the geotechnical properties of flow materials. More attention could be paid to these processes in future investigations.

3.7. Need for future work and conclusions

The problem of uncertainty in debris flow studies deserves more research attention. Using the method employed, while two mapping teams may obtain similar measurements of travel distance and flow behaviour (i.e. whether deposition or erosion dominates a reach), the estimates of the volume of deposition or erosion may vary considerably. To obtain more certain estimates of eroded and deposited volume, a detailed series of before and after observations of channel morphology are needed, such as those currently being gathered at the Illgrabin catchment in Switzerland (Berger et al., 2010; McCoy et al., 2010; Schlunegger et al., 2009). Unfortunately, the conclusions of these studies will likely not be valid everywhere; erosion rates and runout behaviour may be specific to the region and type of debris flow (e.g. Busslinger, 2010). Therefore, repeated, detailed topographic surveys of several debris flow paths in New Zealand would be extremely beneficial in understanding erosive and depositional processes. This work could also be compared to simple mapping methods, such as the one presented here, to quantify the lack of precision involved in field mapping.

Despite these limitations, the technique summarized here works well to characterize the volumes eroded and deposited and travel distance of a past debris flow event. It is best for small debris flow events with event magnitudes between 100 m^3 and 10,000 m^3. Recording upper and lower bounds for erosion helped communicate the amount of uncertainty in estimating eroded volumes. Using this method, one can collect the data needed to run most simple empirical-statistical or one-dimensional mathematical models for runout (Rickenmann, 1999; Fannin and Wise, 2001; Prochaska et al., 2008a; Benda and Cundy, 1990; Corominas, 1996). The method could be used to calibrate 2-D models which incorporate lateral spreading, but higher resolution topographic data would be needed.

4. Morphology of torrent and hillslope debris flows in New Zealand alpine catchments

This chapter begins by summarizing the literature dealing with the differences between hillslope and torrent debris flows. Where typologies do exist in the literature, they often ignore the fact that hillslope and torrent events exist on a spectrum from first-time debris flows on a truly planar hillslope to debris flows in a well-defined stream channel confined by a major topographic feature. This chapter argues that the differences between hillslope and torrent flows are due to their location along the geomorphic system from hillslope to sea.

Using this framework, the chapter then describes the geology, climate, and qualitative flow behaviour of 21 debris flow paths in four regions within New Zealand. Four flows are located in the Orongorongo field area, in the southern Rimutaka ranges of the North Island; twelve in the vicinity of Cass, just east of Arthur's Pass National Park; four in the Birch Hill catchment, located in the Ben Ohau Range near Mt. Cook National Park; and two near the Franz Josef Glacier (Figure 4.1). The potential for hillslope events to coalesce in channels to form large magnitude torrent events is also discussed.

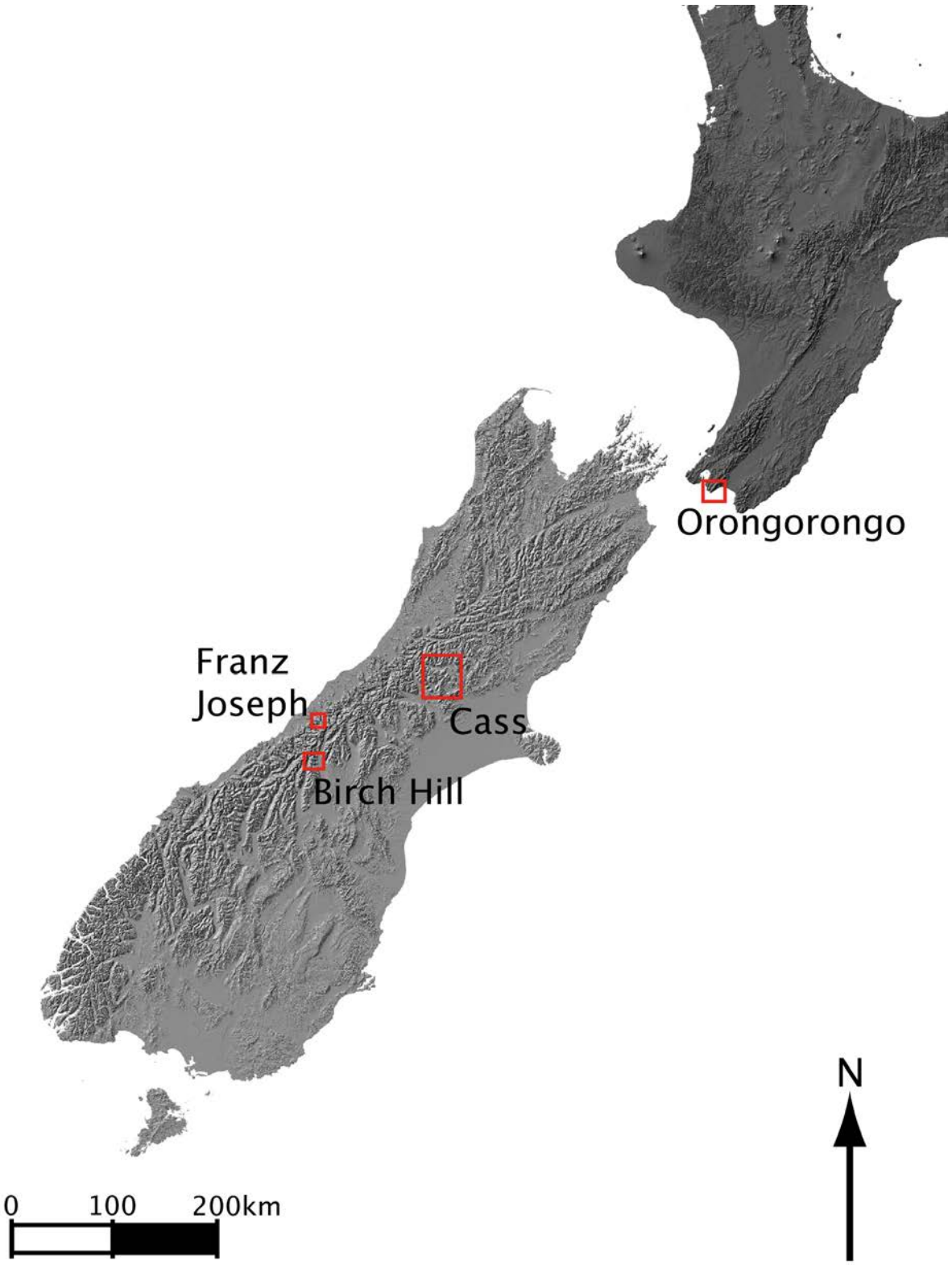

Figure 4.1.: Hill-shaded digital elevation model of the North and South Islands of New Zealand. The field areas are outlined in the red boxes.

4.1. Definitions

Explicit definitions of hillslope and torrent (i.e. channelized) events in the literature are rare. While debris flows which occur on open, planar hillslopes have been recognized in the literature (Zimmermann, 1990; Conway et al., 2010; Glade, 2005; Brideau et al., 2006; Paudel and Law, 2006), they have attracted less academic and engineering interest than larger, channelized debris flows (Conway et al., 2010). This is because most homes and infrastructure exist on debris flow fans formed by torrent flows. Hillslope flows, however, can be extremely hazardous to life and property directly adjacent to hillslopes (Conway et al., 2010). They are also critical agents of geomorphic change which supply sediment to the channel system (Benda et al., 2005).

The most concise typology of hillslope and channelized flows belongs to Glade (2005). According to Glade (2005), debris flows initiate from two main sources; slopes and channels. Debris flows that originate in the channel are termed channelized-type flows. They are also sometimes called torrent-type events. In this study, the term torrent is preferred, the reasons for this will be discussed later in this section. Glade (2005) identifies two types of channelized flows; those which initiate from a failure in the channel or channel bank, and those that form from mobilization of sediment in the channel (Table 4.1).

Events that originate from hillslopes are often called hillslope, open-slope, slope-type events. Glade (2005) splits hillslope debris flows into two categories; those originating from open talus slopes and those that originate from the contact of talus against a bedrock headwall (Table 4.1).

Table 4.1.: Types of debris flows classified according to source of material (from Glade, 2005)

Hillslope debris flow	Channelized type debris flows
Type 1a Source is a talus slope which is regularly subject to retrogressive erosion Type 1b Source is a shallow translational failure which changes into a debris flow when it reaches the channel Type 2 Source on the border between rock wall and talus slope. Water is channelled in the upper headwall and drains into the highly permeable talus slope	Type 3 Source is sediment mobilized along drainage lines Type 4 Source is remobilized sediment of previously deposited material

Based on their name, one might assume that hillslope events are all unconfined and that the distinction between a channelized event and an open slope event may always be easily

made on this basis. However, based on the field mapping in this study, the term open-slope, slope-type, or hillslope debris flow may be misleading. Confinement is still important in these events. While it is true that the first debris flow event on an open, planar hillslope may be completely unconfined, it will often initiate a gully feature which will be used by subsequent events. For example, all the hillslope events mapped in this study were confined to some extent by a linear, incised gully feature or in natural levees from previous events. In fact, much of the debris volume in some flows was sourced from within these gully features.

In this way, classification schemes which classify these flows based on the sediment source, or whether the flow is confined along its length, often create confusion. For example, what happens if a flow which begins on an open talus slope becomes confined? Should straight, linear gullies incised in otherwise planar hillslopes be counted as "previous drainage lines" (Table 4.1) and hence be classified as channelized? Emphasizing the source of debris may also be misleading; the magnitude of the a debris flow is often controlled by how much sediment the flow entrains or deposits as it proceeds down-slope, not the size of the initiating event. In these situations, it is the dominant morphology and processes occurring along the path which determine severity.

For these reasons, the term torrent event is preferred to the term channelized debris flow in this dissertation. The label "channelized" flow, when compared to hillslope flows, erroneously suggests that hillslope flows are completely unchannelized. The term torrent also emphasizes the tendency of torrent flows to hold year-round stream flow; in fact many Europeans use the term "torrent" (or in Italian "torrente") for a mountain stream. In much of the European literature then, debris flow channels (i.e. the landform) are called torrents, and debris flows (the process) are often referred to as "debris torrents". Adding some confusion, Slaymaker (1988) also uses the term torrent to describe coarse-grained, rapid channelized flows with high organic content in the Pacific Northwest.

Throughout the field mapping exercise and even during post-processing, it was clear that categorizing the flows strictly in terms channelization or sediment source was not very useful. This eventually led to thinking about the differences between hillslope and torrent flows in terms of geomorphic unit and stream order, as discussed in the next section.

4.2. Differentiating hillslope and torrent events based on geomorphic unit and stream order

The differences between hillslope and channelized flows are functions of the location of the flow site along the geomorphic system from hillslope to sea. This location in the geomorphic system can be described by stream order (Figure 4.2). Stream order is a measure of the position of the stream in a hierarchy of tributaries (Leopold et al., 1995).

Figure 4.3 shows the profile of a hillslope or a first order stream channel which is incised in an otherwise planar hillslope (i.e. section A-B of Figure 4.2). The slope angle near the top of the slope will often prevent soil formation and, depending on the climate, limit vegetation. Mechanical and chemical weathering processes in this steep, upper section produce debris that will either fall, slide, or sometimes flow down to lower angle slopes. Once deposited, in order for debris to be carried downslope, they require a mass-wasting process that is inherently more mobile than dry grain flows, i.e. a debris flow.

The behaviour of the debris flow will depend on a shifting balance of processes as the flow proceeds downslope. As the debris flow travels downslope, the gravitational driving force will decrease. Water availability, in contrast, will increase. Whether this water comes from seepage or runoff, the water available at any point will depend on the upslope area draining into that point (Figure 4.3). A large slope parallel driving component high on the hillslope will encourage erosion and mobility, but on the other hand, erosion and flow mobility may be constrained by a high solids concentration due to the lack of free water available.

In Figure 4.3, the angle of the theoretical hillslope decreases downslope to an extent where hillslope flows will deposit. However, in many alpine areas, the slope will run down to a larger order stream channel. An idealized slope profile of this larger order stream is shown in Figure 4.4. This is likely to be the location of torrent (i.e. channelized debris flow) events.

This stream will have higher water availability than the hillslope or first-order channel will, as it will receive water from all tributaries up-valley. However, the same balances of forces apply as in the hillslope case; water availability will increase downstream, but gradient will decrease (as shown in Figure 4.4, which is section B-D of Figure 4.2).

While the increased water availability will increase flow mobility, at some point it will cause the solids concentration to drop below a critical limit and the debris flow will evolve into a debris flood or a hyper-concentrated flow. Where this point occurs will primarily be a function of how much solid material is available to the flow. In basins with ample sources of sediment and water, this transition may occur in higher stream orders and at quite shallow slope angles.

A well known example is the lahar produced by the 1982 eruption of Mt. Saint Helens. In this this case, fluid discharge overwhelmed the sediment concentration after the lahar had travelled 27 km from the Crater rim (Pierson and Scott, 1985). The resulting hyper-concentrated flow travelled another 81 km.

Generally, the thickness of the soil layer which may be entrained actually increases downslope (as shown in Figure4.3), but the stability of the material also increases, reducing entrainment. Hence, entrainment is not simply a question of debris availability, but rather a function of both the debris available and the erosive power of the debris flow.

This approach offers a new way of categorizing hillslope and torrent flows, putting the flows into the context of the larger geomorphic system. It also emphasizes the fact that both types exist on a spectrum, where torrent flows paths are less steep but likely to have lower solids concentrations. The greater mobility provided will, to some extent, counter the effect of decreasing gradient.

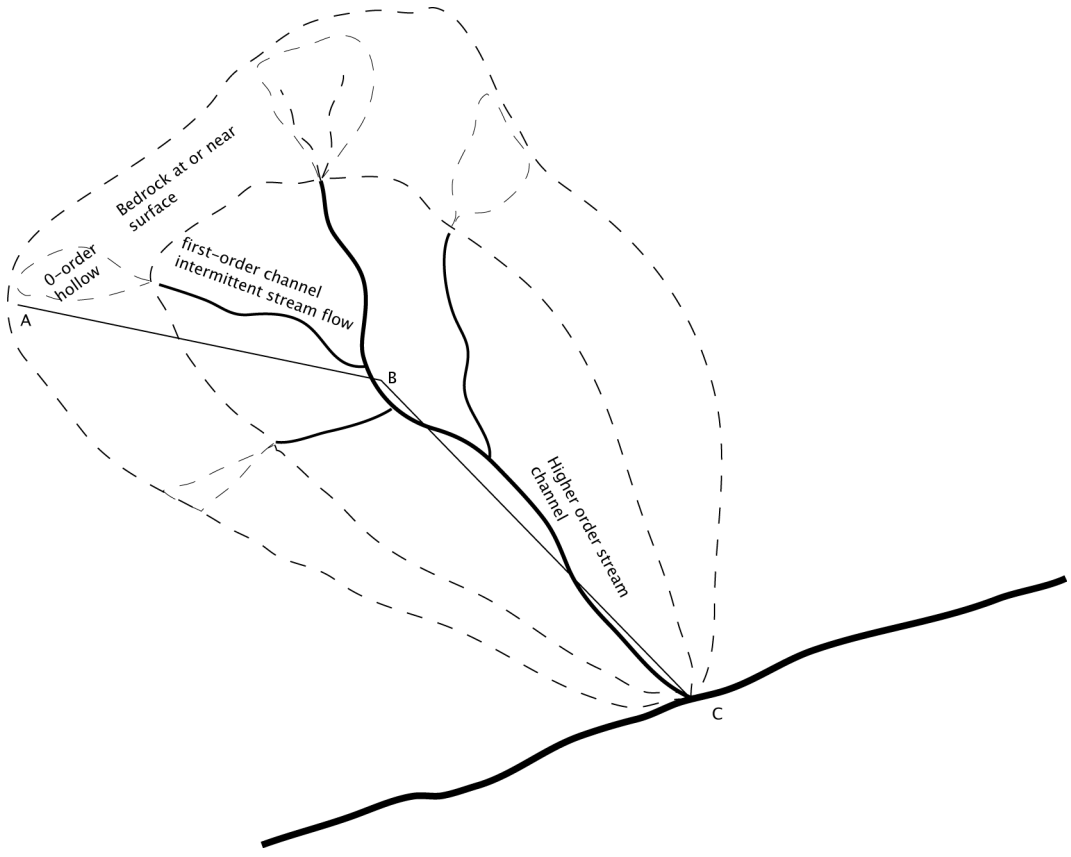

Figure 4.2.: Map view of relation between hillslope and torrent-type flows of various magnitudes. Section A-B and B-C are provided in Figures 4.3 and 4.4.

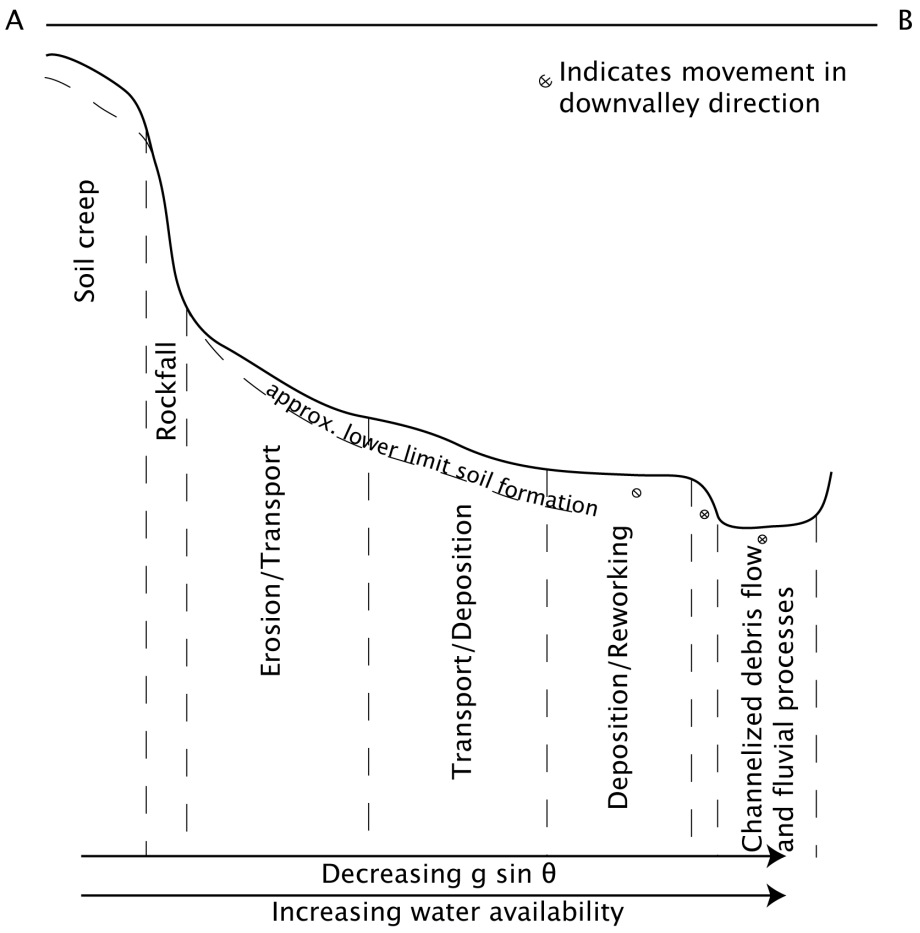

Figure 4.3.: Idealized slope profile of hillslope, 0 order, or 1st order stream subject to hillslope debris flows. See Figure 4.2 for a map view of the section.

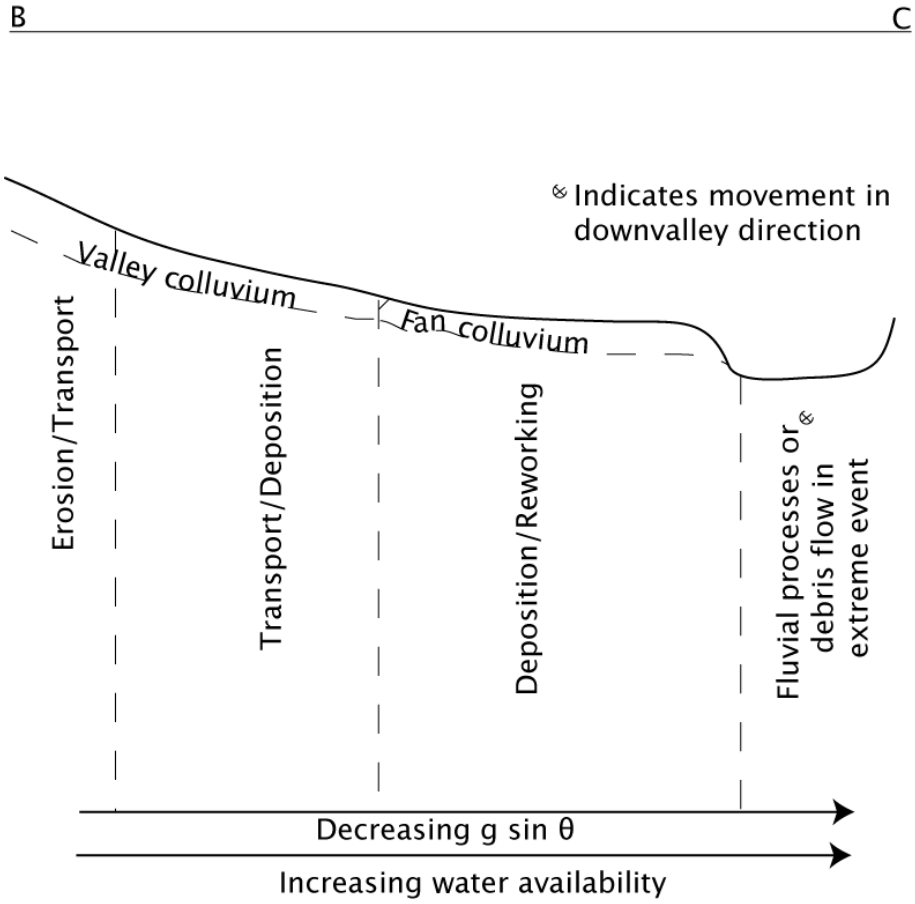

Figure 4.4.: Idealized slope profile of a 1st or 2nd order channel subject to torrent events. See Figure 4.2 for a map view of the section.

4.3. Precipitation data

Table 4.2 shows the maximum expected 1-day rainfall depths for various annual recurrence intervals (ARI) at each field area. These were calculated using NIWA's High Intensity Rainfall System (HIRDS). HIRDS is a web-based tool which that interpolates between known records at nearby climate stations (Thompson, 2011). Maximum rainfall depths for specific precipitation events were taken from the rain gauge closest to each field area, listed in the National Institute of Water and Atmospheric Research's (NIWA) Cliflo database.

The precipitation data are meant to provide the reader with an estimate of the typical rainfall in the field areas. They do not necessarily reflect the rainfall that triggered the events mapped, which could differ depending on microclimate. In some cases, precipitation values

come from stations tens of kilometers away. Also, note that HIRDS does not take into account relevant factors such orographic effects, increased or decreased interception caused by wind, or antecedent soil moisture conditions.

Table 4.2.: Maximum 1 day rainfall depths for the field areas in this study.

24 hour rainfall depths for each field site (mm)				
ARI (years)	Cass	Orongorongo	Birch Hill	Franz Josef
1.58	96	88	189	331
2	101	95	202	349
5	120	118	245	413
10	134	137	280	462
20	150	158	317	515
30	159	171	340	548
40	166	181	358	573
50	171	189	372	592
60	176	196	384	609
80	184	208	404	636
100	190	217	420	657

Based on HIRDS data. ARI stands for Annual Recurrence Interval.

4.4. Orongorongo field area

In the summer of 2008, four debris flows were mapped in the Southern Rimutaka mountain range. This field area is located on the southern tip of the North Island, approximately 15 km east of Wellington (Figure 4.5). The main land use is farming and recreation in a conservation estate. Part of the area is also a scientific reserve. This site is referred to as the Orongorongos, after the main river draining the area. The flows mapped were labeled OR1 through OR4 based on the order they were investigated. OR1 required approximately 4 days to map, OR2 and OR3 required approximately 3 days each, and OR4 required one day. The event volumes and mapped lengths of the Orongorongo flows are shown in Table 4.3.

The lithology in the Orongorongo field area is deeply indurated, deformed Mesozoic greywacke with limited interbeds of conglomerate, argillite, and mudstone. Structurally, the Rimutakas are part of an anticline associated with thrusting of the Wairarapa reverse fault to the east. A spectacular set of beach terraces, the last of which was formed during the 1855 Wairarapa Earthquake, demonstrates the rapid rates of uplift (approximately 1.2 mm/year) in the field area (Begg and McSaveney, 2005). This uplift, direct exposure to southerly storms, and

the instability of the bedrock make debris flows in these catchments relatively frequent events. Based on the amount of vegetation on the debris flow fan, it appears that flows reaching the distal end of the fan occur on at least decadal intervals. From observations of GoogleEarth® imagery, all of the flows mapped in this catchment occurred between 2004 and 2008. Smaller flows not visible on aerial photos may occur even more frequently.

Rainfall data recorded 2.5 km from the Orongorongo flows show the annual rainfall depth averaged 1001 mm from 1997 to 2005. The rainiest months in this field area were in June, July, and August.

Figure 4.6 shows the geology, slope profile, and the major zones of erosion, transport, and deposition of OR1. OR1, OR2, OR3 generally showed a similar morphology, with some slight differences in their entrainment behaviour on the fan, which will be discussed. OR4 showed a much different morphology than OR1, OR2, or OR3. Only intermittent stream flow was observed in this catchment. Limited stream flow may have contributed to a lower moisture content, which may explain this flow's shorter runout distance. The lack of any remolded or fluvial reworked material beyond the main zone of clastic deposition supports this interpretation.

From its initial source high on the bedrock headwall, OR1 entrained coarse colluvium from steep, upper reaches before entering the main-stem channel. These upper, erosional reaches of the flow are shown in zone a in Figure 4.6. Once the flow joined the main stem channel, it entrained enough water from stream flow to mobilize into a mature debris flow.

The occurrence of entrainment or deposition of sediment in the transport zone was unpredictable. This zone is shown in Figure 4.6 as zone b. While confinement, debris availability, and slope all influenced flow behaviour, other factors were relevant. For example, constrictions in the channel either encouraged erosion, or alternatively, caused particle jamming and encouraged deposition. Large clasts clogged at channel constrictions often became knickpoints for subsequent fluvial erosion, as shown in Figure 4.7.

The larger flows in the Orongorongos (i.e. OR1 and OR3) incised and eroded material from the fanhead. This is shown as zone c of Figure 4.6. OR2, which was much smaller in volume, did not erode at the fanhead, but rather deposited. OR4 also deposited at the head of the fan.

Once the flow left the main channel and became unconfined, massive deposition occurred in the form of large lobes of coarse clastic debris (zone d). Further downslope, less continuous lenses of finer sediment were deposited by hyper-concentrated or stream flow which remobilized smaller clasts of the main deposition zone (zone e).

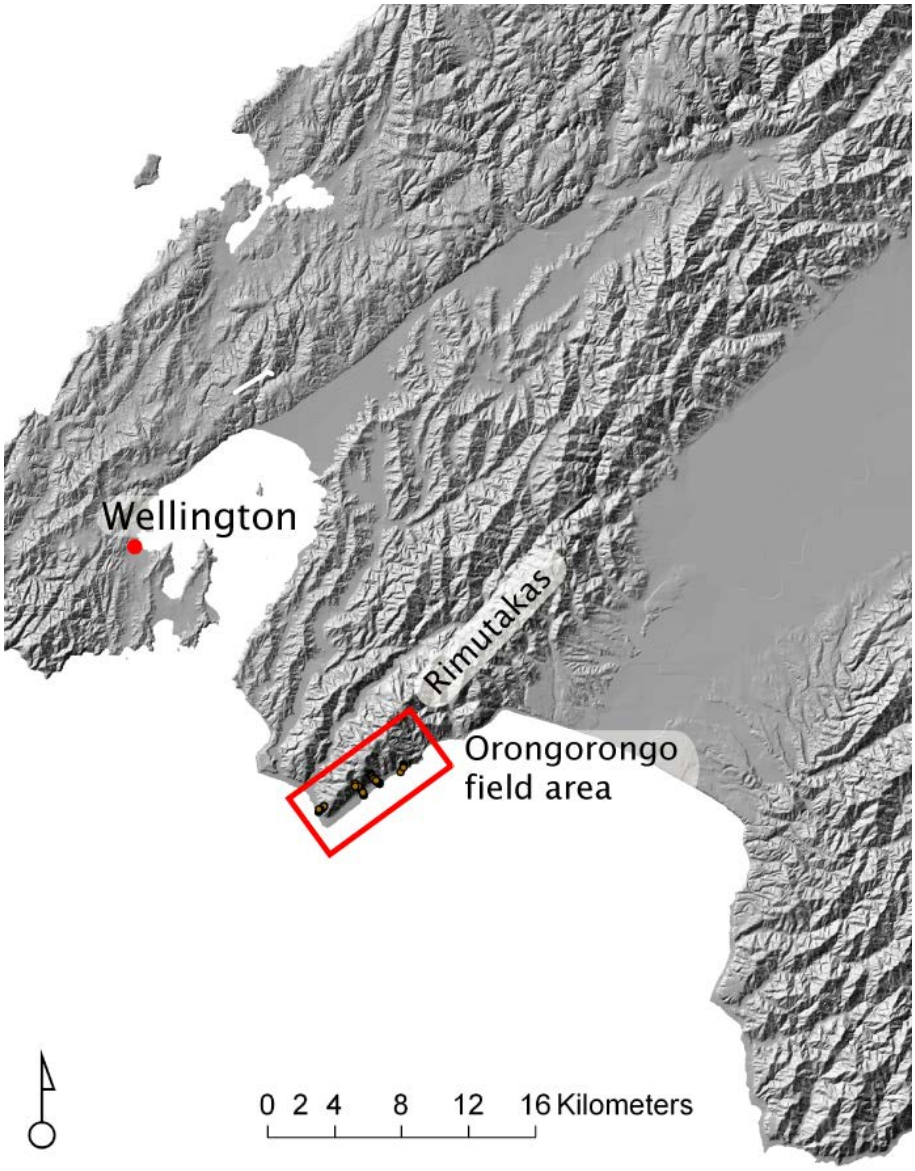

Figure 4.5.: Overview map showing the location of the Orongorongo field area.

Table 4.3.: Event volume and mapped length for flows investigated in Orongorongo field area.

Flow	Event volume (m^3)	Mapped length (m)
OR1	10870	823
OR2	2170	824
OR3	5897	522
OR4	3992	239

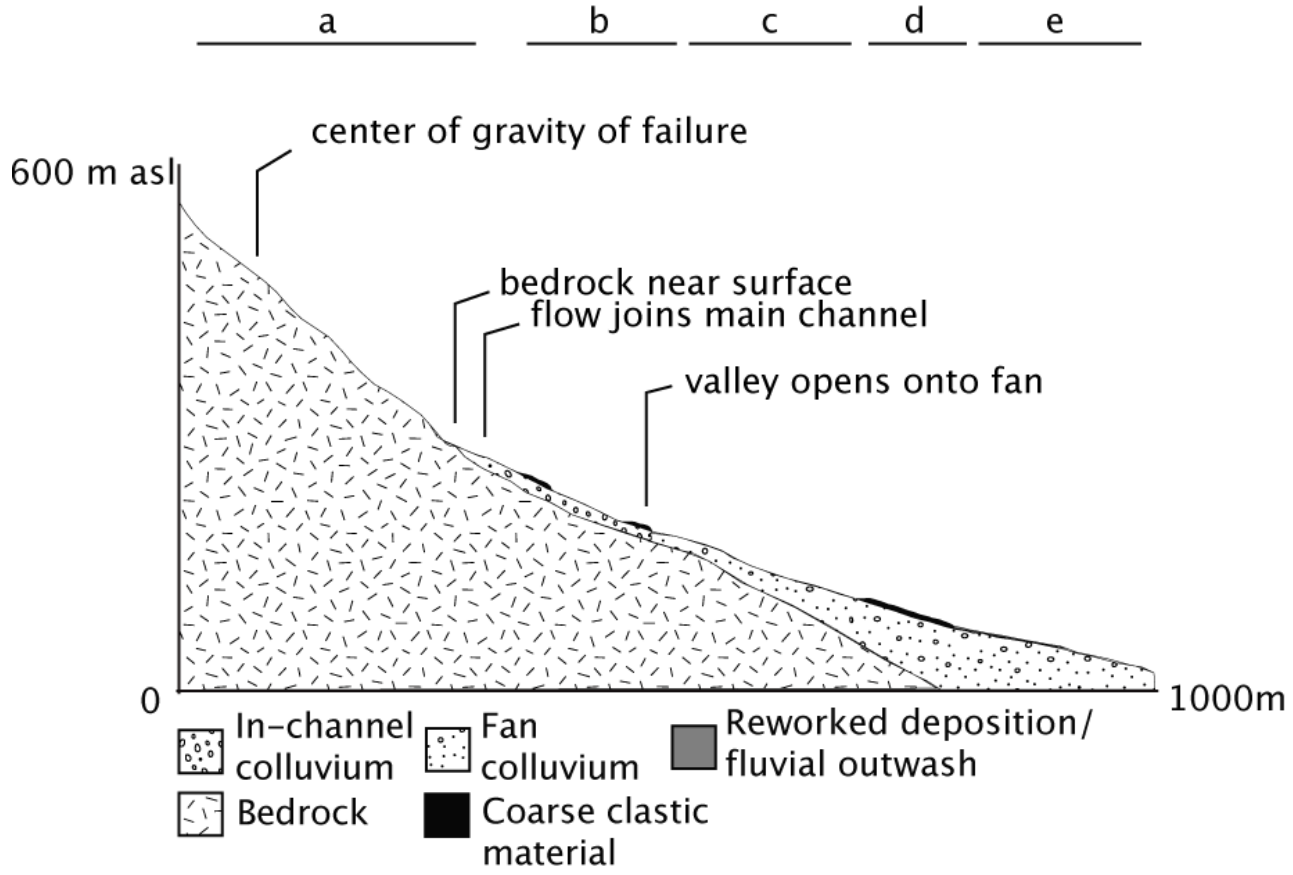

Figure 4.6.: Geomorphic sketch of OR1. (a) Source area in bedrock headwall. (b) Transport zone characterized by stochastic erosion and deposition. (c) Zone of entrainment at fanhead. (d) Massive coarse clastic deposition. (e) Reworked and fluvial material.

Figure 4.7.: A large boulder clogging the channel in OR1. These constrictions later become knickpoints for initiating subsequent fluvial erosion.

4.5. Cass

The Cass study area is located in the eastern Southern Alps, approximately 20 kilometers south-east of Arthur's Pass National Park. Nine flows were mapped and included in the data analyzed in later chapters: four near Purple Hill, two just east of the Broken River near Castle Hill, one near Flock Hill Station from Round Hill, one near of Mt. White Road, and one near Sugarloaf Mountain. Figure 4.8 shows each of these locations. Satellite imagery is also included to give the reader a sense of the basic morphology of each flow. The mapped flows were labeled C1 through C15. C1, C2, C3, C6, C7, C11, C12, C13, and C14 were mapped in detail and included in the data analysis discussed in later chapters. Table 4.4 reports the event volumes

and mapped lengths of these flows.

Six flows were partially or completely mapped in Cass, yet they were excluded from later analysis. These flows included; an event off of Purple Hill (C4), an event on the North side of Sugarloaf (C5), one near Mt. Misery (C8), one North of the Waimakiri River (C9), one near Castle Hill (C15), and one in the Flock Hill sub-catchment (C10). C4 was split by a 30m waterfall with deposition both above and below it. It was unclear if the deposition represented one event or two separate events. C8 was too large to map with the current methodology. C5, C9, C10, and C15 were older events that had been heavily reworked, making meaningful estimates of the volume eroded or deposited very difficult. Further, the upper reaches of these flows were steep, bedrock channels which could not be traversed. While these flows could not be included in the reach data discussed in the following chapters, traversing their transport and deposition zones was helpful in understanding the overall processes and morphology of flows in the Cass region.

Uplift rates in the Cass study area are lower, approximately 0.5 to 1 mm/year, than the Birch Hill or Franz Josef field areas which lie closer to the Alpine Fault (Hales and Roering, 2005). Similar to the Orongorongo study area, the bedrock in Cass is moderate to highly indurated, intricately fractured Triassic sandstone and siltstone interbedded with minor argillite and chert. However, the most important sediment sources for most of the debris flows mapped are not the bedrock outcrops, but periglacial colluvial deposits mantling the bedrock. Above the bushline, these open talus slopes are one of the most striking features of the eastern Southern Alps. Their role in hillslope and landscape evolution has been discussed by several investigators (Whitehouse and McSaveney, 1983; Hales and Roering, 2005; Pierson, 1982). However, no detailed field survey of these debris flows or gullies had occurred since the 1960s (Brundall, 1966). According to Brundall (1966), debris flow movement was associated with high antecedent moisture and moderate rainfall, although the precipitation intensity was not unusually high (recurrence interval of 0.5 per year). Brundall (1966) suggested that flow triggering was limited by debris accumulation in the channel rather than precipitation intensity.

The annual rainfall near Cass, averaged over 2007, 2008, and 2009, was 1812 mm. This fell over an average of 127 rain days. The rainiest months were August, September and October. The maximum one-day rainfall over the last five years (the approximate age of the oldest event mapped) occurred in June 11, 2006 with a total of 141 mm. This falls between a 1 in 10 year and a 1 in 20 year rainfall event rainfall event according to Table 4.2.

None of the flows mapped in Cass deposited into a higher order stream channel which held year-round stream-flow. While active stream flow was observed in some of the flows during

mapping (C8, C10, C12), the stream flow infiltrated into the highly permeable deposits at the base of the slope.

While most of the flows near Cass are of the hillslope type, there were significant local variations in flow morphology. The flows near White Rock Road (C1), Sugarloaf (C2), and Purple Hill (C3, C6, C7, C11) are all of the classic hillslope type. Flows near Castle Hill (C13, C14, and C15) had a similar morphology to those at Purple Hill, but probably had higher moisture contents based on the amount of fluvial reworking present and seepage observed in their paths. Flows near Flock Hill station showed an intermediate behaviour between hillslope and torrent flows (C10 and C12).

Table 4.4.: Event volume and mapped length for flows investigated in the Cass field area.

Flow	Event volume (m^3)	Mapped length (m)
C1	757	841
C2	1091	478
C3	2999	1388
C6	2350	823
C7	883	1054
C11	445	838
C12	2924	907
C13	1328	941
C14	570	836

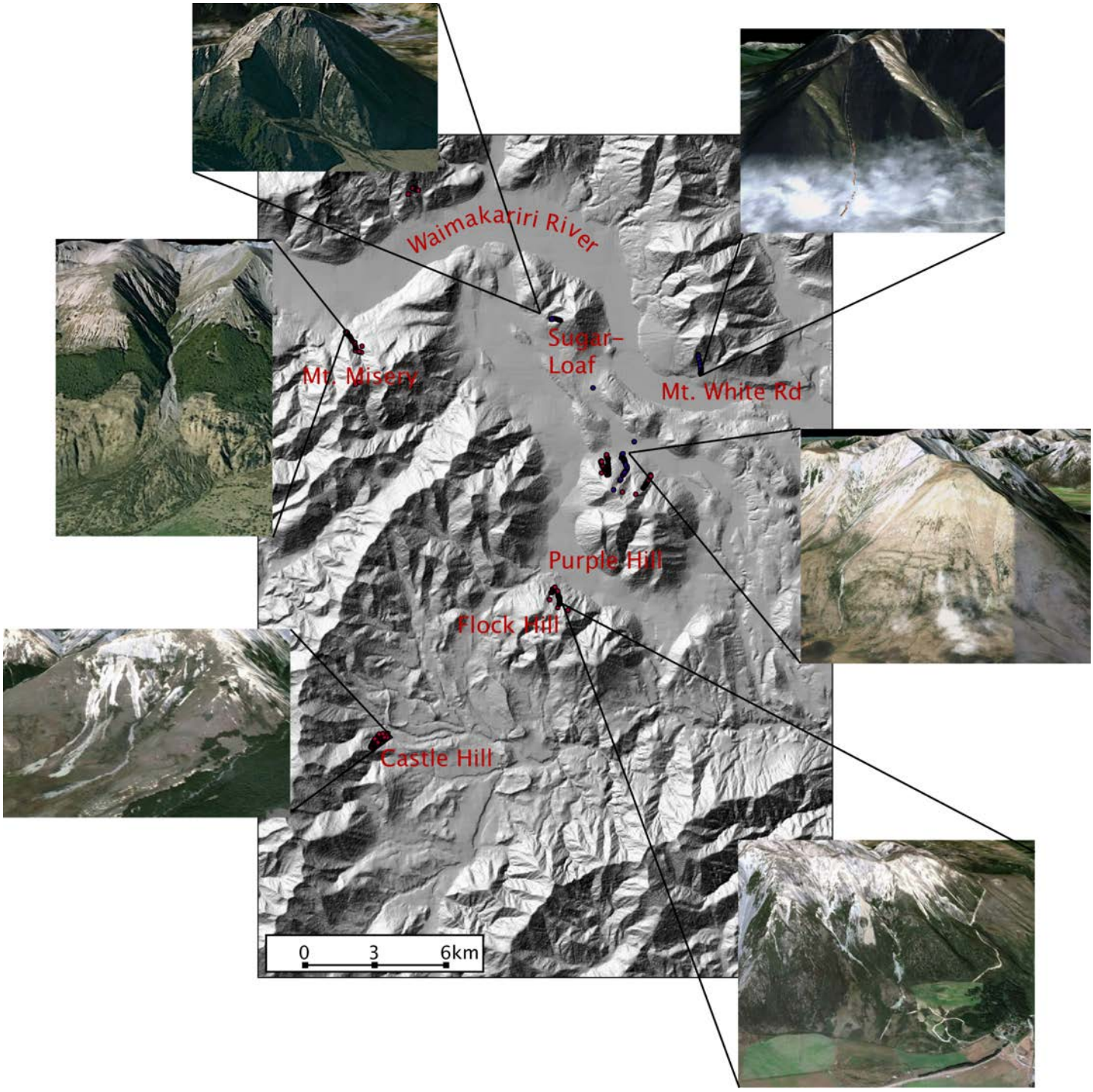

Figure 4.8.: Overview map of the Cass field area. The areas investigated are outlined in red. The dots are GPS coordinates recorded during field mapping.

4.5.1. Purple Hill, White Rock Road, Sugarloaf (typical hillslope type)

The flows mapped near White Rock Road, Sugarloaf, and Purple Hill are all of the classic hillslope type, belonging to the 1a or 1b type in the typology of Glade (2005). An example (mapped flow C2) of the zones of erosion, transport, and deposition typical of these flows is shown in Figure 4.9.

The initial failure mechanism of these small flows was probably seepage from joints in bedrock or surface runoff, or a combination of the two producing small translational failures or slumps. In most flows, there was a small amount of exposed bedrock directly above the source talus slope, which supplied this seepage or runoff. Below these outcrops in the talus slope, bedrock was usually close to the surface, limiting the depth of failure (Figure 4.10). The headwalls of these failures were often subject to retrograde erosion. This zone of failure is shown in Figure 4.9 as zone a.

This planar initiation area was followed by a steep zone of erosion. Below the bedrock outcrops, a small, v-shaped channel appeared in the talus which was often eroded down to bedrock (Figure 4.11). This feature gradually deepened and widened to become a 10 to 50 m wide gully midway down the slope. The point where the gully deepened usually corresponded to the boundary between bedrock near the surface and deeper accumulations of colluvium. Brundall (1966) called these gully features "canoe shaped" because, in plan-view, their shape resembles a canoe; narrow at the beginning, wide in the middle, and narrow again at the end. This area is illustrated by zone b in the geomorphic sketch of C2 (Figure 4.9).

In the upper part of these gullies the flows mainly eroded material, although often small levee deposits were visible on the gully sides. Sometimes there was a narrow, 0.5m to 1m deep, v-shaped channel cut into the floor of the gully. Small, 0.5 to 1 m high knickpoints were observed in these channels, which means that they were probably associated with headward knickpoint migration in the more turbulent watery tail portion of the flow, or by later stream flow.

In the lower slopes of the gully and the transition back onto unconfined hillslope, flow entrainment and deposition behaviour was unpredictable. The lower slopes of the gullies were sometimes erosional and sometimes depositional. As the slope angle decreased, the gullies gave way to a zone of distinctive levees which created a u-shaped channel (zone c in Figure 4.9). Here, partial confinement was usually provided by levees of older flows, with younger levees inset in or mantling older deposits (Figure 4.13). This zone was sometimes a significant area of deposition, representing nearly 90% of the total depositional volume for C1, for example. Deposition of levees and smaller surges continued for some distance down slope.

At a slope angle between 25° and 15° these levees died out and the final pulse of material deposited. This area of terminal deposition was much less consistent and distinct in the hillslope than in channelized events. Some of the hillslope paths may only have been recently activated and have not yet built up fans at the base of the slope (Brundall, 1966).

Prior accounts, as well as field observation of a small flow during mapping, show that they travel slowly, in a halting fashion. Typical velocities are between 0.25 and 2 m/s during movement (Brundall, 1966).

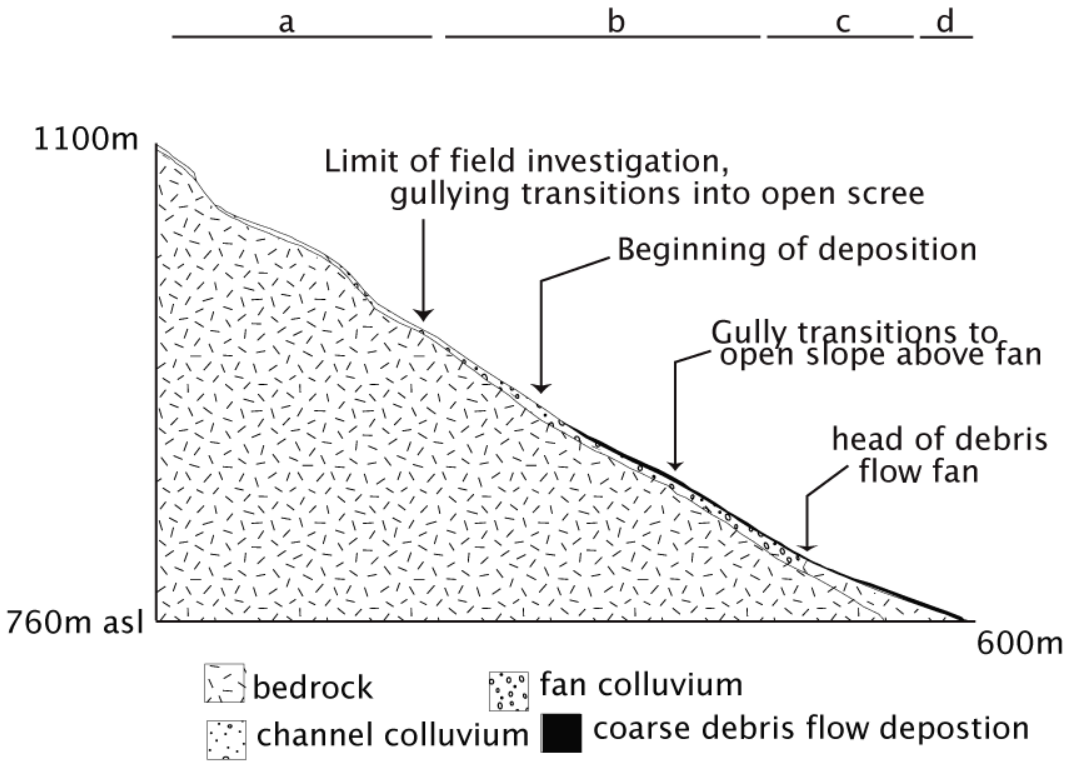

Figure 4.9.: Geomorphic sketch of C2. This behaviour is typical of the hillslope flows. (a) source area. (b) zone of erosion in gully. (c) transport zone on slope characterized by levee deposits (d) terminal lobe of deposit.

Figure 4.10.: The uppermost reaches of C7. The source area is on an open talus slope with bedrock at the surface. The slope angle is 37°.

Figure 4.11.: In the upper reaches of C2. An open talus slope has become a broad gully shown in the photo. A small v-shaped channel is visible in center of the gully which grows in prominence downstream.

Figure 4.12.: This reach in C6 eroded material from the center of the channel, but left a thin levee of debris on the channel sides. The slope angle in this reach is approximately 38°.

Figure 4.13.: Levee deposits in C2. This new material mantled old, buried levees from previous events. The beginning of the gully feature can be seen in the background of the photograph.

4.5.2. Castle Hill

Figure 4.14 summarizes the geomorphology of the three flows mapped near Castle Hill. In their initiation and transport zones (zones a and b in Figure 4.14) , the morphology of the flows was similar to the Purple Hill flows. However, in contrast to Purple Hill, bedrock was generally at or near the surface of the gully floor along its entire length. Also, seepage was observed from a band of bedrock low on the slope (Figure 4.15). This outcrop ran through all three paths, producing a 1-3 m high step in each. Seepage in this zone may have provided more moisture to the flows. Beyond the gully, the Castle Hill flows had short zones of levee deposition before spreading out onto poorly-defined fans (zone d and e in Figure 4.14). From this point, stream flow extensively reworked and spread the debris flow material over a wide area (zone f). These flows displayed more fluvial reworking than the flows on Purple Hill, which suggests there was more water available during or just after to the debris flow event.

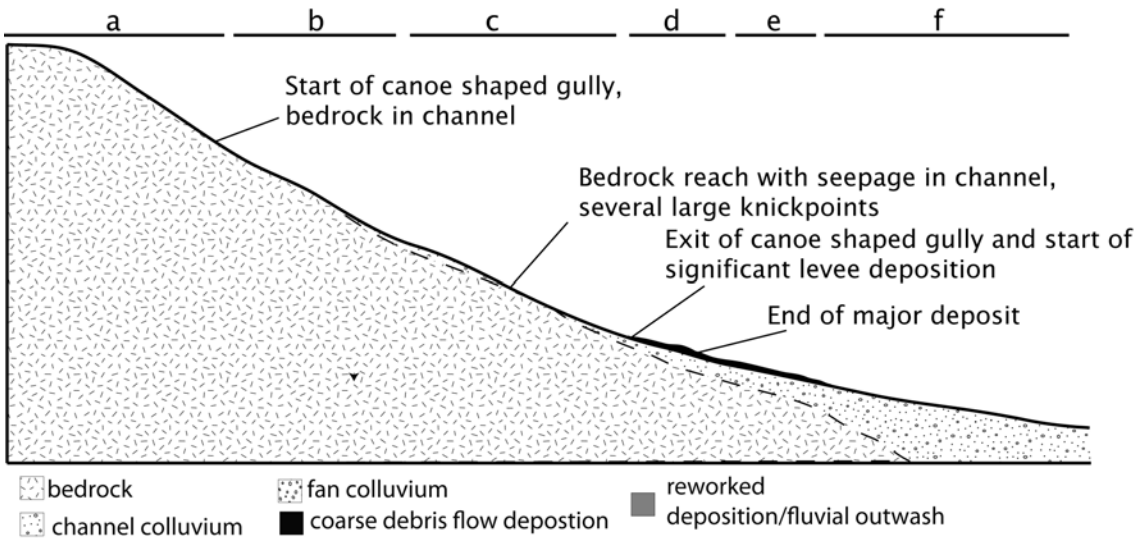

Figure 4.14.: Geomorphic sketch of C13 at Castle Hill. (a) Areas above the flow where bedrock is at the surface, (b) Upper reaches of the bedrock gully, (c) Marks the lower reaches of the gully, where the flow began to deposit levees. (d) Short zone of levees (e) Majority of the coarse clastic debris was deposited here. (f) Long stretch of fluvial deposits that were reworked from e.

Figure 4.15.: Bedrock step in the lower reaches of C14. The slightly darker soil behind the investigator is damp from seepage. Small channels have developed directly under the band of bedrock.

4.5.3. Flock Hill

Two flows were mapped on the north side of Flock Hill. These flows showed an intermediate behaviour between the classic hillslope flows on Purple Hill, and the classic torrent behaviour of the Orongorongos and Franz Josef field areas. Both of the Flock Hill flows are more confined than those on Purple Hill. Sinuous bedrock reaches, rather than a linear colluvial gully, characterized their upper travel paths. Lower in the channel, springs from the bedrock contributed seasonal streamflow to the flows (see Appendix A flow descriptions for more details). Consequently, they probably had more water available to them than the events on Purple Hill. In

addition, no canoe-shaped gully features are observed. Instead, the debris flows incised heavily into their fans. Slope failures from the resulting side-slopes contributed much of the event volume. [1]

Mapped flow C10 demonstrates the morphology of these flows through the lower end of the transport zone. The last few reaches before the final deposition zone were unusually flat compared with the flows on Purple Hill. In C10, these last few reaches appeared to be fluvial. They had a wide, flat bottom and a meandering channel thalweg. Below these reaches, the stream flow suddenly disappeared into the gravel. This disappearance was followed immediately by a break in slope and a return to lobate debris flow deposition. The stream flow reappeared just below this break in slope. This seepage could have created transient pore pressures which temporarily remobilized lobes of material. A similar morphology was also observed in a partially mapped flow C8 off Mt. Misery (Figure 4.16).

Figure 4.16.: Left: The deposition in this flat (slope angle 11°), wide reach off Mt. Misery was reworked by streamflow (shown by the degredational terrace on the left). After the reach shown on the left, there is a sharp break in slope and a return to lobate, coarse deposition on a 25° slope (right).

[1] The incision of the canoe shaped gullies and fans may suggest either that debris production has decreased (perhaps in response to decreased periglacial activity), or that precipitation has increased since the debris fans were originally built.

4.6. Birch Hill

In early February 2010, four debris flows were mapped in the Birch Hill catchment in the Ben Ohau range. These flows were coded BH1, BH2, BH3, and BH4. This area is located in Aoraki/Mt. Cook National Park, approximately 10 km east of the Main Divide of the Southern Alps (Figure 4.1). BH1, BH2, and BH3 flow down north facing slopes slopes from Mt. Loyd. Occasionally, the flows may deposit material into Birch Hill Stream, which drains the catchment. While the fan of Birch Hill Stream is primarily built by debris flood processes (de Scally and Owens, 2005), old, lobate debris flow deposits show that large, torrent flows must also occur. The Birch Hill stream drains into the Tasman River. The event volume and mapped length of these flows is shown in Table 4.5.

Table 4.5.: Event volume and mapped length for Birch Hill flows.

Flow	Event volume (m^3)	Mapped length (m)
BH1	336	821
BH2	638	536
BH3	2606	1039
BH4	387	487

Climatic, geomorphic, and geologic characteristics of the Birch Hill catchment differ markedly from those in the Orongorongos and Cass field areas. While still on the eastern side of the Southern Alps, Birch Hill's proximity to the Main Divide creates more orographic precipitation compared to Cass. The Mount Cook Ewes climate station is located approximately 6 km north of the mapped flows, at a very similar elevation (765m). Between 2005 and 2010, it recorded an average annual precipitation of 3712 mm. The rainiest months were May through October. However, the catchment receives rainfall throughout the year. For example, the maximum recorded 1-day precipitation over the last five years was 312 mm in December 2010. The second highest value was 236 mm in September 2008. According to Table 4.2, the December event had a recurrence interval of between 10 and 20 years.

The bedrock in this area is more highly metamorphosed than in Cass. It is characterized by harder, more intact greywacke to semi-schist facies with closely to moderately spaced joints. The uplift rates of approximately 5 mm/year are also faster than in Cass (Williams, 2004). The mass-wasting processes in the Birch Hill catchment also vary more widely than in the other field areas. Fluvial, debris flow, and snow avalanche processes are evident. Many fans and channels are products of all three processes acting in concert (de Scally and Owens 2005; de Scally et al.

2010, Figure 4.18).

Figure 4.17 summarizes the typical morphology of the Birch Hill flows. Flow behaviour was typical of the hillslope type events. However, unlike at Cass, the paths of these flows started in the bedrock headwalls. While possible, it is unlikely that rockfalls or debris flows from these bedrock reaches contributed material to the flows. Evidence of debris flow process was scant above the boundary between the headwall and colluvium for the first two flows mapped (BH1 and BH2). Runoff or hyper-concentrated flow from these reaches probably infiltrated into the talus slope immediately below. Here, seepage triggered shallow retrogressive failures which provided the bulk of the debris. This situation corresponds to type-2 hillslope flows of Glade (2005) (Table 4.1).

In BH3, some evidence of debris flow was observed in the upper, bedrock reaches (zone a in Figure 4.17). These upper reaches had lag deposits, as well as deposition behind boulders jammed in the narrow channel. However, the vast majority of the flow volume could be accounted for by failure of scree near the bedrock/colluvium boundary. The flow from this point on was similar to BH1 and BH2.

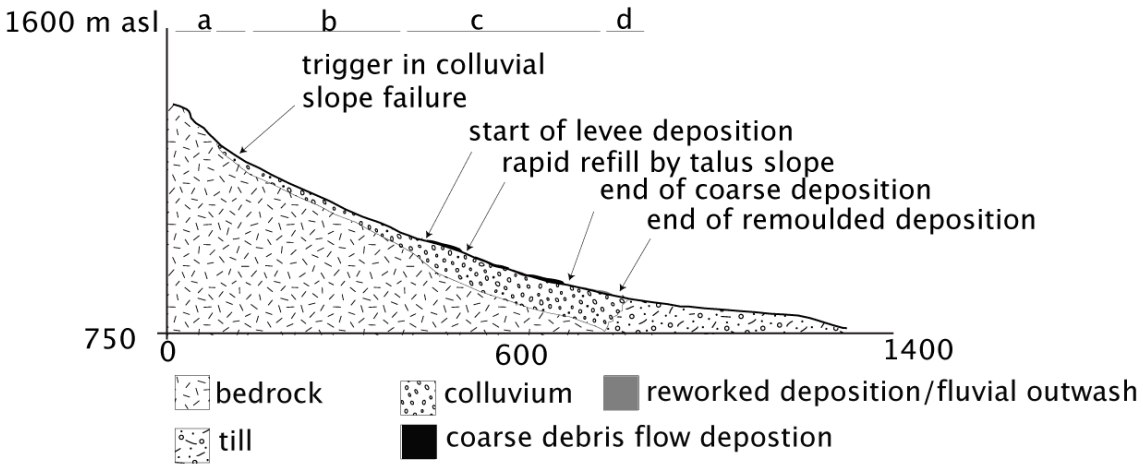

Figure 4.17.: Geomorphic model of BH3. (a) Initiation as shallow colluvial failure. (b) Area of erosion and transport. (c) Transport and levee deposits. (d) Reworked material.

The channel morphology through the transport zones of BH1, BH2, and BH3 was similar to that at Cass, although they lacked the 'canoe shaped' gully feature. Confinement was usually provided by a shallow, incised channel within the talus slope or within the levees of old flows (zone b and c in Figure 4.17). Levees and abandoned channels from older flows were obvious all over the hillslope. Similar to C1 and C2 at Cass, progressive levee formation was a dominant form of deposition (Figure 4.19, zone c in Figure 4.17). In BH2 and BH3, short zones

of reworked material were observed downhill of the terminal, coarse clastic lobe of deposition (zone d).

BH4 was channelized in a bedrock gully for much of its length, which made its behaviour much different from BH1, BH2, and BH3. The majority of material from this flow came from large slope failures in the gully side-wall. From its source, the flow travelled down a bedrock gully before depositing on a steep, unconfined fan. BH4 would probably be classified as a channelized flow using Table 4.1, however, this is not appropriate in this case. The flow deposited on a steep fan on a truncated spur, not in the outlet of a discrete catchment. The flow also lacked any streamflow, similar to a hillslope flow. However, material was sourced from the gully wall, which is similar to a typical torrent event. Because of these complications, BH4 was classified as an "intermediate" flow type in the data-analysis presented in later chapters.

Figure 4.18.: View up the Birch Hill Catchment. Mapped flows, BH 1, 2, and 3 are seen on the left. They initiate from translational failures at the bedrock/colluviums boundary. The central channel in the background of the picture is dominantly affected by snow avalanches triggered on Jamieson saddle or Mt. Edgar Thompson headwalls, rather than debris flows.

Figure 4.19.: Looking down the path of mapped flow BH2. The deposition from BH3 is seen on the left. The bottom of the initial failure is on the right side of the photograph.

4.7. Franz Josef

In March of 2010, four debris flows (FJ1 through FJ4) were investigated on the west side of the Waiho River near the terminus of the Franz Josef glacier. However, only two of the flows could be mapped fully, as the travel path of FJ1 and FJ2 proved too steep and dangerous to traverse. The event volume and mapped length of FJ3 and FJ4 are shown in Table 4.6.

Table 4.6.: Event volumes and mapped lengths for FJ3 and FJ4.

Flow	Event volume (m^3)	Mapped length (m)
FJ3	2483	678
FJ4	1548	544

This field area is located 40 km northwest of the Birch Hill catchment, on the other side of the Main Divide. Uplift rates in this area are the highest in the study at approximately 10 mm/year (Williams, 2004). The field area is also covered in dense bush. Figure 4.20 shows GoogleEarth Imagery of the Franz Joseph field area.

Moisture laden westerly airflow from the Tasman Sea encounters and is forced over the Southern Alps, producing intense rainfall. Rainfall values here far exceed the other debris flow sites visited. According a climate station 5 km away in Franz Josef township, the average annual rainfall between 2005 and 2010 was 5543 mm. The rainiest months tend to be in early to late spring, between August and September, but it can be wet at any time of year. For example, the recorded monthly rainfall for December, 2009 was 1168 mm. Immediately following this period of extremely wet weather in December 2009, there was another large rainfall event in early January 2010. On January 7th, the Franz Josef station recorded a 24 hour rainfall depth of 207 mm. Maximum hourly rainfall on that day was 36 mm. This precipitation event is thought to have triggered the events mapped. According to Table 4.7, which shows the annual recurrence interval for 24 hour rainfall depths, this intensity of rainfall should be expected every other year.

According to Department of Conservation employees in the area, the number of slips which occurred in the area during this event only happens once every several years; perhaps once a decade. This would suggest that the area is sediment-supply limited; the channels had been reloaded with enough sediment to generate debris flows in response to a fairly average rainfall event. However, the precipitation values in the field area were doubtlessly much higher than at Franz Josef; maximum values of yearly precipitation just 5 km to the east of the flows are on the order of 10000 to 15000 mm/year. Further small precipitation cells with much higher rainfall intensities than reported in town probably occurred on the northern side of the Waiho catchment. Such intense rainfall is often extremely localized and it is exceptionally difficult to measure. Without more data, whether this field area is transport or supply limited is an open question.

Table 4.7.: ARI and 1 hour rainfall depth for the Franz Josef field area.

ARI	1 hr rainfall depth (mm)
1.58	36
2	38
5	47
10	54
20	62
30	67
40	71
50	74
60	77
80	81
100	84

The lithology in Franz Josef differs markedly from the other field areas in this study. The bedrock consists of moderately jointed chlorite schist. Clasts of higher metamorphic garnet-bearing schist and lower metamorphic facies were also found in the deposition. Both of the flows mapped traveled down creeks with perennial stream flow before depositing on the outwash plain of the Franz Josef glacier. The flows were channelized by a deep, incised gully for almost their entire length.

Figure 4.21 summarizes the geomorphology of mapped flow FJ4. While large, bedrock waterfalls limited the mapped extent of FJ3 and FJ4, lack of mudlines, levee deposition, lag deposits, or disturbed vegetation directly below the waterfalls suggest that flood-flow or hyper-concentrated flow dominated these upper reaches. The events in these upper reaches had not scoured enough bedrock or colluvium to mobilize into fully mature debris flows.

The location of the stream channel appeared to be structurally controlled. Figure 4.22 shows the first reach of FJ4. The bedrock on the right hand side appeared to be a smoothed, relatively intact fault plane, while the bedrock on the left side had been badly damaged by fault motion. Colluvium and failures in this left gully wall were the major source of debris (see zone a in Figure 4.21). This zone of erosion was relatively short, only 80m in the case of FJ4, but extremely confined (Figure 4.22). These dominantly erosional reaches quickly gave way to a transport zone characterized by intermittent erosion and deposition (zone c in Figure 4.21).

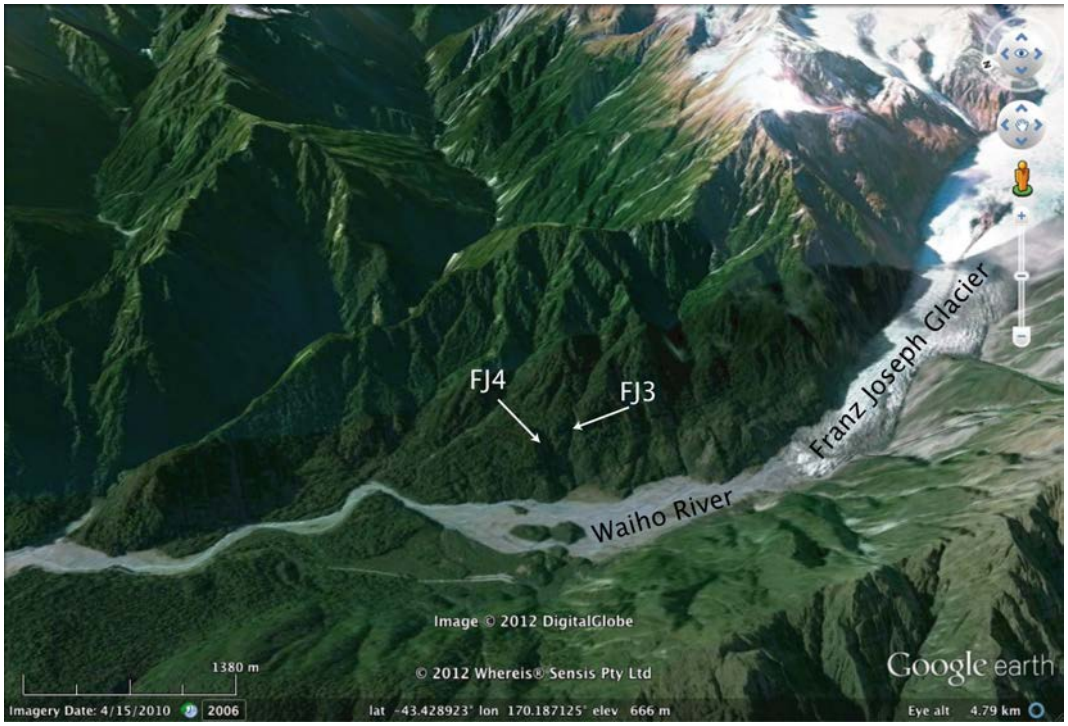

Figure 4.20.: GoogleEarth® imagery of Franz Joseph field area. The location of the two debris flow paths investigated are labeled.

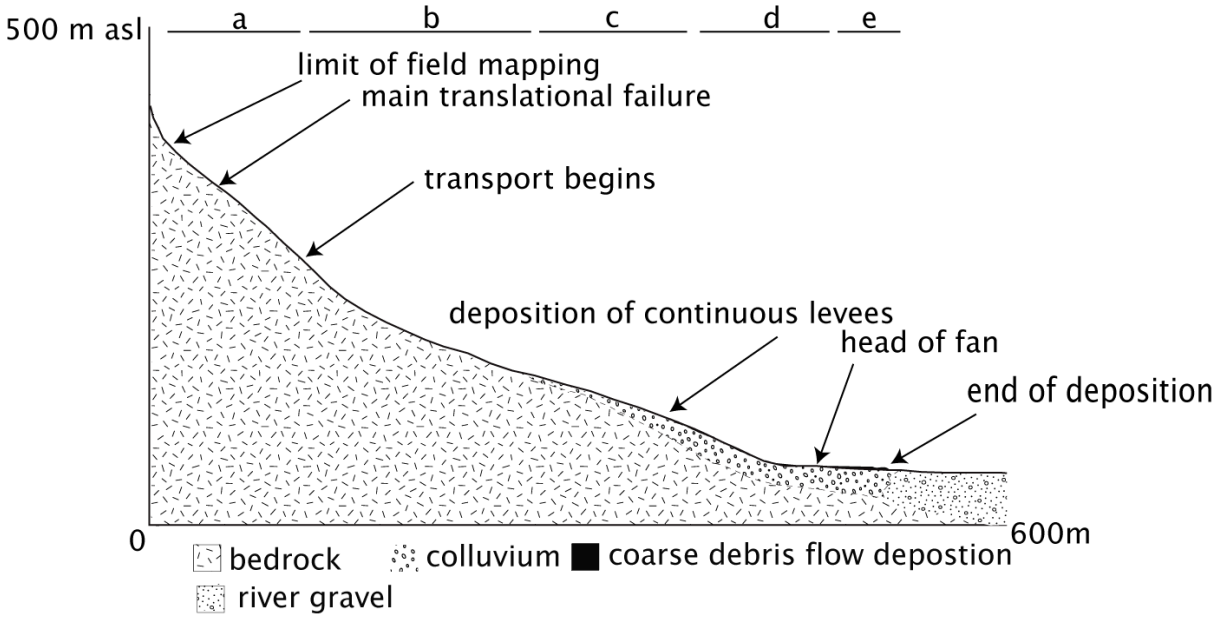

Figure 4.21.: Geomorphic sketch of mapped flow FJ4. (a) Hyper-concentrated stream flow above mapped reaches. (b) Main source of debris in event, erosional reaches. (c) Transport zone of intermittent erosion and deposition. (d) Beginning of deposition. (e) Massive deposition and unconfinement.

Figure 4.22.: Looking down the first, extremely confined reach of mapped flow FJ4. The dominant source of debris came from failures in the left channel bank.

In the transport zone, both FJ3 and FJ4 were still dominantly confined by the gully. Both paths displayed knickpoints formed by 2 to 4 m diameter boulders, which is larger than the 1 to 1.5 m diameter boulders found in the Orongorongos. The flow often trimmed one side of the channel bank while depositing levees on the other side. Disturbed vegetation was also common.

The presence of dense forest differentiates Franz Josef from the other field areas. Fallen trees acted to increase channel roughness by damming the channel and acting as sediment traps. The hillslope flows mapped on the eastern side were primarily bare of vegetation. The importance of woody vegetation in mediating channel recharge has been discussed by several authors (Benda and Dunne, 1997; Lancaster et al., 2003; May and Gresswell, 2004) and is doubtlessly an important process in the densely forested catchments on the west coast of New Zealand as well. The vegetation helps stabilize steep hillslopes, limiting the formation of lower magnitude, but higher frequency hillslope type flows. Instead, the presence of vegetation alters the magnitude-frequency relationship to less frequent, higher-magnitude events (Bloomberg

and Davies, 2012).

The channel in both FJ3 and FJ4 remained confined until abruptly depositing unto short, low angle debris flow fans on the Waiho river floodplain (Figure 4.23). These fans are often truncated by the Waiho River, which transports debris flow material away during flood events. Luckily, the flows were investigated before the river migrated to the west side of the flood plain and removed the deposits.

Figure 4.23.: The last depositional reach of FJ4.

4.8. Discussion

4.8.1. Debris flow size

If hillslope flows occur primarily high in the geomorphic system on hillslopes and in low-order channels and torrent events occur in higher-order channels, it follows that hillslope and torrent flows have different spatial and temporal scales. Hillslope flows are high frequency events that occur at the sub-basin scale, transporting material from steep hillslopes and zero-order gullies to lower angle slopes and sometimes into the main-stem channel of the basin. Less frequent, torrent flows occur along the axis of a basin, transporting material from one stream channel into another of a higher order.

These different spatial and temporal scales will also loosely correspond to event magnitude. Jakob (2005) proposed a ten-fold classification system for debris flows based on the total volume, peak discharge and area inundated. While Jakob was primarily concerned with channelized events which occur in British Columbia and the European Alps, hillslope flows can be placed into the scheme.

Table 4.9 places the flows mapped in this dataset into Jakob's classification. Table 4.9 lists the volume mapped past the last confined reach; this is the event magnitude used in the Jakob's classification. Note that this volume estimate discounts much of the debris deposited in levees by the hillslope flows.

The smallest, Class 1 magnitude flows will typically be hillslope-type events. They will initiate from small, planar, translational failures, zero-order colluvial hollows, or translational failures at the boundary of bedrock and colluvium. The travel path of these flows will be dominated by slope and gully processes. Class 2 and even Class 3 hillslope flows may occur as well, resulting from either larger failures or in areas with expansive, unvegetated talus slopes (e.g. Birch Hill and Cass).

According to Jakob, Class 2 torrents will typically occur on small, supply limited creeks where debris flow activity is limited by the material in the channel. This would be an accurate description of FJ3 and FJ4, which sourced their debris from bedrock failures in an undercut bank.

Class 3 encompasses a typical size range that produces channelized debris flows at decadal return periods in non-volcanic, supply-limited watersheds or higher return periods in supply-unlimited watersheds Jakob (2005). Class 3 flows in this dataset are exemplified by the Orongorongo flows. All of these flows traveled down the main-stem channel of the catchment and flowed out onto a well defined geomorphic fan. From accounts of property owners in the Orongorongos, debris flows occur on sub-decadal intervals, suggesting that these are supply-unlimited watersheds. This is not surprising considering the weathered, unstable nature of the bedrock in this field area.

At longer return periods and in larger basins, debris flow catchments in the Orongorongos may produce larger Class 4 flows which are between 10^4 and 10^5 m^3 in magnitude. Larger basins near Franz Josef and Mt. Cook are almost certainly capable of this magnitude of flow as well, but probably at return periods of hundreds of years rather than decades. For many supply-limited catchments of less than 4 km^2 in size, Class 4 flows may be the maximum that may be achieved even for very long return intervals (Jakob, 2005). Figure 4.24 summarizes this behaviour in a conceptual sketch, modified from Jakob (2005).

Table 4.8.: Debris flow classification for bouldery debris flows (after Jakob 2005).

Size class	Volume (m^3)	Q range (m^3/s)	Potential consequences
1	$<10^2$	<5	Very localized damage, known to have killed forestry workers, damage small buildings
2	10^2-10^3	5-30	Could bury cars, destroy a small wooden building, break trees, block culverts, derail trains
3	10^3-10^4	30-200	Could destroy larger buildings, damage concrete bridge piers, block or damage highways and pipelines
4	10^4-10^5	200-1500	Could destroy parts of villages, destroy sections of infrastructure corridors, bridges, could block creeks
5	10^6-10^7	1500-12000	Could destroy parts of towns, destroy forests of 2 km^2 in area, block creeks and small rivers

Q is the peak discharge in m^3/s. The volume referred to is the volume of the flow deposited on the debris flow fan.

Table 4.9.: Debris flow classes for the flows investigated in this dataset.

Flow ID	Type	Volume past last confined reach or in terminal lobe (m^3)	Class
BH1	Hillslope	14	1
C1	Hillslope	76	1
C11	Hillslope	157	2
C2	Hillslope	231	2
BH4	Hillslope	328	2
C14	Hillslope	540	2
C13	Hillslope	580	2
FJ4	Torrent	810	2
C7	Hillslope	840	2
OR2	Torrent	1524	3
C15	Hillslope	1864	3
FJ3	Torrent	2000	3
C6	Hillslope	2300	3
C3	Hillslope	2426	3
C10	Torrent	2600	3
C12	Intermediate	2740	3
OR4	Torrent	3550	3
OR3	Torrent	4930	3
OR1	Torrent	7610	3

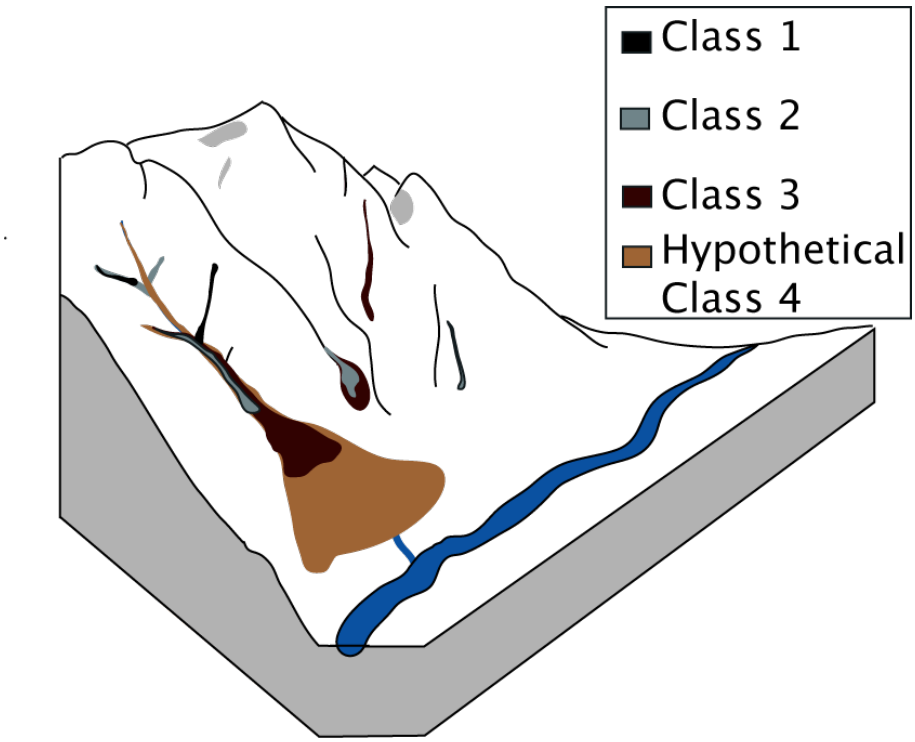

Figure 4.24.: Conceptual sketch for debris flow classes investigated in this chapter.

4.8.2. The relationship between small, hillslope events and larger torrents

Using the geomorphology-based categorization is useful in understanding how small hillslope events can coalesce to form larger Class 3 or 4 torrent flows. Events larger than Class 4 usually originate from volcanoes, lack bouldery fronts, and have high fines contents. Consequently, they are often significantly more mobile than the bouldery flows that are typical in alpine catchments. In fact, Jakob (2005) stops his classification of alpine debris flows at Class 5. Class 4 and 5 events do occur in unusual circumstances in alpine catchments or areas with extremely abundant sediment sources, such as the Jiangjia ravine in southern China (Chen et al., 2007, 2005; Jakob, 2005).

Hillslope flows begin as amalgamations consisting of stone-falls, scree, and small slurries from the open-slopes, swales, or small, 0-order gullies. In light or moderate precipitation, this material may move into the gully and immediately flow down to accumulate in lower angle reaches. In more intense rainfall, this process becomes more widespread. Small surges pick up material already lying in the bed and grow in volume.

These small surges often halt in response to large clasts or when the bouldery front

becomes too large to push out of the way. For a debris flow to continue downslope, it must either go around the dam, overtop it, or build up enough pressure to move through it. This exact process was observed in a series of small surges (approximately 0.005 m^3 in volume) in the upper reaches of C6 during field mapping. The morphology of the deposition from these miniature flows was similar to the morphology of the larger deposits mapped downstream.

In more intense rainfall events, some surges will grow enough to entrain material deposited from earlier debris flows. In hillslope flows like those mapped in Cass and Birch Hill, the flow eventually leaves the gully, becoming channelized in subtle swales on the hillslope or by levees left by previous events. Since the slope angle is gradually reducing and there is no more material from the gully side-slopes to entrain, the flow deposits. For small hillslope flows like the ones in this dataset, this process explains much of their morphology.

In large catchments where Class 3, 4 or 5 debris flows regularly occur, the process of deposition and subsequent remobilization may continue as the flow enters higher order stream channels. The contributing gullies each provide sediment to the main channel. The larger, higher order channel will often have a stable discharge of stream flow available to re-entrain and erode material. In this way, the process of deposition and remobilization in progressively larger channels is continuous from the smallest hillslope flow to the large catastrophic event.

Coalescing of hillslope flows similar to the above description have been noted at Mt. Thomas, New Zealand (Davies et al., 1992). Coalescing hillslope debris flows and debris avalanches also contributed to the May 18, 2005 debris flow disaster at Matata, New Zealand (McSaveney et al., 2005). However, this description of how hillslope flows evolve into larger, torrent debris flow events remains speculative without more detailed studies on sediment transfer, hydrology, and debris flow processes on steep hillslopes. This is an avenue for future research.

4.8.3. Increasing moisture content

The mechanical differences between small hillslope and larger, catastrophic channelized debris flows are largely explained by increasing water availability downslope. The limiting factor for channelized flow in higher order stream channels is material, rather than water. This is a major difference from hillslope debris flows. In talus, material is readily available, however, precipitation usually disappears quickly into the highly permeable debris, emerging as seepage lower down on the hillslope. Hillslope flows may have much higher debris availability than torrents, but less available water for saturation.

In contrast, the water table of higher-order, channelized reaches with nearly constant stream flow is, by definition, at the surface. The amount of saturation in channelized flows is

probably always higher than their contributing hillslope flows. Water availability increases as the flow moves downslope into higher order channels. This helps explain the higher mobility of these flows discussed in subsequent chapters.

4.9. Summary and conclusions

This chapter summarized the geology and overall morphology of debris flows typical of four field areas in New Zealand. Flows were classified into two different types, hillslope or torrent flows. Torrent flows are found in first or second order streams. Hillslope flows are dominated by slope and gully processes on open slopes or steep zero-order or first-order channels which usually lack permanent stream flow.

The most prominent aspects of each field area can be summarized as follows:

- Debris flows in the southern Rimutaka ranges (Orongorongos) were of the bouldery, channelized type and were most likely triggered by rockfalls or hillslope flows from steep, bedrock sources reaches. In larger events, the head of the fan became an important area for entrainment. Volume ranges from 1,000 m^3 to 10,000 m^3 were observed.

- Debris flows in Cass were of the hillslope type, which are typically less dangerous, and deposit on higher slope angles than in the Orongorongos. This may be due to higher solids concentrations and less confinement. Volumes reaching the fan ranged from 100 m^3 to over 1,000 m^3, although significant amounts of deposition occurred in levees further upslope.

- Debris flow behaviour at Birch Hill was generally of the hillslope type, but some reaches in upper bedrock gullies displayed clogging at constrictions similar to that observed in the Orongorongos. Volumes of deposition ranged from 100 m^3 to 1,000 m^3.

- Flows near Franz Josef were of the torrent type, but appear to be characterized by a larger maximum particle size and more woody vegetation than in other field areas. This contributed to channel roughness. Volumes of deposition ranged from approximately 800 m^3 to 2,500 m^3.

Hillslope type flows tended to deposit at higher slope angles and have smaller discharges. This can be explained by lack of confinement once they moved out of the gully and a high solids concentration (low moisture content). Hillslope debris flows are primarily hazardous to infrastructure or residences directly adjacent to steep slopes. They are also extremely important

in transferring sediment to the main channel. This process of channel recharge is important in generating larger Class 3 and 4 channelized flows.

Channelized events travelled down first or second order stream channels, which were in some cases very confined over their length (e.g. in mapped flows FJ3 and FJ4) and held year-round stream flow. Hence, these flows had enough water available to support a lower solids concentration which increased mobility. In places with large areas susceptible to hillslope flows and very high debris production rates, coalescence of many hillslope events may produce catastrophic, Class 4 or 5 debris flows.

5. Empirical-statistical differences between torrent and hillslope type debris flows

This chapter analyzes and compares the reach data from 11 hillslope flows, 4 torrent flows, and 2 flows with an intermediate morphology. The reach data for each mapped flow were amalgamated into a single, larger dataset and analyzed. The intention was to quantify differences in slope, confinement, and erosion/deposition volume between reach types, as well as provide geologists and engineers who may work in these field areas useful empirical data.

The differences found between flow types supported the qualitative observations discussed in Chapter 4. Hillslope flows began to deposit at higher slope angles. Slope angles of erosional and transport reaches were higher in the hillslope than in torrent flows. Hillslope flows also had smaller width to depth ratios, indicating less confinement and smaller discharges. Intermediate reaches were similar to hillslope flows in terms depositional slope and erosion behaviour.

Compared to several larger magnitude events in British Columbia, the New Zealand flows displayed smaller yield rates. Possible reasons for lower yield rates in the smaller, more frequent events studied are discussed.

5.1. Introduction

The mechanics of debris flow motion are extremely complex. Purely mechanical models which adequately simulate debris flow motion at the field scale are still at an early stage of development. Where these models are available, measuring input parameters such as solids concentra-

tion, unit weight, and viscosity at the field scale is both difficult and dangerous. Consequently, debris flow professionals often must rely on empirical-statistical rules to predict volume of debris entrained, depositional slope angle, or total travel distance. These rules are usually based on factors such as slope angle, confinement, and the geology along the flow path (Fannin and Rollerson, 1993; Fannin and Wise, 2001; Hungr et al., 1984; Rickenmann, 2005; Benda and Cundy, 1990; Rickenmann, 1999). The problem with these empirical rules is that they are usually only valid for similar types of flows in similar localities (or the same locality) as that in which they were derived.

While empirical rules for torrent events are common (see Table 2.1), most of these are based on debris flows in Europe or North America. At present, no attempt has been made to systematically collect debris flow data in New Zealand from which empirical rules could be established. For hillslope flows, empirical rules for depositional slope and entrainment are rare anywhere in the world (Zimmermann, 1990; Conway et al., 2010). This chapter begins to fill this gap in knowledge by reporting the typical slope angles of erosion and deposition, flow widths, and eroded volumes for small hillslope and channelized events in New Zealand.

Four of the flows originally mapped and noted in previous chapters were excluded from this analysis. In the case of FJ3, mapped volumes of erosion did not compare well with the mapped volumes of deposition. OR4, as discussed in Section 4.4, was more reminiscent of a debris avalanche than a debris flow and was excluded from the analysis for this reason. In C12 and C15, large amounts of fluvial reworking made estimating the amount of erosion or deposition by the debris flow event difficult. The remaining dataset contains data from 276 reaches and 17 debris flow paths.

5.2. Slope

During field mapping, each reach was given a "reach type" designation (source, erosion, transport, deposition, reworked, or fluvial). The mean slope angle and depth of entrainment (-) or deposition (+) for each reach behaviour is summarized in Tables 5.1, 5.2, and 5.3, for hillslope, torrent, and intermediate flows, respectively.

If source and erosion reaches are simplified as one zone of erosion, and deposition, reworked, and fluvial simplified as depositional, the typical slope angles of erosion, transport, and depositional zones can be crudely summarized. Hillslope-type events tended to be erosional between 40° and 30°. Transport reaches occurred between 30° and 20°, while deposition usually occurred below 20°. For the torrent events, erosion dominated at slope angles over 27°. The

volume change of the flow was marginal in transport reaches at intermediate slope angles (mean of 19°). The mean angle of deposition, 13°, was much lower than for hillslope-type events (20°). For intermediate flows, the typical slope angles of erosion, transport, and deposition were similar to hillslope events (Table 5.3).

The reach types were also analyzed to see if there were statistically significant differences between them. A one-way ANOVA with a Tukey test showed statistically significant differences between the slope angle of several reach types. For hillslope flows, significant differences existed between erosion, transport, deposition, and reworked reach types. There was little difference between source and erosional reaches; this is because the difference between a source and an erosional reach is somewhat arbitrary (both supply debris to the flow). There was also little difference between reworked and fluvial reaches, which reflects the difficult distinction between material deposited by watery-debris flow surges and debris flood surges.

For the channelized flows, there were significant differences between erosion, transport, and depositional reach types. There was no significant difference between deposition and reworked, or reworked and fluvial types. This is due to the fact that, by definition, both debris flows, flood flows, and normal stream-flow occur in torrent channels. The lack of a significant difference between the fluvial, reworked, and coarse deposition may also point to a lower solids concentration in torrent flows.

BH4 and C12 were categorized as intermediate flows, because while they occurred in first order streams with only intermittent stream flow (higher in the geomorphic system than most torrents), they still displayed some properties typical of torrents, such as clogging at constrictions, well-defined fans, and confinement in a gully. Based on the data given in Table 5.3, the intermediate flows were much more like the hillslope than the torrent flows, even though they were channelized over much of their length. This may be related to higher solid concentrations and lack of stream flow in lower order streams, as mentioned in Section 4.8.3. Slope angles of depositional reaches were similar to angles observed in hillslope depositional reaches. The high mean slope angle of transport reaches shown in Table 5.3 is caused by BH4. The transport zone of this flow was dominated by a steep, bedrock channel. If there had been more debris availability in these reaches, they would have been erosional.

Table 5.1.: Summary of the mean slope angle and E' by reach behaviour, for the hillslope dataset.

Hillslope-type debris flows							
behaviour class	Mean slope (°)	Standard deviation	Mean E' (m)	Standard deviation	Flow W/H	Standard deviation	n
Source	35.8	5.4	-0.46	0.79	24.0	40.7	14
Erosion	32.0	4.5	-0.46	0.31	5.0	3.8	37
Transport	26.8	6.0	0.07	0.33	5.0	3.7	63
Deposition	20.1	7.3	0.48	0.47	13.4	16.6	23
Reworked	13.0	3.3	0.13	0.14	41.5	66.4	24
Fluvial	10.8	2.1	0.13	0.12	37.7	39.2	11

E' is the volume balance for the reach divided by the flow area. Flow W/H is the channelization ratio, or flow width divided by the flow height. Deposition is positive. Erosion is negative. n is the sample size (i.e the number of reaches in the dataset).

Table 5.2.: Summary of the mean slope angle and E' by reach behaviour, for the torrent dataset.

Torrent type-debris flows							
behaviour class	Mean slope (°)	Standard deviation	Mean E' (m)	Standard deviation	Flow W/H	Standard deviation	n
Source	36.0	3.5	-1.0	0.53	2.0	0.7	3
Erosion	26.8	7.0	-1.05	0.61	3.4	1.8	21
Transport	18.9	5.5	0.01	0.16	7.4	7.4	35
Deposition	13.1	2.8	0.67	0.48	22.0	17.7	9
Reworked	8.6	1.2	0.20	0.043	289.6	169.7	3
Fluvial	3.0	1.4	0.005	0	106.0	8.4	2

E' is the volume balance for the reach divided by the flow area. Flow W/H is the channelization ratio, or flow width divided by the flow height. Deposition is positive. Erosion is negative.

Table 5.3.: Summary of the mean slope angle and E' by reach behaviour, for the intermediate dataset.

Intermediate-type debris flows							
behaviour class	Mean slope (°)	Standard deviation	Mean E' (m)	Standard deviation	Flow W/H	Standard deviation	n
Source	30.2	2.54	-1.0	0.8	2.8	0.2	2
Erosion	29.0	2.6	-0.9	0.3	3.0	1.7	13
Transport	31.5	7.4	-0.4	0.2	1.7	0.7	7
Deposition	19.7	2.1	0.4	0.3	22.2	8.3	9

Flow W/H is the channelization ratio, or flow width divided by the flow height. E' is the volume balance for the reach divided by the flow area. Deposition is positive. Erosion is negative.

5.3. Confinement

5.3.1. Differences in confinement type

Confinement is the other significant geometric constraint on flow (Hungr et al., 1984). Figures 5.1, 5.2, and 5.3 show the proportion of reaches in the various confinement categories for torrent, hillslope, and intermediate datasets, respectively. The hillslope dataset has a higher percentage of unconfined and partially confined reaches than the torrent dataset (56% versus 41%). This was expected—hillslope flows are, by definition, less confined than channelized types. Despite this, there are a higher percentage of CIG (confined in gully) reaches in the hillslope dataset. These were reaches that were confined in canoe shaped gully features observed at Cass, as discussed in Section 4.5.1.

The torrent-type flows were often confined in the channel, rather than in a gully. Through their transport zones in second-order channels, the torrent flows often traveled down channels which were incised into a wider gully feature (see Figure on page 41). This explains the dominance of the CIC (confined in channel) categorization for torrent type flows shown in Figure 5.1. The intermediate-type flows were, like the torrent flows, dominantly confined by the channel through their erosional and transport reaches before suddenly becoming unconfined on steep fans (Figure 5.3).

5.3.2. Channelization ratio

While the relative proportion of the reach classifications in each dataset qualitatively indicates the type of confinement which dominated, it says little about the degree of confinement. The ratio of flow width to depth (flow W/H) is a more quantitative measure of the degree of confinement (see Tables 5.1, 5.2, and 5.3). The higher the width to depth ratio, the less confined the reach.

Through source and erosional reaches, the mean flow W/H was much lower for torrent (2.0 and 3.4, respectively) than for hillslope-type flows (24.0 and 5.0). In transport reaches, the ratio was higher for torrents (7.4 versus 5.0), indicating that these reaches were relatively wider and less confined. This is because the transport zones in the Orongorongo and Franz Josef flows were dominated by relatively wide, second-order channels where stream-flow was more common. In contrast, the W/H ratio in the transport zone of intermediate events was very low (1.7). This low W/H ratio reflects the confined nature of the small, 0 or 1st order, bedrock gullies that make up the transport zones of these flows.

The width to depth ratio was much higher in the depositional zone for torrent and intermediate flows (22.0 and 22.2) than it was for hillslope events (13.4). This may be related to the way in which the torrent and intermediate type flows suddenly become unconfined and deposit on the debris flow fan, rather than the progressive deposition observed in hillslope events.

5.3.3. Significance of confinement type to volume behaviour

An interesting question with regard to confinement is whether or not there was a significant difference in the entrainment or depositional behaviour between confinement types. ANOVA results show that while there was significant differences between both the CIG and CIC reaches and partially confined reaches, there was no significant difference between partially confined reaches and unconfined ones. This indicates that the distinction between partially confined and unconfined reaches did not reflect any quantitative difference in entrainment or deposition behaviour. In the future, partially confined reaches could be grouped under the unconfined category, as usually done in most other debris flow studies.

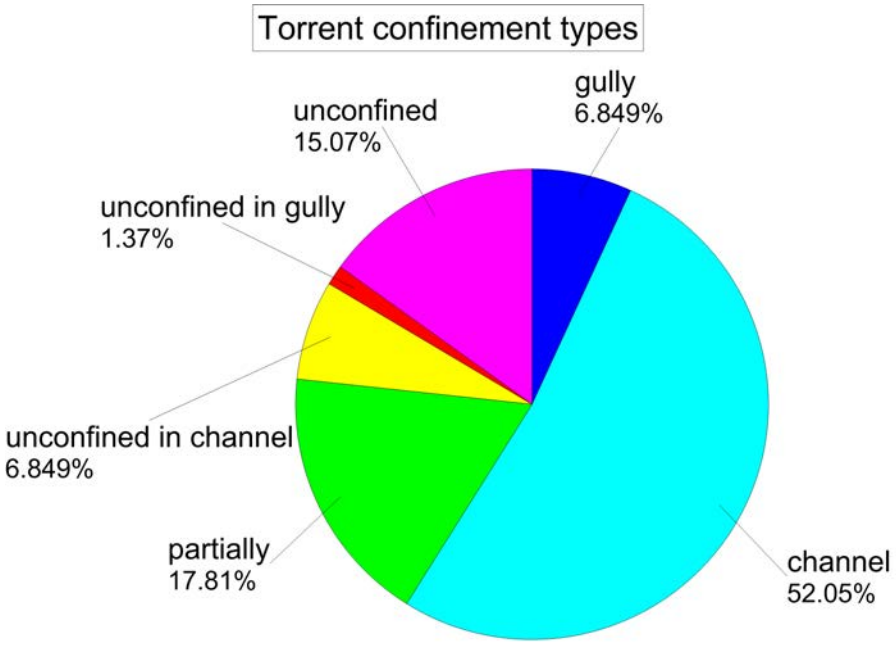

Figure 5.1.: The confinement categories of torrent type flows in this dataset.

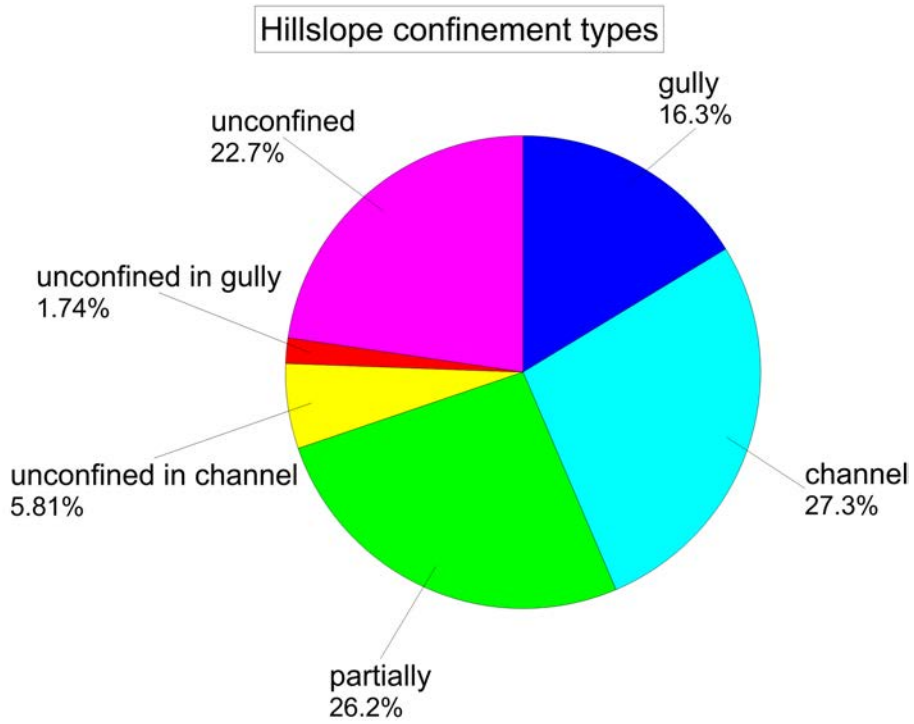

Figure 5.2.: The confinement categories of hillslope type flows in this dataset.

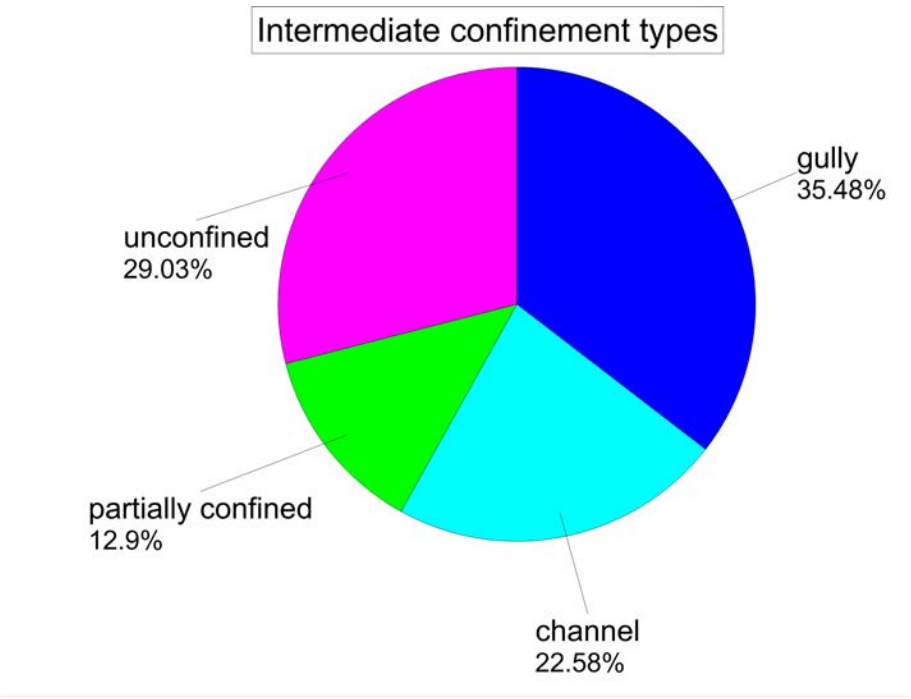

Figure 5.3.: The confinement categories of intermediate type flows in this dataset.

5.4. Volume passing

5.4.1. Calculating yield rates

To understand controls on the erosion and deposition, the rate of volume change was calculated for each reach in the dataset by dividing the volume balance of erosion and deposition by the reach length (m^3/m). This is a common metric in debris flow studies (Hungr et al., 1984; Bovis and Jakob, 1999; Jakob et al., 2005; Hungr et al.; D'Agostino and Marchi, 2003; Marchi and DAgostino, 2004; Fannin and Rollerson, 1993; Fannin and Wise, 2001). If the reach is erosional, the metric is often referred to by different authors as the erosion, entrainment, or yield rate. If depositional, this rate is called the deposition or lag rate. In this study, the terms yield and lag rate are preferred.

Choosing the most appropriate eroded volume for each reach to calculate the volume change rate was challenging. As previously mentioned in section 3.5.1, during field mapping a lower and an upper bound of eroded volume were estimated in each reach. The upper bound represented a scenario where the debris flow had largely created the channel, while the lower bound represented a scenario where the flow had only marginally widened, or simply transported

material through an already formed channel. During data analyses, these individual, reach-by-reach estimates were summed to give a lower bound and upper bound estimate of total eroded volume for the flow. These values were then compared with the total volume deposited by the flow to estimate whether the lower bound, upper bound, or median value of erosion was most accurate.

For five flows in the dataset, the upper bound of erosion was deemed to be the most accurate estimate. For C3 and C14, the total volume deposited was 17% and 18% more than the upper bound of mapped erosion, respectively. In C3, this extra volume can be assumed to represent material unaccounted for in source reaches that were too dangerous to traverse. In C14, there were several lobes of deposition that were likely slightly older events than the one being mapped. It is possible that some of these should have been included in the event deposition. The remaining three flows in which the mapped volume of deposition was much larger than the mapped upper bound of erosion were OR1, OR2, and OR3. The source reaches of all three flows were too steep to be investigated safely. It is assumed that the unexplained volume came from these reaches.

For seven (the majority) of the flows discussed in this chapter, the median between the upper and lower estimate of erosion was very close to the total volume of deposition mapped. The average difference between this figure and the total volume deposited was 9% of the total volume mapped. For these events, the mean erosion estimate in each reach was used to calculate the yield rate and volume passing.

For three of the flows in the dataset, the lower bound of erosion was very close to the mapped deposition volume. The upper bound estimate most likely took into account events older than the one mapped in the depositional zone. The mean difference between the lower bound of erosion and the volume of the mapped deposit was 7.3% of the mapped deposition. For these flows, the lower erosion estimate in each reach was used to calculate the yield rate and volume passing.

5.4.2. Calculating volume passing

To plot the volume passing the end of a reach, an estimate had to be made of how much material was entrained upslope of each reach. This could not simply be calculated as the sum of the eroded volume estimates, because in the Orongorongos approximately 50 to 80% of debris came from source reaches which were not traversed. For the Orongorongo flows, and for the flows where the most accurate estimate was lower than mapped deposit volume, the discrepancy between the estimated eroded volume and volume deposited needed to be accounted for. This

was done using Equation 5.1.

$$V_{passing} = D_{total} - \sum E_{after} - \sum D_{before} \tag{5.1}$$

where $V_{passing}$ is the volume of debris passing the end of the reach, D_{total} is the total deposition calculated for the flow, E_{after} is the volume eroded downslope of the reach end, and D_{before} is the volume deposited uphill of the reach. In this way, the "extra" material (the deficit between mapped erosion and deposition) is treated as entering the first reach (both in the volume passing discussion below and in the UBCDflow modelling in Chapter 6). This calculation results in 0 volume passing the final reach.

However, Equation 5.1 is not appropriate when the mapped erosion was slightly more than the total deposition, as at some point Equation 5.1 will calculate a negative volume balance entering a reach. In these cases, it can be reasonably assumed that the minimum volume passing had to have been at least equal to the volume deposited in subsequent reaches. Therefore, for reaches where Equation 5.1 calculated a negative volume balance, the volume passing was set to the volume deposited downhill of the end of the reach, minus the volume which was entrained from these reaches (Equation 5.2).

$$V_{passing} = \sum D_{after} - \sum E_{after} \tag{5.2}$$

While this approach to calculating yield rate and volume passing is not perfect and significant errors could exist (as discussed in Section 3.5.6) this method gives an approximate estimate of the volume balance amount of material passing each reach. Other debris flow studies have also had to adjust field data to reconcile the differences between erosion and deposition (i.e. Fannin and Wise 2001).

5.4.3. Volume passing results

Figure 5.4 plots the volume passing each reach against the slope angle of the reach. The upper red data points represent the volumes passing in OR1 and OR3, the two largest torrent flows in the dataset. The red line through this data gently slopes up from the right, indicating that these flows progressively entrained material through the fanhead. When the reach slope angle decreased to 16°, deposition dominated and the flows deposited quickly.

The lower red line is an envelope representing the behaviour of OR2 and FJ4, the two smaller magnitude torrent events. These events entrained most of their material in steeper, source reaches and generally transported most of this material down to the fan with little deposition or entrainment in reaches of intermediate slope angle. The peak volume passing for the torrent events generally occurred between 25° and 15°.

The black line in Figure 5.4 is an envelope representing the behaviour of the hillslope flows. The largest of the hillslope flows, C6, was similar in size to the two smaller torrent flows. The rest of the hillslope flows were much smaller. The hillslope flows started depositing on higher slope angles than the torrent flows, but when they did deposit, they did so more progressively. The peak volume passing occurs at slope angles of approximately 30° to 35°. The intermediate flows are not plotted, as the emphasis of this chapter is the contrast between hillslope and torrent events. The intermediate events, however, display a volume passing behavior that is transitional between the torrent and hillslope events, with peak volume passing values occurring at 25°.

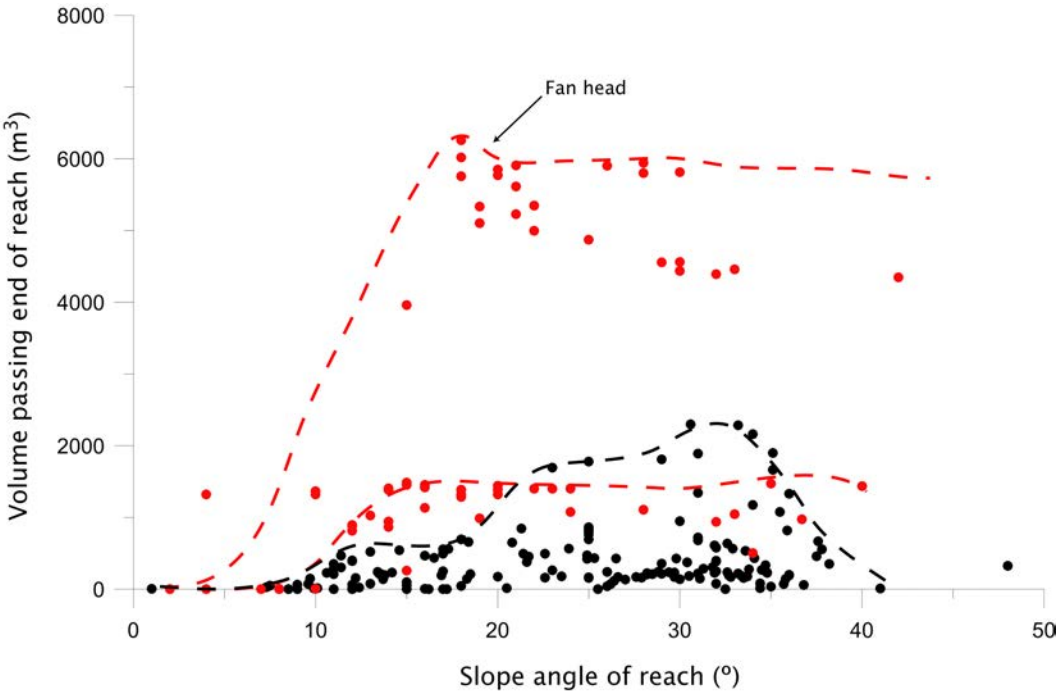

Figure 5.4.: Plot of slope angle of reach and volume passing reach. The red dashed lines indicate the typical volume passing behaviour of the torrent flows. The upper line represents the behaviour of OR1 and OR3, while the lower line is for FJ4 and OR2. The black dashed lines are the typical volume passing behaviour for the hillslope type flows.

5.5. Controls on erosion in each reach

Figure 5.5 shows the yield rates typical of hillslope and torrent events. The average yield rate for erosional hillslope reaches was approximately 2 m^3/m. For torrent type flows, the mean yield rate for erosional reaches was much higher, at approximately 5 m^3/m.

Although the torrent flows have a higher mean erosion rate, this could be due to the reaches simply being wider, rather than a true difference in the mechanism of erosion. To explore this, the net volume balance in each reach was divided by the area of flow to give an indication of the the effective depth of erosion (E'). Taking into account only the erosional reaches, the E' was -1.0 m for torrents, -0.38 m for hillslopes, and -0.85 m for intermediate reaches.

However, if the deposition in each reach is excluded from the volume balance calculated, the measurement becomes simply the eroded volume in each reach divided by the area of the flow. This value was found to be -1.6 m, -0.4 m, and -1.0 m for torrent, hillslope, and intermediate channel types, respectively.

The change in calculated mean depth from -1.0 to -1.6 m for the torrent dataset was unexpected. Upon further inspection of the reach data, the difference was found to be caused by reaches in the torrent dataset with significant amount of erosion and deposition, primarily from levee deposition and smaller surges which halted due to boulder constrictions or vegetation blocking the channel. The differences in E' between the torrent and hillslope flows suggests there is a difference in the mechanism of erosion between flow types.

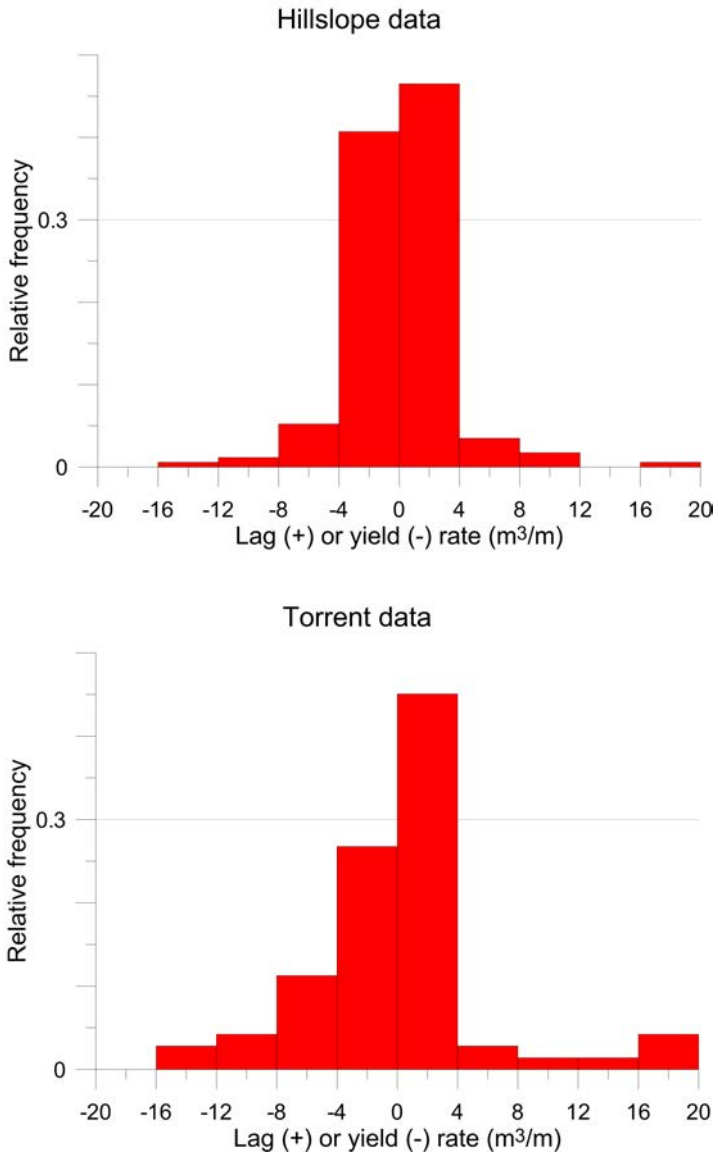

Figure 5.5.: Histogram of deposition (+) or erosion (-) rate for each torrent and hillslope reaches.

5.5.1. Comparison with debris flows in British Columbia

The mean erosion depths calculated above includes material which was entrained from failures in the channel bank or side-slopes, as well as vertical erosion, reflecting channel stability and flow properties.

Accordingly, there have been some attempts in other debris flow studies to estimate entrainment based on the channel geometry and geomorphology (Hungr et al., 1984; Degetto

et al., 2011; D'Agostino and Marchi, 2003). Hungr et al. (1984) suggest tentative estimates for channel debris yield rates for typical stream channels of the southern coast ranges of British Columbia based on bed material, slope angle, and side-slope stability (Table 5.4). The data in Table 5.4 comes from flows that are generally an order of magnitude larger than the flows in this study. The global yield rates[1]of the coastal British Columbia flows were between 6 and 18 m^3 per m of channel length Hungr et al. (1984). In contrast, global yield rates in this study range from 0.5 to 12 m^3/m.

Table 5.4.: Yield rates for stream channels in the southern coast range of British Columbia Hungr et al. (1984) compared to values in this study. For the British Columbia flows, estimated values are based on flows between 10,000 and 55,000 m^3.

Slope (°)	Bed material	Side slopes	Channel debris yield rate (Hungr 1984)	Torrent flows in this study	Hillslope flows this study
20-35	Bedrock	Bedrock or thin colluvium	0-5	1.25-5	2.1-6.5
10-20	Thin debris or soil	Bedrock or thin colluvium	5-10	NA	NA
10-20	Deep talus, colluvium, moraine	Stable	10-15	NA	0.4-3.95
10-20	Deep talus, colluvium, moraine	at repose	15-30	5.0-13	NA
10-20	Deep talus, colluvium, moraine	potentially unstable (active failure)	Up to 200	0.2*	NA

*Based on a single data point.

[1]The global yield rate is defined as the event volume divided by the distance from initiation to point of major deposition on fan.

5.5.2. Influence of bed-type, sideslope height, and slope stability

To see whether or not the factors identified as important in the coast range of British Columbia were applicable to this study, the influence of bed type, side-slope stability, and side-slope height on yield rate for the erosive reaches in the NZ dataset was explored. Bed type was classified as bedrock, thin debris or soil cover, or thick colluvium. Side slope heights were categorized as <5 m, 5-10 m, 10-15 m, 15-20 m, and > 20 m in height. The stability of the channel bank was also categorized. If the reach had no side-slopes, in other words the channel was simply incised into the valley floor or confined by natural levees, the stability category was assigned as "planar". If the reach was characterized by relatively unweathered bedrock or gentle side-slopes, the stability category was "stable". If the side-slopes were composed of talus slopes or scarps near their angle of repose which were stable during mapping, but may be destabilized by saturation, then the category was assigned "at repose". Finally, if translational failures were observed, the stability category was assigned "active failure" .

The relative frequency histograms in Figure 5.6 compare the proportion of reaches in each category for the torrent and hillslope data. The torrent dataset has a higher proportion of reaches with unlimited colluvium, side-slopes between 5 and 15m high, and a larger proportion of side-slopes which are just at their angle of repose.

Figure 5.7 shows how debris availability, sideslope height, and the bank stability category affected entrainment for the erosional reaches in the dataset. Erosion increases as the channel transitions from bedrock to thin colluvium, just as British Columbia, but then decreases as colluvium becomes deeper. This may be due to the decrease in slope angle with increasing debris depth. The amount of erosion also increases with increasing side-slope instability. However, the magnitude of erosion observed is far less than in Hungr et al. (1984).

The comparison illustrates the difficulty in applying yield rates developed in one field area to another field area with a different climatic and geologic setting. The categories in Table 5.4 themselves make comparison difficult. For example, while in British Columbia reaches with bedrock in the channel floor and gully sideslopes were associated with low yield rates, in New Zealand they were associated with large yield rates.

Point sources of sediment from unstable bedrock were the major contributor of debris in the torrent dataset. Slope failures or debris availability explained the large yield rates of the majority of unusually erosive reaches in the dataset. For example, in reach 3 of FJ4, confinement by a more competent, near-vertical layer of schistose bedrock caused the flow to downcut into the channel and undercut a gully wall of very unstable, fault-damaged rock which then failed. Similarly, the upper reaches of C12 had unusually high yield rates of between 6

and 12 m^3/m. This was due to a very active, steep talus slope feeding straight into the gully, which was walled by vertical bedrock on the other side. The flow was forced to downcut and undercut the active talus slope. A mud line 3.5 m above the channel floor showed evidence of a large flow depth and/or vertical erosion in these reaches. This demonstrates the ability of flows to generate high yield rates on very moderate slope angles, if they are confined and have active sources of sediment directly connected to the channel system.

Lower-angle slopes were generally much less erosive in New Zealand than for the larger magnitude flows discussed by Hungr et al. (1984). In British Columbia, lower-angle slopes with unlimited colluvium yielded entrainment of up to 30 m^3/m of length. In New Zealand, entrainment on lower slope angles only occurred when the flow had incised a channel in the head of the fan, which only occurred in the larger-magnitude torrent events (e.g. OR1 and OR3). The factor limiting erosion in these reaches was the capacity of the flow to mobilize sediment, which was controlled by the volume of the passing surge and its moisture content. This behaviour is typical of larger Class 3 or 4 torrent type flows and contributes to the potential for high yield rates.

5.6. Controls on deposition

5.6.1. Volume entering

Confinement is a first order control on whether or not a flow will deposit. Once the flow is unconfined the lag rate is controlled by the second-order controls of slope and the volume entering the reach. Figure 5.8 shows the slope angle of the unconfined reaches in the dataset plotted against the rate of deposition observed in the reach (m^3/m). The size and color of the points indicate the volume entering the reach, with larger and darker dots indicating larger volumes. Notice that the largest lag rates occur on intermediate slope values between 15° to 25°. At slope angles below 15º, the flow is generally spreading out over the fan or unconfined zone and is running out of material for deposition. Hence, the points on the left-hand side of Figure 5.8 are fluvial and outwash deposition (2° to 10°). From inspection of the reach by reach data, the largest deposition rates were from coarse clastic deposition in torrent reaches. The points between 20º to 30º are generally from clastic deposition of hillslope flows.

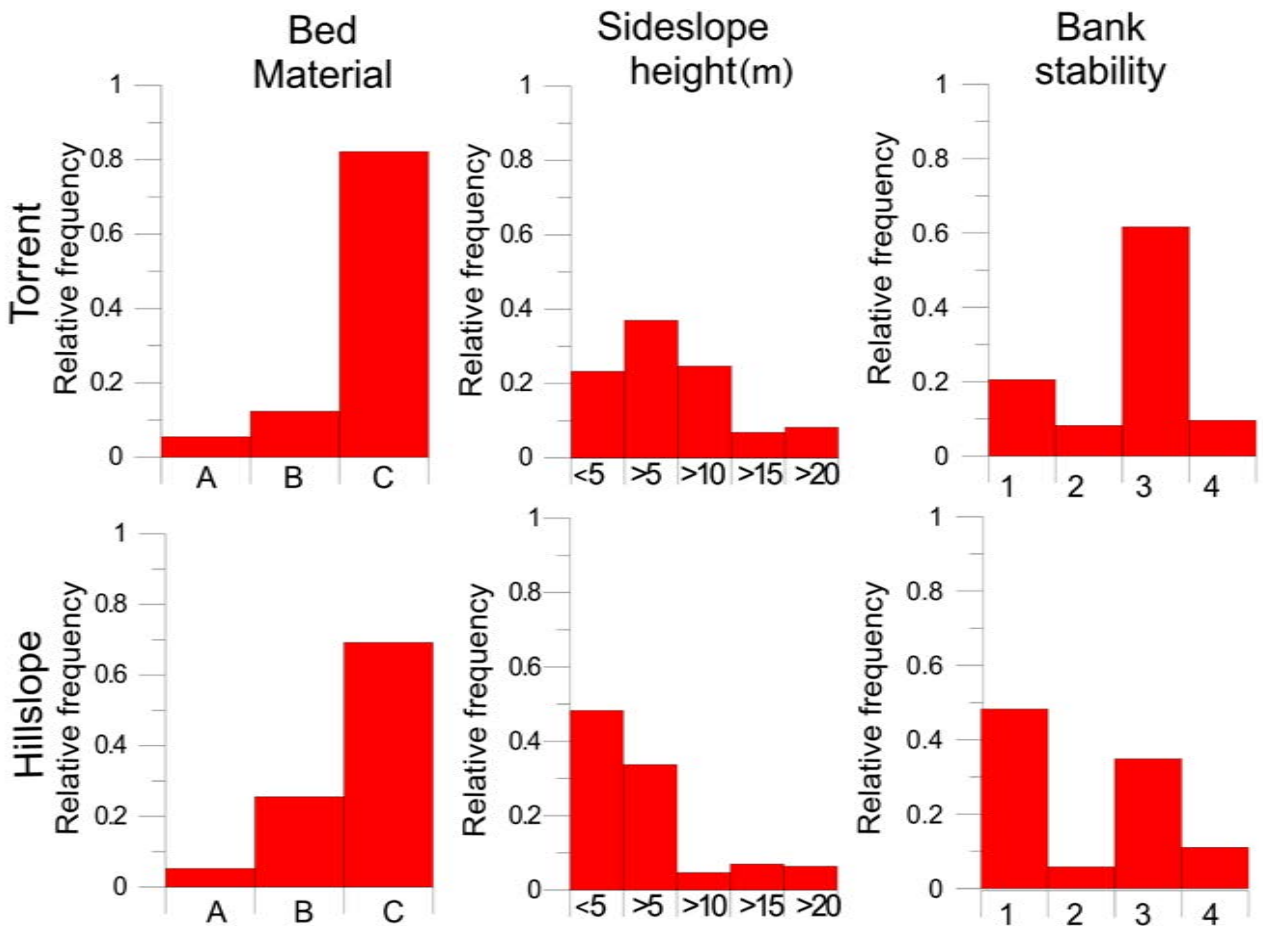

Figure 5.6.: Relative frequency histograms of the proportion of reaches in each category for the torrent and hillslope data. First row: reaches where material in channel floor is bedrock (A), shallow colluvium (B), and deep colluvium (C). Second row: height of channel sideslope height (m). Third row: bank-stability rating of either planar (1), sloped but stable (2), at angle of repose (3), or an active failure was observed (4).

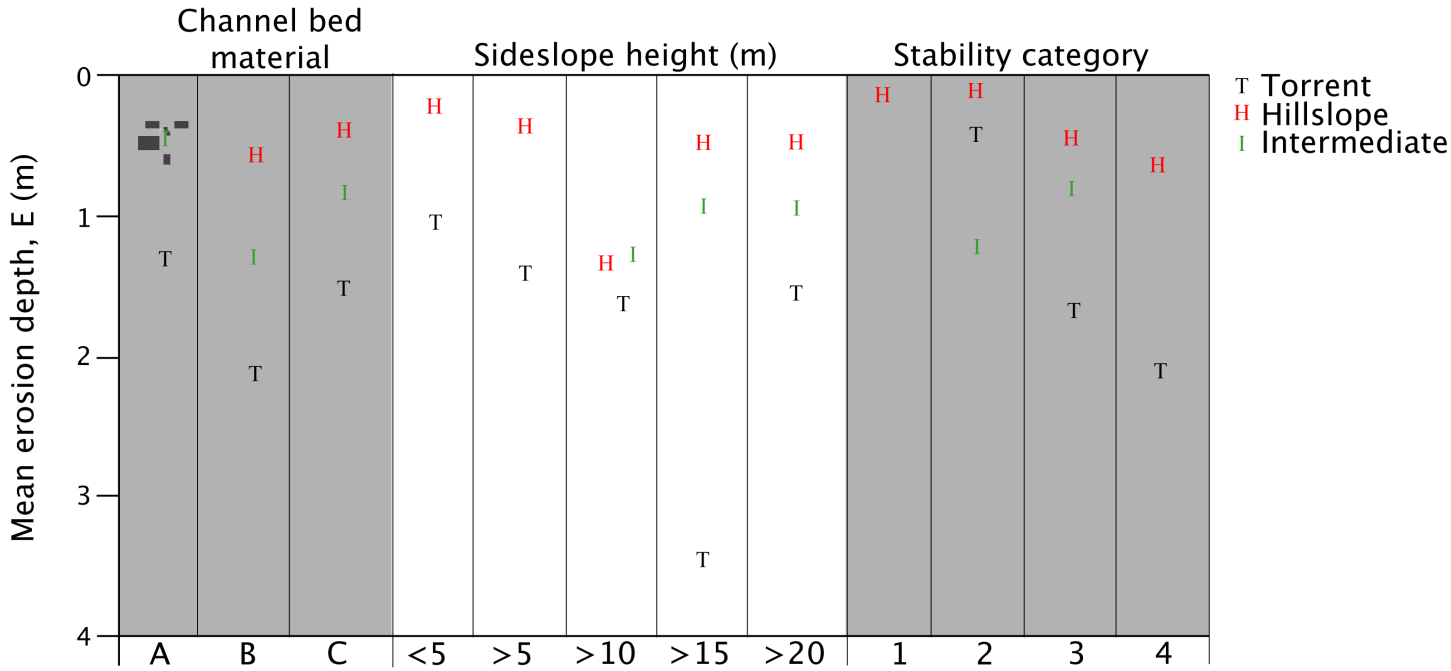

Figure 5.7.: First column: reaches where material in channel floor is- (A) bedrock , (B) shallow colluvium , and (C) deep colluvium. Second column: height of channel sideslope (m) where the sideslopes are <5m , 5-10m , 10-15m , 15-20m, and >20m . Third column: bank-stability rating of either (1) planar , (2) sloped but stable, (3), at angle of repose, or (4) an active failure was observed .

5.6.2. Particle clogging

In transport reaches controls on entrainment were more complex. Unusually high deposition rates in transport reaches were generally associated with clogging of debris at channel constrictions or the halting of smaller surges which were unconfined in the bottom of the channel or gully. The clogging appeared to relate to the channel width and flow depth relative to larger clasts in the flow. While clogging of boulders at constrictions is often observed in alpine debris flow channels (Davies, 1997; Miyazawa, 2001), analyses of on the influence of jamming in debris flow channels remains rare. Previous studies in hydraulics have found that particles in tubes tend to form blockages when the maximum particle size exceeds 1/6 of the pipe diameter (Nedderman, 1992). From a fluvial geomorphology perspective, the 1/6 ratio of maximum particle size in the channel to channel width also seems to be an important threshold. For example, bed stability diminishes in flood events when the ratios of maximum clast size to bed width drops below 1:6 (Zimmermann et al., 2010).

Evidence collected in this study shows the development of clogging in debris flows channels also follows a critical clast size/width ratio. Boulders clogging the channel and subsequent backing up of debris was observed in OR1, OR2, BH2, BH3, and C1. In reach 7 of OR1, boulders choked in an 8 m wide constriction had an a-axis dimension of 1.5 to 1.8 m and a b-axis dimension of approximately 1.5 m. In reach 9, a 2 m diameter boulder created a jam in a 6 m wide constriction. In BH3, a 1.2 m diameter boulder acted as a keystone in a 5 m wide channel. In these examples the channel width to particle diameter ratio varied from approximately 1:3 to 1:5, below the blockage threshold ratio of 1:6. The average channel width in the dataset of both flow types was 4.7 m (hillslope) and 6.4 (torrent). Given that maximum boulder size in torrent reaches was just over a 1.1 m and just over 1 m in most hillslope flows, it is likely that many reaches in the dataset were susceptible to clogging of larger particles at channel constrictions.

The maximum boulder size is also important when a flow transitions from greater to less confinement. The average flow depth for torrent and hillslope style flows was 1.4 m and 1.0 m, respectively, which is very close to the maximum particle size observed in both flow types. According to Davies (1997) small, alpine flows will tend to halt when the flow depth drops below the maximum particle size. This factor helps explain why some smaller surges stopped in transport zones when other, larger surges were able to carry on.

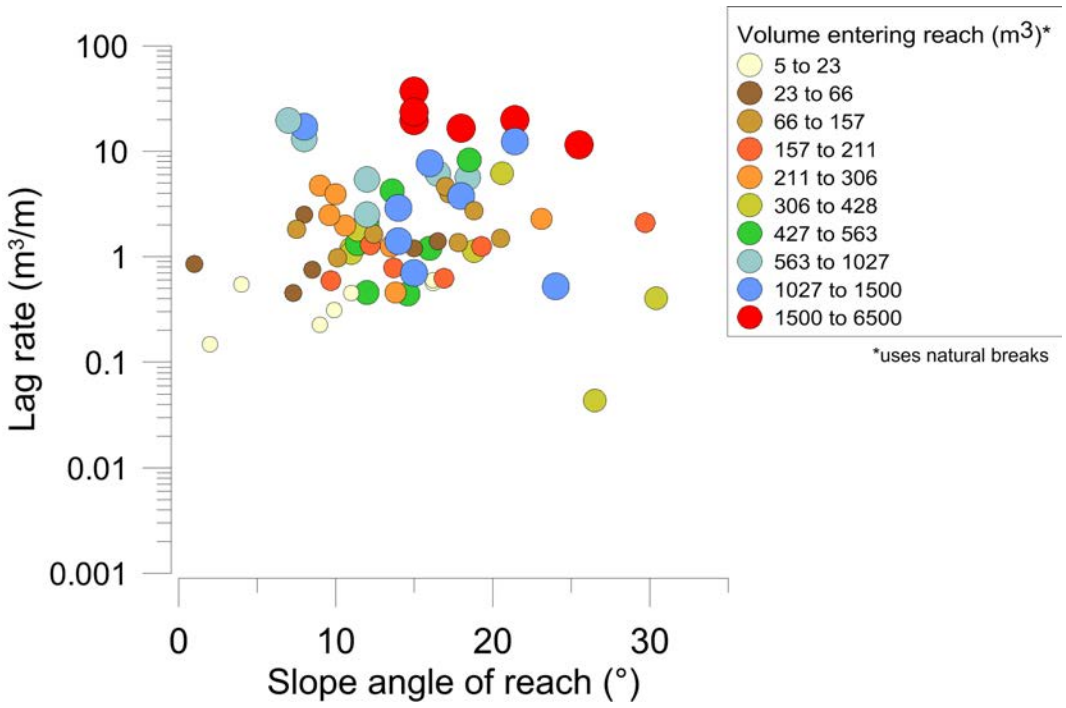

Figure 5.8.: Scatter plot of slope angle of reach and the lag rate in that reach.

5.7. Discussion

5.7.1. Differences between small hillslope and larger torrent events

Many of the differences between hillslope, small, high-frequency torrent events, and larger, lower-frequency torrent events can be explained using the conceptual model discussed in Section 4.2. Hillslope flows are dominant higher in the geomorphic system on open slopes and low order streams. As these flows enter drainage paths lower on the slope (and hence travel down lower angle reaches) they become torrent events. Infrequent, catastrophic, debris flow events may travel down to even higher-order, lower angle channels.

How much material the debris flow erodes or deposits along its path, as well as the physical properties of the material, will determine how far the flow is able to travel. The yield rate will depend on two principle factors; the material available to the flow, and the ability of the flow to entrain that material. Smaller yield rates and values of E' suggest that for hillslope flows studied in Cass and Birch Hill, both material availability and the ability for a flow to mobilize the material were lower than for torrent events mapped in the Orongorongos and Franz Josef. In the hillslope flows, bedrock was closer to the surface, gully sideslopes were lower and

were less prone to large failures. These smaller flows had smaller surges which were inherently less confined, in contact with less erodible material from the channel floor and banks, had lower flow heights and velocities, transmitted smaller amounts of stress to the bed and channel banks. It is also possible that the moisture content of the flows was lower.

In contrast, it appears both material available for entrainment and capacity to entrain material were greater for torrent flows studied, as evidenced by larger E' and yield rates. This may have been caused by a greater frequency of larger failures in the channel and gully walls, the availability of unlimited colluvium at the fan head, greater confinement, and larger peak discharges. However, while most of channelized reaches of torrent flows in this study were floored by deep colluvium, they still displayed small yield rates when compared to larger, more catastrophic events from the literature (i.e. Hungr et al. 1984). Large yield rates observed in this study usually came from point sources of sediment, rather than vertical channel incision.

The depth of colluvium did not appear to be the determining factor in entrainment in this dataset, indicating that erosion was entirely controlled by debris availability. While slope angle and degree of confinement were first-order controls on whether or not sediment could be mobilized, second-order controls such as clast size (both in flow and bed) and clogging may have also been important.

Further, the entrainment behaviour will differ depending on the size of the overriding surge. Channel armoring could limit entrainment of small surges, but not constrain larger surges which have a larger D_{90} and higher velocities. Smaller surges may flow through channel constrictions, but are more likely to halt due to low confinement ratios. A larger surge may be more prone to clogging at channel constrictions, but it also has more power to abrade the channel walls, entrain large clasts already present in the bed or sidewalls, and override smaller constrictions. Conceptually then, certain characteristics of the channel may inhibit entrainment, up to a critical point where the flow discharge is capable of overcoming them.

5.7.2. Relationships between torrent and hillslope debris flows

While torrent and hillslope flows may be different, they exist along a continuum; a hillslope flow high on a slope may enter a channel and evolve into a torrent. In fact, many small translational failures and hillslope events observed elsewhere have grown into large, catastrophic debris flows. The size of the initial event sometimes has little to do with how a debris flow evolves (King, 1996; Jakob and Jordan, 2001). What controls whether or not a hillslope flow will evolve into a torrent flow, then, is a question of some importance.

Sediment availability in the channel could be one factor. If a small hillslope flow or

translational failure enters a channel, but there is not enough sediment stored in the channel for the flow to entrain material and grow in volume, a debris flow will not be produced. This is the "supply limited" concept proposed by Bovis and Jakob (1999). In this type of supply-limited situation, a triggering event will not produce another debris flow until the channel has "recharged" with sediment from adjacent flows.

However, some research has found that larger accumulations of in-stored sediment actually inhibit a joining hillslope flow or bank failure from turning into a torrent event (Brayshaw and Hassan, 2009). Looking at channelized debris flows which had mobilized from translational failures and hillslope flows on gully side slopes in British Columbia, Brayshaw and Hassan (2009) found that the deeper the debris stored in the reach where the landslide entered the channel, the larger the landslide (or hillslope flow) required to mobilize a debris flow. Thus, failures into scoured channels were actually more likely to continue downslope than channels that had been recharged. Gullies that experience frequent flows were scoured, which in turn perpetuated the high frequency of smaller flows.

The findings of Brayshaw and Hassan (2009) also imply that if a debris flow occurs in a channel which has been stable for a long period, the event will likely be very hazardous, as both the initiating failure and the amount of sediment available for entrainment will be large. Following this rationale, logging, fire, or any other sudden change in channel processes will be particularly hazardous. The event may destabilize the starting zone, channel banks, and a large volume of in-channel sediment simultaneously. It may also mobilize multiple tributary gullies (i.e hillslope flows), leading to increased discharges in lower order reaches and larger potential for erosion, even in reaches that are primarily transport or depositional in smaller events.

In a related way, debris flow mitigation measures which stabilize in channel sediment such as sabo dams or ring nets need to be treated with caution. Such measures may reduce the frequency of debris flows by inhibiting the mobilization of small events, but in practice might simply shift the debris flow magnitude frequency response of the catchment to rarer, but much more catastrophic flows (Bloomberg and Davies, 2012; Davies and Hall, 1992). Adequate maintenance and clearing of debris trapped behind the artificial obstruction is pivotal.

None of the flows in this dataset originated from large, anthropogenically influenced (i.e. logging or fire) failures. Nor were the paths in this dataset altered by debris flow mitigation structures, as is the case with many other debris flow studies. Therefore, this study represents debris flow catchments in a relatively natural state, where frequent debris flows of class 1, 2, and 3, both scour and refill parts of the debris flow path.

In places where debris flows are frequent events, the research of Brayshaw and Hassan

(2009) suggests that smaller initial failures will be needed to trigger an event, but there will be less in stored sediment available for entrainment. Therefore, such flows will typically have smaller average yield rates than more catastrophic events. They will also tend to runout far less, coming to rest on the proximal fan, or even on intermediate slope angles in transport reaches.

This may help explain entrainment behaviour observed in this dataset. In this study, the average lag rate in transport reaches at intermediate slope angles was 0.3 m^3/m. It is easy to imagine many of these reaches becoming sources of erosion in a larger event. For example, the smallest flow mapped in the Orongorongos, OR2, deposited near the start of the geomorphic fan. In all the larger flows in the Orongorongos (larger class 3), the proximal fan was an important zone of entrainment.

These factors, as well as field observations indicate that small class 1, 2, and 3 debris flows (using classification system of Jakob 2005), especially in unanthropogencially influenced catchments, have the potential for extremely variable erosion and deposition behaviour. These small, yet frequent flows may exhibit lower velocities and lower moisture contents than many higher-magnitude flows, and hence may stop or begin to deposit in response to small changes in confinement or slope. The evolution of the flow is also subject to local channel conditions, such as point sources of sediment in side-slopes and the degree of armoring of the channel bed. The state of the channel, and the subsequent behaviour of the flow, is dependent on whether or not the last debris flow event scoured or refilled key areas along the travel path.

5.8. Conclusions

This chapter compared the hillslope, torrent, and intermediate reach data. Slope and confinement were the primary controls on flow behaviour for each type. Hillslope flows had smaller width to depth ratios than torrent events, indicating less confinement and smaller discharges. The hillslope flows also began to deposit at higher slope angles. Slopes of erosional and transport reaches were significantly higher in the hillslope than in the torrent flows.

While deposition for both flow types was controlled primarily by slope and confinement, clogging at channel constrictions was also found to be important. This was generally found to occur when the maximum boulder size was over 1/6 of the channel width.

Differences in erosion depth between hillslope and torrent flows suggest that the method of entrainment differed between the flow types. Lower and less extensive side-slopes in hillslope events meant they were not supplied by large translational failures in gully walls, but instead

were supplied by a more progressive raveling from adjacent talus slopes. In addition, less confinement in hillslope flows inhibited debris mobilization and encouraged deposition at steeper slope angles.

While the distinction between hillslope and torrent events was generally useful, the complex categorization of confinement type was not. There was no significant difference in erosion behaviour found between partially confined reaches and unconfined ones, which suggests that partially confined reaches can simply be treated as unconfined reaches in future work. The distinction between confined in channel and confined in gully reaches could also be dispensed with, as there was no significant difference in erosion behaviour between these two confinement types.

A comparison of torrent events in this dataset with others from the literature reveals that yield rates for the New Zealand data are substantially lower than those observed in larger, catastrophic debris flows. Higher-magnitude, lower frequency events travel further, often down higher order stream channels with large amounts of in-channel colluvium available for entrainment. It is possible that greater water availability and larger discharges in these larger events may help mobilize this sediment. It is also possible that the frequency of events in the field areas studied could explain the lower yield rates, as the events represent relatively high frequency flows which scour the channel and prevent large amounts of sediment from accumulating.

While the geology and the morphology of the channel can explain some of the entrainment and depositional behaviour between torrent and hillslope flows, there are also differences in key flow parameters and rheology. Field observation of a very small hillslope flow in the field, as well as observations from other hillslope flows, suggests that these flows may have a higher average solids concentration than torrent-type flows. Although we did not sample any flows as they occurred, lower solids concentrations and deeper flow depths in the torrent-type flows may facilitate higher velocities, mobility, and lateral spread. These differences should be expressed in the friction parameters needed to simulate the different flow types. This is the subject of the next chapter.

6. Modelling travel distances of small debris flow events in New Zealand

This chapter applies two models for debris flow travel distance, DAN-W and UBCDFlow, to the field data described in previous chapters. Input parameters in DAN-W are back-calculated so that simulated travel distances match those observed in the field. These back-calculated input parameters are shown to be higher than those associated with most large, channelized debris flows discussed in the literature, but lie within the range of smaller channelized and hillslope flows found elsewhere (Brideau et al., 2006; Bertolo and Wieczorek, 2005; Rickenmann, 2005). The large scatter in input coefficients for small events is thought to be caused by the increased susceptibility of small surges to changes in confinement, clogging at constrictions, and being impeded by vegetation. Smaller friction coefficients for larger flows reflect lower depositional slope angles and increased mobility.

The New Zealand debris flow events are also modelled with UBCDflow. Despite being an empirical model developed in a field area with a different geology and climate, the model predicted the event volumes and travel distances of the torrent events well, but generally over-predicted the travel distance of the hillslope flows. Further, UBCDflow is limited in its ability to help the modeler visualize a debris flow event. Finally, a method to combine the strengths of both DAN-W and UBCDflow is presented. The results from this chapter should be useful to hazard modelers performing preliminary hazard analysis in the field areas studied.

6.1. Introduction

Predicting debris flow travel distance, along with event magnitude and velocity, are primary challenges for debris flow investigators. These predictions rely on careful observation and

interpretation of the potential flow path, as well as the investigator's prior experience in the field area. The qualitative interpretation and judgement of the investigator are often supported by empirical and semi-empirical modelling tools which provide quantitative estimates of important debris flow parameters such as travel distance and discharge. While each model is limited, the models are never-the-less important decision support tools in hazard mitigation. Two of the most popular models used are DAN-W and UBCDflow. DAN-W is a 1-D modelling software package based on the shallow water equations proposed by Savage and Hutter (1989) (Hungr, 1995). UBCDflow is an empirical model based on reach data from torrent and hillslope events in the Queen Charlotte Islands (Fannin and Wise, 2001).

Both of these models were developed in British Columbia, Canada. Like New Zealand, British Columbia's mountainous terrain and mid latitude position in the roaring 40s make it prone to debris flows and other types of landslides. UBCDflow has been used in several areas of British Columbia (Fannin and Wise, 2001; Busslinger, 2010), while DAN-W and similar shallow-water equation based models have become standard modelling tools used throughout the world. In both North America and Europe, investigators have calibrated these models with many moderate to large magnitude debris flow events (Rickenmann, 2005; Naef et al., 2006; Bertolo and Wieczorek, 2005; Medina et al., 2008; Hurlimann et al., 2008).

While there have been some studies devoted to debris flows in New Zealand (McSaveney and Davies, 2005; McSaveney et al., 2005; McSaveney and Glassey, 2002), this work has tended to focus on large-magnitude, relatively low-frequency events. No quantitative model is widely used or calibrated to field data, especially for high frequency, low magnitude events like those mapped in this study. This chapter begins to fill this gap in knowledge by applying UBCDflow and DAN-W to New Zealand debris flow paths.

6.1.1. Background to DAN-W

Many common mathematical models of landslide motion, including DAN-W, are based on the shallow water equations (Savage and Hutter, 1989). These equations are derived by depth-integrating the Navier-Stokes equations. The assumptions of the shallow water equations are:

- The landslide has a small aspect ratio (the length is much greater than the depth).
- The path is fairly smooth.
- The interior of the landslide can be described by constitutive rules. In DAN-W, usually either Savage-Hutter, Rankine, or modified Savage-Hutter rules are used.

- There is a nearly uniform velocity profile throughout the depth (the failed mass moves as a slightly deforming block or plug).
- Flow resistance takes place at the bed only.
- The density of the landslide remains constant.
- Pressures within the landslide mass are hydrostatic

In an overview of the limitations of the Savage-Hutter model in the context of snow avalanches and laboratory sand avalanches, Hutter et al. (1994, 2005) found the model was capable of simulating small sand avalanches in a flume. However, even in a simplified laboratory experiment, the predictive power of the model was limited. While the model performed relatively well in experiments with a smooth bed surface, the authors cautioned that the model did not perform well when the bed was bumpy due to the violation of the assumption that the velocity profile is fairly uniform throughout the flow (Hutter et al., 2005).

While the motion of laboratory scale avalanches violate some of the assumptions of the shallow water equations, debris flows violate nearly all of them. The channel bed is typically very rough, much rougher than in flume experiments. The concentration and bulk density of the flow change as the flow moves downslope. By definition, shearing is pervasive through the body of a debris flow, violating the assumption of a relative uniform velocity profile with a small zone of shear at the base. Pressures inside the flow, especially at the base, are above hydrostatic (Iverson, 2005b; Sassa et al., 2004; Wang et al., 2003). Entrainment and deposition of material causes the flow to change solids concentration. Segregation will cause some parts of the flow to have different particle sizes and solids concentration. Despite all these limitations, the use of the shallow water equations endures because they are computationally simple, convenient, and flexible. Most popular mathematical models used to predict debris flow and avalanche motion use them.

Shallow-water equation-based models can broadly be classified into two types: an "equivalent fluid" approach which requires extensive calibration with field events (Bertolo and Wieczorek, 2005; Brideau et al., 2006; Hungr and McDougall, 2009; Medina et al., 2007; Pirulli and Sorbino, 2008), and more complex, but more mechanically sound two-phase approaches (Iverson and Denlinger, 2001). While the latter do not require empirical calibration in different field areas, they do require extensive knowledge of flow parameters that are rarely known in the field. The more simplistic equivalent fluid approach models the friction on the bed as sliding friction governed by a specific rheological friction model. The flexibility to back calculate

the frictional coefficients used in the chosen rheological friction model makes the use of the "equivalent fluid" method more common in practice.

One of the most common commercial equivalent fluid models is the Dynamic Analysis model (DAN) introduced by Hungr (1995). The DAN-W software package is its current, GUI-based, 1-D incarnation. In DAN-W, the slide mass is represented by a number of blocks which contact each other and are free to deform as they move downslope. Assuming the conservation of momentum and mass, the model solves for the longitudinal displacement of the block and the flow height normal to the path at each time step. The solution is referenced to a Langrangian mesh in curvilinear coordinates (Hungr, 1995). The net driving force acting on each block consists of the tangential gravitational driving force (G), the basal resisting force (T), and the tangential internal pressure (P) (equation 6.1).

$$F = G + P - T \tag{6.1}$$

P includes pressure contributed from adjacent blocks as well as the internal resistance to deformation. This internal resistance depends on the lateral pressure coefficient, κ, which is the ratio between the tangential and normal stress in the flow. This depends on the magnitude of strain and the internal friction of the flowing material.

The methods for calculating κ are based on a constitutive law chosen by the user. In DAN-W, the user chooses between Savage-Hutter, a modified Savage-Hutter, and Rankine methods. The modified Savage-Hutter method is used in this study (this is the default in DAN-W and is recommended by (Hungr, 2003)). The value of κ for each block depends on whether the block is being compressed (passive) or extended (active). The variables used to calculate κ are the internal friction angle (entered by user), the magnitude of strain for the time step in question, and a stiffness coefficient, although the latter has little effect on the model (Hungr, 1995). The equations that DAN-W uses to calculate the P component due to Coulomb-friction are:

$$P = -k\,\gamma\,\frac{d_h}{d_s}\left(1 + \frac{a_c}{g}\right)\,H\,B\,cos\alpha\,ds \tag{6.2}$$

where d_h/d_s is the pressure gradient, γ is the bulk density, $a_c$is the centrifugal acceleration, g is gravity, H is the flow height, B is the flow width, θ is the slope angle, ds is the infinitesimal width of the boundary element; and

$$k = k' + S_c\,\Delta\epsilon \tag{6.3}$$

where k' is the value of the earth pressure coefficient at the last time step, S_c is the stiffness coefficient, and $\Delta\epsilon$ is the magnitude of strain. The value of the stiffness coefficient is calculated differently depending on whether the block is under extension or compression by:

$$S_{extension} = \frac{k_p - k_a}{0.025} \; or \; S_{compression} = \frac{k_p - k_a}{0.05} \tag{6.4}$$

where k_p is the passive earth pressure coefficient and $k_a$is the active earth pressure coefficient. The value in the denominator is set by the user (the default and recommended values are 0.05 and 0.025, as shown).

The basal resistive force used (T in equation 6.1), depends on the specific rheology chosen to model the flow. This is one of the most important considerations in the modelling exercise. DAN-W provides a choice between seven rheologies: plastic, frictional, Newtonian laminar, turbulent, Bingham, Coulomb viscous, and Voellmy. The discussion below considers the frictional (Equation 6.5 and 6.6) and the Voellmy rheologies (Equation 6.7). For the purely frictional rheology,

$$T = tan\,\phi\,\gamma\,H\,\cos\theta \tag{6.5}$$

where T is the resistive force, ϕ is the friction angle, H is the flow height, and θ is the slope angle. The friction coefficient term (μ) in the Voellmy equation (Equation 6.7) is related to the friction angle Equation 6.6.

$$\mu = \tan\phi \tag{6.6}$$

From a practical perspective, the frictional rheology is limited because the flow accelerates and decelerates much too quickly compared to debris flows observed in the field (Rickenmann, 2005). The flow velocities cannot be back-calculated independent of the travel distance.

The Voellmy equation (Equation 6.7) resolves this problem by the addition of a turbulent drag term ($[\gamma V^2]/\psi$). The Voellmy equation was originally developed to model the travel distance of snow avalanches, and has since been used to model many other types of landslides (Rickenmann, 2005).

$$T = \mu\,\gamma\,H\,\cos\theta + \frac{\gamma\,V^2}{\psi} \tag{6.7}$$

where V is the velocity of the flow. The coefficient in denominator of the turbulent drag term, ψ (m/s^2), is analogous to a Chezy term (C) used in hydraulics.

The introduction of the second term makes it possible to manipulate the velocity behavior of the simulation somewhat independently of the travel distance. Since the turbulent term dominates the frictional behaviour at high velocities and the Coulomb term dominates at low velocities, the Voellmy rheology allows the model to be calibrated to estimates of both flow velocity and the travel distance. Very low values of ψ will dampen flow velocities, while large values will make the flow velocities more similar to those observed if the flow was modeled with a frictional rheology (e.g. the flow will both decelerate and accelerate quickly). This flexibility and the popularity of the Voellmy rheology in commercial practice are the primary reasons this rheology was chosen in this study.

While DAN-W was designed to simulate some of the physical mechanics of flow motion, in practice, the simulations are highly idealized. In reality, the debris volume mapped in each flow may have been deposited by a series of individual surges of much smaller volume. Some of this material may have been in the initial failure, but much of the volume may have been entrained along the flow path. This study, however, uses a simple approach where the flow is modelled as a single surge with a starting volume equal to the entire deposition volume of the flow. Voellmy frictional coefficients were systematically altered until the simulated travel distance approximately matched the travel distance mapped for the coarse clastic material. Details regarding the methodology are discussed further in Section 6.2.1.

This simplified approach allows comparison of empirical, back-calculated friction values for flows in this dataset with others around the world and has been used by various investigators (Hürlimann et al., 2003; Bertolo and Wieczorek, 2005). The model should be treated not as a rigorous simulation of the mechanics involved in the flow, but rather as a decision support tool which allows the user to model various scenarios. This may add weight to judgement based on geomorphic evidence.

DAN-W also allows the user to set a maximum erosion depth for each reach. As a block passes over this reach, a fraction of this depth (and hence, volume) proportionate to the passing discharge is eroded. The total volume is only removed once the entire slide mass has passed over the given reach. The mass of the block is increased by the amount of volume entrained. As this material is eroded, a momentum correction is applied to account for the momentum required to accelerate the added increment of stationary mass, ΔM, to the current velocity of the block, v. This is achieved by subtracting a quantity $\frac{\Delta M}{\Delta t}$v in each time step for the duration of Δt from the right side of Equation 6.1 (Hungr, 2003). Modelling entrainment adds an additional level of complexity that is addressed for a sub-set of flows in Section 6.4.1.

6.1.2. Background to UBCDflow

UBCDflow was briefly mentioned in Chapter 2, but the background to the model is expanded here. UBCDflow is an empirical-statistical model based on 131 events and 533 channel reaches in the Queen Charlotte Islands, B.C. (Fannin and Wise, 2001; Fannin and Rollerson, 1993). As discussed in Chapter 3, the methods used to collect the original field data in the Queen Charlotte Islands were very similar to the ones used in this study.

The terrain in the Queen Charlotte Islands is a heavily dissected plateau with elevations of up to 700m. The climate is cool and maritime with a annual precipitation of approximately 1 to 4 m/year. The geology consists of metamorphosed volcanics mantled by Pleistocene glacial soils and colluvium (Fannin and Wise, 2001).

Given a user-defined entry volume, the model predicts whether the flow will entrain material, resulting in a positive addition to flow volume (+dV), deposit material (-dV), or transport material (0 change) in the reach (note the change is sign convention from yield and lag rate terminology). This determination is based on the mode of flow (confined, unconfined, or transitional) and the slope angle of each reach (Figure 6.1). The magnitudes of erosion or deposition are determined by the regression equations in Table 6.1.

As an example, FJ4 will be used to illustrate how UBCDflow determines erosion, transport or deposition. The observed and modelled volume passing the end of each reach is shown in Figure 6.2.

The user must first enter a starting volume for the flow. Approximately 500m^3 of erosion was mapped in the first, source reach of FJ4. This volume was modelled as the starting volume in UBCDflow. The material then flowed down through five consecutive confined reaches with slopes angles between 34° and 28°. The flow eroded material through these reaches because according to the UBCDflow decision tree (Figure 6.1), confined reaches between 10.5° and 55° will be erosional.

FJ4 then entered an unconfined reach at a slope angle of 24°, which according to the rules of UBCDflow, is treated as a transitional reach. As the slope angle is between 20.5° and 55°, the flow volume did not change (see the right-hand branch in figure 6.1). From this point, the modelled event flowed down a series of confined reaches with slope angles above 10.5°, and thus erosion was predicted. In reach 8, the flow went from confined to unconfined (a TF reach) on a slope angle of less than 20.5°, and therefore UBCDflow modeled deposition. The next two reaches were confined and over 10.5° (see middle branch of 6.1), and thus were predicted to be erosive. Finally, the flow became unconfined on a 14° slope, which is classified as a transitional reach (TF). As the slope angle was below 20.5°, deposition was predicted. The

flow was predicted to run out of material by the next reach. Therefore, UBCDflow modelled the flow to stop somewhere within this reach.

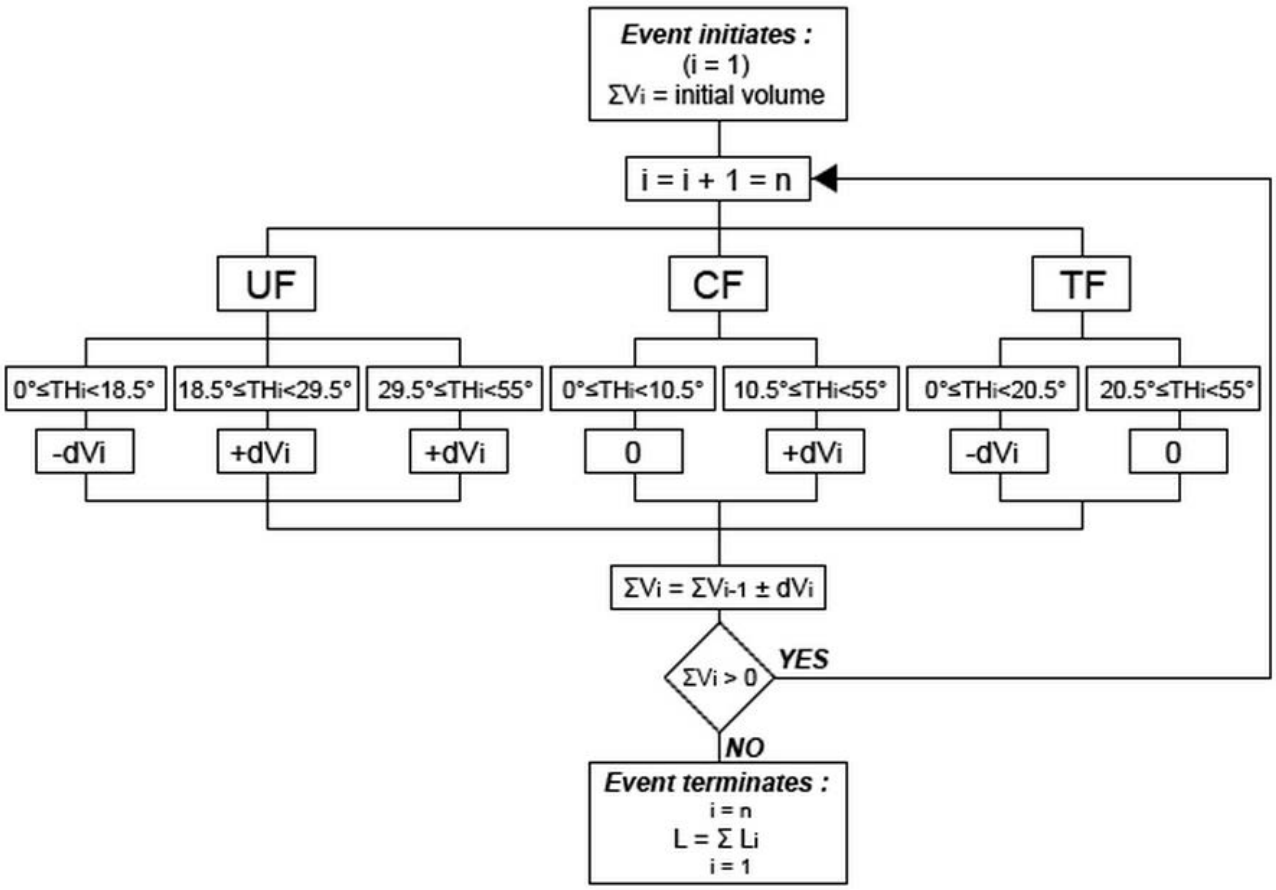

Figure 6.1.: Decision tree explaining which regression equation UBCDflow uses to calculate volume change in each reach (Fannin and Wise, 2001).

Table 6.1.: Regression equations used by UBCDflow (Fannin and Wise, 2001).

Flow behaviour	Mode of Flow	Regression equation	No. of reaches	R^2	Slope angles, Th_i (°)
Unconfined	Deposition	$\ln(-dVi) = -0.514 - 0.988 \ln(W_{d_i}) - 0.101(BAF_i) - 0.731 \ln(L_i) + 0.0155(Th_i)$	127	0.88	0-24
Unconfined	Entrainment	$\ln(+dVi) = 1.13 \ln(W_{e_i}) + 0.787 \ln(L_i) - 0.0636 \ln(\Sigma V_{i-1})$	94	0.76	19-29
Unconfined	Entrainment	$\ln(+dVi) = 0.728 + 1.31 \ln(W_{e_i}) + 0.742 \ln(L_i) - 0.0464(Th_i)$	82	0.79	30-55
Confined	Entrainment	$\ln(+dVi) = 0.344 + 0.851 \ln(W_{e_i}) + 0.898 \ln(L_i) - 0.0162(Th_i)$	82	0.76	10-5
Transitional	Deposition	$\ln(-dVi) = -1.54 \ln(W_{d_i}) - 0.90 \ln(L_i) + 0.123(BAF_i)$	191	0.95	0-20

The subscript i denotes the reach in question, while i-1 denotes the previous reach. $W_{e_i}$is the reach width (m). $BAF_i$is the Bend Angle Function defined by $cos(dTh_i)\, cos(dAZ_i)\, ln \sum(V_{i-1})$, where dTh_i is the absolute value of the , change in slope angle (°), dAZ is the absolute value of the change in reach azimuth (°), and $\sum V_{i-1}$ is the volume entering the reach in question (m^3). $L_i$is the reach length (m). $Th_i$is the slope angle of the reach (°).

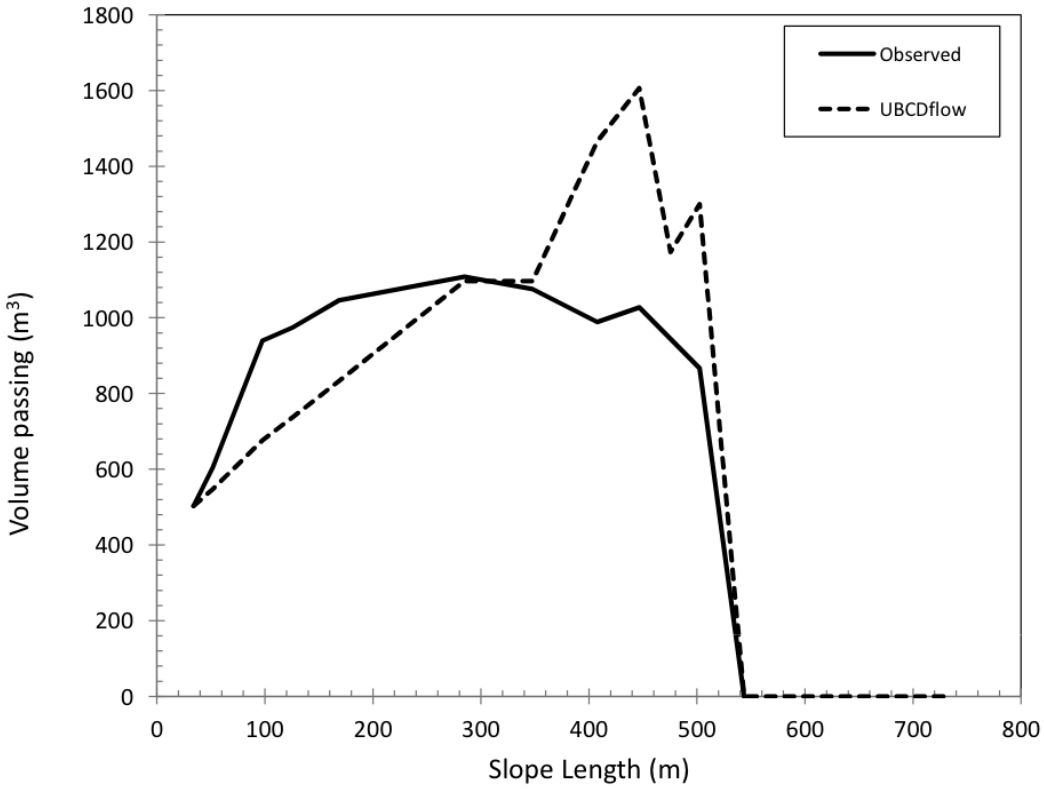

Figure 6.2.: Plot of volume passing the end of each reach based on field observations (observed) and model (UBCDflow).

6.2. DAN-W analyses

6.2.1. Methods

The methodology used to calibrate input parameters in DAN-W is discussed below. Calibration proceeds by finding a pair of "best fit" μ and ψ—the pair which, when using the Voellmy rheology in the DAN-W simulation, best approximate the behavior observed in the field (Mckinnon, 2010). Ideally, the model approximates the velocities, travel distance, flow heights, and depositional shape observed in the field. However, in many studies (including this one) not every relevant flow parameter is known. Even if all these parameters are known, it is often impossible to match all of them exactly. For example, the coefficients used may simulate the flow depth well, but not the velocities or travel distance. The modeler must choose which aspects of the behaviour are most important. This study focuses on matching the two most important parameters in determining the flow severity; velocity and travel distance.

6.2.1.1. Flow path data

The first step in using DAN-W is to prepare an elevation-distance slope profile for the model debris flow to run down. Data points containing elevation and horizontal distance need to be chosen based on data collected in the field or topographic data. To do this, the slope distance (L_s) of each reach was converted to horizontal distance (i.e. horizontal length or map length, L_h) by $L_s \cos\theta$, where θ is the slope angle of the reach. The vertical drop for each reach was calculated by $L_s \sin\theta$. In this way, data points representing elevation above the toe and horizontal distance from the initiation of the debris flow were calculated. In order to model the travel distance beyond the mapped extent, elevation-distance profiles derived from GoogleEarth topographic data were added to these mapped profiles. The mapped field data were supplemented with data from GoogleEarth in mapped flows OR1, OR2, OR3, OR4, C6, C1, C2, C3, and C11. In these flows, the entire starting zone of the flow could not be mapped because access was too dangerous.

Each point in the DAN-W elevation-distance profile also requires a flow width (i.e. the width of the flow at the beginning and end of each reach). This was inferred from field sketches and estimates of flow width in the field. For the initiation zone not traversed in the field, the widths were based on air-photo and GoogleEarth imagery. The widths of reaches beyond the mapped extent were based on the width of the flow in the final reach mapped.

The next step was to input the top profile of the landslide mass—i.e., the starting mass of the material. The volume of each flow was modelled as a slab of material of uniform thickness lying in the starting zone. The length and width of the starting zone were based on the field data collected or GoogleEarth imagery, as noted above. Each starting slab is split up into 50 slices—the model elements that interact as the flow proceeds downslope. The thickness of the slab was set to accommodate the volume of the flow.

Once the data input is complete, DAN-W constructs the flow paths geometry by interpolation between the input data points using a spline function. Figure 6.3 shows a screen shot of the resulting flow path and starting slab of flow FJ4, as well as the final deposit for the simulation.

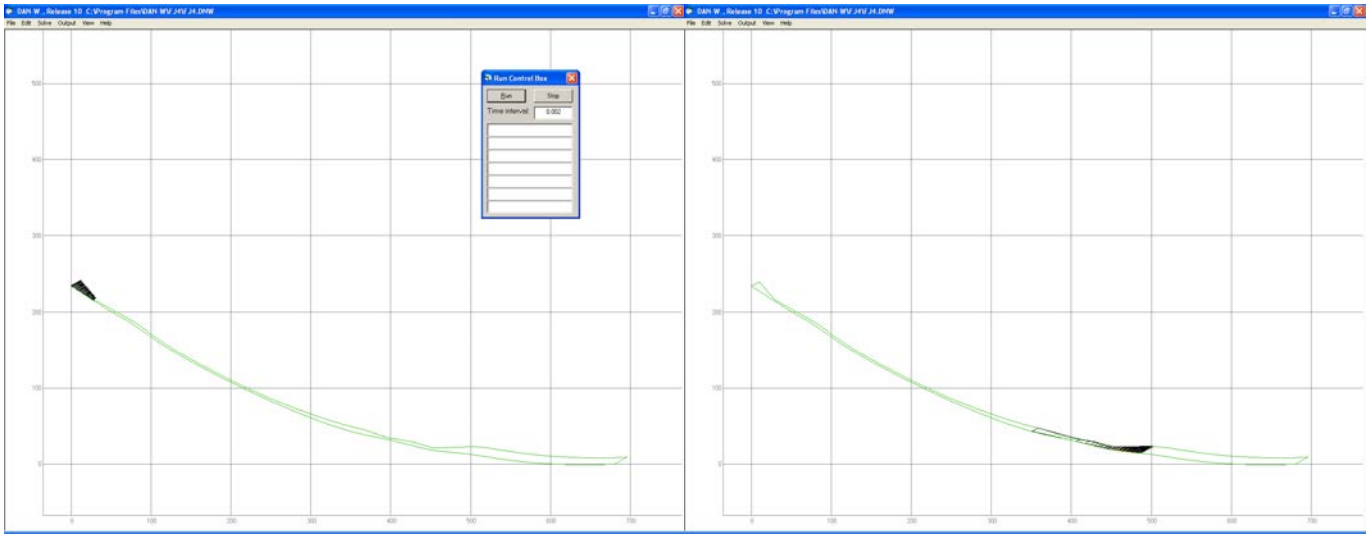

Figure 6.3.: Left-screenshot of the starting slab and flow path of FJ4 in DAN-W. Right-Screen shot of final deposit.

6.2.1.2. Other DAN-W parameters

DAN-W also requires that the internal friction angle and flow density of the flow material be defined. These parameters were set to 35° and 2000 kg/m^3, respectively. These are the DAN-W defaults and the parameters recommended in the DAN-W manual (Hungr, 2003). The program also allows the user to set the constitutive law used to calculate the pressure term. This was set to the modified Savage-Hutter, as recommended by Hungr and McDougall (2009). The rest of the parameters required by DAN-W follow the default values for the program, and are summarized in Table 6.2.

Table 6.2.: Input parameters in DAN-W for each simulation

Input parameter	Value
Volume of starting mass	Equal to mapped volume of deposition (m^3)
Topography	Surveyed and supplemented by topographic data from GoogeEarth® in inaccessible reaches (m)
Number of slices	50 slices
Time step	0.002 seconds
Internal friction angle	35°
Density	2000 kgm^{-3}
Centrifugal force setting	On
Tip ratio	0.5
Stiffness coefficient	0.05
Stiffness ratio	5
Pressure term	Modified Savage-Hutter
Lower limit of (ψ)	10 ms^{-2}
Upper limit of (ψ)	Value which gave a peak velocity of approximately 10 ms^{-1}

6.2.1.3. Travel distance

The choice of an appropriate travel distance to match in the simulation depends on the judgement of the investigator. Travel distance could be defined as the horizontal distance from the head of the failure to; the maximum extent of deposition, the extent of coarse clastic material, or extent of the main surge (Prochaska et al., 2008a). Most studies do not report which definition they use, although if the observations came from remotely sensed data, travel distance is likely to be based the maximum extent of any material deposited by the flow. This will take into account material that has been remobilized by subsequent, small surges or has been fluvially reworked after the main event. This material is less important to engineers because the highest impact forces and hazard accompany the main surge, not subsequent smaller surges

or stream flow. The inclusion of outwash also conflates mass-movement with fluvial processes. For this reason, the friction coefficients in this study were back-calculated using the distance from the head of the failure to the end coarse clastic deposits.

6.2.1.4. Calibration procedure

Once the path geometry and other parameters of DAN-W were set, the μ and ψ were altered by trial and error until the simulated travel distance matched the travel distance observed for the coarse clastic debris.

As noted above, while both the μ and ψ influence the momentum of the flow, μ primarily determines the travel distance because the friction term is dominant during unconfined runout at lower velocities. It was the more important coefficient calibrated in this study, as the travel distance of the coarse clastic material was known with some confidence, while flow velocities were poorly constrained. Hence, μ was first adjusted (to the second decimal place) using a ψ value of 100 ms^{-2}.

Once the approximate best-fit μ was determined, ψ was adjusted to achieve reasonable flow velocities. Unless the flow is observed directly, estimates of flow velocity usually must be determined from other field observations. One of the most common methods is to derive the velocity from observations of super-elevation in channel bends (Hungr et al., 1984). Unfortunately, there was very little evidence of super-elevation observed in the flows in this study. In the absence of these observations, instead of finding a singular, best-fit value, an upper and a lower bound of ψ were determined.

The lower bound of ψ was set to 10 ms^{-2}. This was below any ψ values found in the literature, and is quite conservative. Using a μ value of 10 ms^{-2} generally causes peak velocity values to be under 5 ms^{-1} in the channel and velocities in unconfined, runout reaches to be well below 1 m/s. Using this low ψ value, the flow front generally creeps down hill in the runout zone at speeds of 0.1 ms^{-1} before coming to a halt. The simulation was stopped when the front velocity reached 0 ms^{-1}.

The upper bound of ψ produced a simulated peak velocity of approximately 10 ms^{-1}. This upper bound on velocity was based on the work of Prochaska et al. (2008a). Using observations from British Columbia, Utah, and Italy, Prochaska et al. (2008a) observed a weak (R^2 of 0.45) empirical, linear relationship between the square of the flow height (in m) multiplied by the sine of the channel slope (S), and velocity (Equation 6.8) .

$$v = 0.35(h^2 S) + 5.36 \tag{6.8}$$

All of the h^2S values for reaches in this study were below 3 m^2. From Prochaska's data, for reaches where the flow was under 3 m^2, all flow velocities within two standard deviations from the mean were below 10.6 ms^{-1}. Based on this data, 10 ms^{-1} was thought to be a reasonable upper limit on velocity for the simulations in this study, especially since eyewitnesses of hillslope flows report velocities of no more than 2 ms^{-1} (Brundall, 1966). For the torrent flows, maximum velocities were arguably no higher than in flows reported in Prochaska et al. (2008b), which were of similar or larger magnitude than those in New Zealand.

The ψ value was back-calculated to the nearest 50 ms^{-2} for ψ values above 100 ms^{-2}, to the nearest 10 ms^{-2} if the best fit was below 100 ms^{-2}. In this way, two pair of friction parameters were determined for each flow, each resulting in a simulated travel distance which approximately matched the travel distance of the coarse clastic material. Figure 6.4 shows a plot of the deposit depth and peak velocity for the upper and lower bound simulations of FJ4.

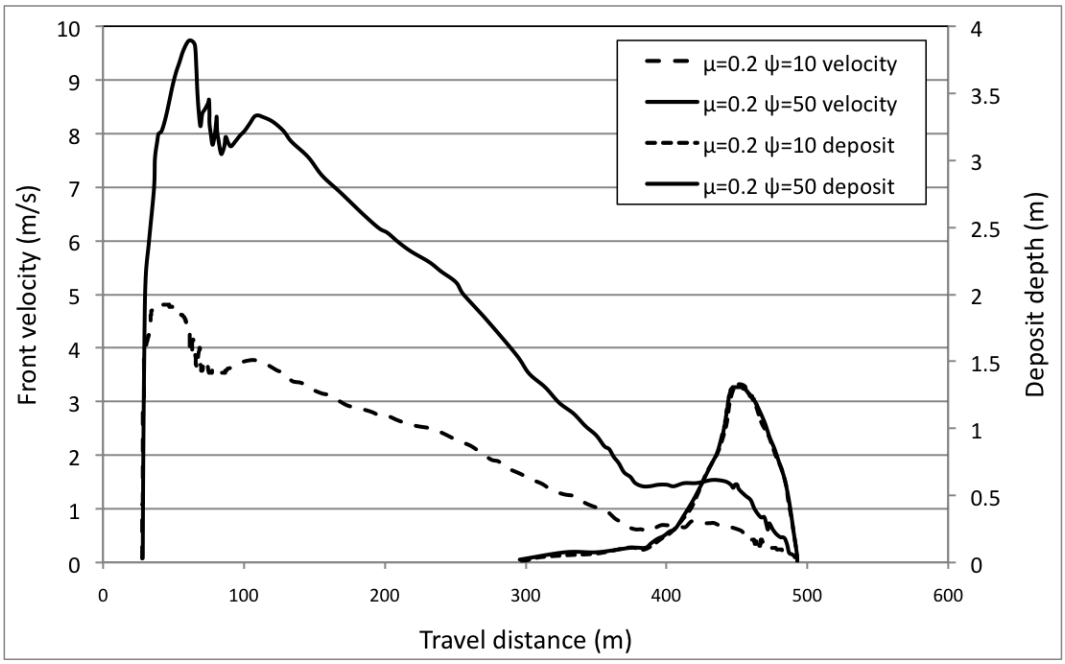

Figure 6.4.: Comparison of the peak front velocity and deposit depths predicted by DAN-W for FJ4. The upper bound simulation (μ = 0.2, ψ=50 ms^{-2}) and lower bound simulation (μ = 0.2, ψ=10 ms^{-2}) are compared.

6.2.2. Results of DAN-W simulations

6.2.2.1. New Zealand results

The Voellmy resistance parameters back-calculated for 18 New Zealand events are shown in Figure 6.5. The black lines indicate an alpine-torrent type flow, the red lines indicate a hillslope event, the red-dashed lines indicate an intermediate event. The intermediate events are represented by red-dashes because they were found to be similar to the hillslope events. The endpoints of each line represent the upper and lower bound discussed above.

The best-fit μ value was, in general, not very sensitive to ψ. The upper and lower bound of ψ sometimes varied over 2 orders of magnitude, yet the best-fit μ was a unique value for the majority of the flows. The exceptions were in C6, C2, C1, and C14, where greater momentum caused by higher flow velocities (a consequence of a higher ψ) necessitated the use of a higher μ to slow and stop the flow at the appropriate travel distance.

The range of back-calculated μ for the torrent events was 0.16 to 0.3, while the range for the hillslope and intermediate events ranged from 0.22 to 0.46. For simplicity and to compare with other datasets discussed later in this chapter, Figure 6.6 plots a single, best-fit μ and ψ for each flow. It should be noted that the values of ψ used are approximate. For the hillslope flows, the median between the upper and lower bounds is used, rounded to the nearest 10 ms^{-2} . For the torrent flows, the ψ values are closer to the upper bound, as the upper bound bound often produced velocities of approximately 4 to 7 ms^{-1} in the mid to lower, confined reaches of the path. Velocities in this range are in agreement with the findings of Prochaska et al. (2008a) (see Equation 6.8, which has an intercept of 5.36 m/s).

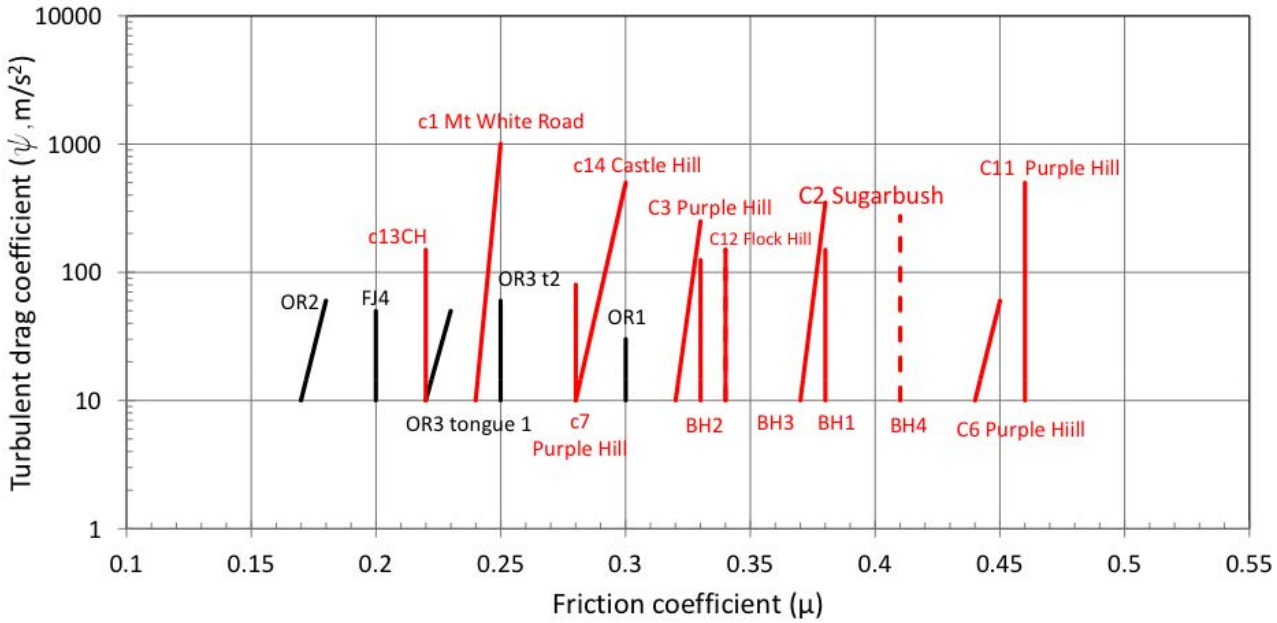

Figure 6.5.: Voellmy friction parameters calculated for New Zealand dataset. Hillslope are shown in red. Intermediate flows are the red, dashed lines. Torrents are in black. Each line connects the lower and upper bound of μ and ψ back-calculated for each flow.

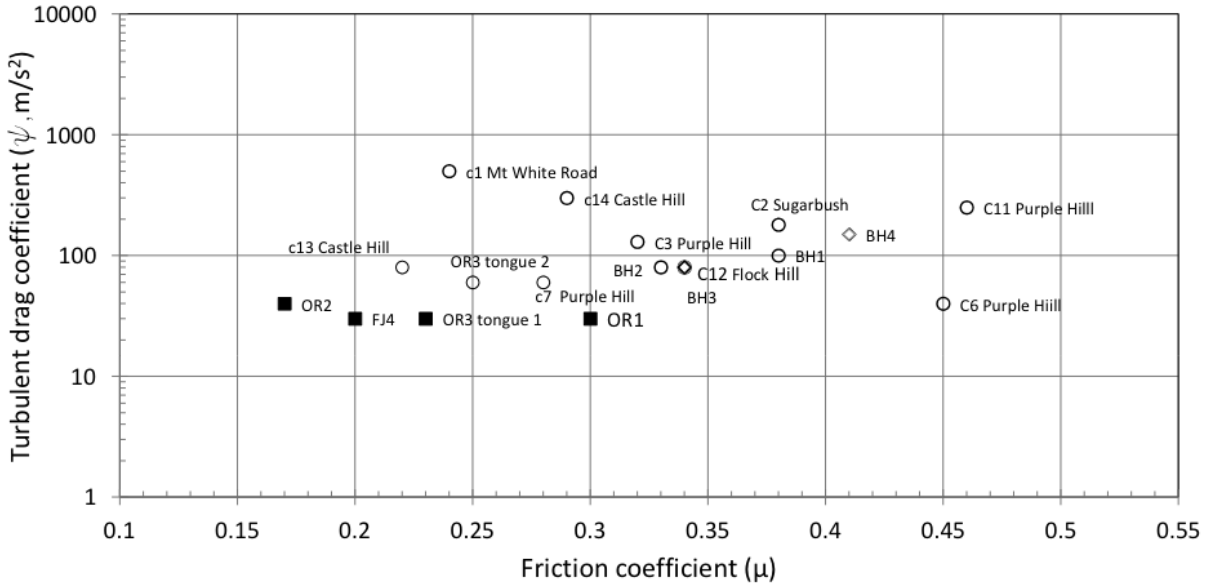

Figure 6.6.: Best-fit friction coefficients for the New Zealand dataset. Torrent flows are shown by black squares. Intermediate flows are shown by hollow diamonds. Hillslope flows are shown by hollow circles.

6.2.2.2. Variation in coefficients due to choice of travel distance

The end of the coarse clastic deposit is sometimes not a definitive point, but rather a gradual facies change to finer material. In addition, some investigators may be interested in the deepest point of deposition, which could be interpreted as the stopping point of the main surge. Other investigators may prefer a more conservative maximum which takes into account outwash material.

To represent these differences, the friction coefficients were also back-calculated to match approximately ± 5% of the travel distance of the coarse clastic material. One simulation was back-calculated to match a shorter travel distance ($L_{observed}$ -5%) using the highest coefficients possible (i.e. the ψ which gave a maximum velocity of 10 m/s). Another simulation modelled a longer travel distance ($L_{observed}$ +5%) and used a ψ value of 10 ms^{-2} , which required a lower μ value.

Figure 6.7 plots the results of these simulations. The black lines indicate an alpine-torrent type flow, the red lines indicate a hillslope event, the red-dashed lines indicate an intermediate event. The endpoints of each line are the upper and lower bounds discussed above. Any combination of μ and ψ along the line will give a reasonable value of the travel distance for each event.

A representative simulation, however, did not necessarily lie exactly on the line, because velocity can be modeled somewhat independently of runout. The different μ values found for the upper and lower bound are primarily determined by the travel distance chosen, while the range in ψ is primarily a function of the choice of acceptable velocities. In reality then, the range of values which may reasonably approximate the travel distance should be represented as rectangle, where the width of the rectangle represents range of acceptable travel distance, and the height represents a range of acceptable velocities. These ranges are represented in rectangles in Figure 6.8. The lower-left and upper-right corners of each rectangle correspond to the endpoints in Figure 6.7.

Figure 6.8 is useful because it indicates of the range of Voellmy parameters which might be reasonable for each flow. If an investigator wanted to model a flow with a shorter travel distance but higher velocities, such as would be expected from a granular debris flow with a high solids concentration for instance, they would choose a value from the upper-right hand corner of the rectangle. If the behavior of a slower, but more mobile flow was desired, the investigator would select values towards the lower left hand corner.

Figure 6.8 also illustrates the range of coefficients which could simply be a function of different modelling methodologies. For example, if the maximum extent of any deposition was used (including outwash), the back-calculated best-fit μ will be significantly lower than if the simulation used the travel distance of the coarse clastic material.

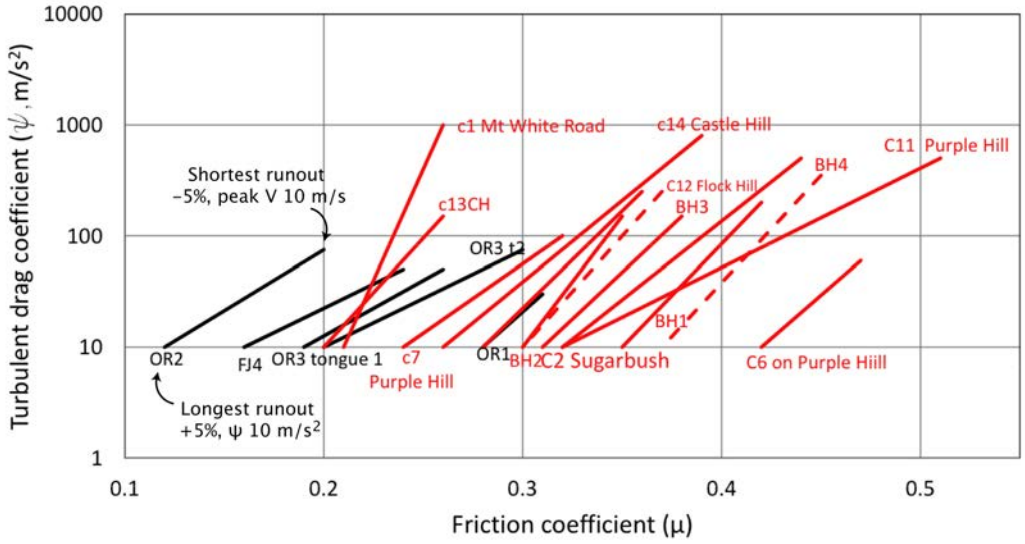

Figure 6.7.: Voellmy friction parameters calculated for the New Zealand dataset. Hillslope flows are shown in red. Intermediate flows are the red, dashed lines. Torrents are in black. Each line connects the friction parameters used to model the lower bound ($L_{observed}$ -5%, high ψ) and upper bound ($L_{observed}$ +5%, ψ of 10).

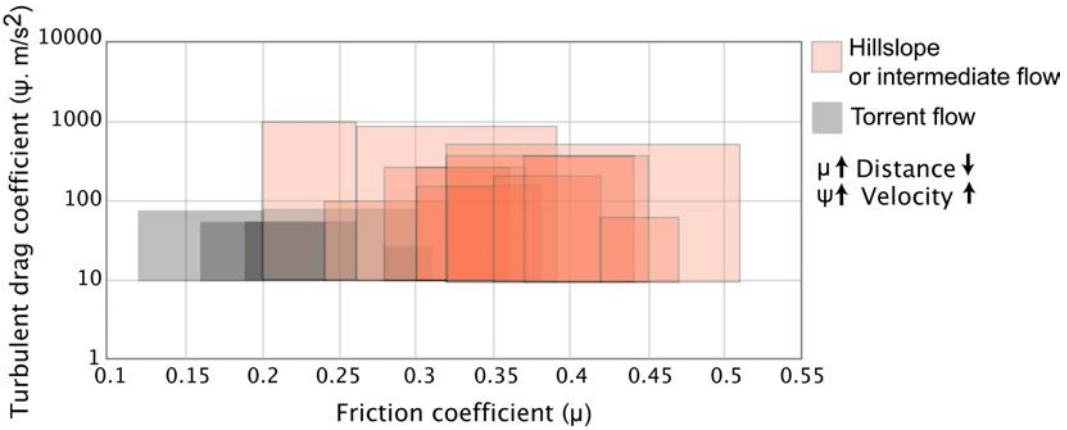

Figure 6.8.: Plot showing the approximate range of friction parameters suitable to model each flow to ± 5% of the travel distance of the coarse clastic material.

6.2.3. Discussion

6.2.3.1. Comparison with other debris events

Figure 6.9 compares the New Zealand best-fit Voellmy friction parameters with other flows from the literature. The friction coefficients are very scattered, with μ values ranging from 0.01 to over 0.5. Most previous reports of this range in the literature were narrower, from approximately 0.01 to 0.3, and focused on torrent flows (Hürlimann et al., 2003; Gamma, 2000; Rickenmann, 2005; Zimmermann, 1990). In contrast, the small torrent and hillslope events modeled in New Zealand required higher friction coefficients. However, they were still within the range back-calculated for small open-slope flows on Vancouver Island (Brideau, 2009).

The low, average ψ values found for the New Zealand flows was probably a consequence of both the upper limit imposed on the velocity, the conservative lower bound of ψ, and the boundary conditions of the model. The upper bound of 10 m/s is an overly conservative upper bound for some of the flows, as modelling the flows as a starting slab equal to the mapped volume sometimes produces unrealistic flow heights (and therefore higher velocities) as the debris bottle-necked in narrow reaches. For example, DAN-W simulates a flow height of 10 m in the upper, narrow transport reaches of OR1. This was by far the worst example, however, and even in this case, DAN-W models a deposit thickness of 2.5 m, which was approximately the deposit depth observed in the field. Further, the low ψ values have little effect on the rest of the discussion in this chapter, which focuses on μ. If the flows were modelled with higher ψ values, the friction coefficients may shift slightly upward, but will remain largely unaffected, as illustrated by Figure 6.5.

Comparing the scatter of points in 6.9 shows that points within individual datasets cluster together (Figure 6.9). Assuming this is not entirely due to differences in modelling methods (some flows used modelling software other than DAN-W and may have slightly different methodology), it suggests that debris flows from different field areas exhibit distinctly different physical characteristics and that these differences are reflected in back-calculated friction values. Hence, friction values calculated for one field area are unlikely to be transferable to another.

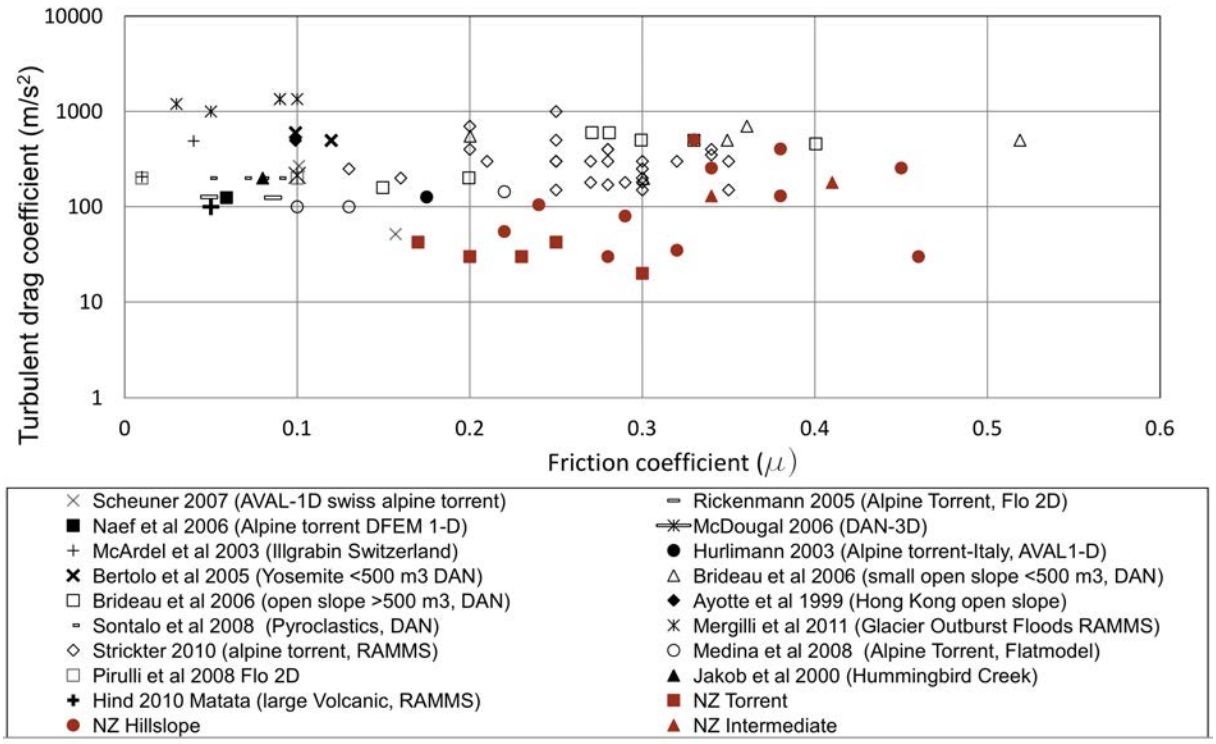

Figure 6.9.: Back-calculated values of μ and ψ for the New Zealand datasets and various other flows from the literature.

6.2.3.2. Influence of event magnitude

Previous investigators have found a relationship between increased debris flow mobility and event volume or watershed area (Zimmermann, 1990; Rickenmann, 1999; Gamma, 2000). To investigate this, the best-fit μ value was plotted against event volume for the New Zealand data. Figure 6.10 shows that, for this dataset, there is no relationship between the average friction coefficient and event volume (R^2 of 0.1). The upslope area (the uphill area which would contribute runoff to the flow) was approximated using GoogleEarth. If upslope area is plotted against μ, the relationship slightly improves to an R^2 of 0.28 (Figure 6.11). This suggests the upslope area is acting as a proxy for the amount of water or debris available to the flow.

Compared to torrent events, the active area which contributes water and debris to the channel of a hillslope event may be very small. The path of these flows is often incised into a planar hillslope rather than a mature basin. At any point in the channel, water and debris are only contributed by the gully wall or the channel immediately upslope of the flow. This may contribute to lower moisture contents and therefore lower mobility in hillslope type flows. In addition, torrent flows which enter lower order stream channels are more likely to encounter

stream flow and incorporate water. In a torrent flow, the corresponding area is the entire area of the catchment up-slope of the point in question.

While the relationship between mobility and event volume does not hold in this dataset, when friction coefficients from datasets around the world are plotted over a large range of event volumes, a weak correlation (R^2 of 0.4) becomes apparent (Figure 6.12). The lower μ values of larger magnitude events reflects the lower slope angle where these events come to rest. This is because the frictional resistance defined by μ is the dominant component of the Voellmy resistance at low velocities in the runout zone. Thus, μ follows the same trend as the slope angle of deposition; small, hillslope flows will deposit on higher angle slopes and thus have high friction coefficients. Larger alpine flows and volcanic lahars travel down gentler, larger order streams, deposit on lower angle fans, and therefore display lower friction coefficients.

In Chapters 4 and 5, emphasis was placed on differences between event volume, entrainment behaviour, and the geometry of the flow path. The fact that larger debris flows come to rest on lower angle slopes and have higher mobility than small debris flows is not simply due to larger initial failures. DAN-W explicitly accounts for the momentum balance and deformation of the flow. Any difference in the friction parameters must have to do with either channel geometry not accounted for in DAN-W or other parameters intrinsic to the frictional resistance to flow, rather than event volume. These differences could include fines content, type of fines, presence of vegetation, moisture content, or differences in particle size distribution. While non of these parameters were measured in this study due to time and access constraints, they doubtlessly effect the mobility of the flow. The input parameters back-calculated for the Voellmy rheology in DAN-W reflect all these various factors.

Although the correlation between flow volume and μ in Figure 6.12 is weak, the plot highlights some trends which may be useful to debris flow investigators. At first approximation, flows over 50,000 m^3 will almost always to have μ values of less than 0.1, while debris flows with volumes of less than 50,000 m^3 will tend to have μ values greater than 0.1. The frictional parameters back-calculated for small flows are more variable than for the larger, more catastrophic events. However, smaller torrent type flows will generally have values between 0.1 and 0.3. Open-slope or hillslope type flows are variable, but may have very high friction values in excess of 0.3.

The physical meaning behind the increased scatter in the friction coefficient with lower event volume is explained by smaller flow depths, lower velocities and a consequent increased sensitivity to small changes within the channel. Debris flows tend to stop if the flow depth drops below the size of the maximum particle diameter (Davies, 1997) or if they run out of

material. For small flows, either of these situations may occur if the flow enters a reach having low confinement. Lower velocities will also make a small flow more prone to being impeded by vegetation or channel constrictions. These factors will increase the net friction to movement, and are generally randomly distributed in the channel, giving rise to more stochastic, scattered friction values at lower event volumes. As the flow becomes larger, it will be less prone to these factors.

Stochastic channel processes explain the high variability in small events, while both channel morphology and mechanical differences in flow may explain the decreasing friction with larger event volume. As previously discussed, larger flows may have a lower solids concentration made possible by bulked stream flow. It is also possible that longer drainage pathways in larger flows will prevent consolidation and enhance mobility.

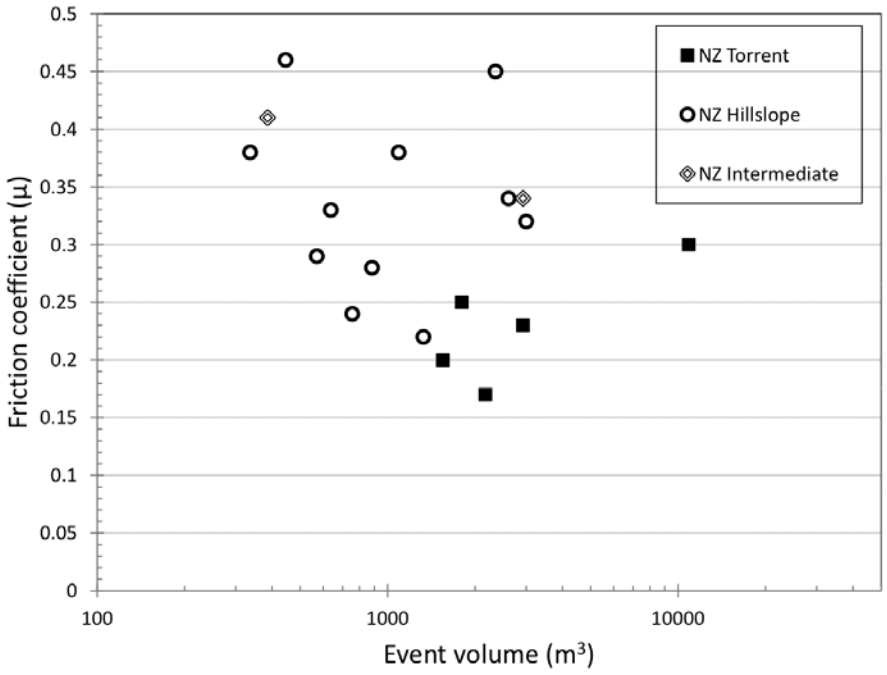

Figure 6.10.: Event volume of New Zealand debris flows plotted against the back-calculated friction coefficient.

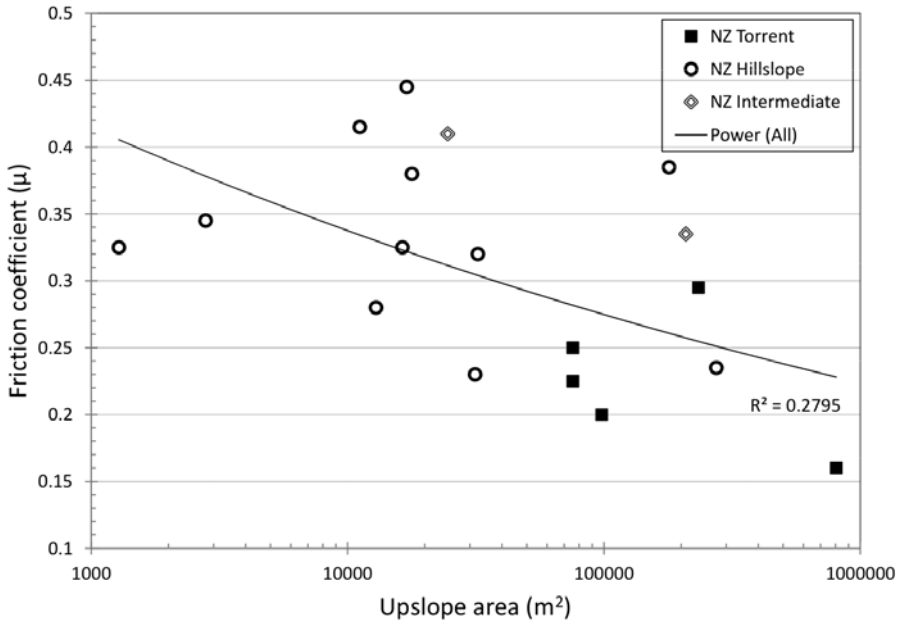

Figure 6.11.: The friction coefficient for each flow in the New Zealand dataset plotted against the approximate upslope area that contributed to the debris flow.

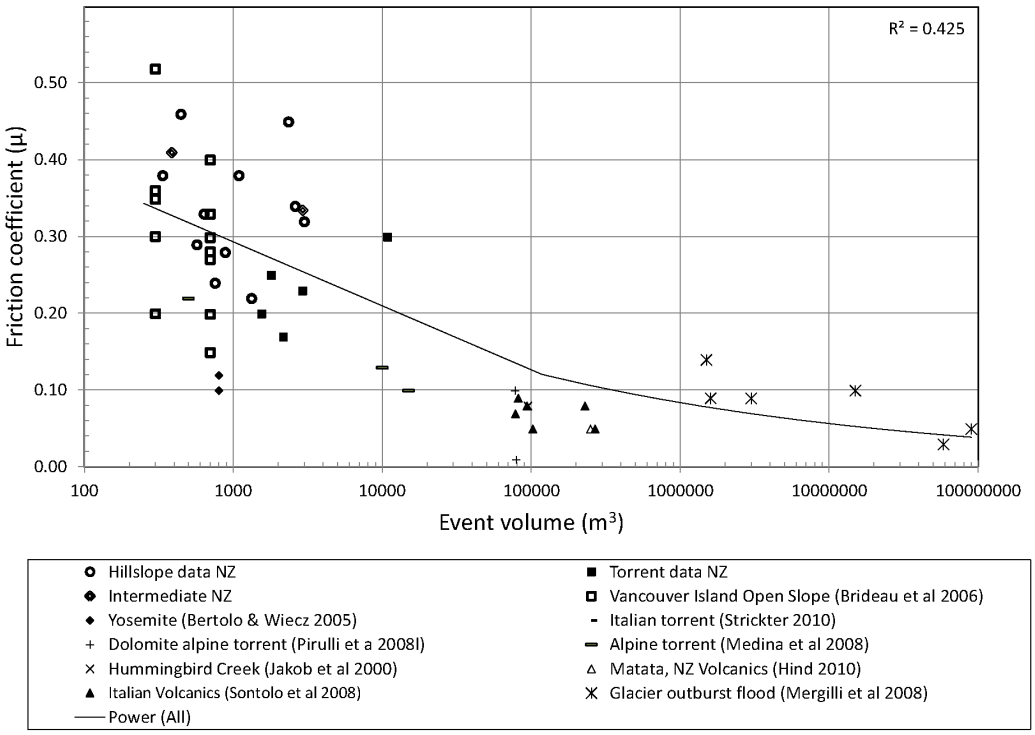

Figure 6.12.: Figure shows the friction coefficient plotted against the event volume.

6.3. UBCDflow

6.3.1. Methods

UBCDflow requires the following data for each reach; slope length, the mode of flow (confined, unconfined, or transitional), the azimuth, the slope angle, and the average width of each reach. Since all of these data were recorded in the field, setting up UBCDflow was straightforward. UBCDflow also requires a starting volume coming into the first reach modelled. If the flow was fully traversed and the starting volume of the flow in the first mapped reach was known with some confidence (e.g. mapped flow FJ4), this volume was set to the starting volume in UBCDflow. If the entire starting zone was not traversed and the deposition volume was greater than the mapped erosion, the starting volume of the flow was set to the remaining volume unaccounted for (e.g. mapped flow C3). Using these inputs, the model predicted the volume change and cumulative flow volume in each reach. When the volume dropped to zero, the flow stopped.

6.3.2. Results

6.3.2.1. Torrent flow results

The four-torrent type flows modelled with UBCDflow show that this model performed relatively well in terms of predicting travel distance. Table 6.3 summarizes the modelling results and error. Plots of the UBCDflow output for individual flows are shown in Appendix B. In three cases, the model accurately predicted in which reach the coarse clastic material stopped. The model over-predicted the travel distance of OR2 by one reach, which is only +1.3% of the total travel distance.

UBCDflow matched the entrainment and deposition amounts mapped in the field less closely. UBCDflow over-predicted the peak passing volume by an average of +53.5% compared with the volume passing estimated using field measurements. The model was better at predicting the total event magnitude; the average overestimate of the volume deposited by the flow was only +10.3%.[1] It must be stressed than even the over-prediction of +53.5% is still well within the estimated error of field measurements. UBCDflow estimated the observed

[1]The maximum volume passing is equal to the total event volume only if there is no sporadic erosion or deposition. The maximum volume passing will also be less than the event volume if there is both deposition and entrainment in a single reach. For example, consider a section of path that is five reaches long. If there is 100 m^3 of deposition and 110m^3 of erosion in each reach, then total volume passing will only be 50m^3(i.e. 5 x 10m) at the end of the fifth reach. The total volume deposited, however, will be 500m^3(5x100m^3).

entrainment values quite well.

While the model performed well at predicting the travel distance of torrent type debris flows, UBCDflow's success hinged on an accurate characterization of the mode of flow in each reach. Reach confinement was known and entered post-hoc. In predictive modelling, deciding if a reach is unconfined or confined may be more difficult. For example in OR1, the flow downcut and became channelized at the head of the fan. In a predictive analysis done before the event, these reaches would likely have been classified as unconfined and UBCDflow would have significantly underestimated the travel distance. If used for predictive modelling, multiple runs should be conducted with multiple confinement settings, especially in reaches near the head of the fan.

6.3.2.2. Hillslope flow results

13 hillslope flows were also modelled with UBCDflow. Despite being developed primarily with data from channelized flows (Fannin and Wise, 2001), the model still provided a useful estimate of passing and event volumes of hillslope debris flows. For 10 of the 13 flows, the model predicted the event volume within the error of the dataset. UBCDflow's average error in predicting the maximum passing volume and total event volume was 197% and 105%, respectively. In two mapped flows, C11 and BH1, UBCDflow massively over-predicted the material entrained. Excluding these flows, UBCDflow's predictions of total volume was only +39%. This is well within the error of the mapped volume estimates.

UBCDflow over-predicted the travel distance, so much so that the simulation did not run out of volume even when extra reaches were added, for four flows. For the other nine flows, the average overestimate of travel distance was +20%. As discussed in the previous section, UBCDflow's predictions of travel distance are based on event volume and very sensitive to where the flow becomes unconfined. UBCDflow's success at predicting the travel distance of torrent flows largely depends on identifying reaches where the flow will become unconfined on the fan. Unlike torrent flows, hillslope flows don't suddenly become unconfined on a debris fan, but generally become unconfined after leaving a gully mid-slope, where they then progressively deposit levees as they make their way down to lower slope angles. Old natural levees often provide at least some confinement as the flow moves through this zone. Colluvial fans, if present, are poorly delineated (see Section 4.5). The definition of confinement is therefore much more subjective than for torrent type flows. Given this subjectivity and the tendency of UBCDflow to over-predict volume passing and event volume for the flows assessed here, it is not surprising that UBCDflow tends to strongly over-predict travel distance (Table 6.4).

Table 6.3.: UBCDflow modelling results for torrent type flows.

Volume data for torrent flows (m^3)					Travel Distances (m)		Error (%)		
Flow	Observed total deposited	UBCDF total eroded	Estimated max passing	UBCDF max passing	Travel D Observed*	Travel D UBCDF	V passing	Total V deposited	Travel Distance
OR1	10869	8020	6258	8020	725	725	+28	-26	0
OR2	2170	3820	1469	3640	877	866	+148	+76	+1.3
OR3	5897	4681	5267	4884	435	435	-7	-21	0
FJ4	1548	1732	1108	1606	543	543	+45	+12	0

*The travel distance observed refers to the travel distance of the coarse clastic material. A value of 0 does not mean UBCDflow predicted the travel distance perfectly, but rather that UBCDflow predicted that the flow stopped in the correct reach.

Since different investigators may interpret confinement differently, another round of UBCDflow modelling was done where all reaches were classified as unconfined. Results are shown in Table 6.5. Setting all of the reaches to unconfined generally yielded better travel distance predictions. For C12 and BH1, the travel distance predicted was longer than the flow path input into the model (i.e. the volume had not reached zero, even at the end of the last extra reach, which was well beyond any evidence of any debris flow deposition). However, setting the reaches of the remaining flows to unconfined lowered the average error in travel distance from +20% to +11%, and accurately predicted the travel distances of C1, C2, and C7.

Setting all reaches to unconfined also improved volume predictions. The average percent passing error was lowered to 132%, down from 192%. For event volume, the average error decreased to +58%. When the outliers C11 and BH1 were removed, UBCDflow over-predicted event volume to less than 1%.

As an example, Figure 6.13 plots the simulated and observed volume passing each reach for mapped flow C2 against slope length. In this instance, both predictions underestimate the amount of erosion from the upper-most, unconfined reaches. UBCDflow also predicts that the flow will erode at lower slope angles, where in fact the flow deposited a large amount of material in levees. However, once the slope angle drops below 20°, very rapid deposition in the UBCDflow simulation causes the flow to stop in the correct, final reach. This illustrates a case where UBCDflow provided a correct travel distance prediction and a useful event volume, but did so for reasons that were not physically correct.

Table 6.4.: UBCDflow modelling results for hillslope type flows.

Volume data for hillslope flows (m^3)					Travel Distances (m)		Error (%)		
Flow	Observed total deposited	UBCDF total eroded	Estimated max passing	UBCDF max passing	Observed*	UBCDF	V passing	Total V deposited	Travel Dist
C1	756	2234	399	2106	769	PME	+428	+195	PME
C2	1091	760	946	760	478	635	-19	-30%	+32
C3	2998	4500	1888	4500	1354	PME	+138	+50	PME
C6	2350	3851	2297	3851	823	1071	+67	+64	+30
C7	883	1014	863	1014	925	1054	+17	+15	+14
C11	445	2175	236	2175	802	911	+821	+388	+13.6
C12	2924	3385	2633	3593	907	PME	+33	+23	PME
C13	1327	1004	853	1004	624	529	+18	-24	-15
C14	570	1000	567	1000	560	616	+76	+75	+10
BH1	336	2205	309	2205	797	PME	+613	+494	PME
BH2	638	1363	427	1363	497	691	+219	+113	+39
BH3	2606	1803	651	1803	709	989	+177	-31	+39
BH4	386	290	384	290	247	280	-24	-25	+13

PME stands for past model extent (i.e. the simulation did not come to a stop before the end of the model flow path, even when extra runout reaches were added which were well past any debris flow deposition observed in the field). *The travel distance observed refers to the travel distance of the coarse clastic material.

Table 6.5.: UBCDflow modelling results for hillslope type flows with all reaches set to unconfined.

Volume data for hillslope flows, all reaches modelled as unconfined (m^3)					Travel Distances (m)		Error (%)		
Flow	Observed total deposited	UBCDF total eroded	Estimated max. passing	UBCDF max. passing	Observed*	UBCDF	V passing	Total V deposited	Travel Dist
C1	756	1083	399	1083	769	769	+171	+43	0
C2	1091	473	946	473	478	478	-50	-56	0
C3	2998	1953	1888	1953	1354	1632	+3	-35	+21
C6	2350	3567	2297	3567	823	1071	+55	+52	+30
C7	883	711	863	711	925	925	-18	-20	0
C11	445	1624	236	1624	802	878	+588	+265	+9.5
C12	2924	3497	2633	3436	907	PME	+29	+18	PME
C13	1327	676	853	676	624	529	-20	-49	-15
C14	570	670	567	670	560	530	+18	+17	-5
BH1	336	1996	309	1996	797	PME	+545	+556	PME
BH2	638	1055	427	1055	497	638	+147	+65	+28
BH3	2606	1657	651	1657	709	919	+154	-36	+30
BH4	386	363	384	363	247	312	-5	-6	+26

PME stands for past model extent (i.e. the simulation did not come to a stop before the end of the model flow path, even when extra runout reaches were added which were well past any debris flow deposition observed in the field). *The travel distance observed refers to the travel distance of the coarse clastic material.

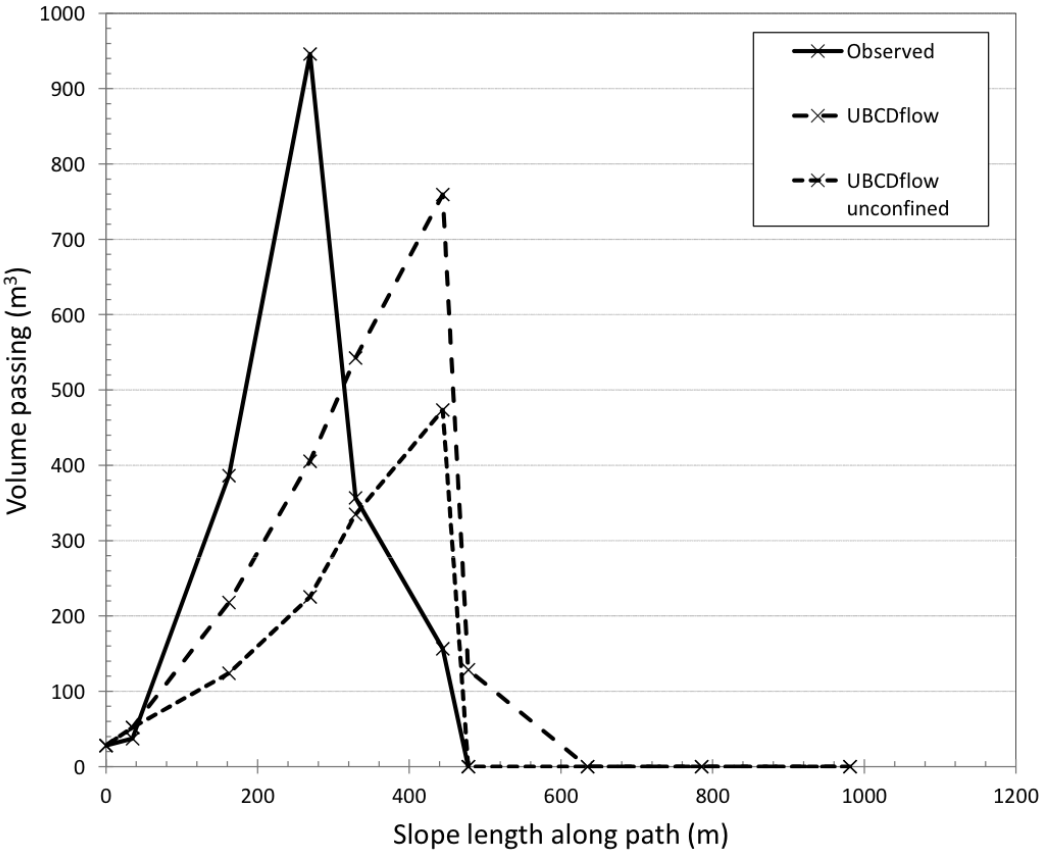

Figure 6.13.: Plot of the volume passing each reach for C2. UBCDflow unconfined refers to the simulation where all reaches were set to unconfined.

6.4. Evaluating potential travel distance and event volume: a combined modelling approach

Greater modelling capability may be gained from combining the strengths of UBCDflow and DAN-W. The following section explores the effect of modelling entrainment in DAN-W on travel distance, velocity, and event volume for a subset of the data. The erosion depths predicted by UBCDflow are then used in each DAN-W simulation. Finally, C3 and FJ4 are used as examples of how UBCDflow, the back-calculated parameters from this study, and DAN-W may be used together.

6.4.1. Effect of entrainment on travel distance and maximum velocity

Thus far, the analyses has approximated the volume of the starting slab to be equal to the entire event volume. This starting slab of material was then allowed to flow down a fixed bed and then deposit. In order to use the volume behavior predicted by UBCDflow in a DAN-W simulation, the effect entrainment on the frictional parameters discussed earlier needed to be evaluated.

To this end, a subset of four of the most typical hillslope flows, C2, C6, C7, and C11 were modelled using the entrainment option in DAN-W. The friction parameters used in the simulations were set to the best-fit shown in Figure 6.6. The estimated eroded volume for each reach was divided by the trace area. This was exactly what was done in Chapter 5 to compare depths of erosion (E'). These values were then entered into DAN-W as the maximum erodible depth in each reach.

Table 6.6 shows the original volume of the sliding mass used to model each flow from Section 6.2.2, the event volume predicted by DAN-W using observed erosion depths. The change in travel distance and flow velocity are also shown.

Incorporating entrainment into the simulations had very little impact on the predicted travel distance, but significantly decreased the maximum velocity in 3 of the 4 flows. Based on this subset of simulations, if all flows were modelled with entrainment, the back-calculated μ values would likely change very little (by approximately 0.01), but values of Ψ may increase significantly. Entrainment also shifted where the maximum velocity was recorded downslope and yielded more realistic flow depths. For example, the maximum observed velocity changed from approximately 8 m/s to approximately 4 m/s for mapped flow C6 (Figure 6.14). This maximum value shifted approximately 200 m downslope to the last confined section of the travel path. Figure 6.14 also shows that modelled flow depths were also much more in line with flow depths inferred from field evidence.

Event volumes of simulations incorporating entrainment were marginally less than those observed in the field. The simulated event volumes are lower because DAN-W simulated the maximum depth of erosion only if the entire flow passed over the reach. In all simulations, a long, narrow tail was left behind the flow front. Consequently, DAN-W did not always simulate the maximum volume of entrainment, which led to a decrease in simulated event volume.

Table 6.6.: Differences in modelled flow behaviour between simplified block release and simulations with entrainment for C2, C6, C7, and C11 using best-fit friction coefficients.

Flow ID	Original modelled volume (m^3)	Volume with simulated erosion (using observed depth of erosion, m^3)	Change in travel distance (%)	Change in max velocity (%)
C2	1083	1036	-1.5	-1
C6	2350	2309	0.3	-49
C7	871	754	0.6	-38
C11	433	423	0.1	-36

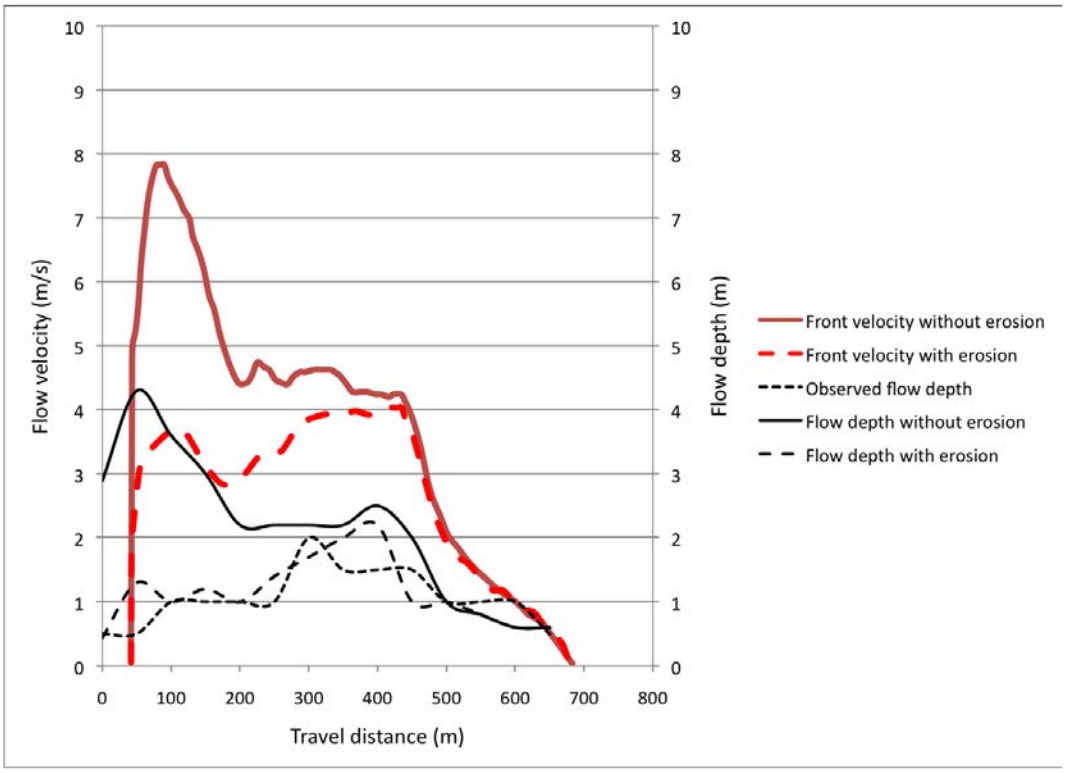

Figure 6.14.: Front velocity and flow depth modelled in DAN-W, with and without entrainment, for flow C6. The flow depth inferred from field evidence is also shown.

6.4.2. Use of UBCDflow eroded depths

To explore whether the erosion volumes predicted for hillslope flows by UBCDflow, instead of those mapped, could be used in the DAN-W simulations, the travel distances of hillslope flows C2, C6, C7, and C11 were remodelled using the maximum eroded depth predicted by UBCDflow. The depth of erosion was calculated by dividing the volume change predicted by UBCDflow by the trace area (L x trace width) for each reach.

These erosion depths were then input into DAN-W. The simulations were run using the best fit parameters shown in Figure 6.6. Table 6.7 reports changes in travel distance when the UBCDflow erosion depths were used. As discussed earlier, the event volume simulated with the maximum erosion depths predicted by UBCDflow were generally higher than the event volume recorded in the field. However, these large over-estimates in volume made very little difference to the travel distance simulated by DAN-W. For example, while UBCDflow over-predicted the volume of C11 nearly three-fold, this increase in volume made very little difference in the DAN-W simulation. The change in travel distance was only +3%, which equates to an over-prediction of only 20m. DAN-W dampened the effect of over-predicting the volume entrained, since it is not very sensitive to changes in the flow volume. This is because at low velocities, the runout is a much more a function of μ, rather than size.

Table 6.7.: Comparison of modelled flow behaviour between simplified block release and simulations incorporating entrainment, using UBCDflow erosion depths, for C2, C6, C7, and C11.

Flow ID	Volume with simulated (erosion depth predicted by UBCDflow, m^3)	Change in travel distance (%)	Change in modelled volume (%)
C2	1783	-0.2	+139%
C6	3568	+0.9	+54%
C7	906	+3.5	+4%
C11	1497	+2.9	+256%

6.4.3. Application to hillslope event

To investigate how a combined approach using both UBCDflow and DAN-W would perform in a predictive hazard analysis, the travel distance and entrainment of mapped flow C3 were modelled using none of the field data other than the path geometry.

Two groups of simulations were run in UBCDflow. In the first simulation, all reaches

were set to confined in UBCDflow. This provided a conservative estimate of the volume entrained in each reach. In the second group of simulations, all reaches were set to unconfined, which as discussed in Section 6.3.2.2, gave more realistic values of entrainment for most of the flows in the dataset. The modelled volume change of the flow in reach, according to UBCDflow, was divided by the reach area to yield an eroded depth. These erosion depths were used DAN-W. The results are shown in Table 6.8.

The initial volume of simulated failure was largely arbitrary. In this case, a failure volume of 100 m^3 was modelled above the highest reach mapped. While this was smaller than starting volume inferred from field measurements, it would be similar to the starting volumes of mapped flow C6 and C7, which were also located on Purple Hill. Nevertheless, the amount of entrainment predicted by UBCDflow is relatively insensitive to the starting volume.

Three combinations of μ and ψ were used in each group of simulations in DAN-W. A conservative μ value of 0.17 was based on the lower bound of μ found for hillslope debris flows. The highest μ, 0.38, was the average of the upper bound values for the hillslope flows. Finally, a fairly typical μ value of 0.34 was used, based on Figure 6.8. The ψ value was chosen to be twice the average of all the hillslope flows back-calculated in Section 6.2.2, as modelling entrainment in DAN-W tended to significantly decrease the velocity observed in the flows.

The best-fit simulation used the erosion depths predicted by the confined UBCDflow results and μ value of 0.34. This simulation under-predicted the travel distance of the coarse clastic by 3% (40m). It under-predicted the event volume by 13%, which is negligible given the possible errors in the field measurements of between -50 and +150%. Interestingly, while the most conservative estimate (μ of 0.17) over-predicted the travel distance of the main surge, it came within 40 m of the travel distance of smaller surges of remolded and outwash material. (Figure 6.15).

Figure 6.15.: Left: Overview of C3 from GoogleEarth. Right: Enlarged picture of final depositional reaches. The 'upper bound' is the DAN-W simulation run with μ of 0.38, 'average' is μ=0.34, and lower bound of μ is 0.17.

Table 6.8.: DAN-W simulation results using the erosion depths predicted by UBCDflow for mapped flow C3.

μ	ψ	Event volume (m^3)	Max velocity (ms^{-1})	Extent (m)	Error travel distance (%)	Error volume (%)
0.17	330	1370	9.2	1628	+37.7	-54.3
0.34	330	1367	6.9	1127	-4.7	-54.4
0.38	330	1365	6.3	1100	-6.9	-54.4

All reaches were set to unconfined. Percent error in travel distance compares the simulated value to that observed in the field. The percent error volume compares the event volume modelled to the figure calculated from field observations. The initial starting volume used for this simulation was 100 m^3.

6.4.4. Application to torrent event

While UBCDflow was found to be useful in predicting the travel distance and event volume for torrent debris flows in Section 6.3.2.1, UBCDflow does not provide an estimate of important parameters such as flow height, flow velocity, or depositional shape. DAN-W does provide these parameters. It is possible to run a UBCDflow simulation to estimate a travel distance and volume for a torrent event, then use this data to back-calculate input parameters for the Voellmy rheology in DAN-W. The resulting simulations in DAN-W may give the investigator an idea of the velocities, discharges, and deposit area involved in a potential flow.

To test this, hypothetical starting volumes of 100 m^3, 500 m^3, and 1000 m^3 were simulated entering reach 2 of FJ4 with UBCDflow. Regardless of the starting volume, the simulated flow always deposited in reach 12 due to lack of confinement and low slope angle. Also, the depths of erosion remain the same for each simulation, as the entering volume is not included in the function which calculates the volume change.

The eroded depths predicted by UBCDflow in each reach were then entered into DAN-W as the maximum erodible depth in the corresponding reach. The flow was then simulated with starting volumes with 100 m^3, 500 m^3, and 1000 m^3. Using a maximum velocity of 10.6 m/s, the best fit μ for each simulation was 0.21. The best-fit ψ was 200, 100, and 50 ms^{-2}, respectively. Figure 6.16 plots the depths of erosion and deposition observed in the field, as well as predicted those predicted by UBCDflow for the run with 500 m^3 starting volume. It also shows the shape and depth of deposited material.

In this case, UBCDflow predicted the total event volume well, to within 12% of the volume observed. However, as Figure 6.16 illustrates, it did so for reasons which did not reflect field observations. The model under-predicted the erosion observed in the upper reaches, where a bedrock failure in weak, fault damaged rock contributed most of the event volume. It over-predicted entrainment in the lower part of the transport zone. In this case, the two errors cancel each other, which yields a remarkably accurate, and lucky, prediction of the event magnitude.

Figure 6.16 also illustrates some of the limitations of DAN-W. Both models, in fact, significantly overestimate the depth of material deposited on the fan and correspondingly underestimate the amount of material deposited as levee or lag deposition in the transport zone. This effect must be considered when dealing with low magnitude events.

Despite these limitations, DAN-W is quite useful in visualizing the potential velocities and flow depths in the event (Figures 6.17 and 6.18). The simulated peak velocities occurred in the mid to upper reaches of the flow path. At a point 200 m along the path, the flow velocity was 8 m/s and the flow depth was 2 m. While the actual flow velocity was unknown, inferred

flow depths from field evidence were approximately 1.5 to 2m. This information would not be provided by just UBCDflow or another empirical model for travel distance.

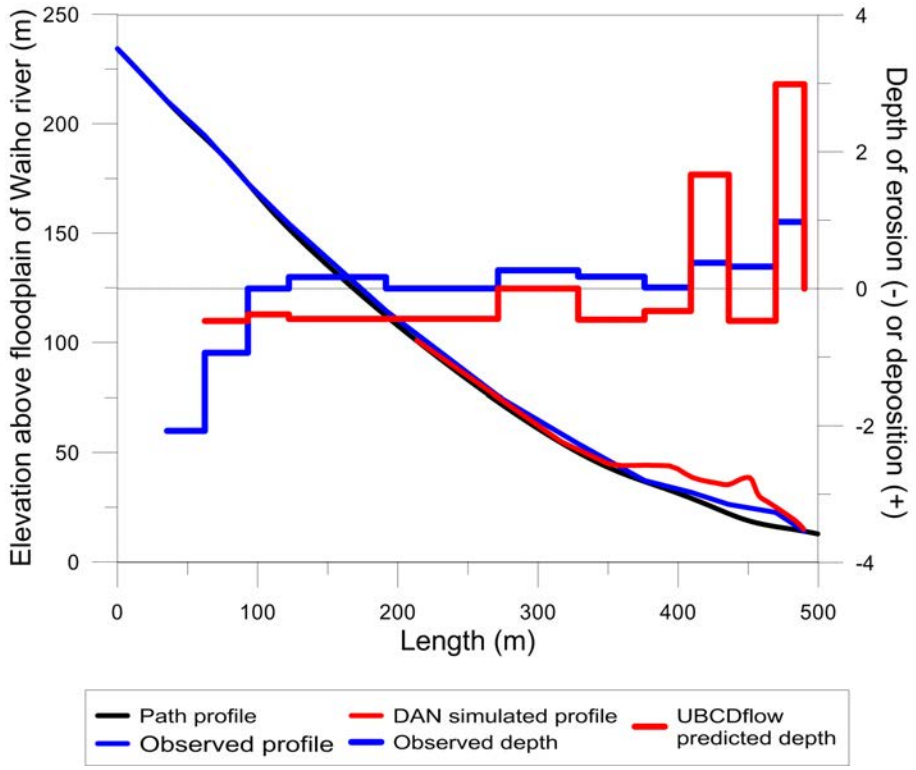

Figure 6.16.: Combined output for simulation using 500m^3 starting volume, μ of 0.21, and ψ of 100 ms^{-1} Observed and predicted depth of effective erosion or deposition by UBCDflow and observed in the field. The deposition shape along the path observed and that predicted by DAN-W is also shown. The depth of deposition is exaggerated by a factor of 10.

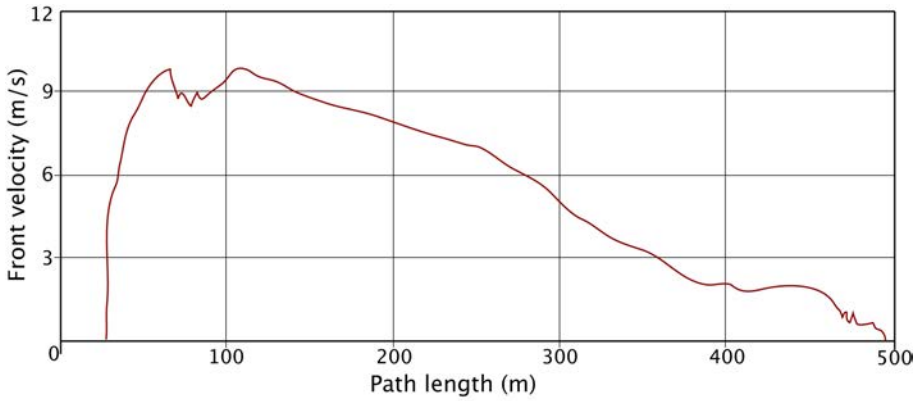

Figure 6.17.: Velocity plot for simulation of FJ4. The line represents the velocity at the flow front.

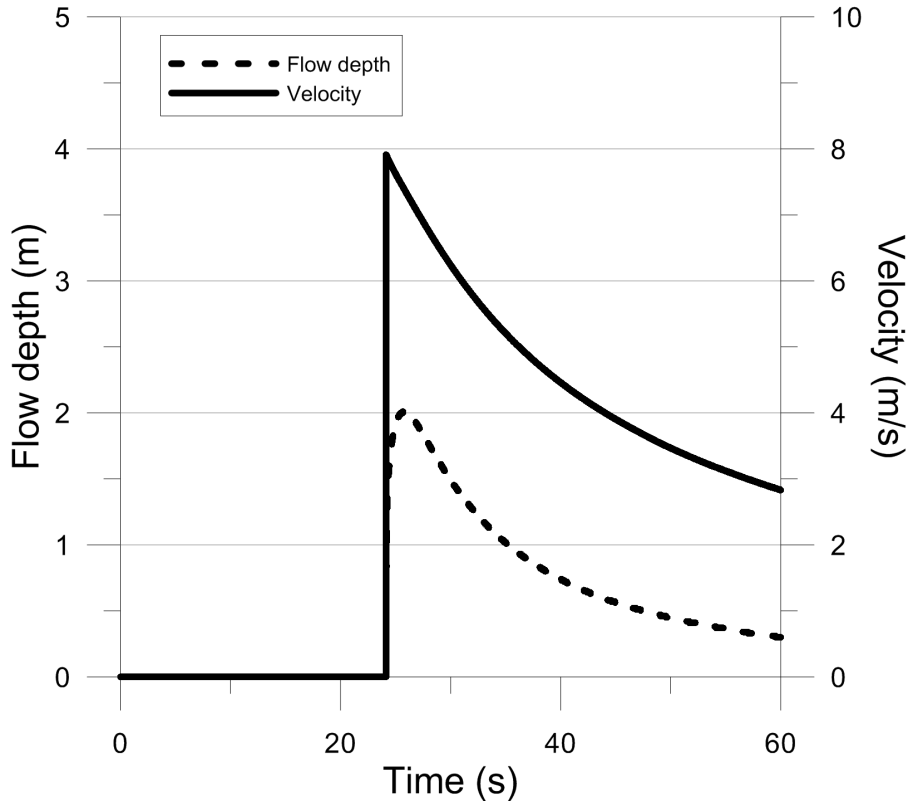

Figure 6.18.: Flow depth and velocity for simulation of FJ4 using a 500 m^3starting mass at a control point 200m along the horizontal. Flow depth is shown in red, while flow velocity is in black. DAN-W simulates a flow front 2 m deep and moving at approximately 8 m/s.

6.5. Summary and conclusions

This chapter summarizes the methods used to simulate 17 debris flows in New Zealand with DAN-W and UBCDflow. The results may be useful to debris flow investigators, especially when trying to predict the travel distance and event volume of small debris flows in one of the field areas studied.

- The back-calculated Voellmy friction coefficients for the debris flows simulated in this study were generally higher than reported elsewhere in the literature for torrent type debris flows. This is thought to be related to the relatively small magnitude of the events and the steepness of the paths. Smaller events are more likely to be effected by in-channel vegetation, channel constrictions and roughness, and small changes in confinement, increasing the overall frictional resistance of the channel.

- Friction parameters for hillslope flows were higher than for torrent type flows. This may be due to a lack of confinement and smaller contributing area to these flows.

- When the dataset is supplemented by data from the literature over a wide-range of volumes, the Voellmy friction coefficient tends to decrease with increasing flow volume. In general, flows above 50,000 m^3 will have a back-calculated μ of less than 0.1. Flows smaller than 50,000 m^3 will have a μ greater than 0.1, but vary considerably among flows of similar magnitude. The increased mobility of larger could be due to the decreased susceptibility discussed above, but may also be related to rheological differences between large and small magnitude events.

- UBCDflow predicted the travel distance of torrent type flows with well-defined unconfined reaches in 3 out of the 4 cases tested. The maximum volume passing was often over-predicted. Care should be taken to identify the mode of flow correctly (confined, unconfined, or transitional), as the model is very sensitive to this input. The model's success is a result of the tendency for torrent, granular debris flows to begin depositing in unconfined reaches at approximately 20°, regardless of event volume.

- UBCDflow generally over-predicts the runout and entrainment for hillslope type flows. Both UBCDflow and DAN-W over-predicted volume passing, as neither one could adequately simulate progressive levee deposition. Setting all reaches of hillslope flows to unconfined gave more accurate predictions of travel distance, as UBCDflow's rules for unconfined reaches reflected the slope angles where hillslope flows tended to erode and

deposit. In some cases, however, UBCDflow dramatically over-predicted both entrainment and travel distances. UBCDflow is best applied when there are large accumulations of colluvium which can be entrained from the channel floor or sides.

- Modelling entrainment in DAN-W, as opposed to the simplistic method of modelling the flow as one large starting mass, did not change the back-calculated μ substantially for the flows tested, but did increase the ψ value needed to simulate higher velocities. It also provided more realistic flow heights as the flow proceeded down-slope.

- Using UBCDflow and DAN-W in combination may be a useful decision support tool in preliminary hazard analysis. UBCDflow is able to give good approximations of event volume and entrainment behaviour for torrent flows, and reasonable approximations of event magnitude for hillslope events. For hillslope events, the eroded depths from UBCDflow and the back-calculated friction parameters found in this and similar studies can be used together. For torrent events, the outputs from UBCDflow can be used to back-calculate friction parameters in DAN-W.

7. Modelling debris flow processes in a geotechnical centrifuge

This chapter summarize 18 geotechnical centrifuge tests. The tests were designed to investigate the influence of flow volume, moisture content (or solid concentration), and pore fluid rheology on model debris flow behaviour. The response variables measured were flow velocity, flow depth, runout, and deposit shape. Both increasing flow volume and increasing moisture content increased the flow velocities observed, although the effect of moisture content was much more pronounced. The flow depths observed varied little between tests of different moisture content and volume because of the boundary conditions of the tests.

The tests also compared the effect of using different pore-fluid rheologies (Newtonian versus pseudo-plastic) with the same soil. The flows using a pseudo-plastic pore fluid accelerated to much higher velocities in the flume, but also decelerated much faster than the Newtonian flows. This behavior is related to the dropping viscosity of the pore-fluid during acceleration in the confined flume.

Four flows were tested with an erodible bed. The main mechanism of erosion in these tests was single particle scour by the watery tail and knickpoint retreat. Levees were also observed in the tests, indicating that the flows were relatively unconfined in the channel.

Two flows using a finer soil and water (but scaled to match the consolidation behavior coarse soil used in the rest of the tests) displayed very different flow heights and velocities than the tests using a coarser soil and a higher viscosity pore-fluid. The results indicate that the viscosity of the pore fluid needs to be scaled with the g-level (N).

The morphology of the deposits and dimensional analyses showed that while the centrifuge was able to model many features of large scale tests and mitigate some of the scaling issues associated with small-scale tests, the flows were very viscous compared to granular,

bouldery-type debris flows. Perhaps the most useful element of the centrifuge is not that it is able to simulate prototype-scale processes perfectly, but that it provides the opportunity to alter the g-level, and therefore the frictional nature of the flows, independently of other variables. By doing so, centrifuge testing has the potential to greatly complement other physical modelling techniques.

7.1. Introduction

As discussed in Chapter 2, small scale flows may not reflect the dominance of Coulomb stresses and the decreasing importance of viscous stresses in field scale flows (Iverson and Denlinger, 2001). A geotechnical centrifuge was presented as a means of increasing the self-weight of the model, to achieve stress levels similar to a small debris flow in the field and thereby mitigate this problem.

While centrifuges have been used to model a variety of static and dynamic processes including seismically induced liquefaction, rockfall behaviour, fluid flow and erosion (Chikatamarla et al., 2006; Schofield, 1980; Garnier et al., 2007), debris flows are a relatively new phenomenon to be tested on a centrifuge. Initial studies (Bowman et al., 2010, 2007) focused on experimental set-up, and proving repeatability with some preliminary fixed bed tests and several erodible bed tests. The goal of this study was to extend this work by further refining the experimental set-up and to test whether debris flow parameters found to be important in 1-g and field studies could be tested in the drum centrifuge.

Debris flow volume is often cited as the most critical parameter in estimating debris flow hazard, as larger flows travel faster and farther than smaller flows, both at the lab and field scale (Hungr et al., 1984; Rickenmann, 1999, 2005). Further, previous work has shown that the peak discharge of the flow can be related to the total debris flow volume (Rickenmann, 1999).

Moisture content is also an extremely important control on flow behaviour. For example, in field and laboratory investigations of runout distances in the Dolomites, moisture content was found to control runout almost regardless of event volume D'Agostino et al. (2010). Takahashi (2007) discusses the importance of grain concentration, which decreases with increasing moisture content, in controlling the velocity distribution of particles with depth. That is, the greater the moisture content, the less the frictional contact between particles, and the lower the resistance to flow. Thus, the moisture content has a profound influence on shear rate, peak discharge, and peak velocity, which in turn affect impact pressures on any structures or natural

materials in the path of the flow.

This study refers to moisture content by mass rather than solids concentration by volume, as often used elsewhere in the debris flow literature. The relationship between them is:

$$v_s = \frac{1}{G_s w + 1}$$

where v_s is the solids concentration by volume, G_s is the specific gravity of solids (2.65), and w is the moisture content by mass. A moisture content of 33% or 0.33 corresponds to a solids concentration of 0.53 by volume.

7.2. Apparatus and instrumentation

Details regarding the design and instrumentation used in the experiments have been discussed in Bowman et al. (2007) and Bowman et al. (2010). However, a brief description of the apparatus and some minor changes to the flume for these sets of tests is given below.

Experiments were carried out using the ETH Zurich Geotechnical Drum Centrifuge in Switzerland over a week long testing period in December 2009. A previous week of centrifuge testing in June of 2008 focused on testing instrumentation and qualitative observations of several erodible bed tests.

The ETH centrifuge has a maximum working radius of 1.1 m, a maximum design acceleration of 440g, and a maximum load carrying capacity of 2000 kg (Springman et al., 2001). The flume configuration is sketched in Figure 7.1. The debris flow flume apparatus consisted of a flume to guide the flow to the runout zone, a strut which attached the head of the flume to the drum, and a curved support to spread the load of the flume over the drum surface. Originally, the flume was 600 mm long (Bowman et al., 2010, 2007), but it was lengthened in this set of tests to 700 mm.

The flume width in this round of tests was decreased from 160 mm, as used in previous tests (Bowman et al., 2010, 2007), to 60 mm to provide increased channelization. This had the effect of producing flow velocities more representative of field scale flows than had been achieved in previous trials. The greater degree of channelization also increased flow depth, which, when combined with a coarser particle distribution, enabled individual particles to be tracked in the high speed camera images.

Six pore pressure transducers (PPTs) were mounted in the base of the flume to measure

pore pressure during the experimental debris flows (Figure 7.2). Coarse sand particles glued to the base provided a rough bed surface. Smooth aluminum and Perspex walls created relatively plane strain behaviour. The upper, clear Perspex channel wall allowed a small monochrome high-speed digital camera (500 fps at full scale of 240 × 240 pixel) to observe a cross-sectional view of the flow during the test (Figure 7.3). Small markers painted on the window enabled tracking of the flow. The flow was lit by a close array of 8 LEDs embedded in the Perspex window. The camera was started by the tripping of a light barrier at the head of the flume as the flow front passed. The unconsolidated debris flow material was introduced "in flight" to the channel by a flexible feeder tube. The tube extended from the central axis of the centrifuge, where material was delivered via a funnel, and was guided by an actuator on the centrifuge tool plate to the head of the channel. Material was then able to flow outward under centrifugal acceleration down the slope. This system enabled the material to be prepared and maintained as a slurry external to the drum (in which it would otherwise consolidate during spin-up).

After each test, measurements were taken of the maximum runout and lateral spread of each flow. In addition, reference marks running vertically and horizontally on the drum surface were used as a grid to record spot depths of the flow deposit (as shown in Figure 7.3). This data was then used to compare the morphology of deposition and runout. Originally, a laser-line scanner was installed to record deposit morphology and depth. The black dots shown in Figure 7.2 were meant to mark the locations where the laser would scan a cross-section. Unfortunately, the laser failed to record any meaningful data—the results were simply noise. The material used was probably too reflective because the moisture on the surface of the deposit scattered the laser.

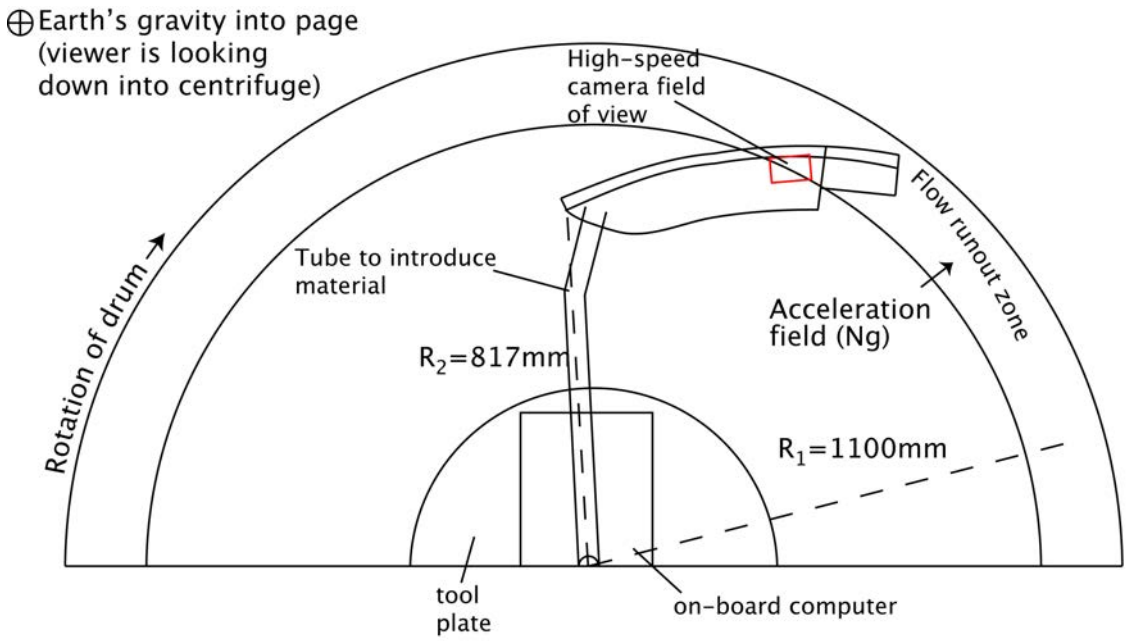

Figure 7.1.: Plan cut-away schematic view of the debris flow channel within the drum centrifuge (only half of the drum shown). In this round of tests, the chute was extended by 100 mm and the average angle of the chute was 24°.

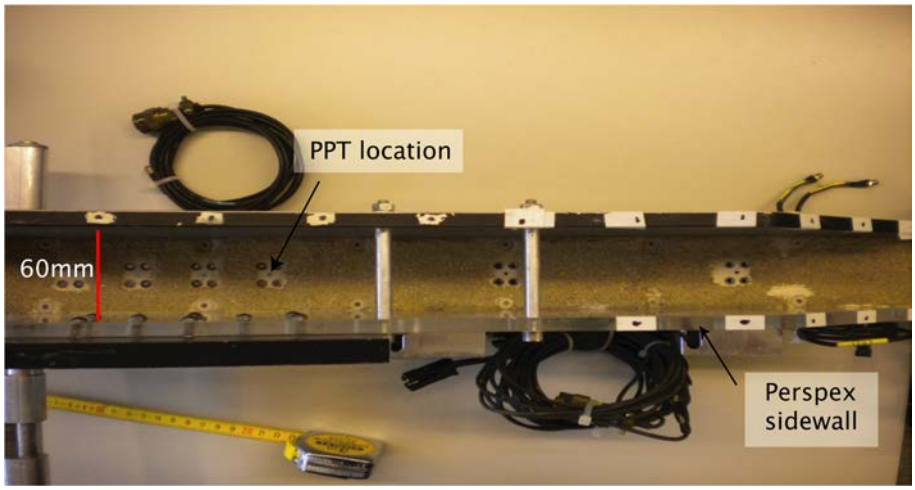

Figure 7.2.: Close-up of flume when not installed in the machine. The width of the chute is 60 mm. The roughened base and pore-pressure transducers (PPTs) positioned in the base of the machine can also be seen.

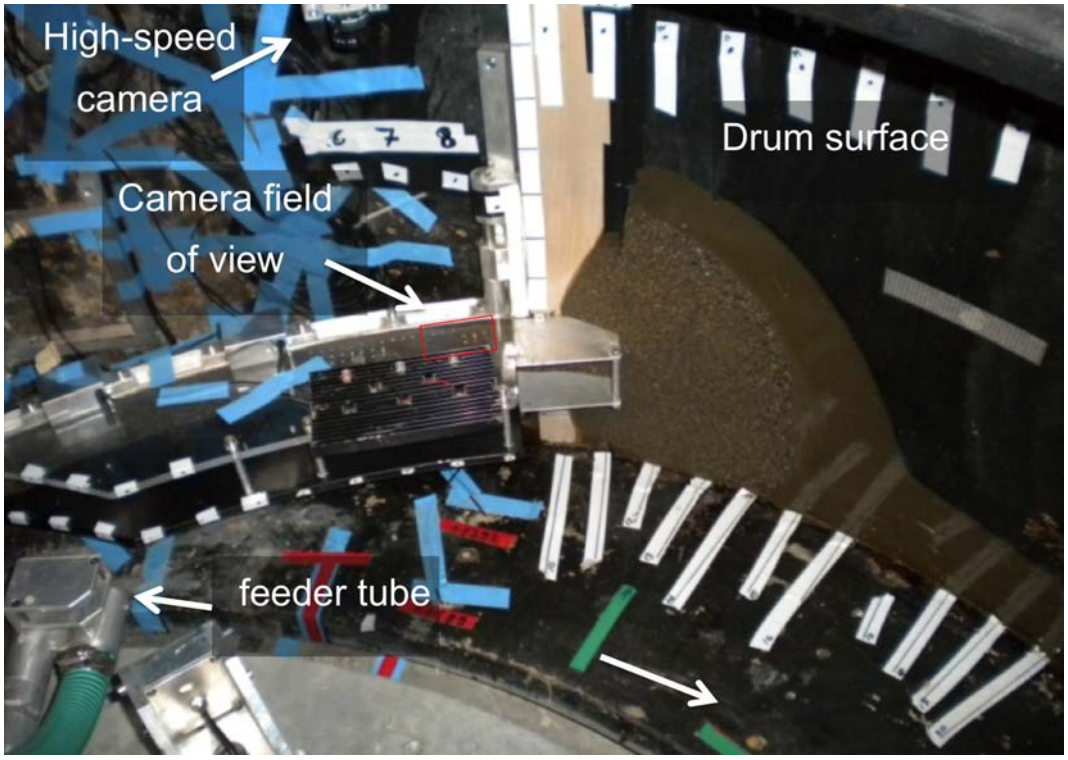

Figure 7.3.: Photograph of experimental set-up and deposition from test T14, which has consolidated on the drum surface after spin-down. The markers in the top/bottom of the photograph serve as reference points for measurements of depth. Note that the photo was taken obliquely, the deposition is plastered vertically to the inner wall of the drum.

7.3. Scaling

7.3.1. Centrifugal acceleration

As discussed in Chapter 2, there is slight variation in the acceleration through the model. The vertical acceleration field is $\omega_r^2 r$, where ω_r is the angular rotation speed of the centrifuge and r is the radius to any element in the soil model. At the maximum centrifuge radius, 1.1m, the centrifugal acceleration produced by the centrifuge in this round of experiments was 392 ms^{-2}, 40 times the earth's gravity (N=40). However, at the head of the flume (at a radius of approximately 0.817m) the vertical acceleration was 291 ms^{-2}. This means that there was an approximate 35% increase in effective g from the beginning of the channel to the end. Since all of the experiments decribed here were conducted at the same angular rotation (ω_r) the effect of the changing radial acceleration was the same for all experiments. This makes comparisons between tests rather straightforward. However, while the influence of the changing g-level is quantifiable, it does add a complicating element to attempting direct comparison with experiments at 1-g.

7.3.2. Coriolis acceleration

Additionally, there is a small increase in the effective N due to the velocity of the flow. The full equation for centrifuge modelling also includes a Coriolis term $2v_r\omega_r$, where v_r is the radial velocity of the element of interest in the model and ω_r is the angular velocity at that point (Taylor, 1995). For most centrifuge tests on relatively static geotechnical processes the effect can be ignored. However, for testing of high speed processes, the effect of Coriolis can be significant. While this does add complication, the Coriolis effect can be quantified. At the position of the high-speed camera (r of 1.025m and slope angle of 20°) test T16, which recorded the fastest flow in the tests, had a velocity of 3.66 ms^{-1}. This velocity produces a tangential acceleration of 47.3 ms^{-2}, which is approximately 13% of the radially generated centrifugal acceleration at this point. This is not inconsequential, however, most of the flows in the experiments had velocities well below this maximum. A more typical flow moving at 1 ms^{-1} as it passes the high-speed camera position produces a Coriolis acceleration of only 4% of the overall acceleration field. Coriolis accelerations of less than 10% tend to be ignored in geotechnical modelling (Taylor, 1995). The effect is quantifiable and it is unlikely that it would significantly impact the trends observed in this set of experiments. In the runout zone, where the flows are moving slower and perpendicular to the centrifugal acceleration field, the coriolis force had minimal effect.

7.4. Pore-fluids

There are two reasons for substituting a higher viscosity pore fluid for water in centrifuge modelling; to match the consolidation behavior between the model and prototype scales and to test the effect of changing pore-fluid rheology on flow behavior.

7.4.1. Matching consolidation in model and prototype

As discussed in Chapter 2, the pore fluid viscosity must be increased, or the particle size decreased, to match consolidation time-scales in the model and prototype. The most common viscous solutions used for this purpose in geotechnical centrifuge modelling are glycerine/water, silicone oil, and hydroxypropyl methyl cellulose/water (Dewoolkar et al., 1999). Silicone oil has numerous drawbacks; it is a hazardous waste, it is very difficult to clean (as it is resistant to most solvents), and it is expensive (Stewart et al., 1998). As all of the flows in this study were saturated, an inexpensive and relatively easy to clean pore fluids were needed. Therefore, glycerine and hydroxypropyl methyl cellulose were used.

After silicone oil, a glycerine/water solution is the second most common pore-fluid used in geotechnical modelling (Taylor, 1995). Its pore fluid rheology is Newtonian (discussed below), which means it will have many of the same rheological characteristics as water. However, glycerine is hygroscopic; it attracts water molecules from the atmosphere. Consequently, it cannot be fully dehydrated once mixed with water. This prevents any determination of moisture contents or sieve analysis after the test, since the mixture cannot be oven dried.

Methyl cellulose has an advantage over glycerine in tests in which knowing the final particle size distribution or moisture content is important. It is not hygroscopic and dries to a fine powder at 100°C, allowing the fluid to evaporate and solid materials to be sieved out. It also has the advantages of relative insensitivity to changes in temperature and a unit weight almost identical to pure water (Stewart et al., 1998). However, unlike water, it is not a Newtonian fluid.

7.4.2. Rheologies

Different fluid rheologies which could be applied to debris flows are shown in Figure 7.4. The simplest rheology is Newtonian; the fluid's stress versus strain rate curve is linear. A solution of glycerine and water is Newtonian.

Bingham fluids exhibit a linear shear resistance-shear rate relationship after an initial

yield shear stress has been reached. Dilatant fluids display a convex stress versus strain rate curve. Shear-thinning (pseudo–plastic) fluids show the opposite behavior; viscosity decreases with increasing shear rate. Methyl cellulose is shear-thinning.

The use of either a Newtonian or a pseudo-plastic pore fluid will depend on the type of flow one wishes to model. Granular debris flows tend to have low quantities of fines in the form of clay and silt ($< 5\%$ by mass, Takahashi (2007)), hence such flows are generally modelled as Newtonian and frictional. Conversely, muddy debris flows (Takahashi, 1991, 2007) tend to have their coarser clasts mixed within muddy suspensions. Such suspensions are often modelled as Bingham fluids. However, since mud suspensions are generally pseudo-plastic, this is an over-simplification. It may be more appropriate to use a truly pseudo-plastic material and model the fluid behaviour as such.

The use of a non-Newtonian pore fluid may not reflect all field debris flow conditions (i.e. for typical stony or granular debris flows), however, in this case, that is not the intention. Isolating the pore fluid as a variable has the potential to clarify aspects of the interaction between the solid and fluid phases of the flow. For example, it may possible to assess how the dominance of particular mechanisms such as viscous shearing or pore pressure diffusion shift as the flow transitions from confined flow to unconfined flow. These interactive mechanisms have hitherto been difficult to separate experimentally.

Figure 7.5 shows the viscosity versus shear rate of both methyl cellulose and glycerine fluids, as well as the range of global shear rates encountered in the tests. These shear rates were calculated by dividing the flow height by the typical flow velocity at the high-speed camera position. According to this calculation, over the range of shear rate encountered in the tests, the viscosity may drop by approximately 1/3 for the methyl cellulose flows, while the viscosity of the glycerine flows should not change.

While this approach to calculating the shear rate is appropriate for homogenous, viscous fluids, it does not strictly apply to granular flows which are mixtures of solids and fluids. As shown in Couette cell experiments (Bagnold, 1954) and flume tests (Takahashi, 1978, 1981; Ancey and Evesque, 2000), the effects of fluid shearing around grains, as well as the presence of grain to grain interactions, make saturated granular flows much more complicated. As discussed later in this chapter, the behaviour of the flows suggests that the viscosity of the methyl cellulose pore fluid may have dropped even further than predicted using global shear rates. This is discussed later in the chapter.

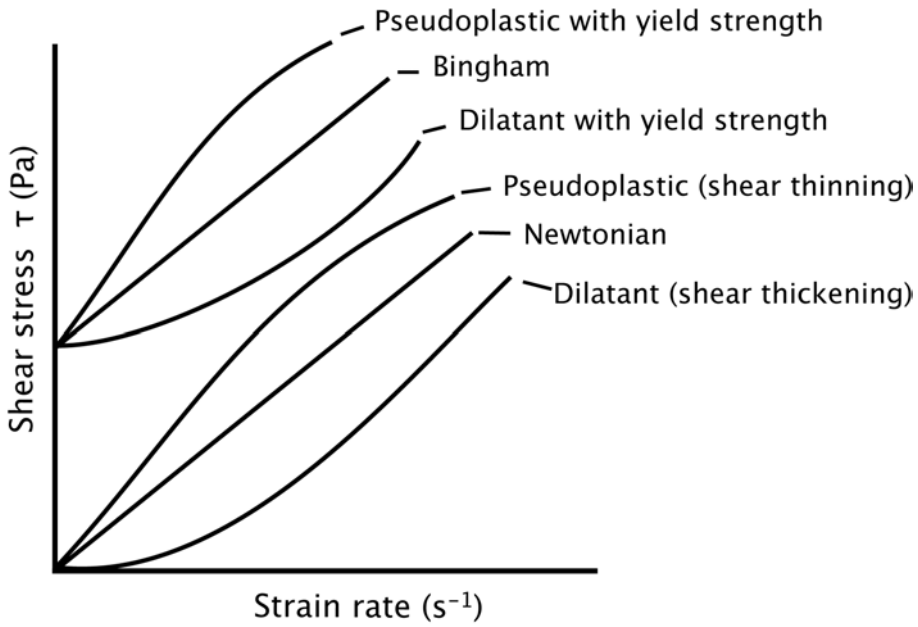

Figure 7.4.: Flow curves for idealized liquid and plastic materials.

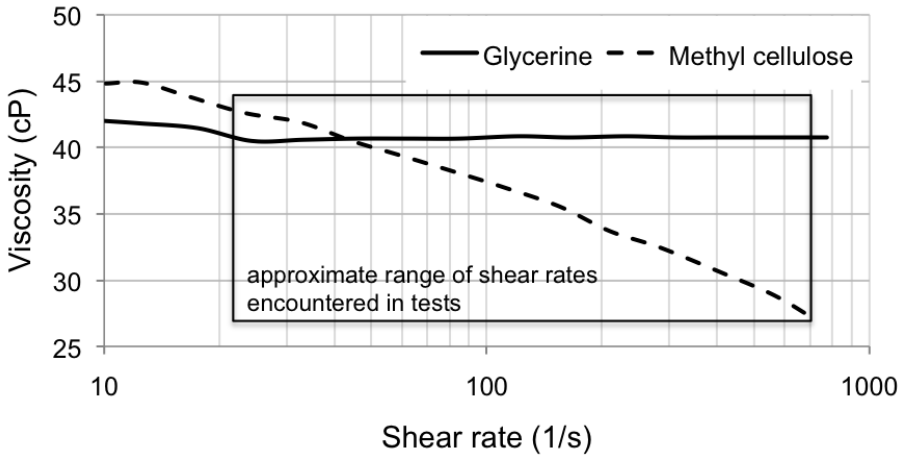

Figure 7.5.: Effective viscosity data for glycerine and methyl cellulose. The range of maximum global shear rates for the tests is also shown.

7.5. Test preparation

7.5.1. Soils

Experimental constraints limit the particle size distribution (PSD) of the soil tested in the centrifuge. The maximum size particle used is limited by the narrowest internal point of constriction in the feeder tube (where the internal diameter is 32 mm). The maximum particle diameter is slightly over 4 mm. Particles larger than this can cause mechanical arching and flow blockage (Bowman et al., 2007). The particle size distribution tested represents a compromise between the largest D_{90} (2 mm) possible, while still allowing a relatively high value of C_u (d_{60}/d_{10}) of 36.7, which is shown to be an important parameter in other physical modelling studies of debris flow behaviour (Bowman and Sanvitale, 2009). The PSDs used in this set of experiments are shown in Figure 7.6.

7.5.1.1. Coarse PSD

The coarse PSD, the main mixture of soil used in the majority of the tests, was a mixture of soil from three separate localities—two in New Zealand and one in Switzerland. The largest fraction used (approximately 48% by weight) was collected from the Mt. Thomas debris flow site in Northern Canterbury. This locality has been a site of ongoing debris flow activity since 1977, when a series of debris flows were triggered on recently harvested cut blocks (Pierson, 1980).

The material from Mt. Thomas was supplemented in the range of 0.6 mm to 0.075 mm with fluvial material available at ETH, since sieving out enough sand and silt strictly from the Mt. Thomas material was impractical. 41% of the PSD tested was made from this fluvial material. The lighter color of this sand also created slightly more texture in the high speed camera imagery, which was helpful for post-processing.

The finest 11% of the mixture came from loess collected from slips in the central north island of New Zealand. This provided the remainder of the fine sand, silt, and clay in the particle size distribution used in the tests, as shown in Figure 7.6. Atterberg limit tests were carried out on both Mt Thomas and North Island loess materials (percentage passing 75μm). These showed that the fines were of low plasticity and hence, applicable to stoney or granular debris flows (Takahashi, 1981)– see Table 7.1 and Figure 7.7 for details.

In the dry form, the dry particle size distribution of the loess was much coarser than when dissolved in solution, due to hard agglomerations of fine material acting as individual clasts. These dissolved readily in solution during wet sieving and hydrometer testing. To ensure

that these clasts desegregated before each test, the coarse PSD was mixed with the viscous solution to the correct moisture content, covered, and allowed to sit overnight. However, some agglomerations of fines were still observed in the depositional material during testing. This is problematic. The fines in these 'pseudo-clasts' were not in solution in the pore fluid, which means that the PSD prepared was effectively slightly coarser than intended. The effect would have been similar in all of the tests conducted, however, which means that comparisons between tests of the same material are still valid.

7.5.1.2. Fine PSD

Two sets of tests used a material with a particle size distribution approximately $\sqrt{N}$ smaller than the particle size distribution used in the rest of the fixed bed tests. This was called the fine PSD in order to test the "model of models", as discussed in Section 7.6.2. The ideal distribution would be exactly $\sqrt{N}$ finer than the coarse PSD. However, hydrometer testing after the experiments showed that the fines used in these tests were slightly finer than originally thought. The actual fine PSD used is shown by the dashed line in Figure 7.6.

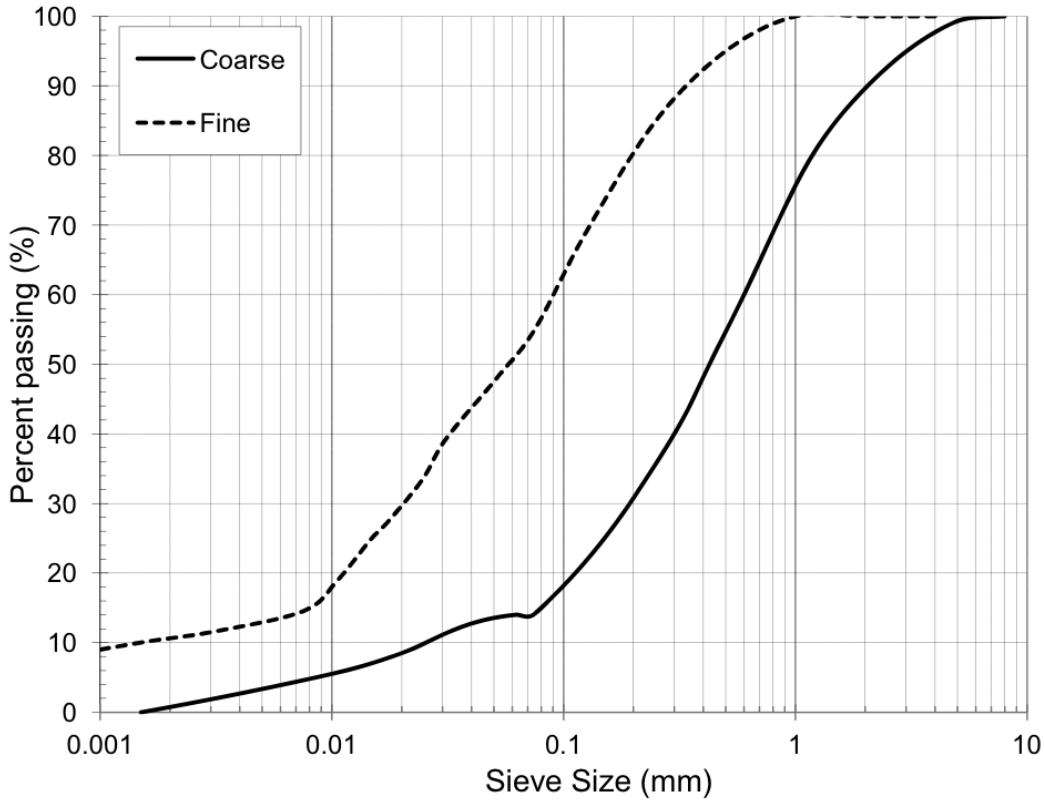

Figure 7.6.: The coarse and fine PSD used in all tests.

Table 7.1.: Soil plasticity parameters for the fines used in the experiments.

Soil origin	Liquid Limit W_{LL} (%)	Plastic Limit W_{PL} (%)	Plasticity Index PI (%)	Classification
North Island Loess	33.7	23.3	10.4	Low plasticity clay
Mt. Thomas	30.1	22.2	7.9	Low plasticity silt/clay

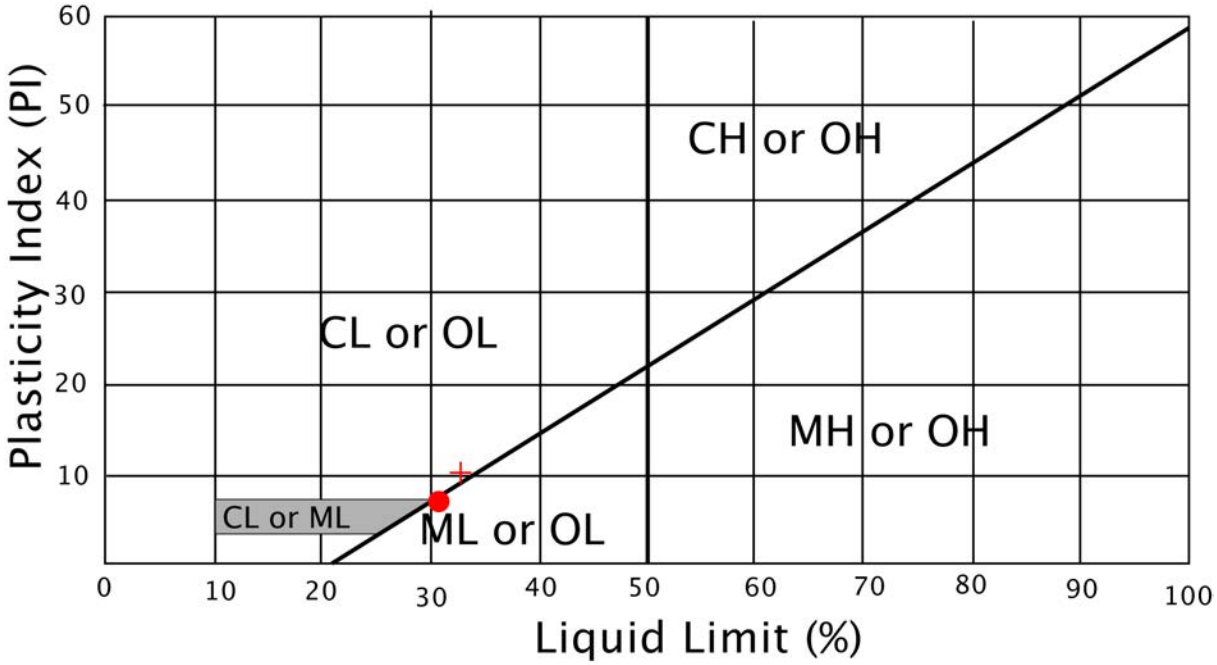

Figure 7.7.: USCS classification of soils based on the liquid limit and plasticity index. CL is inorganic clays of low to medium plasticity. CH is inorganic clays of hight plasticity. ML is inorganic silts which are non-plastic or slightly plastic. MH stands for silts with high plasticity. OL and OH stands for organic clays of low and high plasticity, respectively. The markers are the locations of the fine material (passing $75\mu m$) from the Mt. Thomas material (red dot) and loess material used in the experiments (red cross).

7.5.2. Pore-fluids

Whether methyl cellulose or glycerine was used, the solutions first had to be mixed up to the target viscosity. Both solutions were mixed to the appropriate viscosity using a cone viscometer. The pore fluid solutions were first mixed to the approximate viscosity intended. At this point, more glycerine or methyl cellulose was added, or the solution diluted by trial and error until

the desired viscosity was reached. For glycerine, the target viscosity was between 40 to 42cP. For the methyl cellulose, the target viscosity was between 42 to 45cP at a shear rate of 10 s^{-1}. The methyl cellulose was mixed at a slightly higher viscosity in order to approximately match the viscosity of the glycerin at shear rates between 50 and 100 s^{-1}, which was the range of shear values originally expected. The range of pore fluid tested varied 2 or 3 cP because it was difficult to achieve a viscosity value that was precisely 40cP. The viscosity tests were conducted at a temperature of 20°C, which was the climate controlled temperature of the centrifuge room where the experiments were conducted.

7.5.3. Erodible beds

In five tests, erodible beds approximately 4 cm thick and with a moisture content of 15% were prepared in-situ. Methyl cellulose was used as the pore-fluid in these tests; the same as for the flows. To construct and prepare the beds to a consistent thickness, fixed amounts of soil were packed behind a 40 mm wide polystyrene mold which was formed to match the curved shape of the bed. The surface of each mold was hardened and sealed with a sand and glue to prevent absorption of fluid into the pores of the polystyrene.

The high fluid viscosity of pore-fluid ensured that there was little migration of moisture through the bed at 1g before the centrifuge was spun up. The mold was just flexible enough to be withdrawn without disturbing the bed surface just before each test. The beds were slightly undersaturated at a moisture content of 15% and stayed vertically in place by suction before spin up. Movement was monitored by a video camera placed at the head of the bed. No detectable movement of the bed was noted between removal of the moulds and spin-up to the working g-level for any test. It should be noted that the beds probably desaturated somewhat during spin-up due to evaporation, which was exacerbated by the heat from the LED array and the air flow produced by the spin of the centrifuge.

7.6. Test agenda

The results from 18 debris flow tests are presented. Table 7.2 gives details and test code of each experiment. Note that throughout this chapter, the tests are referred to by a shortened version of the test code: i.e. test T7_V_MC becomes test T7. Each test took, on average, a half day of centrifuge time. A week was spent preparing material and instrumentation. More details regarding the experimental setup and reproducibility of the tests is given in Bowman

et al. (2007) and Bowman et al. (2010).

7.6.1. Fixed bed tests with coarse material

Eleven tests were run using a fixed bed and the coarse PSD. Three variables were tested; flow volume, moisture content, and fluid rheology. The first variable tested was the volume of material used in the test. Using glycerine as the pore fluid, three tests were run using 1.0 kg (T15), 1.75 kg (T14), and 2.5 kg (T20) of material. Each test had a moisture content of 33% by mass.

The second variable tested was moisture content. Two flows were run using 1.75 kg of dry solids with a moisture content of 39% (T23) and 41% (T11) moisture content to compare with the flow of 33% moisture content (T14). The moisture content of the flow with 41% moisture content (T11) is only approximate because the first attempt at T11 became clogged in the feeder tube. Since centrifuge time and time to prepare the material was limited, the test was rerun by adding the approximate volume of fluid lost in the first attempt.

The next variable tested was the effect of using a different pore fluid rheology—methyl cellulose. 1 kg (T9), 1.75 kg (T10), and 2.5 kg (T7) of dry solids were tested at 33% moisture content. Two more tests were conducted at a higher moisture content of 36% (T12) and 39% (T22).

Finally, a single fixed bed test, T5, used the same coarse PSD with water as the pore fluid. The moisture content was 36% by weight. However, there is no velocity or deposit shape data for this flow. The test was conducted in a previous round of tests when the pore pressure transducers were not working and manual depth measurements were not taken.

7.6.2. Fixed bed tests with fine material—model of models

Two tests were designed as a modelling of models; a common strategy in geotechnical testing. A model of models test is a way to check the scaling assumptions of the test. In this case, the goal of these two tests was to check the assumption that, in terms of consolidation behaviour, a material with a particle size distribution scaled down by $\sqrt{N}$ would behave similarly to a test using the original PSD with a pore-fluid viscosity scaled up by N. If consolidation dominates flow behaviour, to the extent that other effects of altering viscosity can be ignored, then the runouts, velocities, and flow heights of these flows should be the same. These experiments were included to test this hypothesis. The tests T21 (1 kg dry solids) and T24 (1.75 kg) were tested at 33% moisture content to compare against T15 and T14, respectively.

7.6.3. Erodible bed tests

During field mapping, it was noted that bed armouring seemed to limit the erosion in some reaches. Further, in the high-speed camera imagery in several preliminary erodible bed tests, erosion was only observed in the watery tail portion of the flow, after the bed had been completely saturated. Accordingly, three tests were set-up to investigate the effect of different bed particle size distributions on entrainment (T17, T18, and T19). A fourth test was set-up to investigate the effect of a bed which was, hypothetically, made more permeable to moisture from the over-riding flow by creating small holes in the bed surface with a nail (T25). This test was conducted in order to see if increased saturation of the bed would increase the amount of entrainment observed.

These tests were all conducted using 2.5 kg of the coarse material over a 1.25 kg erodible bed. All of the flows had a moisture content of 33%. The bed was prepared to 15% moisture content in each test.

In test T16, 825mL of clear methyl cellulose solution was sent down the flume, over an erodible bed using the coarse PSD. The premise of this test was to observe how a clear fluid would erode material, in contrast to the granular flows.

Figure 7.9 shows a picture of the bed in tests T17, T18, T19, and T25 before each test was conducted. In both T17 and T25, the PSDs in the bed was the same as for the flow (the coarse PSD). In T18, the upper layer of the bed was covered with fine gravel. Large particles over 4mm in diameter were placed at random on the bed surface to mimic boulders at the prototype scale. In T19, all of the particles larger than 1 mm were removed. Note that the finer bed test (T19) is much lighter than the other photos, as the most of the gravel has been removed.

Table 7.2.: Test agenda. MC stands for methyl cellulose.

Test Code	Weight of material (kg)	Moisture content (% by weight)	Pore fluid	Material used
T5	2.5	36	water	coarse
T9	1.0	33	MC	coarse
T10	1.75	33	MC	coarse
T7	2.5	33	MC	coarse
T12	1.75	36	MC	coarse
T22	1.75	39	MC	coarse
T15	1.0	33	glyc	coarse
T14	1.75	33	glyc	coarse
T20	2.5	33	glyc	coarse
T23	1.75	39	glyc	coarse
T11	1.75	41	glyc	coarse
T21	1.0	33	water	fine
T24	1.75	33	water	fine
T16	1.25 - bed 825mL MC - flow	15 - bed	MC	fluid flow, coarse bed
T17	1.25 - bed 2.5 - flow	15 - bed 33 - flow	MC	coarse flow, coarse bed
T18	1.25 - bed 2.5 kg - flow	15 - bed 33 - flow	MC	coarse flow, coarser bed
T19	1.25 - bed 2.5 - flow	15 -bed 33 - flow	MC	coarse flow, finer bed
T25	1.25 - bed 2.5 - flow	15 - bed 33 - flow	MC	coarse flow, bed with holes

Glyc stands for glycerine, MC is methyl cellulose.

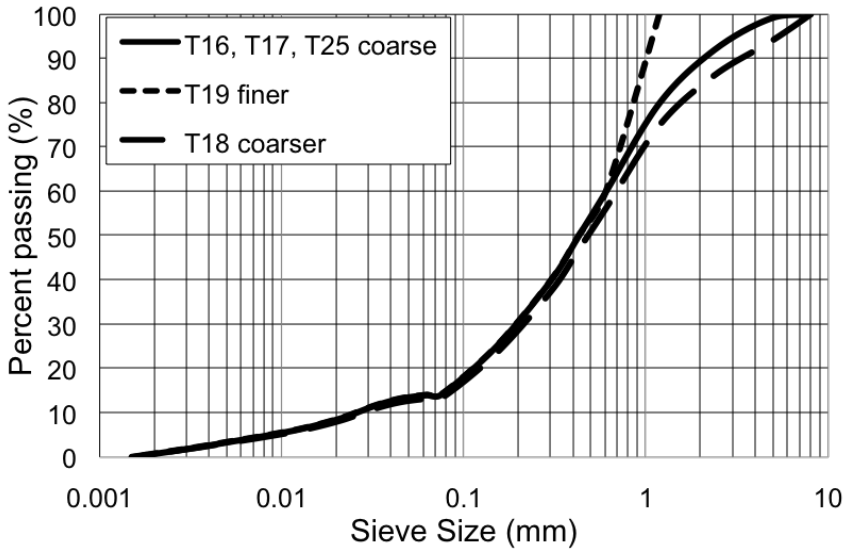

Figure 7.8.: The particle size distribution of the erodible beds.

Figure 7.9.: Plan view of the prepared erodible beds used in test: T17, which was made of the coarse PSD (upper left); T18, which was made coarser (upper right); T19, which was made finer (lower right); and T25, which was prepared with holes (lower left).

7.7. High speed camera images and flow height data

7.7.1. Typical behaviour

Images from the high speed camera gave a view of the debris flow as it passed the Perspex window. A fast, coarse, unconfined flow front dominated by larger diameter solids preceded the peak discharge in every flow (Figure 7.10).

The surface of each flow was often slightly higher in the middle than on the edges because larger particles were often carried in the center of the flow and their edges would protrude from the surface. While particles adjacent to the Perspex window were in focus,

particles near the centre were somewhat blurry and indistinct, because of the limited depth of field in the camera. This can be seen in Figure 7.10.

To explore the change in flow depth over time, the flow heights, both at the free surface at the center and against the window, were measured by use of the high speed camera images. Measurements of the flow depth were taken at least every four frames during front passage, then every several hundred frames in the watery tail portion of the flow when the rate of change of flow height dropped significantly. These measurements were precise to within ±0.5 mm.

Figure 7.11 shows the typical morphology of an experimental debris flow surge and how these features appear on a plot of maximum flow height with time. The depth of flow rapidly attenuated in all the flows with the arrival of the front (or head) of the surge. In some flows, the flow depth was then steady for a short period as the body of the surge passed. This is labeled as the body of the flow in Figure 7.11. After a period of time, the flow depth began to decrease, coarse clasts more or less stopped being visible on the flow surface, and the material at the window became noticeably finer. This was interpreted as a transition to finer material in the tail part of the surge.

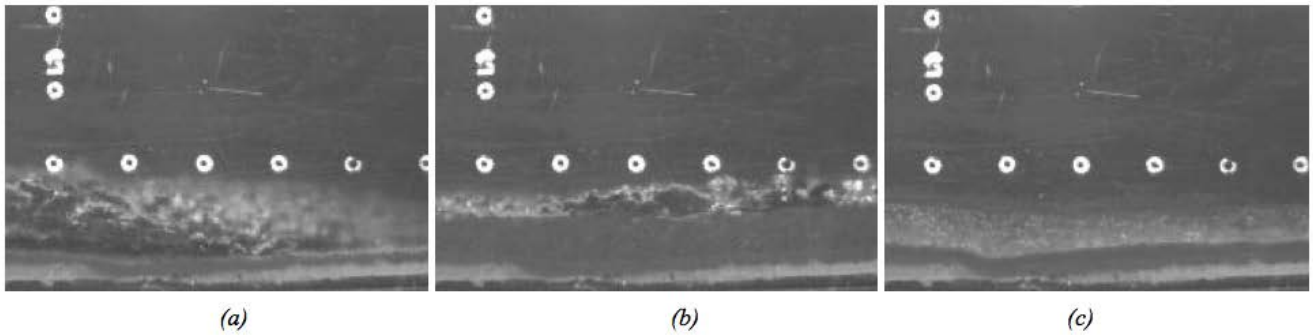

Figure 7.10.: High speed camera images from test T14. Flow proceeds from left to right. The dot spacing is 10mm. The sequence shows (a) the arrival of the front at frame 644 (1.93s after light trigger was tripped), (b) passage of the body of the flow at frame 707 (2.12s), and (c) the the watery tail portion of the flow at frame 1504 (4.5s).

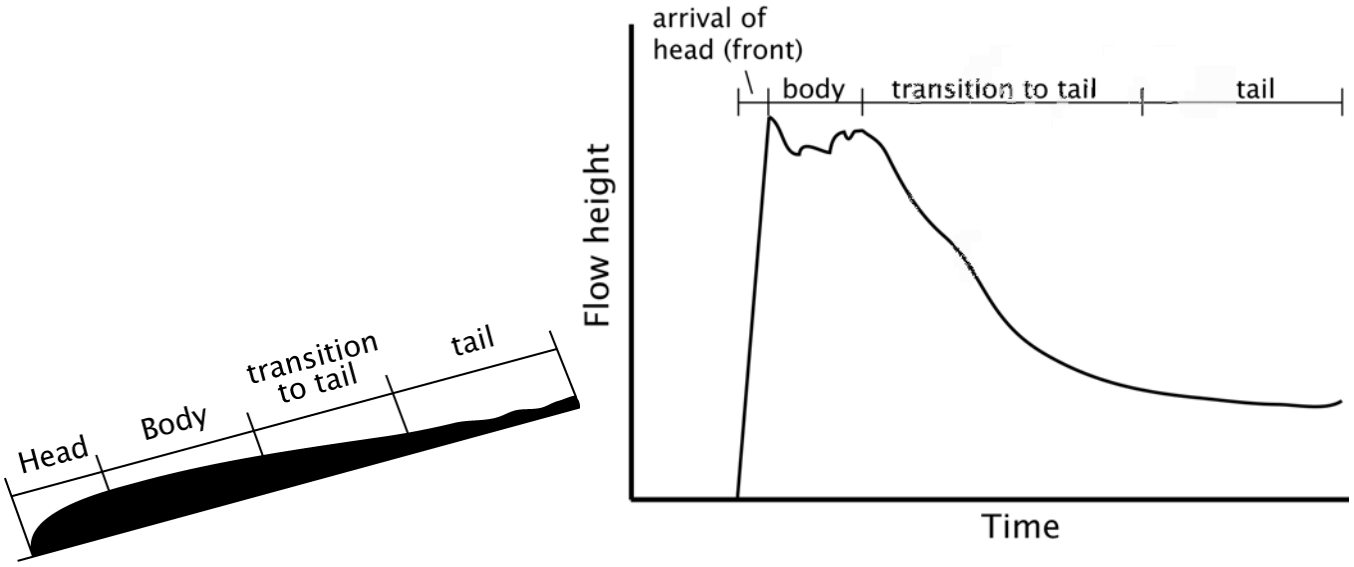

Figure 7.11.: Left: Main features of a debris flow surge. Right: Corresponding features in a plot of flow height and time.

7.7.2. Glycerine flows

Figure 7.12 shows the flow height of the glycerine flows during passage of the front and the transition to the thinner tail part of the surge. The maximum flow heights ranged from 14 mm to 17 mm at the high-speed camera position. There was no systematic difference in the height of the front between different flow volumes, or different moisture contents. However, the flows at higher moisture contents (39% and 41%) had a sharper peak, indicating that the front and body passed the high-speed camera with a higher velocity than the flows with 33% moisture content. Despite this, the surge morphologies (i.e the height and relative lengths of the body and tail) were approximately the same regardless of moisture content. For the tests with increasing mass, since the flow heights were very similar, the extra mass was accommodated in a longer, thicker body and tail.

7.7.3. Methyl cellulose flows

Figure 7.13 shows the flow height of the fixed bed, methyl cellulose flows during passage of the front and the transition to the thinner tail part of the surge. In these tests, the maximum flow height was more variable and slightly less than for the glycerine flows. The depths of the tail varied, especially between the 2.5 kg and 1.75 kg flow. While the 2.5 kg flow went slightly faster than the 1.75 kg flow, the peak flow heights were very similar. Thus, the peak discharges

of the two flows were fairly similar as well, even though much more material travelled down the flume in the 2.5 kg test. This material then, had to be transported behind the front in a longer, thicker body and tail, which can be seen in Figure 7.13.

Following this rationale, one would expect the body and tail of test T9, with 1 kg of material, to be even thinner. However, some of the front material in this flow was deposited at the channel margins, as seen in the high-speed camera. This effectively narrowed the channel as the rest of the flowed passed, producing a thicker (in terms of flow height), longer tail than would have occurred otherwise.

7.7.4. Finer flows

Figure 7.14 shows the height of the flows of the fine PSD and water. The maximum heights of the flows were dramatically less than for either the methyl cellulose or glycerine flows. Notice that the arrival time of these flows is much earlier than for the coarse experiments, indicating a much higher velocity. The shape of the hydrograph also indicates that these flows had a shallower front and longer body than for the fixed bed tests with coarse material and a more viscous pore fluid. In this case, the difference between flows of different volumes is clear. The volume of the flow did not cause a large change in peak flow depth, it increased the length of the flow body and the thickness of the tail portion of the flow.

Interestingly, in all tests except the fine flows, increasing volume did not produce a systematic increase in flow height. In past flume experiments that were conducted at 1-g (Davies, 1988) increasing the flow volume resulted in an increase in the peak flow height. From this, for the centrifuge tests, it is hypothesized that the diameter of the feeder tube largely limited the maximum flow rate as the material was transported to the head of the flume.

7.7.5. Erodible flows

Figure 7.15 shows how the maximum flow height of the erodible bed tests changed over time. The black lines indicate experiments which were designed to test the effect of a coarser or finer particle size distribution in the bed. These tests used 1.25 kg erodible beds, with a 2.5 kg flow. The shape of the hydrograph and peak discharge in each test is remarkably similar. They are also very similar to their fixed bed counterparts. However, the flow heights are approximately 25% larger than in the fixed bed tests. The probable reason for this increase in flow height will be discussed later in the chapter.

The red line is test T16, in which a fluid flow of 40cP methyl cellulose was sent down

the flume over a prepared bed identical to the one used in test T17. The hydrograph shows that this flow arrived at the high speed camera position much sooner and had a very shallow front profile. The front also showed turbulent-like behaviour as shown by the erratic, spiky profile as the front passes. The tail of the flow began to erode material once the flow front had passed. At this point, flow heights became much more stable.

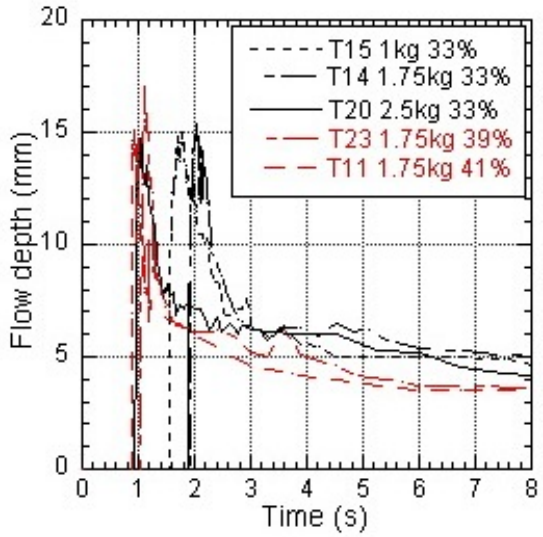

Figure 7.12.: Plot of flow depth over time for the glycerine tests.

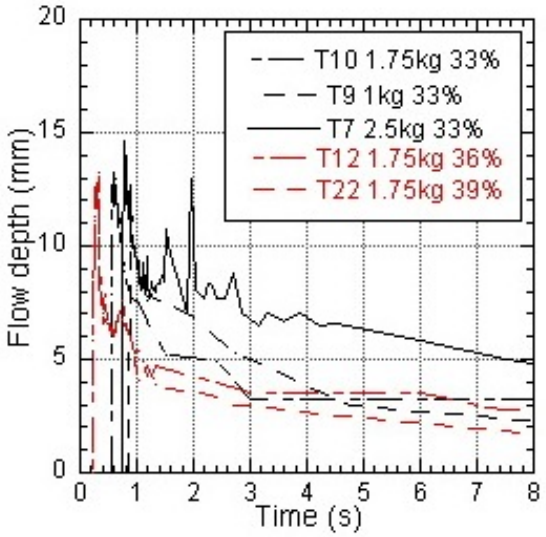

Figure 7.13.: Plot of flow depth over time for tests using methyl cellulose as the pore fluid.

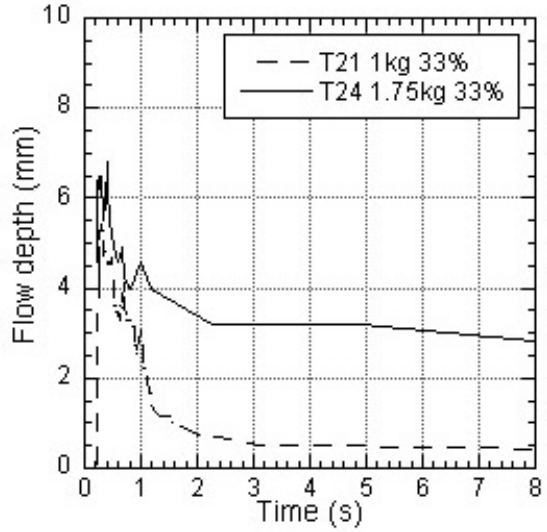

Figure 7.14.: Plot of flow depth over time for tests using the fine particle size distribution and water as the pore fluid.

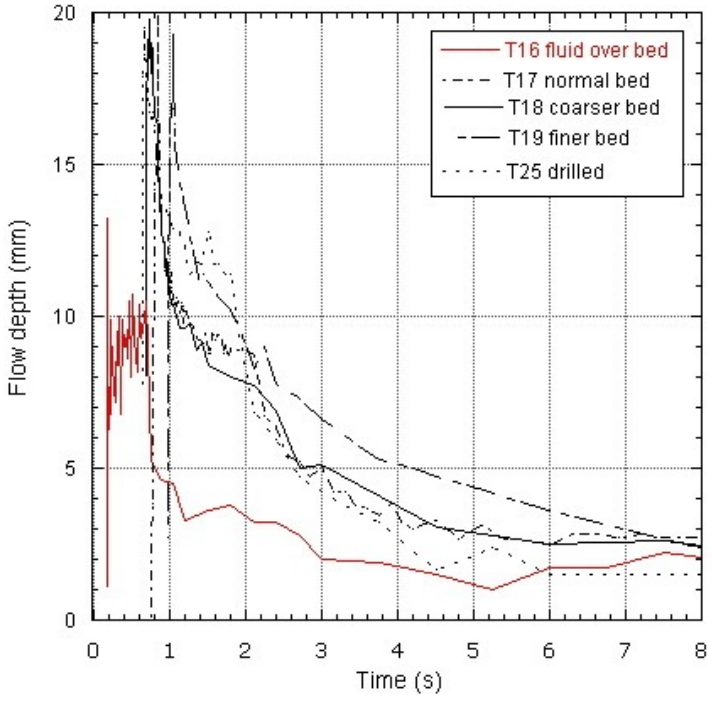

Figure 7.15.: Plot of flow depth over time for erodible bed tests (which use methyl cellulose as their pore-fluid).

7.8. Front velocity data

Data from pore pressure transducers mounted at the base of the flume and the high-speed camera were used to record the front velocity of the flows as they travelled down the flume (Figures 7.16, 7.17, and 7.18). Each pore pressure transducer recorded a spike in pressure as the flow front passed over the sensor. The time between these responses divided by the distance travelled between successive pore pressure transducers gave the average velocity between them. The locations of the data points shown in the Figures are half way between the pore pressure transducers which recorded the responses used to calculate the velocity.

Figures 7.16, 7.17, and 7.18 also show the front velocity recorded by the high-speed camera near the flume outlet. This velocity was calculated by tracking how long it took the flow front to traverse the width of the camera frame. The average velocity in the camera frame is presented as a single data point at the camera position.

7.8.1. Glycerine

Figure 7.16 shows the velocity of the glycerine flows as they travelled down the flume. The velocity of the glycerine flows increased with both flow volume and moisture content. The peak velocity nearly doubled between 1.0 kg and 1.75 kg (T15 and T14, respectively), but only increased slightly when another 0.75 kg of material was added (T20 with 2.5kg).

An increase in moisture content produced a much more dramatic response than an increase in volume. A moisture content increase of 6% (to give a w of 39% by weight) in test T23 caused the peak velocity to triple when compared to T14 (w of 33%). The addition of another 2% to a w of 41% moisture content in T11 caused the peak velocity to increase substantially again.

7.8.2. Methyl cellulose

Figure 7.16 plots the velocity of the methyl cellulose flows as they travelled down the flume. The general trends are the same as for the glycerine flows; velocity increases with volume and moisture content, but the effect of moisture content is much more pronounced. The maximum velocities of the methyl cellulose flows are approximately double that of the corresponding glycerine flows. The use of methyl cellulose appeared to magnify the trends observed in the glycerine flows.

7.8.3. Fine material and water

Figure 7.18 indicates that the fine material flows travelled much faster than either the glycerine or methyl cellulose flows. However, the 1 kg flow actually travelled faster than the 1.75 kg flow. The reasons for this behaviour are unknown.

7.8.4. Erodible beds

Pore pressure data was not available for the erodible bed test (T17, with methyl cellulose pore fluid) as the under-saturated condition of the bed attenuated any pore pressure response at the base. However, the velocities recorded for each flow at the high-speed camera position are shown in Figure 7.19. Figure 7.19 also shows the velocity of the fixed bed tests at the high-speed camera position for reference.

The front of T16 was fluid only; no solid material was entrained by the flow front. Consequently, its front velocity at the high-speed camera position was extremely fast (3.66 ms^{-1}). For tests T17, T18, T19, and T25, the front velocity was similar to the velocity of T7–the analogous fixed bed test with 2.5 kg of coarse material and w of 33%. This was surprising, as it was expected that both increased bed roughness and a loss of moisture into the bed would slow the flow, as occurred in previous tests on more unconfined flows (Bowman et al., 2010).

7.8.5. Coarse material and water

The velocity at the high speed camera of the single flow using the coarse PSD and water (T5) is shown in Figure 7.19. The flow achieved a velocity of just over 2 ms^{-1}—approximately the same as the equivalent 1.75 kg methyl cellulose flow at 36% moisture content (T12). This suggests that the viscosity of the methyl cellulose may have dropped well below the values shown in Figure 7.5 as pore-fluid was forced between particles during shearing.

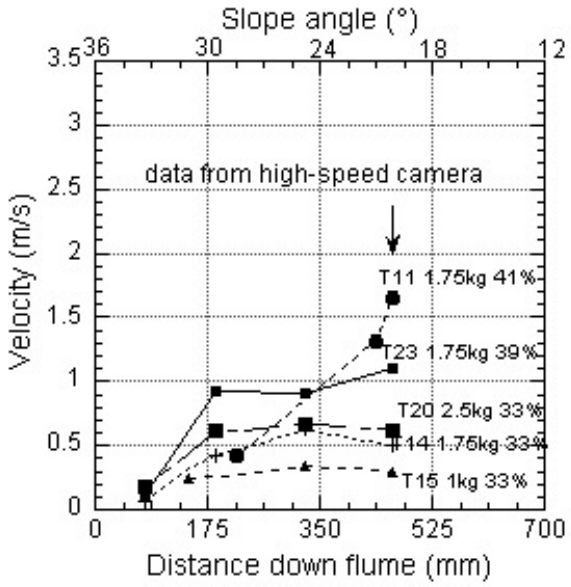

Figure 7.16.: Velocity of the glycerine flows plotted. The far right set of points was calculated from high-speed camera data.

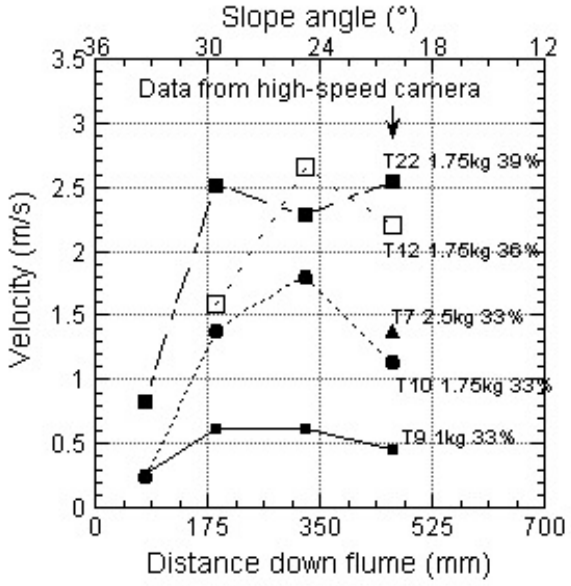

Figure 7.17.: Velocity of the methyl cellulose flows plotted against distance.

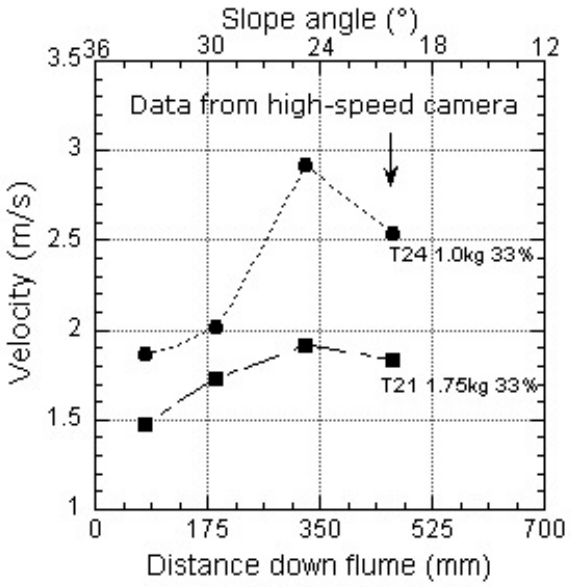

Figure 7.18.: Velocity of the fine flows plotted against distance.

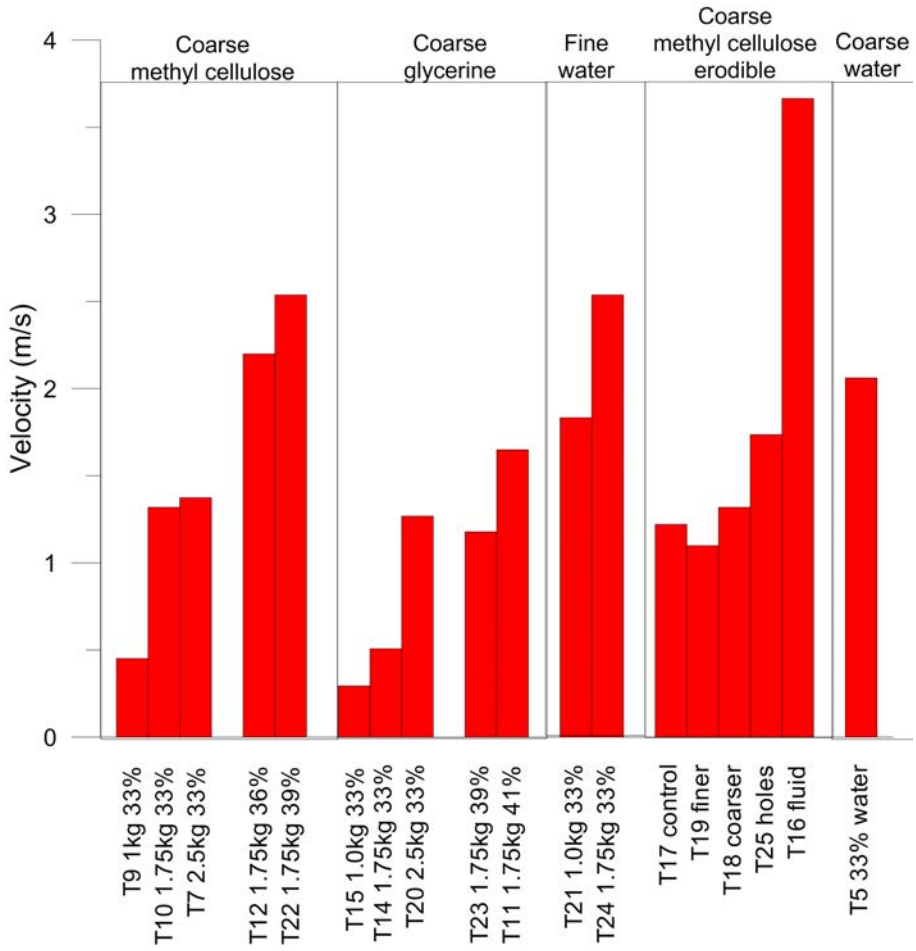

Figure 7.19.: Bar graph to compare the velocity at the high speed camera position for all tests.

7.9. Velocity profiles

7.9.1. Particle tracking

The velocity profile with depth was observed by tracking particles at various depths as the flow passed by the fast-camera position. Velocity profiles were measured as the front and the body of the flows passed the high-speed camera position. While the velocity profiles cover most of the flow depth, unfortunately, the epoxy used to seal the flume and occasional residual material from previous tests obscured the deepest 3 to 5 millimeters of flow, preventing a complete velocity profile to the base of the flume. Velocity profiles also were not possible for the fine flows, as there was not enough texture to track particles. It was also not possible to observe the

velocity profile of test T5, as a different high-speed camera set-up in this test showed a larger field of view, but less detail.

7.9.2. Fixed bed tests at 33% moisture content

Figure 7.20 compares the velocity profiles of test T14 (glycerine flow) and test T10 (methyl cellulose flow). Both tests used 1.75 kg of material at a moisture content 33%. Figure 7.20 shows that the velocity profile of the front is much shallower (i.e. the flow is faster and there is greater shear) than in the body. While the flow does slow with time, the dramatic change in profile is caused primarily by friction against the outer walls of the flume. In the true flow front, the flow front represents the velocity profile without the influence of friction from the walls of the flume. In the receding limb, the particles tracked are sliding against the Perspex wall, creating a much steeper velocity profile. The velocity profile in T14 shows the velocity of a particle tracked in the body of the flow on the surface, which is traveling much faster than particles a the margin of the flow against the Perspex window. This demonstrates that the overall velocity of the body of the flow was probably larger than what is implied by the velocity profile taken against the Perspex window.

Figure 7.20 also confirms that the methyl cellulose displayed a higher velocity, and hence higher shear rate than the glycerine flows (note that the x scales in Figure 7.20 are different). Both profiles are also approximately linear with depth.

7.9.3. Fixed bed tests at 39% moisture content

Figure 7.21 shows the velocity profiles of T23 (the fixed bed glycerine test with 39% moisture content) and T22 (the equivalent methyl cellulose test at 39% moisture content). In this case, both tests are moving at a similar velocity at the front. However, the glycerine test appears to be moving more slowly in the body of the flow. Again, both velocity profiles appear to be approximately linear with depth.

7.9.4. Erodible bed tests

Figure 7.22 shows the velocity profile for T17 (the control erodible bed test with the coarse PSD in both flow and bed) and T7 (its equivalent fixed bed test which used 2.5 kg of material). For test T17, the surface of the erodible bed is at 0 flow depth. Both velocity profiles had similar velocity profiles at the front. However, the body of the fixed bed test (T7) was much slower than the erodible bed case.

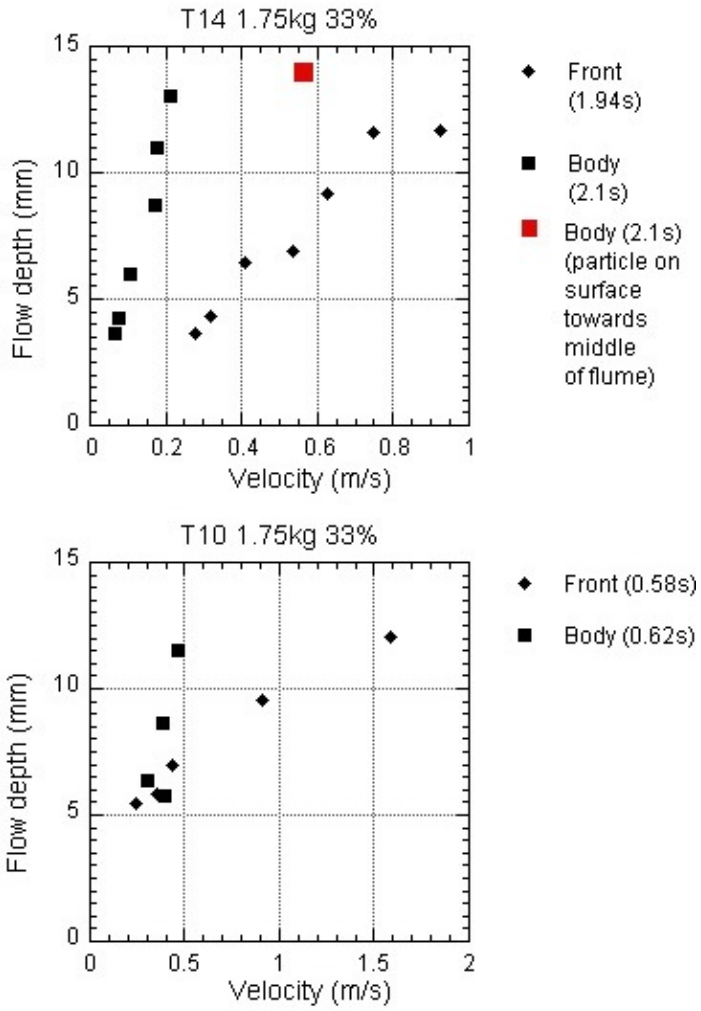

Figure 7.20.: Velocity profiles of the tests for tests T14 (glycerine flow using 1.75kg of material at 33% MC) and T10 (methyl cellulose flow using 1.75kg of material at 33% MC). The methyl cellulose flow's velocity profile at the front is significantly faster. Zero depth represents the bottom of the flow (i.e. the bed of the model).

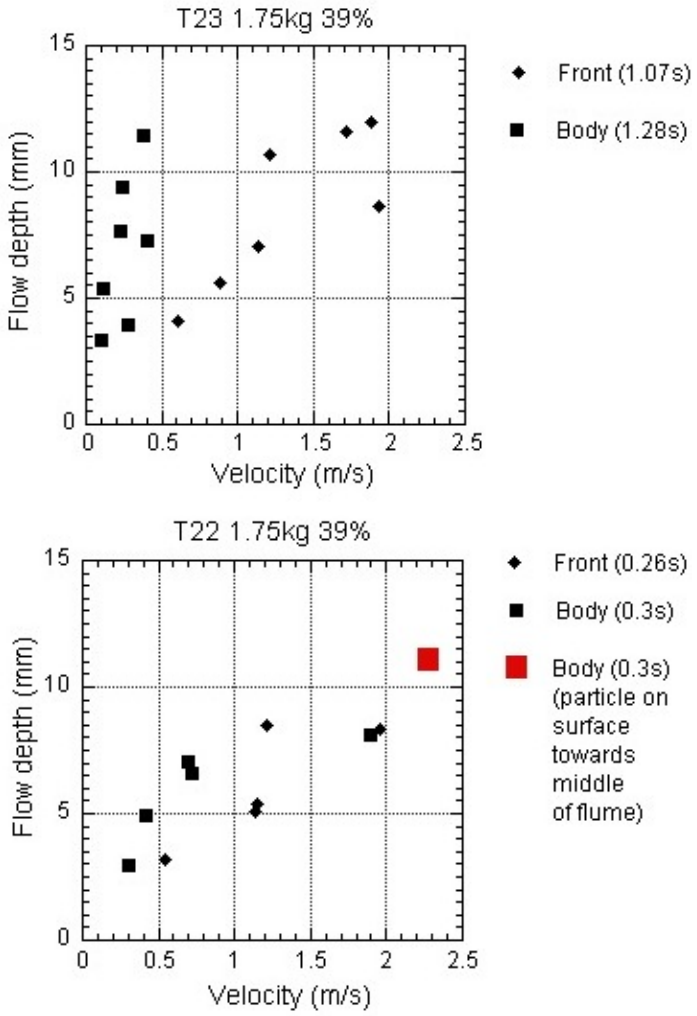

Figure 7.21.: Velocity profiles of the tests for tests T23 (glycerine flow using 1.75kg of material at 39% MC) and T22 (methyl cellulose flow using 1.75kg of material at 39% MC). While the velocity profile at the front is similar, the velocity profile of the body in the methyl cellulose shows more shear.

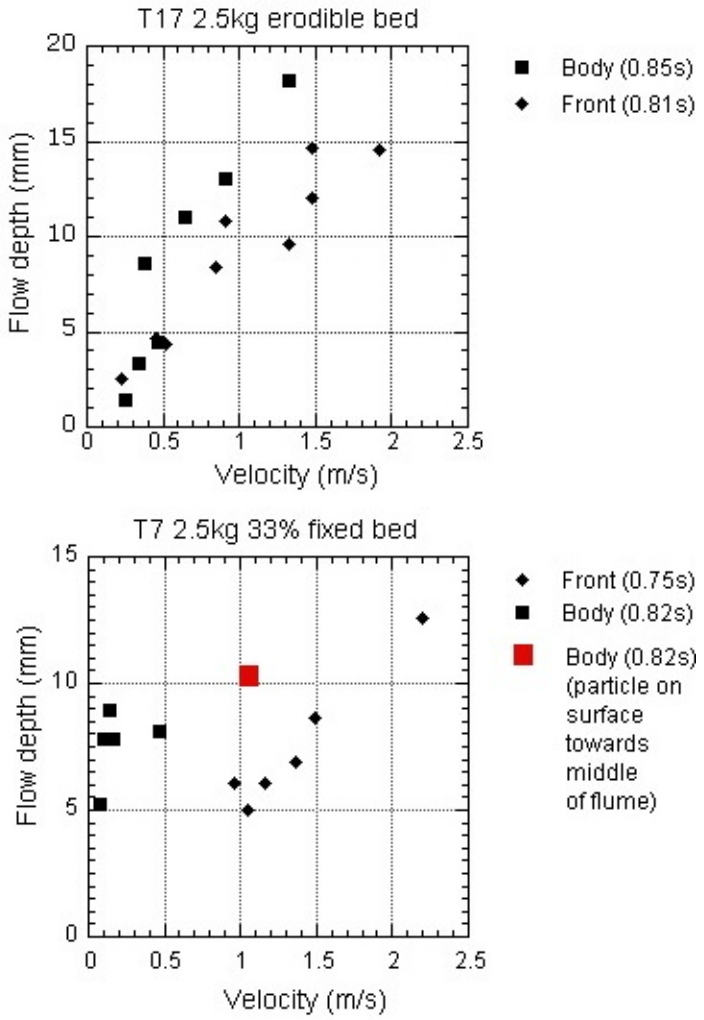

Figure 7.22.: The velocity profile for T17 (the erodible bed test using 2.5kg in the flow at 33% moisture content) and the equivalent fixed bed test, T7 (2.5kg 33% moisture content). Both had methyl cellulose as the pore fluid.

7.10. Deposit shape of fixed bed tests

7.10.1. Data collection

After each of the tests, point depths of the deposit were measured using the grid set-up prior to testing. From this data, a data file with x, y, and z coordinates was constructed for each test. These were post-processed into contour plots using MatLab®. The resulting contour plots of the test deposits are shown in Figures 7.23 through 7.27. The general deposit shape of each

test was quite similar, with lateral spread exceeding the runout. The maximum deposit depths in the runout zone were approximately 3 cm, usually located just outside the flume outlet and thinning towards the end of the deposit.

7.10.2. Coarse material with glycerine and methyl cellulose

7.10.2.1. Data

All of the fixed bed tests showed a similar deposit shape, where lateral spread (the width) exceeded runout (length). Depositional area increased with both increased volume and moisture content. For example, an increase in 1.5 kg of material between tests T15 and T20 produced approximately 5 cm more lateral spread and 5 cm more runout. The depth of the deposit also increased from just under 2 cm in test T15 (1 kg) to just under 3 cm in test T20 (2.5 kg).

The effect of increased moisture content, however, was found to be much more important than an increase in volume. For example, the overall deposition area between tests T20 (2.5 kg at 33% moisture content) and T23 (1.75 kg at 39% moisture content) was nearly identical, despite the fact that T20 was 50% larger in mass than T23. Furthermore, the higher mobility provided by the moisture content of test T23 allowed it to spread thinner and farther than a flow of the same volume and lower moisture content (test T14 at 33%).

Comparing equivalent plots for mass and moisture content between Figures 7.23 and 7.24 (glycerine tests) and Figures 7.25 and 7.26 (methyl cellulose tests), shows that the deposition morphology for the glycerine based tests was virtually the same as for the methyl cellulose tests. From the velocity data discussed earlier, all tests were probably moving so slowly by the time they reached the flume outlet that lateral spread far exceeded the runout of the flows.

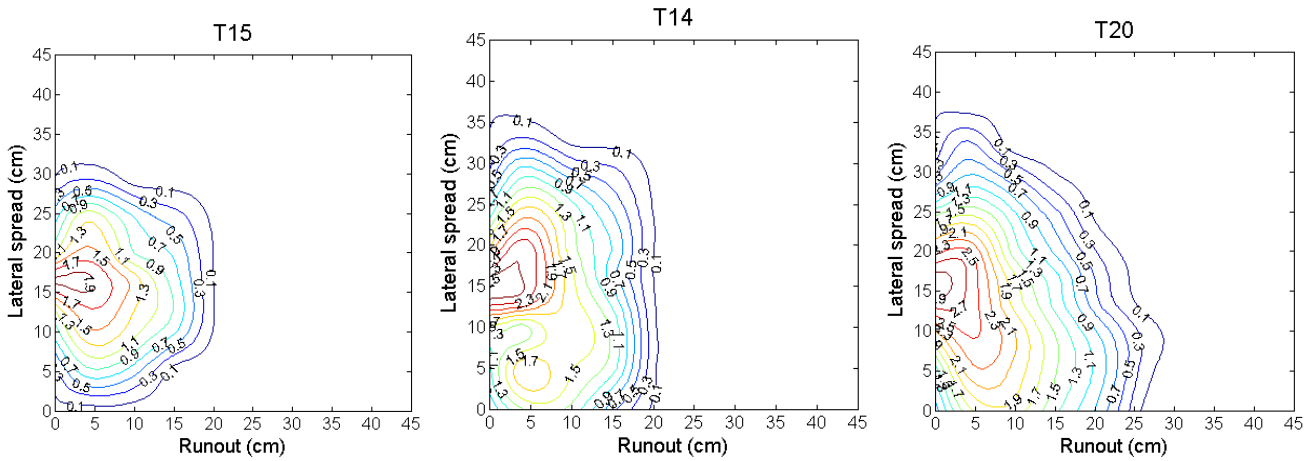

Figure 7.23.: Contour plots of the deposition for T15 (1 kg), T14 (1.75 kg), and T20 (2.5 kg). All flows used glycerine as a pore fluid and a moisture content of 33%. The isobars and labels report the depth in cm.

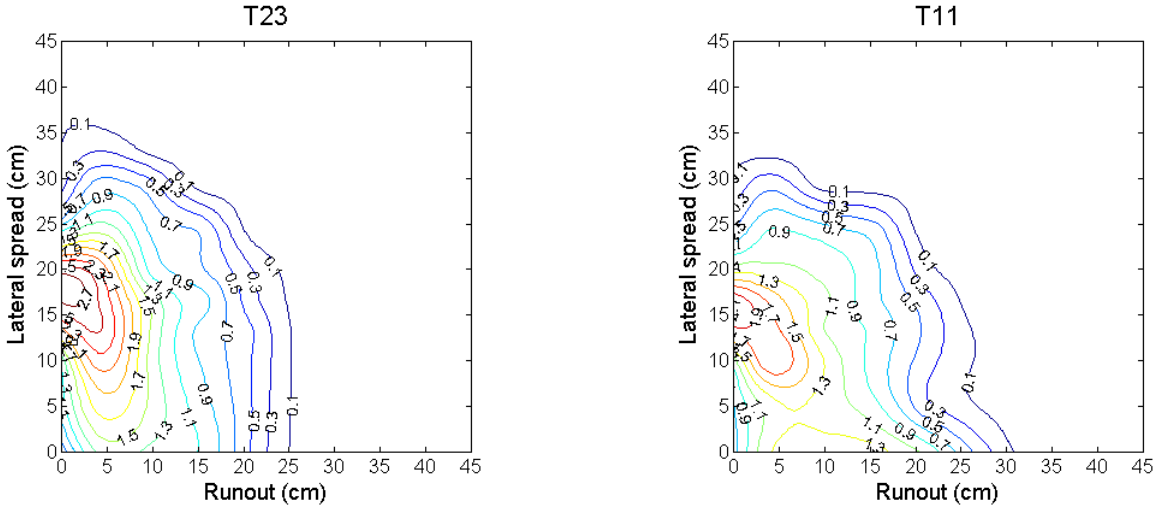

Figure 7.24.: Contour plots of the glycerine flows which used a higher moisture content. T23 used 39% MC, while T11 used approximately 41% moisture content. Both flows had 1.75 kg of coarse material.

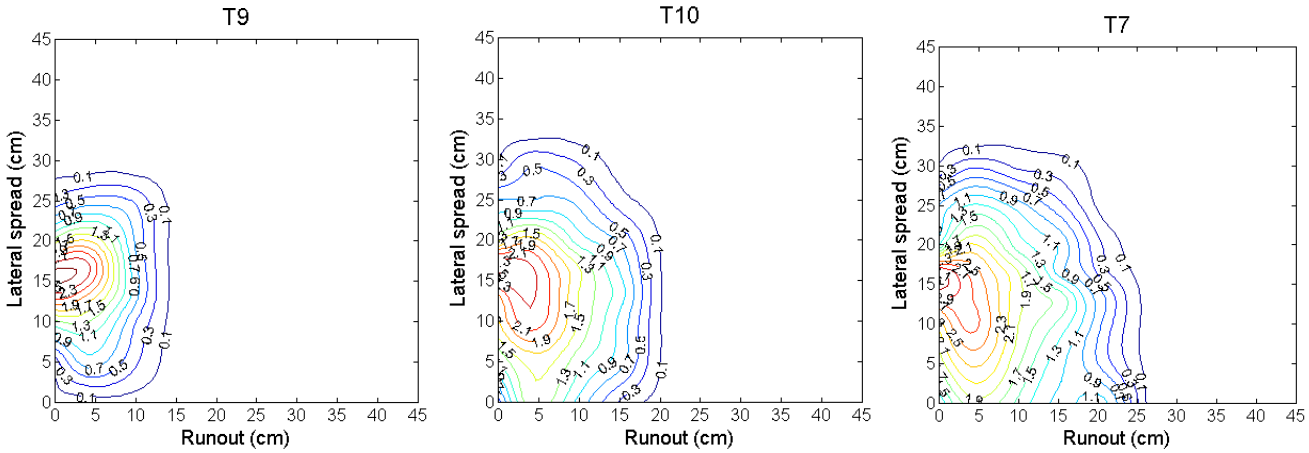

Figure 7.25.: Contour plots of the deposition for T9 (1 kg), T10 (1.75 kg), and T7 (2.5 kg). All flows used methyl cellulose as a pore fluid and a moisture content of 33%.

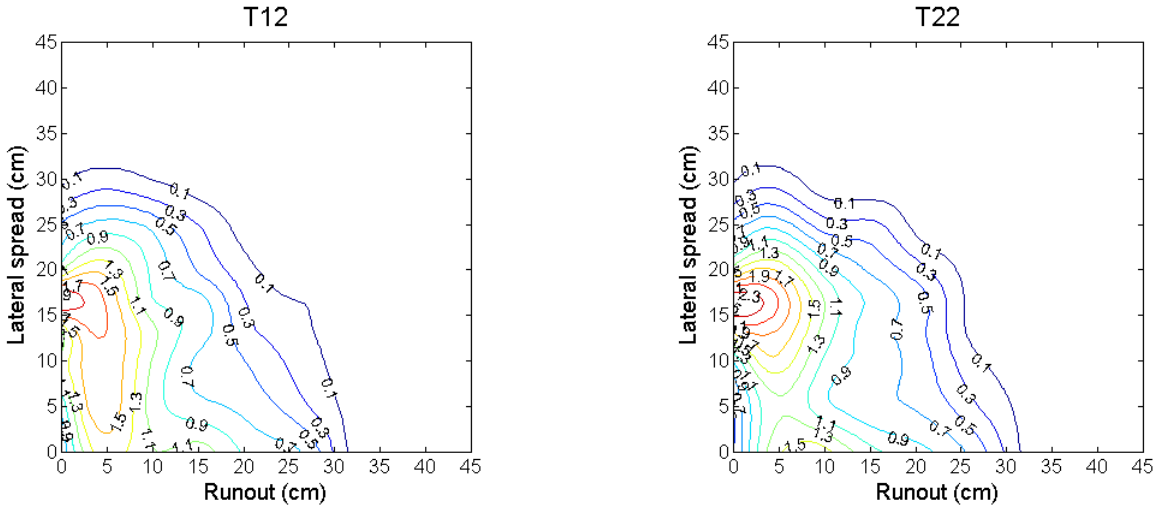

Figure 7.26.: Contour plots of the methyl cellulose flows which used a higher moisture content. T23 used 36% MC, while T11 used 39% moisture content. Both flows had 1.75 kg of coarse material.

7.10.2.2. Discussion

The deposit shape observed in these experiments contrasts with many debris flows mapped in the field and some laboratory flows (Carrol et al., 2007; Iverson and Denlinger, 2001), where the runout usually exceeds that lateral spread of the flow. This is likely due to the rapid deceleration of the flow within the channel, leading to deposition before opening to a horizontal unconfined fan zone (in terms of prototype). This is explained by the slope profile of the

channel. While the channel slope angle averaged 24°, it continuously reduced from the head at 36° to the base at 12°, which is typical for a fan slope angle in the field. However, in this case, the flow was still confined within the channel. Fannin and Wise (2001) suggest, based on a dataset of debris flows from British Columbia, that within confined channels, deposition may occur at slope angles below 9°, whereas for transition zones (at the transition between the end of a confined channel and head of a fan), deposition may occur on slopes below 20°. In these experiments, the exit slope angle lies between these two values, suggesting it may be similar to the transitional situation. Deposition on the fan was noted to back up as far as the camera position at latter stages of the flows, supporting this interpretation.

7.10.3. Fine material with water

The fine flows showed different deposit morphology than the other fixed bed tests. Unfortunately, this is poorly captured in the contour plots (Figure 7.27). Figure 7.28 is a photograph of the deposition of T21 (the 1.75 kg fine flow). The overall deposit shape in plan view is quite similar to the equivalent glycerine test (T14, 1.75 and w of 33%), even though the fine material ran out much further.

The experiments with fine material also displayed different segregation behaviour than the experiments with coarse material. In the experiments with fine material, the coarser fraction of the flow seemed to have separated from the silt fraction in both tests. This coarser deposit appeared to have overridden the finer material, as shown by the two images in Figure 7.28. This suggests that the fine material flowed down the flume first, followed by a surge of coarser material. None of this, however, is visible in the high-speed camera images. While the material was excavated after the test, unfortunately the material was not wet-sieved to quantify the segregation.

From the photograph (Figure 7.28) , there is also evidence of reworking by the fluid in the fine deposits. Figure 7.28 shows a more hummocky appearance than the deposits of coarse material. This may be evidence of separate surges in the fine material. The reasons for this behaviour are unknown. It is possible that there was some clogging in the feeder tube.

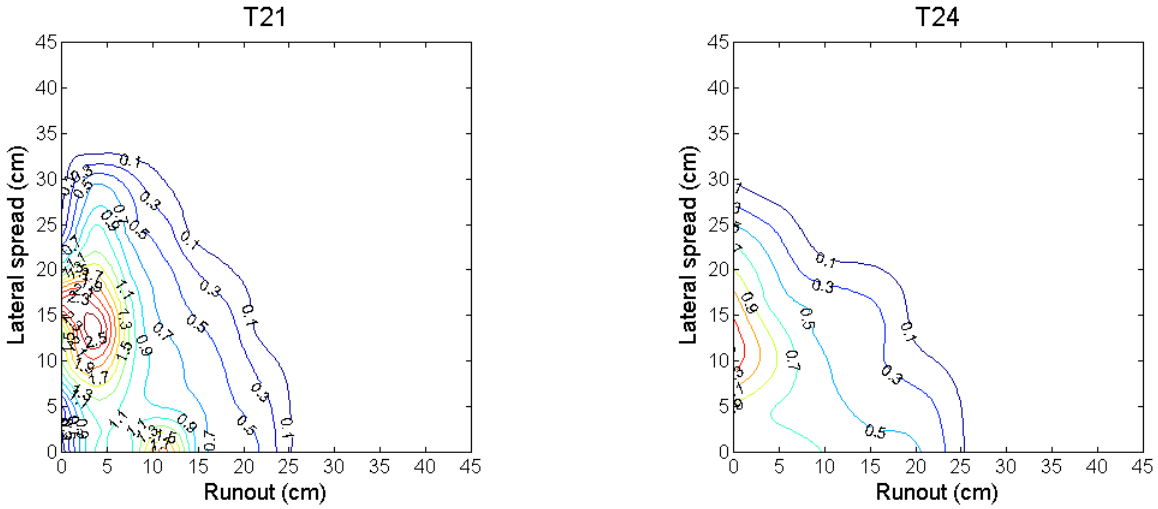

Figure 7.27.: Contour plots of the deposition for T24 (1 kg) and T21 (1.75 kg). Both flows used water as a pore fluid and had a moisture content of 33%.

Figure 7.28.: Deposit of test T21 (1.75kg fine distribution 33% water). The material has separated into coarser and finer fractions. The coarser fraction appears to have run out and over the fine. The image on the right shows small channels in the deposition, suggesting the deposit was reworked by water flow.

7.11. Deposit shape and erosion behaviour in erodible bed tests

7.11.1. Deposit shape

Figure 7.29 and Figure 7.30 are contour plots for the erodible bed tests T16, T17, T18, T19, and T25. The shapes of the deposits were very similar to that observed in the fixed bed tests, where lateral spread exceeded runout. The area of the deposit in tests T17, T18, T19, and T25 was greater than the deposit area in the equivalent fixed bed test (T7, 2.5 kg which used methyl cellulose and w of 33%, see Figure 7.25). The reasons for this greater lateral spread are discussed later in the chapter.

T16 (the flow of clear fluid over an erodible bed) showed a different deposit shape than the other tests. The flow extent was much larger than the flow width and the flow was also very thin (Figure 7.31). Obvious segregation, with larger particles at the distal end of the deposit, is also visible in Figure 7.31.

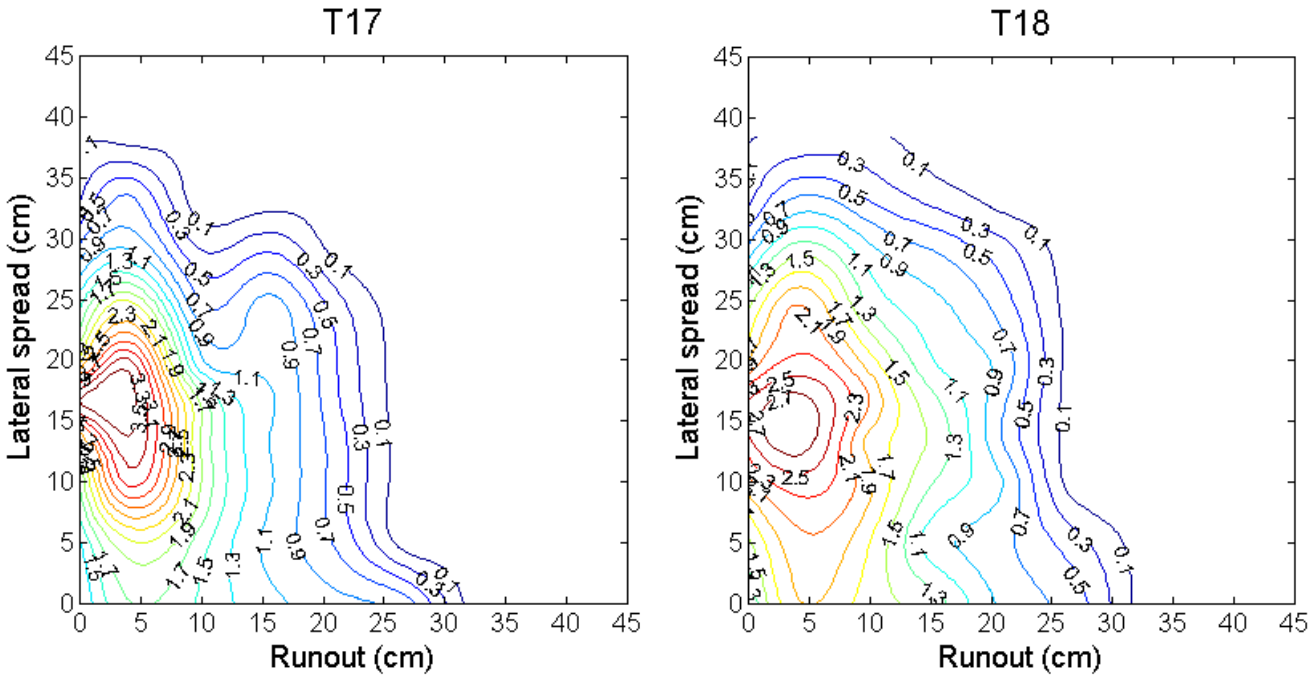

Figure 7.29.: Contour of deposit for T17 (control with coarse PSD in bed and flow) and T18 (armored bed) .

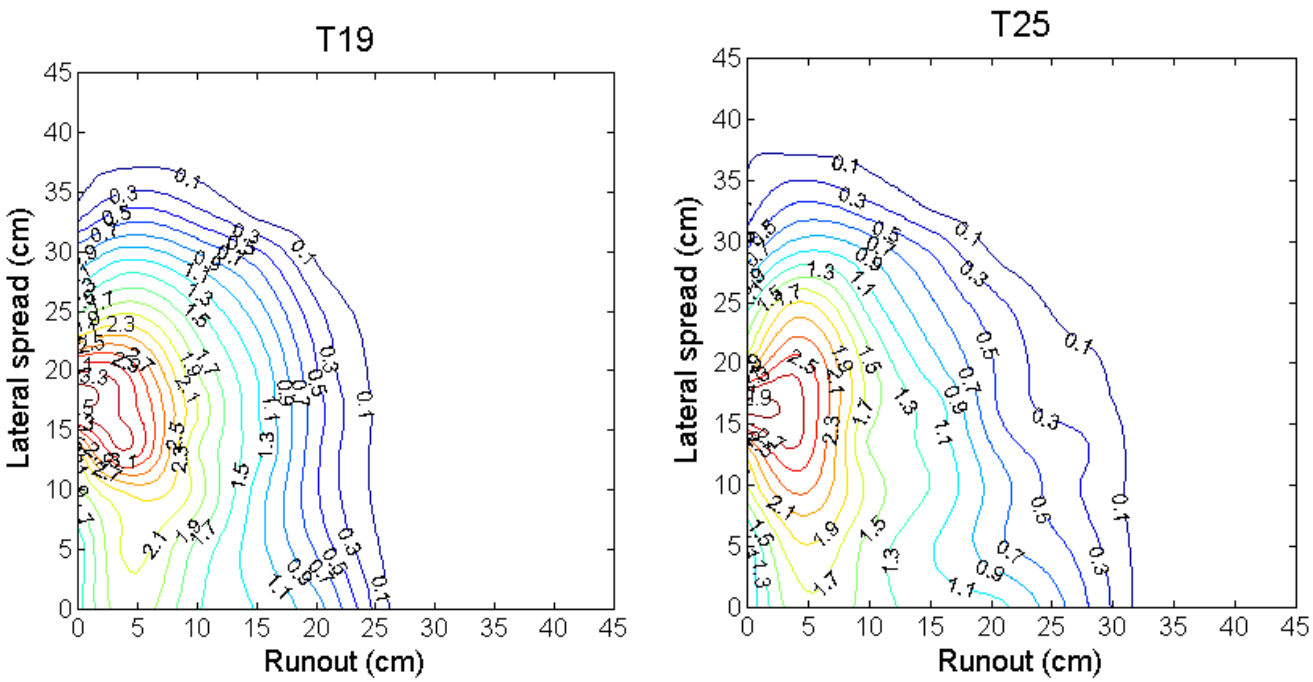

Figure 7.30.: Contour plots of T19 (test with finer bed) and T25 (test on bed prepared with holes for infiltration).

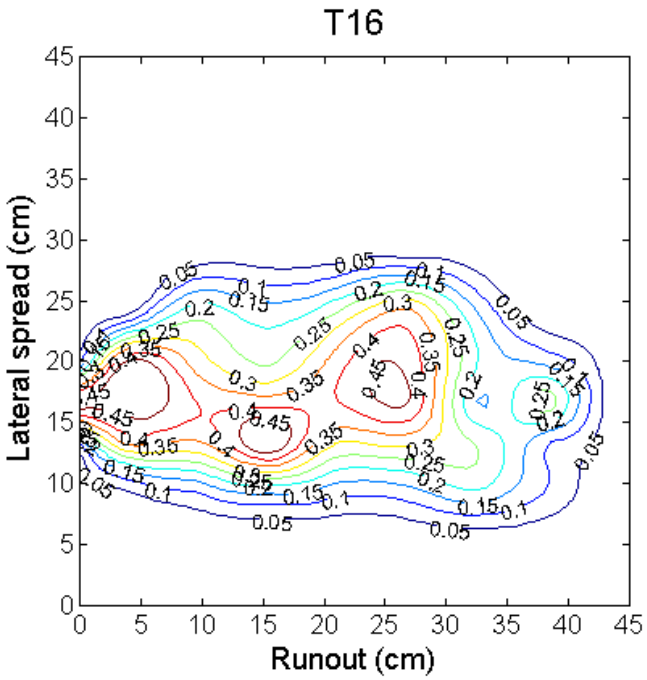

Figure 7.31.: Contour plot and photograph of T16, the test using 2.5 kg of clear, methyl cellulose flow and a 1.25kg erodible bed.

7.11.2. Erosion

Erosion behaviour of the flows was recorded by the high-speed camera. At the camera position, the dominant mechanism of erosion observed was single particle scour by the watery tail portion of the flow. The bed was progressively eroded from the bottom of the channel, which created knickpoints and bank collapse.

The erosion behaviour as the flow front passed in test T17 is summarized in Figure 7.32. The erosion observed in this test was typical. When the flow front arrived in the middle of the camera frame, 0.78 seconds after tripping the light trigger, no erosion was observed. As the front and body of the flow passed, a saturation front became visible which percolated into the bed (0.86s). At 6.3 seconds, well after the transition to the tail portion of the flow, a knickpoint had developed, which is visible in the lower right hand corner of the camera frame. By 14.5 seconds, the knickpoint had retreated headward, creating sidewall collapses. In the fourth picture in Figure 7.32 (14.5s), the presence of failures in channel sidewall is shown by a small gap between the original surface line and the material against the sidewall. In the last frame recorded by the high-speed camera, a wedge of material can be seen in the lower right hand corner of the frame. This is depositional material that has backed up to this position from the end of the flume.

After each erodible bed test, all deposition material was collected from the drum surface and oven dried. The dry weights of the deposits are shown in Table 7.11.2. An estimate of the mass eroded in each erodible bed experiment was calculating by subtracting the weight observed on the drum in test T7 (the 2.5 kg fixed bed test) from the dry weight observed on the drum in each erodible bed test. The assumption was made that the flows would have deposited precisely the same amount as test T7 (i.e. if no erodible bed had existed). While this may introduce a significant amount of error, being based on a single test, it is the only data available to quantify the amount of erosion. The result does, however, give a reasonable comparison of the erosion behaviour between different tests.

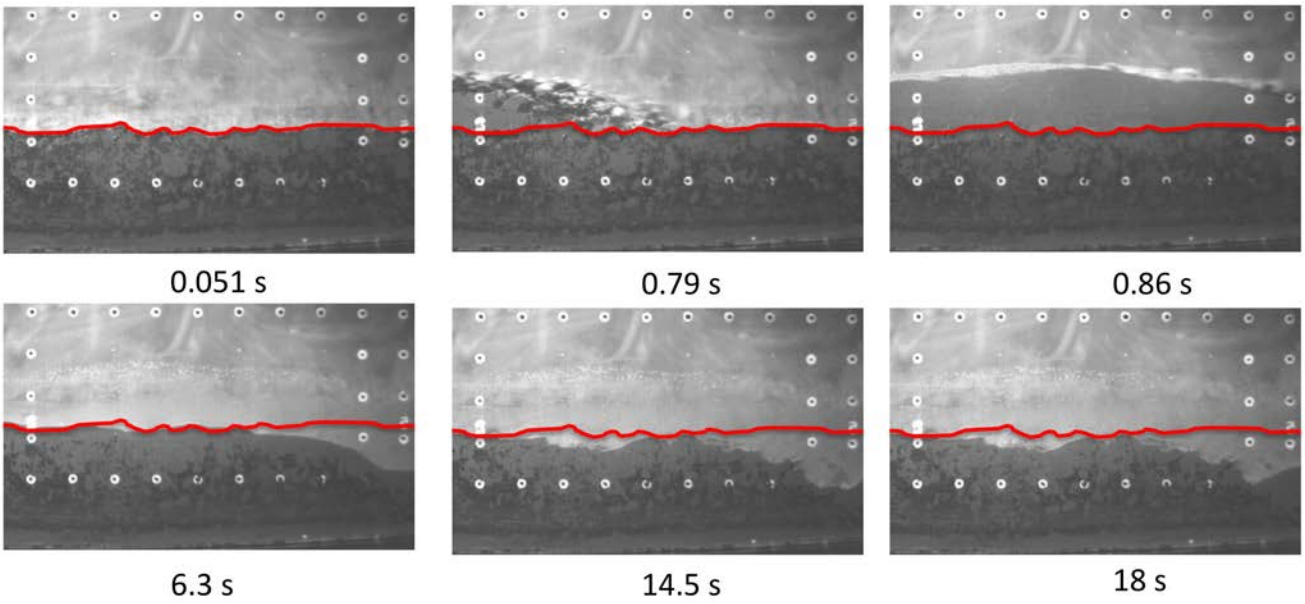

Figure 7.32.: Figure shows the passage of the flow front and subsequent erosion of the bed for T17. The time elapsed is shown below each picture. The red line shows the height of the original bed surface. Erosion proceeds by single particle scour by the watery tail.

Table 7.3.: Eroded material from erodible bed tests.

Test code	Dry weight on flume (g)	Eroded (g)
T7 (fixed bed 2.5 kg)	1572	–
T16 (erodible bed 825mL fluid flow)	1923	193
T17 (erodible bed, 2.5 kg flow)	1736	164*
T18 (coarser bed, 2.5 kg flow)	1896	324*
T19 (finer bed, 2.5 kg flow)	1923	351*
T25 (bed with holes, 2.5 kg flow)	1678	106*

*These figures make the assumption that the dry weight of the erodible bed tests would have been the same as test T7

7.11.3. Discussion

According to Table 7.11.2, the most erosive test conducted was T19 (the finer bed test), followed by T18 (coarser bed), T16 (fluid over bed), T17 (coarse bed) , and T25 (bed with holes). It

was hypothesized that T19 would be more erosive than T18 because armoring would inhibit erosion, especially erosion by particle scour. While this hypothesis proved correct, T19 was only slightly more erosive, probably within the error of the erosion estimate. Further, T18 (coarser bed) was actually more erosive than test T17 (coarse bed). Therefore, armoring seemed to play a small role, if any, in these sets of experiments.

T25, the test where the bed was prepared with holes, was the least erosive of the erodible bed tests. This was unexpected, as it was hypothesized that this flow would be the more erosive due to an increase in bed saturation provided by the holes. In retrospect, the bed was probably made slightly more compact during preparation, which may have decreased erosion. A more compact bed would have been more resistant to erosion by single particle scour. In the other erodible bed tests, erosion at the high-speed camera position was only observed once seepage had saturated the top several millimeters of bed material. A more compact bed would hamper the progress of this front.

Since single particle scour by the more fluid tail of the flow was the dominant agent of erosion in these tests, T16 (the flow of fluid only) would hypothically be the most erosive. However, this was not the case. Since T16 was very fast, most of the flow had passed before this saturation front had progressed. This effect limited erosion.

It is interesting to note that the deposit area of the flows was inversely proportional to the amount of material eroded. Test T25 (the test with holes) showed the greatest spread of any of the flows, yet the least erosion. It also had the highest velocity at the high-speed camera position. Test 19, the most erosive of the flows, had the lowest depositional area (see Figure 7.30).

It is hypothesized that a lower bed permeability in test T25 (due to greater compaction), caused more moisture to remain in the flow. Therefore, the flow spread further, just as observed for the fixed bed tests with higher moisture contents. The higher moisture content also caused the higher velocity (see Figure 7.19). In contrast, the moisture content of the most erosive test, T19, probably dropped both as it eroded material and lost fluid into the bed. This lowered the moisture content of the flow and decreased its lateral spread.

The shape and width of the channel incised by the flows controlled flow confinement and was another major factor in the tests. In general, the shape of the eroded channel changed slightly with distance down the flume. After each test, the centrifuge was allowed to spin for 15 to 20 minutes to allow time for bed and flow deposit to consolidate. This allowed for pieces of the bed to be removed without breaking apart. Figure 7.33 shows two pieces of the bed in T18 which was removed from the flume. The bed on the left was taken from 1/3 the distance

down the flume. The incised channel is approximately 40 mm wide and clearly a half U-shape. The cross-section on right was taken from near the high -speed camera position and is slightly more half V-shaped.

Lateral levee deposition was observed just outside of the eroded channel every erodible bed test. Figure 7.34 shows a levee formed during test T17. The levees were made of larger (>2 mm) clasts, indicating that there was segregation in these flows. Sometimes, these particles were not individual clasts, but agglomerations of loess which had not fully disagregated in solution. In all tests, levees were observed on right side of the channel, on the side opposite the Perspex window.

The width of the eroded channel and location of the levees indicate that the erodible bed flows did not spread out over the full width of the channel. This helps explain the increase in flow height observed in the erodible bed flows. If the wetted perimeter in a erodible bed test is assumed to be similar to a fixed bed test, then a decrease in width of 10 to 15 mm will be accompanied by an increase in flow height of 3 to 5 mm. This is very close to what was observed (see Section 7.7.4).

Clearly, the introduction of an erodible bed adds complexity to the experiments. For example, small changes in the width of the eroded channel will effect confinement, which will in turn effect the velocity, flow height, and erosive potential of the flow. Variables such as the degree of bed compaction are also difficult to control and may have added error to the experiments. However, all of these factors exist in field scale flows. Further, these experiments reproduced many features of field scale flows including levees, knickpoint migration, and bank collapse.

Figure 7.33.: Cross-sections of the bed after flow passage (test T18). The bed on the left was taken from 1/3 the distance down the flume. The incised channel is narrower and clearly half U-shaped. The section of bed on the left was taken lower down the flume, near the high speed camera position. The channel is more half V-shaped.

Figure 7.34.: Photo of levee left by flow in test T17, which used the coarse PSD in both the flow and bed. The view shown here is from the top of the flume, looking down into the runout zone.

7.12. Runout

7.12.1. Measurement

The spot depth measurements, which were used to construct the velocity contour plots (useful for visualizing the shape of the deposit and maximum extent of runout) were further used to analyze the debris flow runout of the center of mass. The mass of material entering the flume was determined by weighing the container which held that the flow material before and after each test.

7.12.2. Mass

As shown in Figure 7.35, approximately linear relationships were observed to exist between flow mass entering the feeder tube and runout to the centre of gravity for flows conducted at a moisture content of 33%. Note that the linear relationships between flows using methyl cellulose, glycerine, and the fine distribution with water were different. The slope of the linear regression for the flows that used a Newtonian pore fluid (glycerine and water) was less steep than observed for methyl cellulose. For the fine flows, the slope of the trend line was similar to the glycerine flows (although with only two data points, any inferences made about the fine flows are speculative). For the fine flows, the line was translated up; the flows ran out far further than a glycerine or methyl cellulose flow of the same volume. Despite the differences, increasing mass was associated with increasing runout in all tests.

The relationship between mass and runout changed with the moisture content of the flow. For both glycerine and methyl cellulose, the flows of a higher moisture content produced a higher runout than predicted by the trend line for 33% flows. This effect was particularly dramatic for the methyl cellulose flows at 36% and 39% (Figure 7.35) .

The erodible bed test with the coarse PSD in both the bed and flow (T17) plotted close to the trend line plotted for fixed-bed, methyl cellulose flows with the same moisture content 33% moisture content. This suggests that it behaved similarly to the fixed bed tests. However, there was significant variation in the runouts observed for the erodible bed tests. This may be due to changes in velocity, confinement and how much moisture was lost to the bed.

7.12.3. Velocity

Previous studies have found that the runout of granular debris flows scale with the square of the flow velocity at the exit to the debris flow fan (Takahashi, 1991, 2007). Figure 7.36 shows the runout to the center of mass plotted against the square of the flow velocities at the high speed camera position, which was located 21 cm from the flume exit. Figure 7.36 also shows trend lines for the flows at 33% moisture content (the glycerine, methyl cellulose, and erodible bed tests).

For both the glycerine and the methyl cellulose, an approximately linear relationship was observed to exist between the square of velocity and centre of gravity for flows at a moisture content of 33%. However, the tests conducted at a higher moisture content did not plot on the same relationship. Instead, a higher moisture content, which led to a higher velocity at the observation point in the channel, did not lead to as much runout as predicted by the plotted

trend for 33% flows. Correlation coefficients, at R^2 of 0.85, 0.76, and 0.53 for glycerine, methyl cellulose, and erodible, respectively, were not as high as for the relationship between mass (or volume) and runout.

As discussed on 7.8.3 on page 185, the fine flows unexpectedly showed a decrease in velocity with increased mass (or volume). However, the runout of the slower, 1.75 kg flow was longer. In this case, it was clear that the volume of the test, rather than the velocity, controlled the runout deposition on the fan.

7.12.4. Momentum

Figure 7.37 shows the product of the total mass entering the flume (kg) and the flow front velocity at the camera (ms^{-1}), which is termed "peak momentum", against position of the centre of gravity. Two trend lines are plotted; one for the entire set of methyl cellulose flows and one for the set of glycerine flows. This shows that data can be collapsed to a single trend line for each pore fluid, in which moisture content and erodible / non-erodible beds are included (with R^2 of 0.89 and 0.91 for methyl cellulose and glycerine, respectively). Peak momentum, as it takes into account both the total mass and the velocity of the flow, shows a strong relationship with runout for all tests. This could, in part, be caused by the boundary conditions in the test, as the diameter of the feeder tube may have restricted the peak discharge. If the flow heights were allowed to vary with different moisture contents and volumes, the relationship between momentum and runout may have changed.

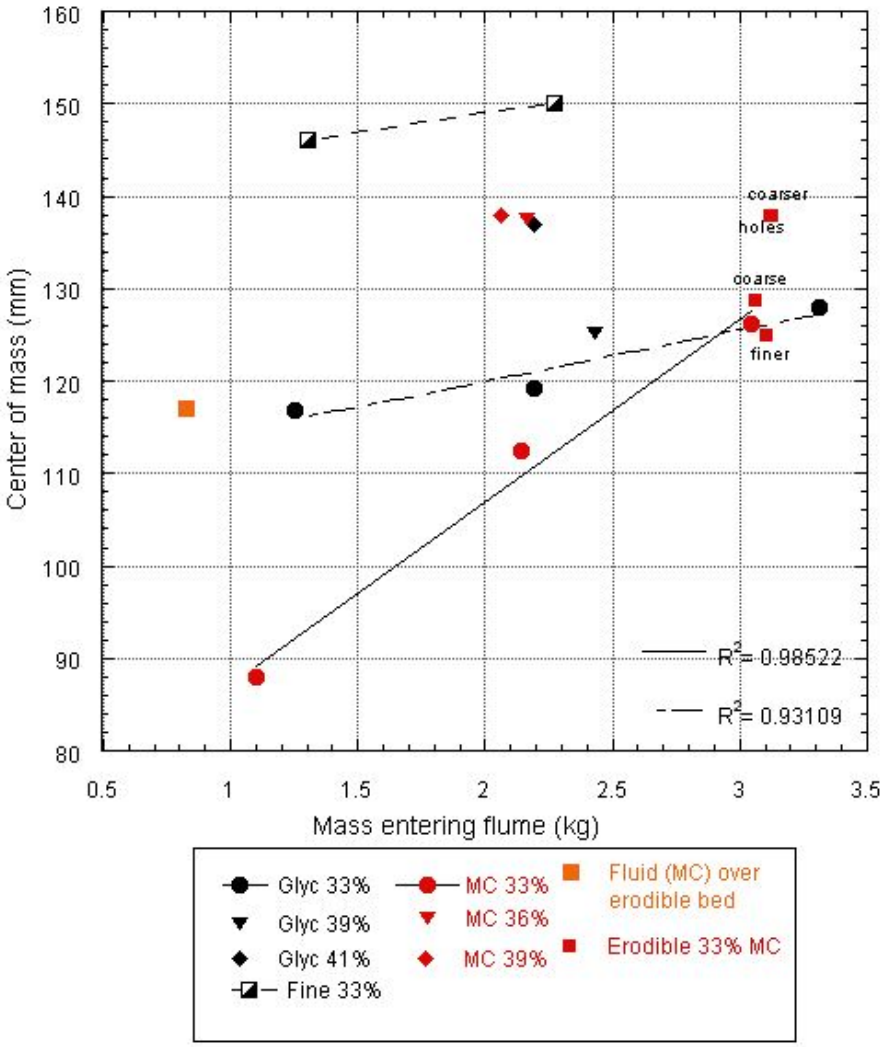

Figure 7.35.: The runout of each test (shown by the distance of its centre of mass from the flume outlet) versus mass entering the feeder tube. MC is methyl cellulose, Glyc is glycerine.

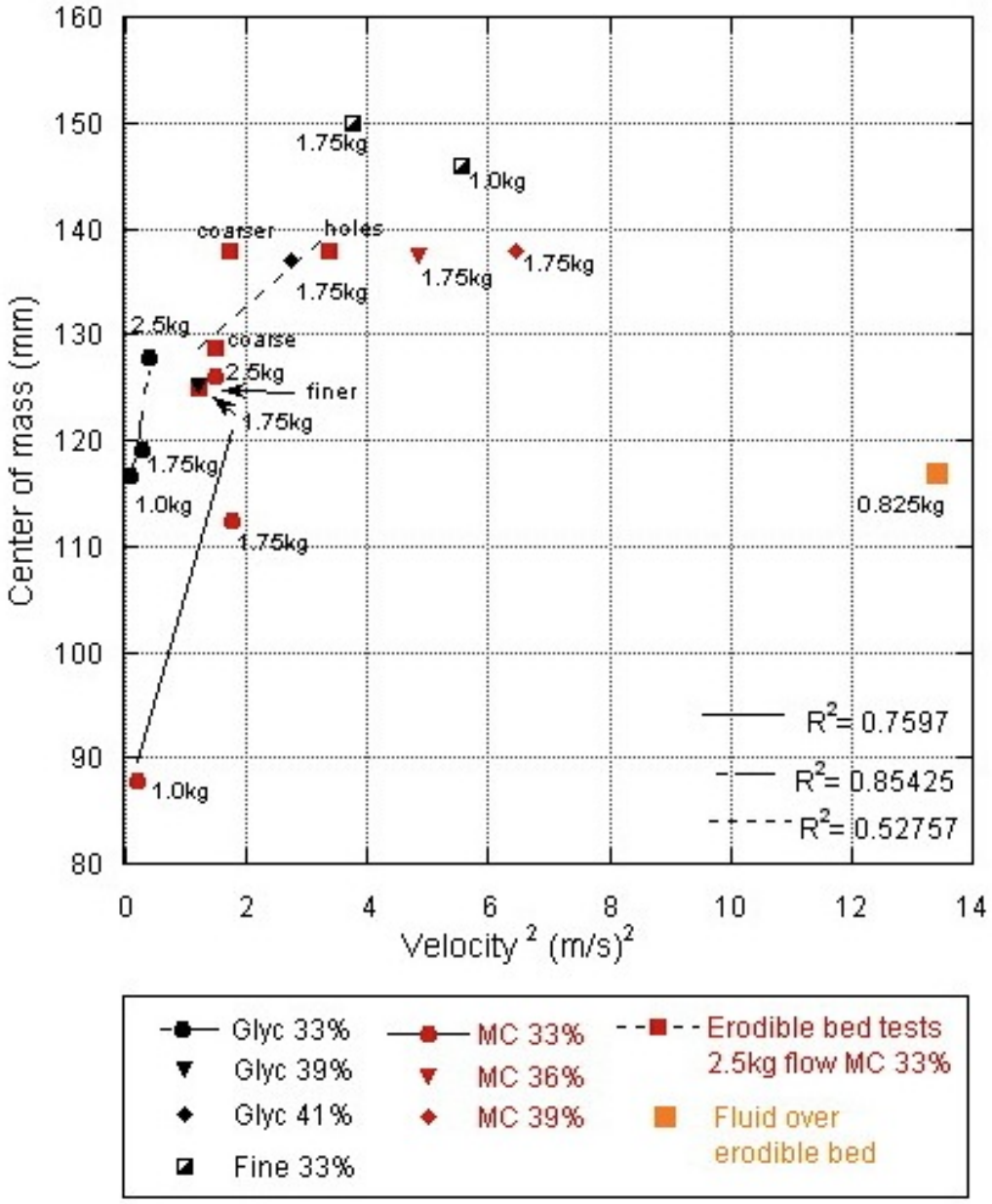

Figure 7.36.: Location of the centre of mass of the deposit (from flume outlet) versus the square of velocity of the flow front at the high speed-camera position. MC is methyl cellulose, Glyc is glycerine.

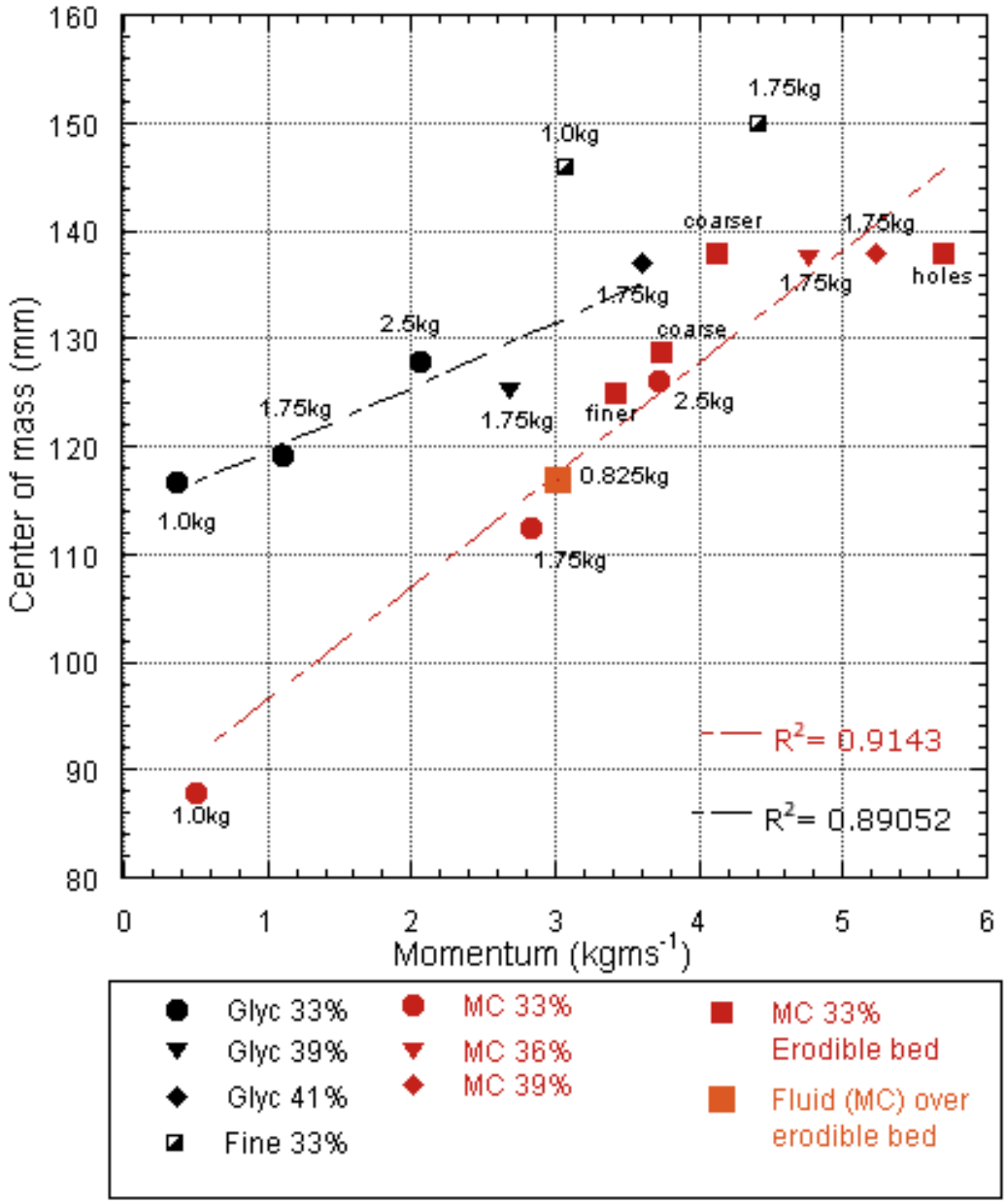

Figure 7.37.: The runout of each test (shown by the distance of its centre of mass from the flume outlet) versus the peak momentum of the flow at the high speed camera position. MC is methyl cellulose, Glyc is glycerine.

7.12.5. Discussion

Flows with an increased moisture content ran out farther than would be expected for a given volume, but less far than would be expected given their velocity at the high-speed camera position. Further, in the fine flow tests, the 1 kg test, which showed a higher velocity at the camera, actually ran out slightly less than the 1.75 kg test.

This behaviour shows that volume is the primary control on runout for these tests, while velocity is secondary. Without camera data in the runout zone, exactly how the flows spread out on the fan is unclear. However, as evidenced by the depths of the deposit, it seems likely that most of the flow is deposited en masse, then the deposit viscously deformed and spread homogeneously. Given that the flow fronts had probably slowed substantially by the time they reached the flume outlet, the major driving force would have not been momentum of the front, but pressure from the body and tail. As the front began to spread laterally, it was also shunted forward by the rest of the flow which was still confined in the channel and traveling down the incline.

For flows with increasing mass but the same moisture content, the driving force of a longer, thicker body and tail explains the increase in flow velocity. The trend line of increasing velocity in Figure 7.36 for the w=33% flows reflects this increase in volume. The primary importance of flow volume is illustrated by comparing tests T7 to T10 and test T21 to T24. T7 (2.5 kg coarse material with methyl cellulose, 33%) had only a marginally higher velocity at the high-speed camera position than test T10 (1.75 kg methyl cellulose, 33%), but ran out 15 mm further. In the case of the fine material, the slower, but larger volume flow (T21 1.75 kg), ran out further than a faster, smaller flow (T24 1 kg).

Velocity is still important. The higher moisture content flows, which are moving faster at the high-speed camera position, do runout further than a lower moisture content flow of the same mass (as shown in Figure 7.36). Plotting the runout against the peak momentum of the flow, as it takes into account both the velocity and volume of flow, explains the variation in runout with respect to both volume and moisture content.

7.13. Dimensionless groups

7.13.1. Background

As discussed in Section 2.4.1, and in the introduction to this chapter, small, 1-g physical models may be limited in their ability to reproduce the mechanics of large scale flows. Iverson and

Denlinger (2001) argued this point by conducting a dimensional analysis of relevant debris flow parameters. Dimensional analysis seeks to simplify a physical situation to as few independent parameters as possible. Using the Buckingham Pi theorem, a situation containing x parameters and n dimensions, can be simplified to x-n, dimensionless groups. One can then evaluate similitude between differing scales of model by comparing the relevant dimensional groups.

The following section expands on the Section 2.4.1 by discussing the dimensionless groups that have been shown to be relevant to debris flow mechanics (Iverson and Denlinger, 2001; Bowman et al., 2010; Iverson, 1997) . These include the Reynolds number, Bagnold number, Savage number, Pore-pressure number, aspect ratio, the Fluidization number, and the Friction number.

7.13.2. Quasi-Reynolds number

The Quasi-Reynolds number, shown in equation Eq. (7.1) , is the ratio between the inertial and viscous stresses present in the flow (Iverson and Denlinger, 2001).

$$N_{qR} = \frac{\rho H \sqrt{NgL}}{v\mu} \tag{7.1}$$

where ρ is the density, H is the flow height, g is the gravitational acceleration, L is the length of the flow, v is the flow velocity, μ is the viscosity of the pore fluid, and D is the characteristic grain diameter. As already noted in Section 2.4, since H is in the numerator of Eq. (7.1), the Quasi-Reynolds number will increase with an increasing length scale. Since g is also in the numerator of the equation, conducting experiments at a higher g-level will also tend to increase the Quasi-Reynolds number. However, as shown in Eq. (7.1), increasing the viscosity by N will more than offset this effect.

7.13.3. Savage number

The Savage number, as shown in equation, reflects the ratio between collisional stresses and stresses due to friction .

$$N_S = \frac{\rho_s}{(\rho_s - \rho_f)} \frac{\delta^2 \dot{\gamma}}{NgH} \tag{7.2}$$

where ρ_s is density of solid, ρ_f is the density of the fluid, δ is the characteristic grain diameter (here taken to be the d_{50}) and $\dot{\gamma}$ is the shear stress. In this equation, an increase in g will increase the dominance of stresses due to sustained grain contacts. Also, it should be noted

that in small scale experiments like in the centrifuge, the characteristic grain diameter will be small. This too, will cause lower Savage numbers. Savage and Hutter (1989) suggest that Ns>0.1 represents the transition to a grain inertial regime, where particle collisions dominate the flow stresses.

7.13.4. Pore pressure number

The pore pressure number reflects the ratio of the time for down-slope motion to the time-scale for pore-pressure diffusion. Field scale flows have N_P<<1, meaning that high pore pressures will persist in the flow long after deposition (Iverson and Denlinger, 2001). The equation is:

$$N_P = \frac{D\sqrt{L/Ng}}{H^2} \tag{7.3}$$

where D is the hydraulic diffusivity (see Table 7.4) and H is the flow height. Note that the flow height is in the denominator of Equation 7.3. Thus, as the scale of the flow is increased, the pore pressure number (which reflects both the permeability of the material and the length of the consolidation flow paths) will decrease. Note that in the centrifuge, an increased g-level (N) will cause N_P to decrease.

7.13.5. Fluidization number

The Fluidization number is the ratio of the velocity scale for fluidization of the mass to the velocity scale of the particle settling. A value of N_{Fl}<1 suggests the solid and fluid phases experience similar velocities and accelerations, and therefore the flow can be treated as an aggregated mixture (Iverson and Denlinger, 2001). The fluidization number is determined by:

$$N_{Fl} = \frac{K}{\mu}\frac{v_s}{(1-v_s)}(\rho_s - \rho_f)\sqrt{Ng/L} \tag{7.4}$$

where v_s is the average solid fraction of the flow and K is the intrinsic permeability (see Table 7.4).

7.13.6. Bagnold number

The Bagnold number represents the ratio of stresses due to grain collisions to the viscous fluid stresses. N_B<40 is regarded as a "macroviscous" regime, where the stresses on the particle are dominantly due to viscous drag. In the macroviscous regime stresses are proportional to the

shear rate. $N_B > 450$ suggests a collision-dominated regime, where shear and normal stresses become proportional to the square of the shear rate (Bagnold, 1954).

$$N_B = \left(\frac{v_s^{1/3}}{v_s *^{1/3} - v_s^{1/3}} \right) \frac{\rho_s \dot{\gamma} \delta^2}{\mu} \tag{7.5}$$

where v_s is the average solid fraction in the flow, and v_s^* is the maximum possible solid fraction in the flow. As Bowman et al. (2010) points out, since N_B explicitly ignores shear stresses generated by Coulomb friction, it is probably most relevant when $N_S > 0.1$.

7.13.7. Aspect ratio

The aspect ration (ξ) is the ratio of flow thickness to flow length (measured from the front of the flow to the end of the tail). The aspect ratio is a measure of flow mobility and there should be no scale dependence between model and field-scale flows (Iverson and Denlinger, 2001).

$$\xi = \frac{H}{L} \tag{7.6}$$

7.13.8. Friction number

The Friction number (given in Equation 7.7) compares the relative effects of particle contact friction and pore fluid shearing Iverson (1997). A large value for N_F (>100) means that frictional stresses dominate over viscous stresses (Zhou and Ng, 2010).

$$N_F = \frac{N_B}{N_S} \tag{7.7}$$

7.13.9. Analysis and discussion

Figure 7.38 plots, on a log scale, the values of these dimensionless groups for four of the tests conducted in the centrifuge, a typical lab flume test, and two field cases. The centrifuge tests compared are T14 (1.75 kg of coarse material. glycerine pore fluid with 33% moisture content), T10 (1.75 kg of coarse material, methyl cellulose pore fluid with 33% moisture content), T24 (1.75 kg fine material and water), and T5 (2.5 kg coarse material and water with 36% moisture content). These are compared with a typical flume test at 1-g (Bowman and Sanvitale, 2009). The two field scale flows chosen for comparison represent the range of debris flow behaviour: the Osceola mudflow (Vallance and Scott, 1997) was an extremely large (peak discharge of $2.5 \text{x} 10^6$ m^3s^{-1}) flow of fine material; the flow at Mt. Thomas, New Zealand (Pierson, 1980) is

a typical, medium sized granular debris flow (peak discharge of approximately $75 m^3 s^{-1}$). The relevant calculations and parameters in the calculation of the dimensionless numbers are shown in Table 7.4.

The method of calculation of the dimensionless numbers and parameters given in Table 7.4 closely follows that used by Bowman et al. (2010). Following common practice, the ''typical'' grain diameter was chosen to equal to d_{50}. However, the truly representative particle size which is relevant to the mechanics of motion may be orders of magnitude smaller or larger than this value, especially for more well- graded materials that are representative of debris flows. For example, the d_{10} particle size controls consolidation behaviour, as shown empirically by Hazen (1892), while larger particles can can limit mobility and influence collisional behaviour(Rombi et al., 2006).

Previous dimensional analysis of debris flows (i.e. Iverson and Denlinger 2001; Iverson 1997) have used the viscosity of the interstitial fluid with the addition of fine particles because over the time-scale of the debris flow, particle sizes of silt size and finer will not settle out of suspension. These fines are therefore considered part of the fluid-phase which increase the viscosity of the pore-fluid.

This study, in contrast, has taken the fluid viscosity in the centrifuge flows to be simply the viscosity of the pore fluid. This is justified in the case of T5, as the particle settling velocity scales with g and the silt-sized particles will behave as if they were $\sqrt{N}$ larger and may not behave as part of the fluid phase. However, the increased viscosity of the glycerine and methyl cellulose flows mean that fines will, in fact, be part of the fluid phase, which may change the effective viscosity of the pore-fluid. In future experiments, it would be interesting to check the rheology of the fluid with suspended fine particles.

The calculations for Darcy's permeability and mixture stiffness follow the approach used by Bowman et al. (2010). Darcy's permeability is a function of intrinsic permeability K, particle density σ, gravity, Ng, and fluid viscosity μ. The hydraulic diffusivity, D, is assumed to relate directly to Darcy's permeability, k, flow mixture stiffness, E_s, and g- level, Ng, by the conventional equation for one-dimensional consolidation of a static saturated soil (Bowman et al., 2010). Estimates for mixture stiffness, E_s, and intrinsic permeability, K, are based on values from the literature (Major, 2000; Iverson and Denlinger, 2001). Note that values of D and K may be one or two orders of magnitude off to due the variable nature of debris flow entrainment, solid concentration, and porosity during downslope movement (Bowman et al., 2010). Also note that one would expect the mixture stiffness to vary between debris flow types, as well as in different parts of the debris flow path. However, this analyses follows the approach

of Bowman et al. (2010) and Iverson (1997) which ignore this variability. The average value of solids concentration C, is assumed to equal the solid concentration of the centrifuge flows and 0.6 for the field scale flows (after Iverson and Denlinger, 2001)

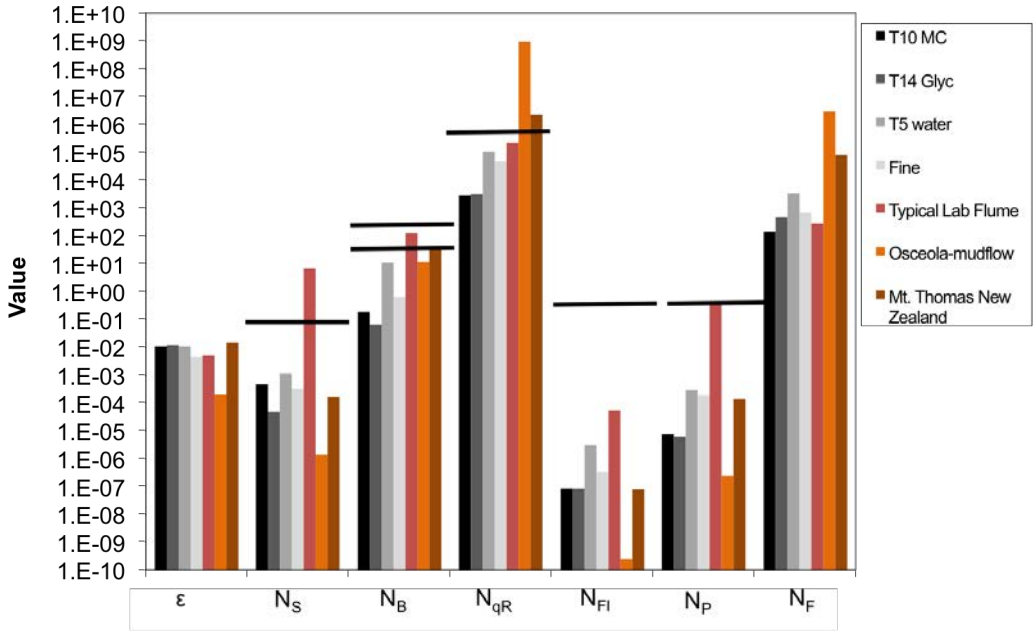

Figure 7.38.: Plot shows dimensionless numbers for T14, T10, T5, and T21, typical lab flumes, and two field scale debris flows. The black lines indicate the boundaries between relevant regimes (Iverson and Denlinger, 2001; Iverson, 1997)

Table 7.4: Parameters used and resulting non-dimensional groups for T10, T14, T5, T21, typical 1-g flume values, Mt. Thomas, and Osceola debris flows.

Parameter/ nondimen- sional group	Symbol (units)	T10 coarse MC	T14 coarse glyc	T5 coarse water	T21 fine water	Typical lab flume	Mt. Thomas	Osceola
d_{50}	δ (m)	0.0003	0.0003	0.0003	$4.7E^{-5}$	0.001	0.01	0.01
Maximum flow thickness	H (m)	0.01325	0.0154	0.01342	0.0054	0.01	1.5	20
Flow length	L (m)	1.2	1.2	1.2	1.2	2	1000	10000
Flow velocity	v (m/s)	1.32	0.52	1.8	2.06	5	5	20
shear strain rate (v/H)	$\dot{\gamma}$ (1/s)	100	34	153	339	500	3.3	1
Solid density	ρ_s (kg/m^3)	2650	2650	2650	2650	2700	2700	2700
Fluid density	ρ_l (kg/m^3)	1000	960	1000	1000	1000	1000	1000
Fluid viscosity	μ $\left(\frac{kg}{ms}\right)$	0.04	0.04[1]	0.001	0.001	0.001	0.001	0.001
Gravity acceleration	Ng (m/s^2)	400	400	400	400	10	10	10
Intrinsic permeability*	K (m^2)	$1x10^{-12}$	$1x10^{-12}$	$1x10^{-12}$	$1x10^{-13}$	$1x10^{-11}$	$1x10^{-12}$	$1x10^{-11}$
Mixture stiffness*	E_s $\left(\frac{kg}{ms^2}\right)$	$1x10^4$	$1x10^4$	$1x10^4$	$1x10^4$	$1x10^4$	$1x10^4$	$1x10^4$
Darcy's permeability*	k (m/s)	$9.8x10^{-7}$	$9.8x10^{-7}$	$3.9x10^{-5}$	$3.9x10^{-5}$	$9.8x10^{-5}$	$9.8x10^{-7}$	$9.8x10^{-8}$
Hydraulic diffusivity*	D (m^2/s)	$2.5x10^{-8}$	$2.5x10^{-8}$	$1.2x10^{-5}$	$1.2x10^{-6}$	$1.2x10^{-3}$	$1.2x10^{-5}$	$1.2x10^{-6}$
Average solid fraction	v_s	0.53	0.53	0.51	0.53	0.6	0.6	0.6

Table 7.4: Parameters used and resulting non-dimensional groups for T10, T14, T5, T21, typical 1-g flume values, Mt. Thomas, and Osceola debris flows.

Parameter/ nondimen- sional group	Symbol (units)	T10 coarse MC	T14 coarse glyc	T5 coarse water	T21 fine water	Typical lab flume	Mt. Thomas	Osceola
Max. possible solid fraction	v_s*	0.6	0.6	0.6	0.6	0.6	0.6	0.6
Aspect ratio	ξ	0.011	0.013	0.01	0.0045	0.005	0.0015	0.0002
Savage number	N_s	$4.8x10^{-4}$	$4.7x10^{-5}$	$1.1x10^{-3}$	$7.9x10^{-8}$	7.01	$1.7x10^{-4}$	$7.9x10^{-8}$
Bagnold number	N_B	0.19	0.06	11.0	0.65	123	39.2	0.65
Quasi- Reynolds number	N_{qR}	2738	3245	109441	446734	223687	2372560	44633
Fluidization number	N_{Fl}	$7.9x10^{-8}$	$8.4x10^{-8}$	$3.1x10^{-6}$	$3.4x10^{-7}$	$5.7x10^{-5}$	$8.0x10^{-8}$	$3.2x10^{-7}$
Pore pressure number	N_P	$7.9x10^{-6}$	$6.2x10^{-6}$	$3.0x10^{-4}$	$1.9x10^{-4}$	0.45	$1.4x10^{-4}$	$3.0x10^{-4}$
Friction number	N_F	$1.4x10^{2}$	$4.7x10^{2}$	$3.4x10^{3}$	$6.7x10^{2}$	$2.89x10^{2}$	$7.9x10^{4}$	$2.9x10^{6}$

MC stands for methyl cellulose. Glyc stands for glycerine.

7.13.10. Results and discussion

Figure 7.38 shows that centrifuge experiments can match some aspects of field scale flows better than typical 1-g flume tests. The centrifuge flows produce relatively low Savage numbers which are more representative of field flows than typical flume experiments at 1-g. This is due to the increased self-weight in centrifuge tests and decreased particle size (see equation 7.2).

Increasing the g-level also has a positive effect on N_P. The physical importance of N_P is emphasized by Iverson and Denlinger (2001); larger volume flows tend to have lower values of N_P because longer drainage paths within the flowing mass create persistent pore pressures. These pore pressures are key to flow mobility, as evidenced by the flow lengths of the Osceola

and Mt. Thomas flows. The decrease in N_P and N_S made possible in centrifuge testing is a key advantage over traditional 1-g flume experiments.

The N_F values, which represents the ratio of frictional to viscous stresses, are in the same order of magnitude for the glycerine, methyl cellulose, and traditional 1-g flume experiments. Using a less viscous pore fluid, however, increases N_F to values more representative of field scale flows.

There are, however, some trade-offs and experimental complications produced by scaling particle size and pore fluid viscosity in the centrifuge. The N_B and N_R were lower than both traditional 1-g flume tests and the field scale flows. This is a result of both the small size of the particles, which is inherent in any small scale test, and the increased viscosity of the pore-fluid needed to match the diffusional and inertial timescale in the centrifuge. Bowman et al. (2010) point out that the lower Bagnold number should only affect flows in the collisional regime, as indicated by high Savage numbers. The centrifuge flows develop low Savage numbers, thus the lower values of N_B may be more acceptable. However, the deposit shape and velocities of the experiments presented here suggest that, even with lower Savage numbers, viscous forces dominated, as is shown in the N_B values.

Low N_{qR} values for T10 and T14 also indicate that viscous forces dominated over collisional forces. Bowman et al. (2010), using a wider flume, a finer PSD, and a PSD similar to the one used in these tests, found the same result; N_R values were too low as compared to both field scale flows and traditional flume-tests. Bowman et al. (2010) stated that increasing the flow velocities in future tests may result in higher Bagnold and Reynolds numbers. This was attempted by a slightly steeper flume angle and a narrower channel in this set of tests. While N_B in these tests was approximately an order of magnitude higher than in Bowman et al. (2010), it appears from the dimensional analyses that dominance of viscous drag was still too high. As shown in Figure 7.38 the use of water instead of a higher viscosity fluid in T5 and T21 resulted in a higher N_R and N_B and mitigated this problem somewhat. In theory, one could use water as a pore fluid and increase the slope angle, thereby increasing the velocity of the flows and N_R still further. Unfortunately, increased velocity comes with its own set of complications–the effect of the Coriolis force will also be increased.

Overall, the dimensional analysis suggests that while centrifuge testing can alleviate some of the scaling problems associated with small scale flumes (i.e. lowering N_S and N_P values), the increased viscosity of the pore-fluid as well as the small particle sizes used in the centrifuge meant that the tests were very viscous, at least compared to large-scale, granular debris flows.

7.14. Controls on velocity in confined flume

Even without using dimensional analysis, there is strong experimental evidence that viscous stresses were important as the flow moved downslope. The velocity at the high-speed camera position was controlled by the volume of the flow, the moisture content, but also, crucially, the viscosity of the pore fluid. The methyl cellulose tests had much higher velocities than the equivalent glycerine tests using the same moisture content and mass. The only variable that differed was the viscosity of the pore-fluid at the high speed camera position. This strongly suggests that viscous stresses were a dominant control on debris flow behaviour during confined, downslope motion.

The centrifuge flows conducted here then, based on dimensional analysis, are definitely not collisional, but probably lie between the frictional and viscous regime. An interesting question, then, is does the dominant regime change as the flow proceeds from a steep confined to shallow confined and then finally to unconfined runout conditions?

Borrowing from the literature on earthquake induced lateral spreading, Bowman et al. (2010) suggested that in a steep, confined setting the experimental centrifuge flows may be in a "forced vibrational regime". In this state, perturbations and large strains cause persistent high fluid pressures which do not dissipate. The length and magnitude of the perturbation, in this case controlled by the velocity of the flow and the slope angle, will cause pore pressures to increase and mixture stiffness to decrease. This will reduce the intergranular friction and influence grain collisions (Iverson, 1997). In fact, if high fluid pressures cause complete mixture fluidization or liquefaction, the grains will mimic the condition of the buoyant spheres used in Bagnold (1954). The closer the flow comes to this condition, the less important enduring grain contacts and intergranular friction will become. The importance of either viscous stresses or collisional stresses, depending on the viscosity of the interstitial fluid, will increase.

This explains the dominance of viscous stresses during downslope motion in the centrifuge flows. As the flows became more and more liquefied, viscous forces became more dominant. Consequently, the viscosity of the pore fluid exhibited a large influence on the velocity observed at the camera position. Since the viscosity of the methyl cellulose dropped with increasing shear rate, these flows experienced less viscous drag than their glycerine counterparts. For the tests that used water as the pore fluid (T21, T24, and T5) the water contributed very little viscous drag during downslope motion, thus they attained higher velocities.

Bowman et al. (2010) successfully used a ''modelling of models'' approach to match flow velocities at the high-speed camera position by matching an increase in Ng with an increase

in fluid viscosity. While these velocity results were interpreted to suggest that the consolidation process was a major influence on flow behaviour, the results could also be interpreted as evidence that viscosity controls downslope velocity and that velocity scales with g. The results in this study corroborate the latter interpretation.

In the context of the flow of a trickle of viscous fluid moving down an inclined plane, Duffy and Moffatt (1995) show (based on the Navier-Stokes equation) that viscosity does indeed scale with g:

$$u_s = \frac{\rho g sin\alpha}{2\mu} h^2 \tag{7.8}$$

where u_s is the surface velocity, ρ is the density of the fluid, g is the gravitational acceleration, α is the slope angle, μ is the viscosity, and h is the flow height. Equation 7.8 shows that if the g-level and the viscosity are doubled, the effect cancels and the same surface velocity is produced as with a 1-g experiment.

Bowman et al. (2010) then, used the correct strategy in their modelling of model tests because both the g-level and pore-fluid viscosity were scaled together. In this set of tests, however, the fine flows were not an appropriate model of models, because the viscosity was changed without changing the g-level. This resulted in different velocities, flow heights, and behaviour. These results suggest that the peak velocity of the flow is not controlled by consolidation behavior, as proposed by Bowman et al. (2010), but rather controlled by the viscosity of the pore-fluid.

7.15. Controls on runout

Consolidation may have been important in the runout phase of movement, although the controls on runout are much harder to identify. As discussed in Section 7.12.5, the differences in runout with increasing mass were explained by the length and thickness of the tail and flow velocity. The flow heights of the methyl cellulose and glycerine tests were similar. The decreased runout of the methyl cellulose flows when compared to the equivalent glycerine flows could be explained by the following mechanisms:

1. The higher viscosity of the methyl cellulose flows at lower shear rates lead to decreased runout and increased viscous damping during the runout phase of the flow. Between the position of velocity measurement and flume outlet, the methyl cellulose decelerated faster than the glycerine flows, creating levees within the channel at the sides of the flows in

T9 and T14. Deceleration would have led to an increase in viscosity and a subsequent decrease in consolidation rate – the former leading to greater deceleration, and the latter leading to a reduced deceleration. Given that deceleration was, overall, greater for methyl cellulose than for glycerine flows this may suggest that viscous effects, which are greater than for glycerine at low shear rate, dominated over consolidation effects in this case. This effect would have been exacerbated by viscous damping in the "free vibrational" phase of movement on the runout surface, which would have effected the more viscous methyl cellulose flows more than the less viscous glycerine flows (Bowman et al., 2010).

2. An additional feedback mechanism may be at work as well; as the viscosity of the methyl cellulose drops, the settling velocity of the particles in the fluid becomes slightly higher. This means that particle sizes which may have been considered as part of the fluid phase, and therefore contributed to increased viscosity of the pore fluid, may now become part of the solid phase. This effect may drop the viscosity of the fluid even further, which may either increase the velocity of the flow, or cause more consolidation, which may slow the flow.

3. It is also possible that even as the flows decelerated and the global shear rate dropped, the shear rate experienced by the pore-fluid as it moved between grains may have been relatively high (as discussed in Section 7.4.2). If this is the case, the viscosity of the methyl cellulose flows would have been lower than the glycerine flows even in the runout phase of movement. The lower viscosity would have enhanced consolidation and dissipation of fluid pressures, making the flows less liquefied and more frictional than the equivalent glycerine flows. This increase in frictional resistance may explain the faster deceleration and decreased runout observed in the methyl cellulose flows. It would also suggest that while the major source of shear resistance was viscous stresses during the confined, acceleration phase of movement, the major source of shear resistance was frictional when the flow decelerated and ran out unto the unconfined drum surface.

4. As noted in Section 7.8, according to the high-speed camera images, segregation appeared to increase with both increasing velocity and increasing moisture content. The more fluidized the flow was during downslope motion, the more pronounced an unsaturated, frictional front became. Unfortunately, evidence of this front was not visible in the deposition of the flows, suggesting that coarse and fine material was, to some extent, remixed as the flow slowed at the bottom of the flume. It is possible that the frictional front might have created a dam and hampered flow mobility at lower slope angles and

hence decreased the runout of the flows. This would have preferentially decreased the runout of the methyl cellulose flows and the flows with increased moisture content. This mechanism may have contributed to the lower runouts observed in the methyl cellulose flows.

7.16. Summary and conclusions

The 18 geotechnical centrifuge tests summarized in this chapter demonstrate several important aspects of debris flow behaviour. They also highlight some of the advantages and challenges of modelling debris flows in a geotechnical centrifuge.

- The fixed bed tests employed variable volumes and moisture contents, at a rotational velocity to produce an acceleration field equivalent to 40g. Three different pore fluids were used to test the effect of pore fluid rheology on flow behaviour. Pore pressure and high-speed camera data were used to construct plots of flow velocity with distance and flow height over time. Both an increase in volume and an increase in moisture content resulted in an increase in peak velocity during downslope movement. However, the effect of increasing the moisture content of the flow was found to be much more pronounced than that of increasing the flow volume. The maximum cross- sectional area of the flow was most likely limited by the diameter of the feeder tube. The use of a non-Newtonian pore fluid increased velocity downslope by a factor of two. This is related to the shear thinning behaviour of the pore fluid and the resulting decreased viscous drag between particles and the interstitial fluid.

- Tests with an erodible bed showed that the main mechanism of erosion was single particle scour by the watery tail and knickpoint retreat. This was surprising, as recent studies have suggested that the debris flow front is the most erosive part of the debris flow in the field (Berger and Schlunegger, 2011; Iverson et al., 2011). It may be that the bed at the high-speed camera position was not saturated or steep enough to produce undrained loading of the debris and subsequent mobilization. It also may be that the granular temperature of the flow may be too small to produce the significant pressure fluctuations at the bed surface, which may be associated with erosion as the bouldery front passes (Berger and Schlunegger, 2011). This explanation would be consistent with the interpretation of the centrifuge flows being in a viscous rather than collisional regime.

- Correlations were found between square of velocity of the flow front at the camera position

and runout and also between total mass and runout for the methyl cellulose and glycerine flows. The influence of mass could be explained by the length and thickness of the body and tail of the flow, which shunted the slow, viscous front out into the runout zone. However, the velocity of the flow front was still important. Peak momentum of the flow at the flume outlet, as defined by the product of flow front velocity and total flow mass, took into account both the length of the tail and the flow velocity, and hence could explain the variance of runout between flows of different moisture contents, as long as the pore-fluid rheology was held constant.

- Tests with a finer PSD and water (but roughly equivalent to the coarser material in terms of consolidation behaviour) acted differently from flows using the coarse material. The velocity for the higher volume test was lower than for the smaller volume test, which is still not explained. However, the increased runout of the larger test, despite having a lower velocity, may be explained by the increased pressure from a relatively long, thick body and tail. This mechanism, along with increased velocity, explains why the fine flows ran out further than the glycerine flow of equivalent mass and moisture content; the body and tail of the flow helped shunt the front forward. The difference in runout as compared to the test with coarse material may also, to some extent, be explained by experimental errors. The material was finer in the tail end of the PSD than ideal PSD, which was to be $\sqrt{N}$ finer than the coarse PSD. This would mean that the materials were not perfectly matched, so that consolidation would proceed slower in the fine material, producing longer runouts.

- Different runout versus momentum relationships were observed for the two fluid types. The non-Newtonian flows ran out less for a given peak momentum than an equivalent flow with Newtonian pore fluid. During downslope motion, the methyl cellulose flows were more mobile (faster) as a consequence of a lower pore fluid viscosity at high shear rates, despite the drop in viscosity also leading to an increased rate of consolidation. This suggests that the glycerine flows were made relatively slower by greater viscous shearing or drag during the acceleration phase. As the flows decelerated, a different response was observed. Between the position of velocity measurement and flume outlet, the methyl cellulose decelerated faster than the glycerine flows, creating levees within the channel at the sides of the flows in at least two tests. This could be explained by either increasing viscosity and viscous drag as the flow decelerated and shear rates dropped, or increased frictional resistance due to greater segregation or faster consolidation, or some

combination of these processes.

- Dimensional analyses of the centrifuge flows and comparison between typical 1-g flume tests and two field scale debris flows shows that the centrifuge has some advantages over traditional 1-g flume testing. By increasing the g-level, the flows become less collisional and more frictional, as shown by decreased values of N_S. The centrifuge is also able to replicate lower values of N_P, meaning that elevated pore-pressures will persist over the length of the test. These are important advantages over 1-g flume tests. However, the introduction of a viscous pore fluid increases viscous stresses, as shown by low N_B. These stresses may be especially important while the flow is accelerating down the flume, as high fluid pressures will decrease frictional resistance and hence cause viscous stresses to increase in importance. The major shear stress acting on the particles will then be controlled by the viscosity of the interstitial fluid.

- In the runout zone, it is an open question whether viscous or frictional forces are more important. The runout behaviour of the methyl cellulose and glycerine flows can be explained by the influence of both processes. In reality, it is likely that both processes operate to some extent.

Both the dimensional analysis and the quantitative measurement of flow velocity suggest that dominance of different mechanisms of shear resistance shifts between channelized down-slope movement and unconfined runout. This has important implications for both the understanding and modelling of debris flow mechanics. It calls into question whether or not a flow can be entirely characterized by collisional, viscous, or frictional regimes. As pointed out by other authors (Hutchinson, 2003; Iverson and Denlinger, 2001) the dominant mechanism of shear stress will be different in the frictional front to liquefied interior. This study suggests that these regimes also will vary depending on location in the debris flow path.

While there are some novel effects and experimental difficulties produced by testing at high-g, overall, the results presented in this chapter suggest that many elements of debris flow behaviour can be modelled in the centrifuge. Perhaps the most useful element of the centrifuge is not that it is able to model prototype-scale processes perfectly, but that it provides the opportunity to alter the g-level, and therefore the frictional nature of the flows, independently of other variables. In this way, centrifuge testing has the potential to greatly complement physical modelling techniques in common use.

8. Debris flow friction slopes

Thus far, this study has focused on the laboratory flows and field scale flows separately. This chapter discusses the concept of friction slope, as defined by the Takahashi/Hungr momentum equation (Takahashi, 1981, 1991; Hungr et al., 1984), in an effort to link and compare mobility between the two scales of debris flow. The momentum equation is also a common tool in preliminary hazard analysis, but the model needs to be calibrated to specific field areas (Rickenmann, 2005). Accordingly, friction slopes were back-calculated for the New Zealand debris flow events discussed in previous chapters.

The analysis showed these values fall within the range of friction slopes presented in the literature. This result is useful from a hazard modelling perspective, as it suggests that the momentum equation can be applied with some confidence to New Zealand debris flows.

Friction slope values from the field were then compared to friction slope values calculated from laboratory flume data (Carrol et al., 2007). In addition, a scaling analysis is presented that takes into account different grain sizes in front and tail of the flow. The results suggest that the rates and mechanisms of energy loss during runout in granular debris flows in the laboratory can be comparable with the those in the field, if the particle size distribution tested is well-graded and the pore-fluid used is not too viscous.

8.1. Introduction

The Takahashi/Hungr (Takahashi and Yoshida, 1979; Takahashi, 1981, 1991; Hungr et al., 1984) momentum equation (Equation 2.1) was briefly discussed in Chapter 2. The equation predicts the runout of a debris flow surge based on the conservation of momentum between an upstream reach and downstream reach. Figure 8.1 shows this simplified surge transitioning from a steep upslope reach to a lower angle runout zone. To apply the equation, the velocity

of the surge (v_u) and flow height (h_u) at the transition point must be known. One must also know the slope angles of the upstream (θ_u) and downstream reach (θ_d) . The flow density, solids concentration, width, and flow height are assumed to be constant from the upstream to downstream reach. The formulation of the equation given by Hungr et al. (1984) is shown below:

$$X_L = V^2/G \tag{8.1}$$

$$V = v_u cos(\theta_u - \theta_d)\left[1 + \frac{g h_u cos\theta_u}{2v_u^2}\right] \tag{8.2}$$

$$G = g(S_f cos\theta_d - sin\theta_d) \tag{8.3}$$

where Hungr et al. (1984) introduced the term friction slope, S_f, by defining:

$$S_f = \frac{(\sigma - \rho_m)\, c_s}{(\sigma - \rho_m)\, c_s + \rho_m} tan\alpha \tag{8.4}$$

where ρ_m is density of the inter-granular fluid, σ is the density of the solid, and c_s is the solids concentration. Thus, the original physical meaning of S_f, according to Hungr et al. (1984) and Takahashi (1991), is related to the grain concentration of the flow (c_s) and the dynamic friction angle between the particles (α). In Equation 8.3, the S_f is assumed to be constant along the runout path.

The value of S_f reflects the equilibrium slope angle at which the flow begins to either accelerate or decelerate. If S_f is equal to θ_d, the flow will continue forever. If $S_f < \theta_d$, then the flow will accelerate. If $S_f > \theta_d$, the flow will decelerate. The model, therefore, is very sensitive to small change in S_f. As the depositional slope itself reflects frictional properties of the flow and this equilibrium angle, values of S_f are often very close to $tan\theta_d$. For this reason, S_f is often related empirically to the θ_d by the equation $S_f = f\, tan\theta_d$, where f is an empirical coefficient.

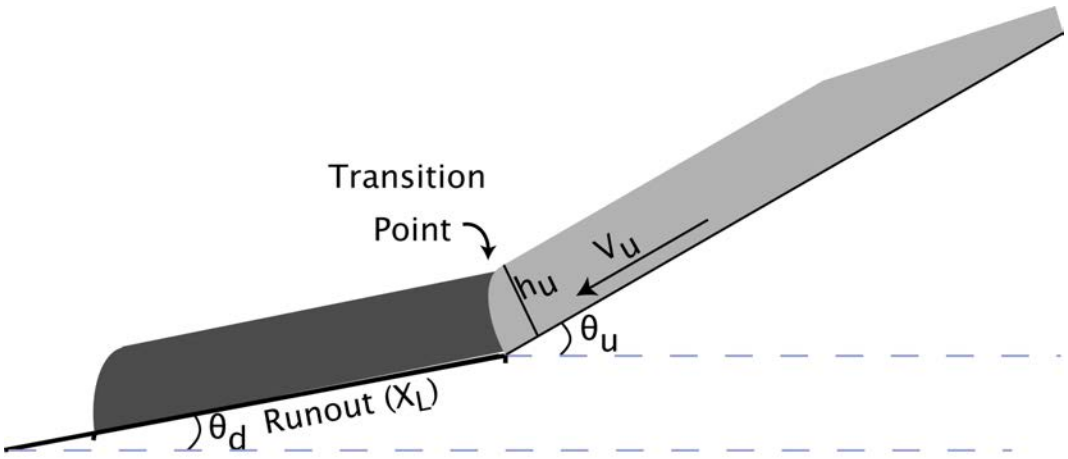

Figure 8.1.: Simplified sketch of a debris flow surge transitioning from the final transport reach to the final depositional reach (modified from Takahashi, 1991).

8.2. Friction slope values in the literature

Practitioners using the Takahashi/Hungr model for preliminary hazard evaluation must choose an appropriate S_f for the area they are working in. Investigators do not usually report the solids concentration (c_v) and dynamic friction angle (α) of the material that is necessary to calculate S_f according to its original definition, since these variables are difficult to measure and may vary from surge to surge. Instead, they report the range of S_f which when used, the modelled runout equals the observed runout. This means that, in practice, S_f is empirical.

Like any empirical parameter for debris flow runout, S_f varies from location to location. Hungr et al. (1984) found that for five large events in Western Canada (event volumes of 20,000 to 50,000 m^3), S_f values of tan(10°) produced good agreement between calculated and predicted X_L. For debris flows in the Southern Alps of Japan a coefficient of f=1.12 yielded better predictions (Okuda and Suwa, 1984). For 12 debris flow events in the Swiss Alps, a coefficient of 1.08 yields more realistic values of X_L (Rickenmann, 2005).

The intent of this chapter is two-fold; to compare friction slope values from New Zealand with other field datasets and thereby evaluate the momentum equation as a modelling tool, and also to use the concept of friction slope to compare the mobility of field and laboratory flows. Friction slope values compared were calculated from the field events discussed in Chapter 2.4, values reported in D'Agostino et al. (2010), and values are taken from a series of experiments on the University of Canterbury laboratory flume (Carrol et al., 2007) which explored the effect

of pore-fluid viscosity and particle size grading on debris flow velocity and runout.

8.3. Data

To compare the best-fit friction slope values from multiple datasets, Equation 8.1 was solved for S_f to yield:

$$S_f = \frac{\left[v_u cos(\theta_u - \theta_d)\left(1 + \frac{gh_u cos\theta_u}{2v_u^2}\right)\right]^2}{gX_L cos\theta_d} + \frac{sin\theta_d}{cos\theta_d} \tag{8.5}$$

The equation also makes several important assumptions. It assumes the flow height, flow density, and the solids concentration of the flow does not change from the upslope reach to the downstream reach.

8.3.1. Field

In order to apply Equation 8.5, the flow height in the final confined reach (h_u), the slope angle in the transport zone (θ_u), the average slope angle in the runout zone (θ_d),the velocity at the transition point (v_u), must be known. In the vast majority of cases, these values are not directly measured, but must be estimated based on indirect field evidence.

8.3.1.1. New Zealand debris flows (hillslope and torrent)

The geometric parameters needed to apply Equation 8.5 were taken from the New Zealand reach data discussed in Chapters 3, 4, 5, and 6. In in order to apply the equation, a suitable transition between the simplified upstream and downstream reaches had to be identified. For confined flows, the end of the last confined reach before the runout zone was chosen. For hillslope flows, the transition point was defined as the end of the last transport reach before major deposition. The value for θ_u was set to be the slope angle of this final confined or transport reach. The length of the runout (X_L) was set to the slope length between the end of this reach and the end of the coarse clastic deposition. If the runout continued over several depositional reaches of different slope angles, the runout slope was set to the weighted average of slope over the runout distance.

Since none of the New Zealand debris flows were directly observed, the entry velocity had to be estimated. For the torrent flows, this was done using the empirical relationship between H^2S (where H is the inferred flow depth and S is the sine of the slope angle in the

reach) and velocity given by Prochaska et al. (2008b) (Equation 8.6). This empirical equation was discussed in Section 6.2.1.4. The flow heights needed to apply Equation 8.6 were estimated from strand-lines, trim-lines, and levees during field mapping, as discussed in Section 3.4.1.4 on page 35.

$$v = 0.35(h^2 S) + 5.36 \tag{8.6}$$

The empirical formula, however, was generated for small torrent flows in the North America and Europe. It may not be realistic for hillslope debris flows in this study. Observations by Brundall (1966) and observations of a small flow during field mapping suggest that many of the flows at Cass travel at a maximum velocity of approximately 2.0 m/s, at least in the lower reaches of their paths. For this reason, the entry velocity of the flows at Purple Hill, White Rock Road, and Castle Hill was set at 2.0 m/s.

Flow velocities in the Birch Hill catchment were poorly constrained. In the absence of other observations, the more conservative (higher) velocities predicted by Prochaska et al. (2008b) were used. The flow height, entry velocity, entry angle, and runout values used for the New Zealand flows are shown in Table 8.1.

Table 8.1.: Values used in Equation 8.5 to back-calculate S_f values for the New Zealand field debris flows.

Flow	Type	Flow height (m)	θ_u (°)	θ_d (°)	v_u (m/s)	Runout (m)
OR1	Torrent	2.0	18.0	15.0	5.8	119
OR2	Torrent	1.5	16.0	12.0	5.6	49
OR3 tongue 1	Torrent	2.0	19.0	15.0	5.8	127
OR3 tongue 2	Torrent	2.0	19.0	15.0	5.8	105
FJ4	Torrent	1.5	14.0	7.0	5.6	41
C12	Intermediate	2.5	25.0	18.3	6.2	320
BH4	Intermediate	1.5	35.7	19.2	5.8	43
BH1	Hillslope	0.25	26.4	23.4	6.0	137
BH2	Hillslope	0.7	21.6	18.0	5.5	55
BH3	Hillslope	1.0	21.7	17.8	5.8	101
C1	Hillslope	0.5	12.0	1.1	2.0	10
C2	Hillslope	1.2	25.0	17.0	2.0	34
C3	Hillslope	1.7	23.0	18.0	2.0	60
C6	Hillslope	1.0	30.6	25.5	2.0	143
C7	Hillslope	0.9	21.3	15.5	2.0	144
C11	Hillslope	1.0	23.0	18.3	2.0	35
C13	Hillslope	0.75	20.0	15.5	2.0	185
C14	Hillslope	1.3	17.0	12.8	2.0	116

8.3.1.2. Torrents in the Dolomites, Italy

The second field dataset discussed was taken from a field study by D'Agostino et al. (2010). These data reported in the study came from a series of debris flows which occurred on July 5th, 2006 at Fiames, located in the Dolomites (Eastern Italian Alps). Debris flows in the region are generally triggered by intense summer thunderstorms. The precipitation provided by these events runs down steep, bedrock basins. At the basin oulets, the runoff progressively mobilizes sediment from talus slopes, eventually evolving into debris flows. The bedrock basins in the area are composed entirely of dolomite, with talus slopes composed of particles from silt to boulder size colluvium. The lower part of the slopes are made up of coalescing debris flow fans.

These events were mapped by D'Agostino et al. (2010) using similar methods to those presented in Chapter 3. However, D'Agostino et al. (2010) calculated the volume deposited by subtracting a digital elevation model (which was produced by LIDAR after the event), from the pre-event topographic surface (estimated from a 1:5000 scale topographic map). D'Agostino et al. (2010) calculated the debris flow discharge by adopting a relation between the estimated

water flood hydrograph and debris flow discharge (given by Takahashi 1978). The flow velocity was calculated using the adapted Chezy equation—$v=Cg^{1/2}\sin\theta^{1/2}$, where C is an empirical, dimensionless Chezy roughness. C was set to 3 based on studies in the neighboring Aquabona watershed (Genevois et al., 1999). Unlike Hungr et al. (1984) and this study, which used the bed-slope near the fan apex as the θ_u, D'Agostino et al. (2010) uses the average bed slope between the initiation point and the beginning of the deposition zone.

Table 8.2.: Field data from D'Agostino et al. (2010).

Flow name	Flow height (m)	θ_u (°)	θ_d (°)	v_u (m/s)	Runout (m)
1	1.39	23.3	19.3	4.17	394
2	1.19	21.9	16.2	3.89	427
3	2.57	21.9	16.0	6.93	312
4	1.5	23.0	21.2	3.96	329
5	1	21.6	21.4	3.15	129
6	0.5	27.9	25.9	4.78	183

8.3.2. University of Canterbury flume

The 1-g flume data presented comes from an unpublished study by Carrol et al. (2007). The flume used in this study, shown in Figure 8.2, was housed in the geotechnical laboratory at the University of Canterbury. The laboratory flume used was 2.5 m long and 1 m high. A metal hopper supported the debris flow material before its release down the curved aluminum chute, which provided a transition to the main channel. The 1 m long, 20 cm wide channel was set at a slope angle of 23°. This test slope ran down to a flat, symmetric runout area which had been roughened with a layer of glue impregnated with sand.

Similar to the centrifuge set-up discussed in Chapter 7, the outward facing wall of the flume was made from Perspex. This allowed a cross-sectional view of the flow to be recorded by a high-speed camera. The velocities given for these experimental flows comes from this high speed camera data.

The experiments were designed to test the effect of particle size distribution and pore fluid viscosity on debris flow runout (Carrol et al., 2007). The d_{50} used in each test was 0.875 mm. The coefficient of uniformity (C_u, defined by d_{60}/d_{10}) of the soils used in the experiments were 4.0 (PSD1), 4.4 (PSD2), and 5.5 (PSD3). The soil tested came from fluvial gravels in the Waimakariri River floodplain, located in Canterbury, New Zealand. Each test was run with a solid mass of 8 kg and a fluid mass of 2.24 kg, producing a moisture content of 0.28, or 28% by

weight. The test labels, coefficient of uniformity, and pore fluid viscosity used in each test are shown in Table 8.3.

,

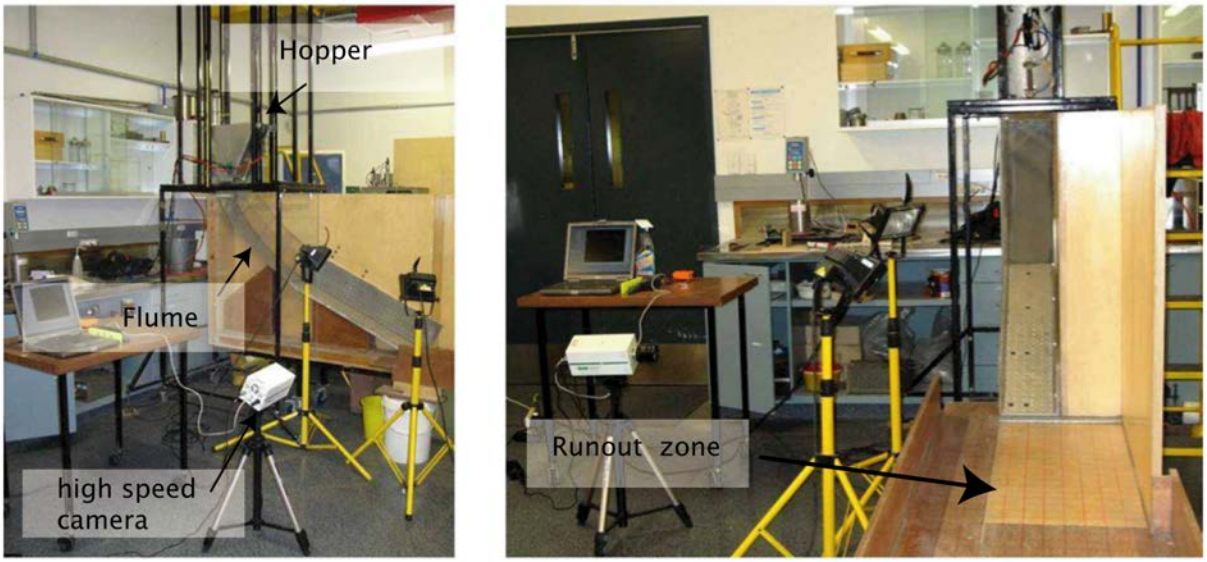

Figure 8.2.: University of Canterbury debris flow flume (Carrol et al., 2007)

Table 8.3.: Description of each test in Carrol et al. (2007)

Test label	C_u	μ (mPa.s)	Flow height (cm)	v_u (m/s)	Runout (cm)
PSD1Visc1	4	1.0	2.6	0.7	32.8
PSD1Visc2	4	3.3	3.3	0.2	29.3
PSD1Visc3	4	176	3.3	0.9	37.1
PSD2Visc1	4.4	1.0	4.9	1.1	71.1
PSD2Visc2	4.4	3.3	3.8	1.3	65.5
PSD2Visc3	4.4	176	3.4	1.8	84.1
PSD3Visc1	5.5	1.0	4.2	1.6	91
PSD3Visc2	5.5	3.3	4.9	1.1	68.1
PSD3Visc3	5.5	176	2.4	1.8	83.6

All flows used a solid mass of 8kg and a fluid mass of 2.24kg.$^{+}$All viscosities measured at 20°C Carrol et al. (2007).

8.4. Results

8.4.1. Field

Figure 8.3 plots the runout angle (θ_d) of the New Zealand data against the back-calculated friction slope (converted to degrees by atanS_f). As found by previous studies (Rickenmann, 2005; Hungr et al., 1984), the back-calculated friction slope was just larger than the runout angle. The friction slope values were larger for the hillslope flows than the channelized flows, reflecting deposition at higher slope angles. To provide an estimate of the error which may be involved in the calculation, the figure also plots "upper" and "lower bound" data points. The "upper bound" data-series in Figure 8.3 uses a velocity and flow height 50% larger than shown in Table 8.1. The S_f must therefore be larger to achieve the same runout. The "lower bound" data-series uses a velocity and flow height 50% smaller, and thus requires a lower S_f to achieve the same runout. Plotting these values gives an indication of the amount of variance in friction slope due to errors in estimating the flow height and entry velocity, as these values are estimates in most debris flow studies (unless flow parameters are measured during the event).

Figure 8.4 plots the runout angle versus friction slope for all the NZ data (mean values) and the D'Agostino et al. (2010) data. The D'Agostino et al. (2010) data plots towards the lower bound of the New Zealand flows. This means that the friction slope values were very close to the depositional slope for the D'Agostino et al. (2010) dataset, which will be discussed later in Section 8.5.1.

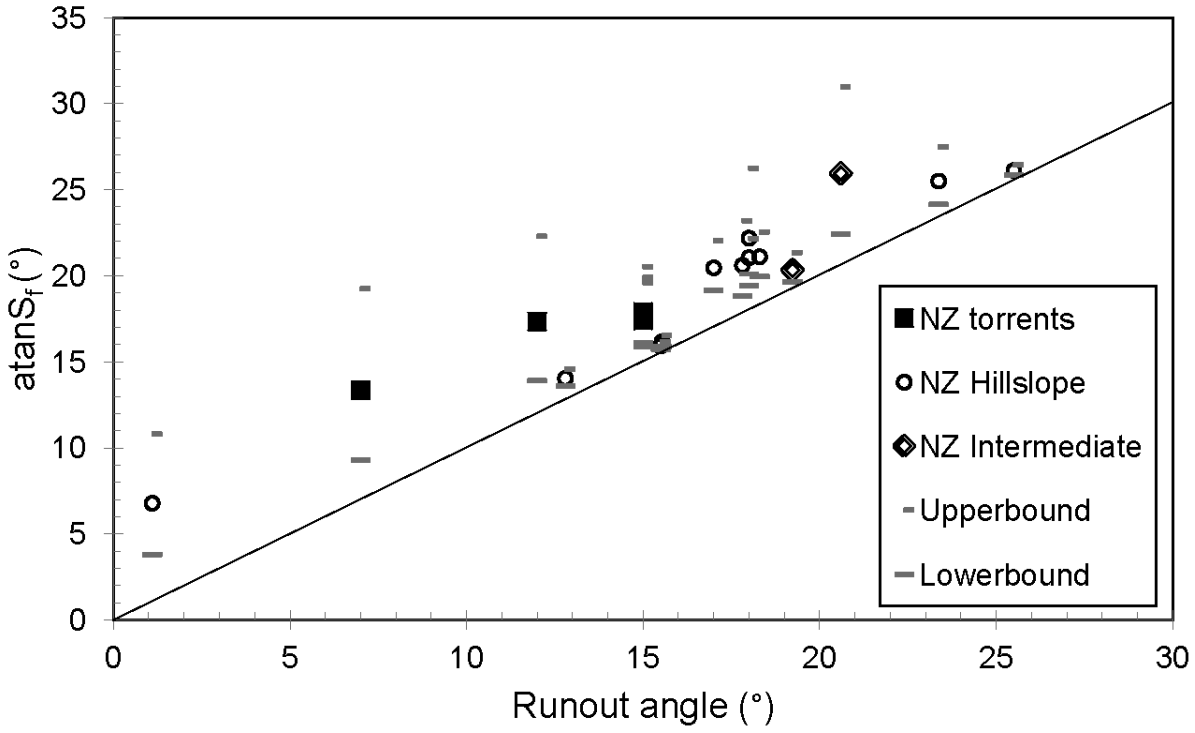

Figure 8.3.: Plot of runout slope angle versus the back-calculated friction slope for New Zealand channelized, intermediate, and hillslope flows. An upper and lower bound for the New Zealand data is given using a entry velocity and entry flow height error of ±50%.

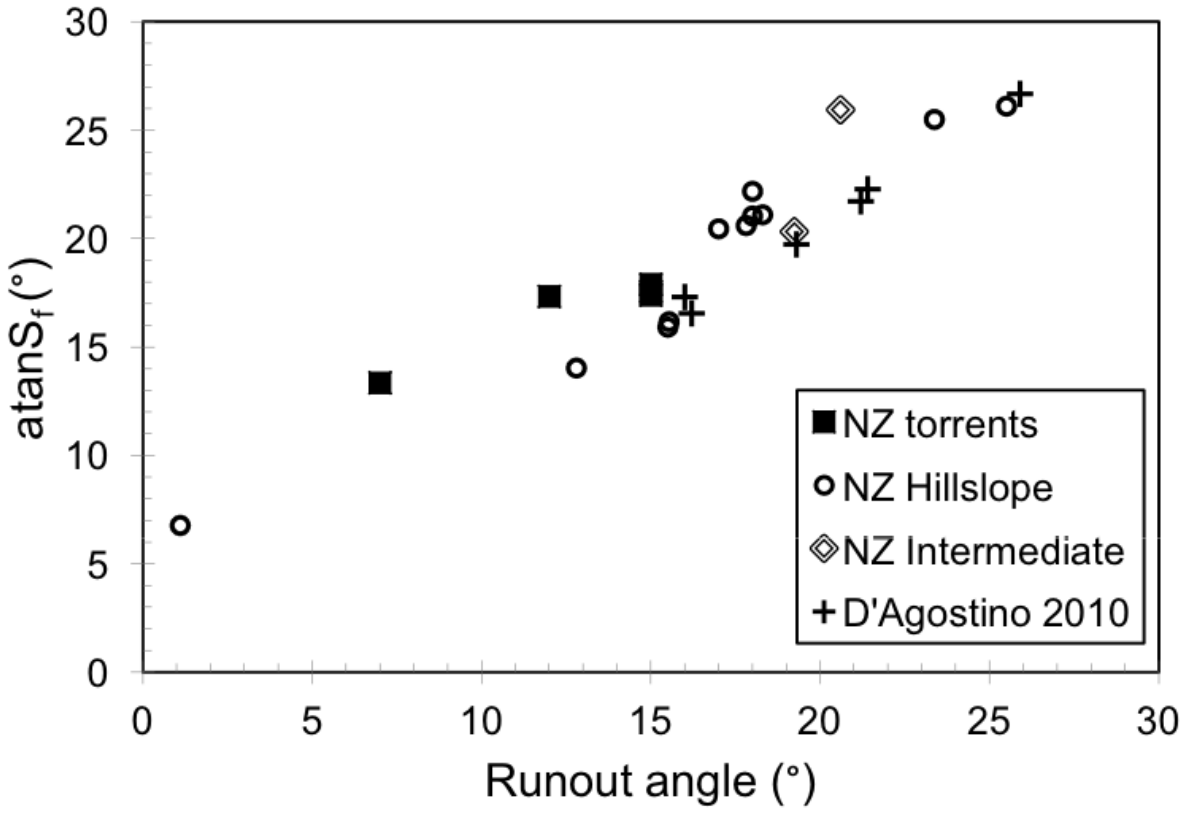

Figure 8.4.: Plot of runout angle versus the back-calculated friction slope for New Zealand and D'Agostino et al. 2010 datasets.

8.4.2. Laboratory

Figure 8.5 plots the square of the flow velocity observed at the high-speed camera position versus the runout from the flume outlet Carrol et al. (2007). Runout increases with increasing velocity. Lower viscosity and higher C_u increased the velocity observed in the tests.

Figure 8.6 plots the back-calculated atanS_f values and the entry velocity squared for each test. The friction slope values generally follow the same trend as the entry velocity; as entry velocity increases, so does the friction slope. However, this relationship breaks down for the flows of high viscosity.

The back-calculated best-fit values of atanS_f range from 21° to 11.5° for the laboratory flows, which is about the same range as for the field debris flows. It is not possible to compare the f values for these flows because θ_d is 0 for a flat runout zone.

Figure 8.7 plots the back-calculated atanS_f and runout for each test. The friction

slope also follows the same trend as runout; higher runout flows have higher friction slope. The reasons for this are discussed in the next section.

It is also interesting to compare the back-calculated S_f values with the values calculated from Equation 8.4. Assuming a dynamic friction angle of 30°, a solid density of 2.7g/cm^3 and a fluid density of 1.0g/cm^3, the atanS_f of all flows is 15.9°— in the middle of the back-calculated range of S_f. This simple exercise demonstrates that while the solids concentration and dynamic friction angle may determine the S_f at first approximation, other factors such as viscosity and the PSD are important as well. This will be discussed further in the next section.

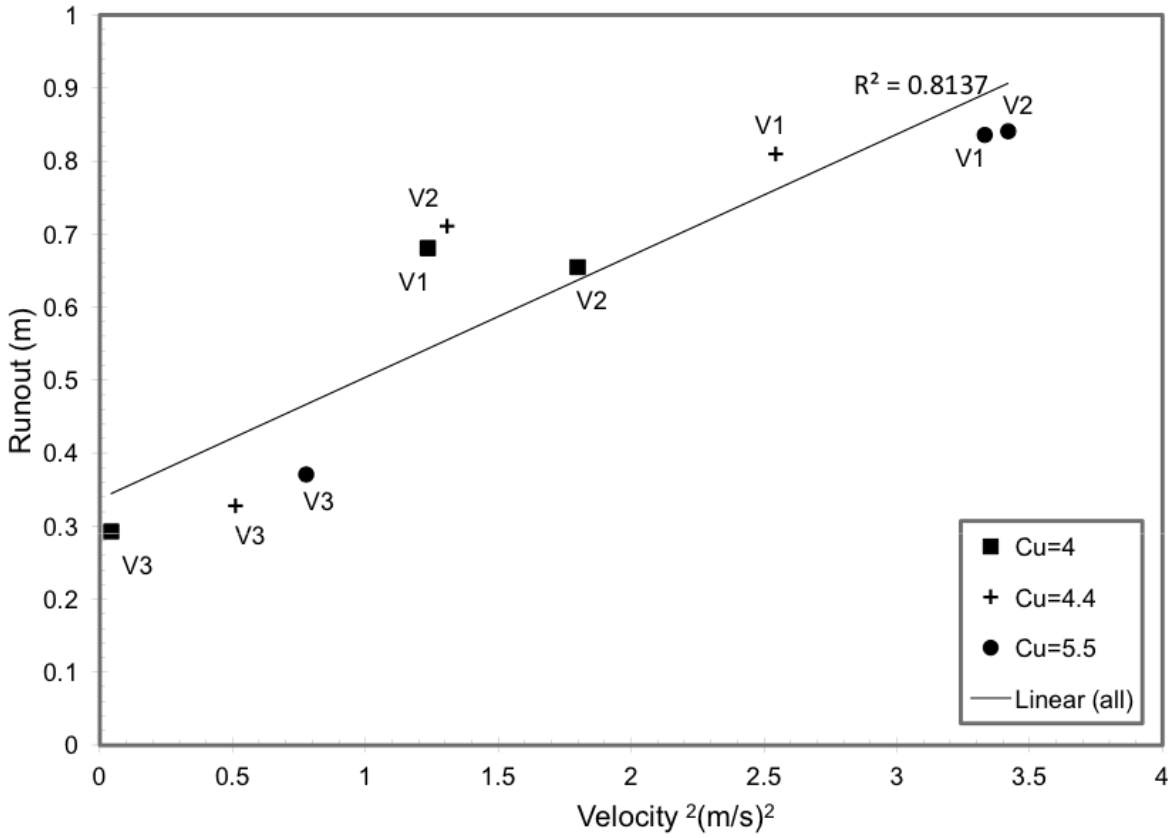

Figure 8.5.: Velocity squared of the 1-g flume data plotted against runout from the flume exit. Viscosity is also labeled V1=1mPa.s (water at 20°C), V2=3.3mPa.s, V3=176mPa.s.

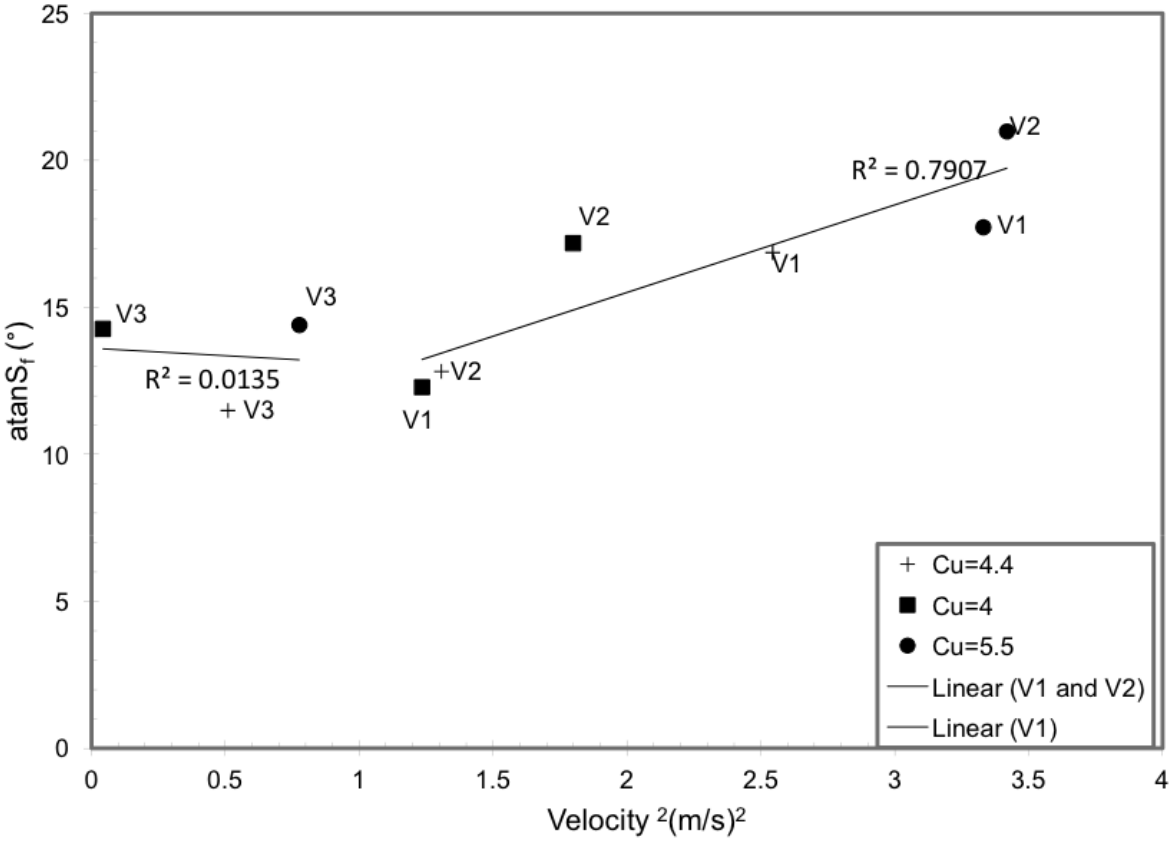

Figure 8.6.: Back-calculated friction slope for 1-g flume tests plotted against velocity squared.

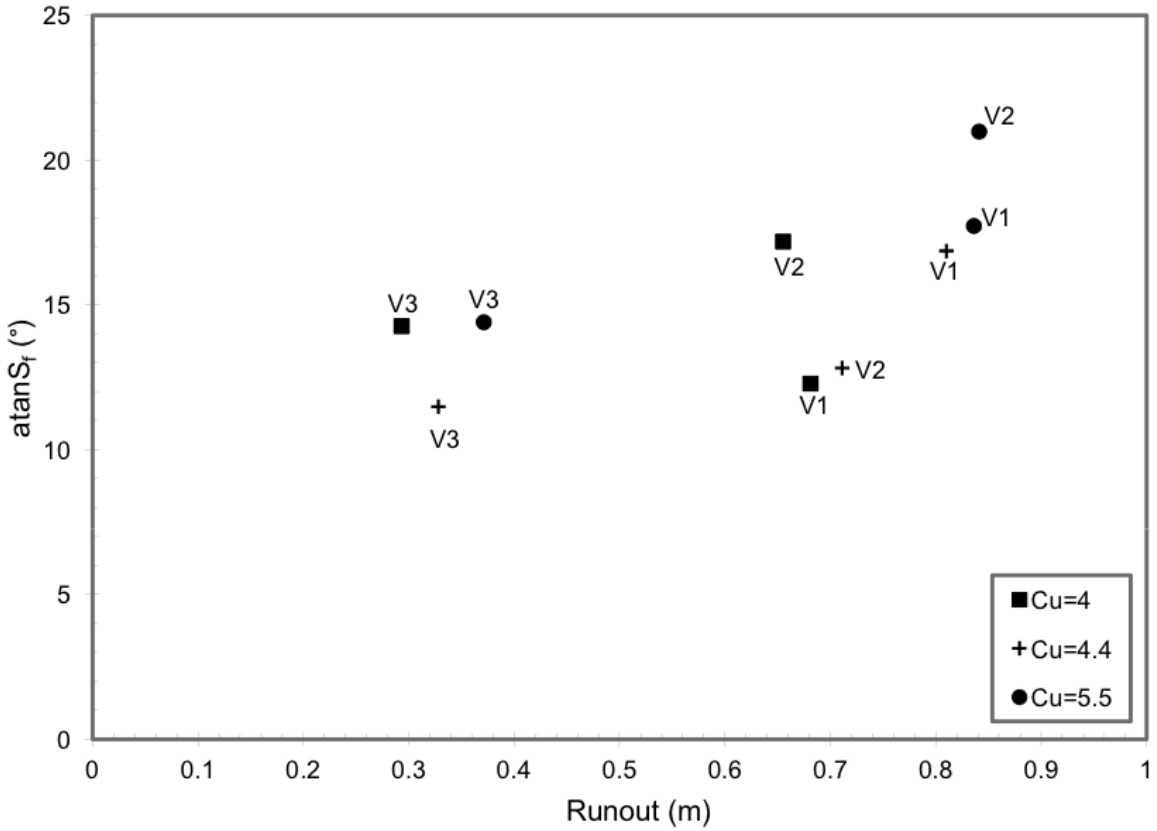

Figure 8.7.: Back-calculated friction slope values for the 1-g flume tests plotted against runout from the flume exit.

8.5. Discussion

8.5.1. Field scale debris flows

The friction slope calculated for each flow was usually just slightly higher than the flow's depositional slope. The exception to this was one of the mapped New Zealand flows, C1, which ran out onto a road with a 1° slope. In this case, the atanS$_f$ was 6.78°, producing a coefficient f of 6.19. This is probably because the slope of the runout surface was artificially modified. For the rest of the New Zealand hillslope flows, values of f ranged from 1.07 to 1.25. For the New Zealand torrent flows, values ranged from 1.01 to 1.37. For the two intermediate flows, BH4 and C12, values for f were 1.29 and 1.06, respectively.

The best-fit values calculated for the New Zealand events are within the range noted by Okuda and Suwa (1984) and Rickenmann (2005). D'Agostino et al. (2010) report values of 1.016 to 1.072 for the torrent dataset in Dolomites, with an average value of 1.030. The best-fit f values for three events in Hungr et al. (1984) (those events in which enough data was included to calculate the best-fit f coefficient) were 1.318, 1.170, and 1.198.

To some degree, the values of coefficient f reflect the abruptness of the transition from the upstream to downstream reaches. The average angle change from θ_u to θ_d in D'Agostino et al. (2010) was 3.3°, while angle changes in the New Zealand hillslope, New Zealand torrent, and Hungr (1984) data were 6.3°, 4.6°, and 6°, respectively. As D'Agostino et al. (2010) point out, "the relationship [between atanS_f and θ_d] can be adequately calibrated, but is too sensitive to f variations to the third decimal place when, as in our case study, the upstream slope θ_u and the fan slope θ_d are very close." The debris flows in the Dolomites incised into their fans, then later deposited onto coalescing fans downslope. The landform did not change, so the slope did not change substantially. When using the momentum equation to model runout in situations with this geometry, very small changes in the S_f used will produce large changes in runout, which may hurt the model's utility.

8.5.2. Laboratory experiments

In the experimental data, entry velocity of the flows to the runout zone largely determined the friction slope. For the two tests with lower pore-fluid viscosity, the friction slope followed the same trend as entry velocity squared—as entry velocity increased, so did the friction slope (see Figure 8.6). This is caused by the dominance of the momentum term (V^2) in Equation 8.5. The runout of the flow is comparatively less important in determining the S_f, as it is not squared in the Equation 8.5. This is reflected in Figure 8.7. The runout of the tests which used water as a pore fluid followed the same trend as the friction slope—a longer runout produced a higher friction slope. While this may be counter-intuitive, it is due to these longer runout flows also having higher velocities, which dominates the momentum equation.

For the flows at higher viscosity, higher velocity did not translate into a very large change in runout (Figure 8.5). Consequently, the relationship with friction slope also breaks down. This is not surprising, as these flows should no longer be considered granular debris flows, but rather viscous debris flows. The momentum equation was developed for fast, granular debris flows and no longer applies in this situation (Takahashi, 1991; Jordan, 1994; Iverson, 1997).

The fact that the S_f value calculated using the the solids concentration (c_s) and the dynamic friction angle (α) (by Equation 8.4) fall within the range of empirical S_f values back-

calculated by Equation 8.5 is interesting. That the empirical values lie on either side of the analytical value demonstrates that the viscosity of the pore fluid and the degree of sorting in the material is also important. Values calculated for atanS_f were between approximately 13° and 23°, which is about the range calculated in field scale debris flows. Differences in empirical S_f then, may reflect differences in viscosity and PSD between different flows.

8.5.3. Comparison of field and laboratory data

The data presented here show that back-calculated friction slopes for 1-g laboratory flows and small scale field flows are similar. The average laboratory atanS_f was 15°, while the typical atanS_f for hillslope events was 20°. This implies that laboratory flumes may be able to adequately represent the mobility of larger scale granular type flows.

Other studies have found the same. For example, D'Agostino et al. (2010) also conducted a series of small scale flume tests which showed that the ratio of the flow length to the vertical drop (a measure of mobility) of the laboratory flows was greater than for the field flows that they measured. This may be surprising, given the apparent scaling problems with small scale experiments which were summarized in Chapter 2 (Iverson, 1997; Iverson and Denlinger, 2001). The results also appears contradictory to the results of Chapter 6, which reported that back-calculated Voellmy friction coefficients (another indicator of flow mobility) decreased with increasing debris flow size over a log scale (see 6.12 on page 142).

However, the decreasing mobility discussed in Chapter 6 mainly reflected the differences between small, hillslope flows which occur in low order streams, and larger, channelized, torrent events which occur lower in the geomorphic system. Most flume studies are explicitly designed to study channelized events. From this perspective, the fact that the typical laboratory values for S_f are lower than the typical hillslope values is unsurprising.

In fact, the results given here suggest that if a laboratory flow segregates into a coarser front and a finer, more liquid tail, the driving and resisting forces during the runout phase of the flow remain similar to what is observed in the larger field scale channelized flows. Crucially, the scaling analysis presented in Chapter 7 and Iverson and Denlinger (2001); Iverson (1997) used the average particle size of the flow (D_{50}), which may not be representative of the important processes at work during runout. Iverson himself states that in granular flows the "deposited coarse debris lacks high pore pressures and typically forms a dam that impedes and eventually halts the motion of ensuing finer-grained debris that retains higher pore pressures. Alternatively, wetter, more mobile debris may have enough momentum to override or breach the dam of previously deposited debris, so that deposits can develop by a combination of for-

ward pushing, mass "freezing," vertical accretion, and lateral shunting of previously deposited sediment." If the mechanics of motion during runout are a function of the relationship between the bouldery front and the finer tail, then rheological similarity should be applied to both parts of the flow.

Figure 8.8 compares the N_S and N_B of the most well-graded, least viscous laboratory flow from Carrol et al. (2007) with that of a coarse, granular debris flow from Mt. Thomas New Zealand (Pierson, 1980). The lighter bars are the laboratory flow, while the darker columns are Mt. Thomas. From left to right, the plot compares the numbers using the D_{50}, D_{90}, and D_{10} grain sizes. The grain sizes used are shown in Table 8.4.

Using the D_{50} to calculate N_S shows that the flows are in different regimes. However, the flows are more rheologically similar at either end of their particle size distributions. When number is compared using the D_{90}, the Mt. Thomas flow comes much closer to the collisional regime. Using the D_{10} to calculate N_S shows that the lab flume is still too collisional, but has moved closer to the frictional regime.

The second set of columns compares N_B. Again, if the D_{90} is considered, the flows are both in the collisional regime. For the D_{10}, the laboratory flow again appears too collisional, however; this analyses assumes the interstitial fluid of the laboratory flow has the viscosity of water. In reality, the viscosity of the pore fluid, which is a mixture of fines and water, is likely to make the flow slightly more viscous and shift N_B lower.

While these collisional, frictional, or viscous regimes of dimensional scaling are important indications of physical processes that dominate flow, one must remember that they were developed and tested with much simpler systems of grain/fluid interaction, i.e. round, buoyant particles with uniform grain sizes. In practice, oxymoronically, these 'thresholds' are known to be gradational. For example, the threshold between collision dominated and viscous processes occurs with N_B between 40 and 240 Iverson (1997).

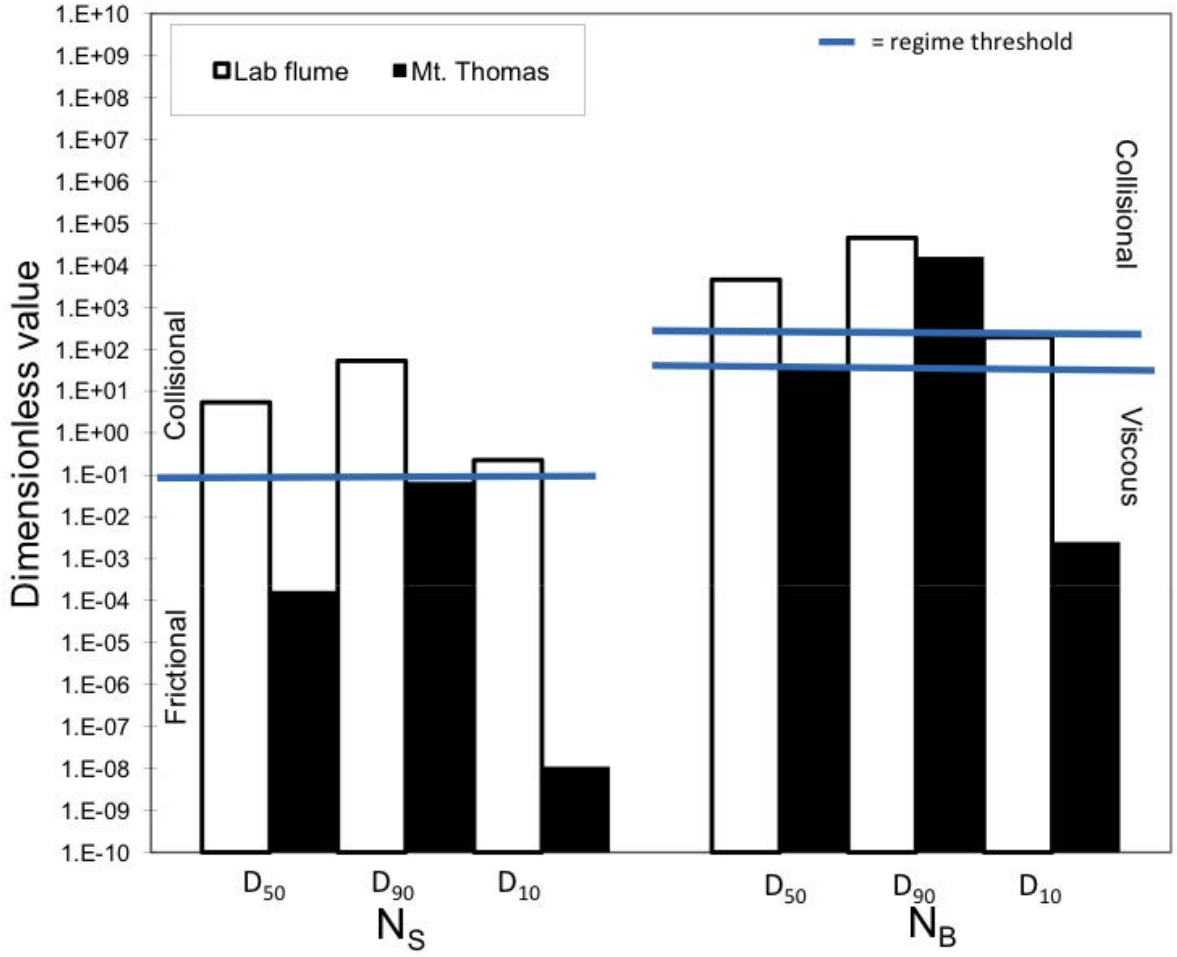

Figure 8.8.: Plot of N_S and N_B calculated for PSD1V1 Carrol et al. (2007) and Mt. Thomas debris flow (Pierson, 1980) using the observed D_{50}, D_{90}, and D_{10}. Laboratory flows are white. Field scale flows are black.

Table 8.4.: Particle sizes used in dimensional analysis.

	Laboratory (mm)	Mt. Thomas (mm)
D_{10}	0.18	0.08
D_{50}	0.875	10
D_{90}	2.75	200

8.5.4. Comparing field and laboratory data–morphology

The morphological evidence that laboratory debris flows act like their larger scale counterparts should not be discounted. Figure 8.9 is an overhead view of the deposit of PSD1V1 (Carrol

et al., 2007). The deposit is coarser towards the front and margins, with finer material in the center of the flow. The more fluid tail overtopped the main deposit after it had stopped, reworking the deposit. This is labeled "Fluid washout" in 8.9. All of these features are typical of field scale deposits (see 2.2.1).

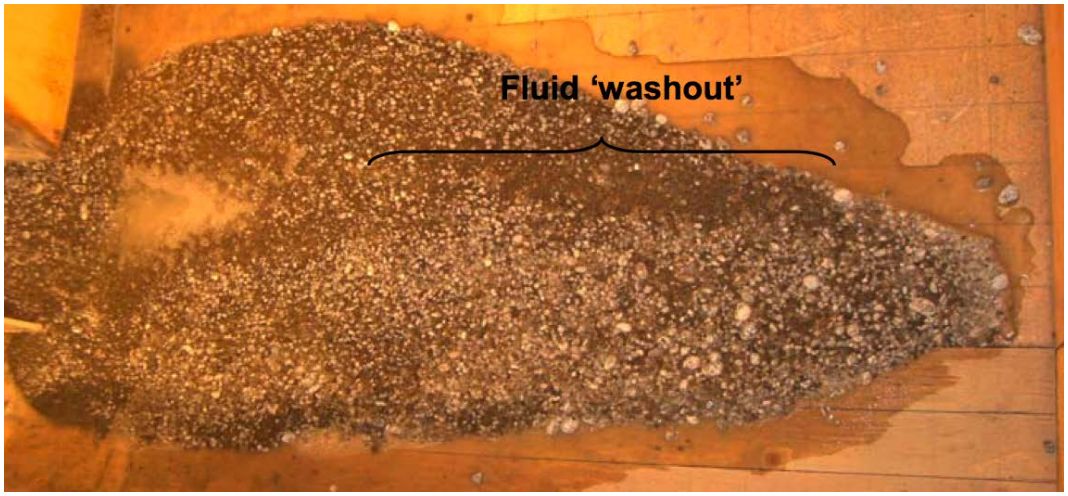

Figure 8.9.: Photo of PSD1V1 from the (Carrol et al., 2007) dataset. The photo clearly shows the formation of a coarser margin and finer tail. Coarser material has even been reworked by fluid tail is labeled by "Fluid washout".

8.6. Summary and conclusions

By back-calculating the best-fit friction slope values in the Takahashi/Hungr momentum equation, this chapter confirmed that the range of empirical friction slope values for the New Zealand dataset is similar to other international datasets. The use of the momentum equation as a decision support tool in preliminary hazard mapping is therefore justified. Caution, however, should be exercised when the entry slope angle is very close to the depositional slope angle, as the model will be very sensitive to even small changes in the friction slope value used.

The range of back-calculated friction slope values in a set of small-scale flume experiments was similar to the range observed in field events. This result suggests that laboratory flows are able to adequately reproduce the mobility of larger scale granular type flows during the runout phase of movement. This implies that the scaling limitations supposedly inherent in small scale flume testing may not be as insurmountable as previously believed. If segregation is achieved, the laboratory flow is able to simulate the relationship between the tail and front of the flow, and thus able to model many of the processes and morphological features observed

in larger scale flows. Since the runout in granular debris flows is controlled by interactions between a finer body and tail and a dryer, more frictional front, it makes sense to apply a scaling analysis to both finer and coarser grain sizes, rather than to the average grain size of the entire flow. This analysis concluded that while there are still some scaling limitations in small scale flumes, the analysis mitigates some of these scaling problems, especially for the bouldery front.

Further, the small scale experiments demonstrate that the friction slope is not simply a product of solids concentration and the frictional properties of the solids, but must also take into account the variance in grain size and fluid viscosity. Experimental flows which use a single particle size, therefore, may be limited in their ability to simulate important processes of granular debris flows.

9. Summary and conclusions

9.1. Introduction

At the outset of this work, the following aims were set forth:

1. To describe debris flow events in New Zealand at a variety of scales and classify them according to debris flow type.
2. To identify the major controls on debris flow behaviour in each field area and quantify volumes eroded, deposited, and travel distance.
3. To model the travel distance of these events using common empirical and dynamic methods and suggest empirical values and methods which could be used by practitioners.
4. To compare the events surveyed with others in the debris flow literature.
5. To increase mechanical understanding of debris flow behaviour using small scale physical modelling. In particular, address the role of flow quantity, moisture condition, and pore fluid rheology in determining downslope velocity and runout.
6. To ascertain whether or not small-scale experiments are able to adequately model the mobility of larger scale flows.

This chapter summarizes the findings in the context of the aims stated above. While the work has achieved much of these aims, it has has also raised some questions and identified avenues for future research.

9.2. Documenting and classifying debris flows in New Zealand

A total of 21 debris flow paths were traversed in four debris flow prone areas in New Zealand. The travel paths were traversed in the summer of 2008/2009 and 2009/2010 by the author and another field assistant.

The field methods used in this study worked well to investigate the general behaviour and eroded and deposited debris volumes of alpine debris flows in New Zealand. The method is best applied to small debris flow events with event magnitudes between 100 m^3 and 10,000 m^3. Recording upper and lower bounds for erosion helped communicate the amount of uncertainty in estimating eroded volumes. Using this method, one can collect the data needed to run most simple empirical or statistical-analytical runout models (Rickenmann, 1999; Fannin and Wise, 2001; Prochaska et al., 2008a; Benda and Cundy, 1990; Corominas, 1996), or one-dimensional mathematical models. With higher resolution topographic data, the field methods could also be used to collect data which could be used to calibrate more complex, 2-D models which incorporate lateral spreading.

The events mapped were classified into three different types; hillslope, torrent (also called channelized events), and intermediate events. The quintessential difference between the hillslope and torrent flows was their location in the geomorphic system from hillslope to sea. Both flow types lie on a continuum from low to high stream order, where the limiting debris flow processes may gradually change from water availability high in the geomorphic system to gradient in higher order streams. Hillslope flows occur on steeper slopes. They are dominated by slope and gully processes in 0-order gullies or first order streams incised into planar hillslopes. Torrent flows are dominated by channel processes in first or higher order stream channels. In these channels, hyper-concentrated flows and high stream flow are also common. The intermediate flows mapped (flows BH4 and C12) were located high in the geomorphic system (in gullies with no or only very intermittent stream flow), but were confined over most of their path. Consequently, they displayed properties of both hillslope and torrent events.

The Cass and Birch Hill field areas were dominated by hillslope flows which deposited between 100 m^3 to over 1,000 m^3 in their terminal reaches, but also deposited significant amounts of material in levees further upslope. The source of material for these flows was small translational failures or progressive bulking of material from gullies incised in the hillslope (Cass) or small failures at the boundary between bedrock headwalls and talus slopes (Birch

Hill).

The Orongorongo and Franz Josef field areas were dominated by torrent type debris flows. Debris flows in the Orongorongos were most likely triggered by rockfalls or hillslope flows from steep, bedrock source reaches. The event volume mapped in the Orongorongos ranged from 1,000 m^3 to 10,000 m^3. In larger events, the head of the fan became an important area for entrainment. While confinement and slope angle were the primary factors in determining whether or not the flow would erode, constrictions in the channel which caused particle jamming and encouraged deposition were also important. These constrictions of large boulders often became knickpoints for subsequent fluvial erosion.

Extremely fast uplift rates (approximately 10 mm/year), extreme rainfall (>10 m/year), and the presence of dense forest separates Franz Josef from the other field areas studied. In this field area, vegetation acted to increase channel roughness and may tend to produce less frequent, higher-magnitude events (Bloomberg and Davies, 2012). The volume of the events was 800 $m^3$to 2,500 m^3. The source of debris for both debris flows was failures in fault damaged bedrock.

9.3. Identifying controls and quantifying flow behaviour

For hillslope events, erosion was observed to occur from approximately 41° to 28° slopes. Deposition occurred from approximately 27° to 13° degree slopes. The mean depth of erosion was 0.46 m. The mean depth of deposits was 0.48 m. Hillslope flows generally tended to deposit levees progressively as they travelled downslope, ending in smaller lobes of debris at the foot of the slope. The average width of the flow path through the transport zone was narrower than for the torrent events.

The controls on deposition were slope angle, and to a lesser extent, confinement. The mean ratio of deposition width to flow height in depositional reaches was 13.4 for the hillslope events, compared to 22.0 for the torrent events. This indicates that for the hillslope events, lateral spread was less than for the the torrent events.

Hillslope type flows tended to deposit at higher slope angles and have smaller discharges than torrent events. This can be explained by lack of confinement once they moved out of the gully and possibly higher solids concentrations. Hillslope debris flows are only particularly hazardous to infrastructure or residences directly adjacent to steep slopes. They are also extremely important in transferring sediment to the main channel. This process of channel recharge contributes to the generation of larger Class 3 and 4 channelized flows.

For the torrent events, erosion was observed from approximately 40° to 14°, depending on confinement. Deposition was observed from 16° to 10.3°, although significant deposition occurred on higher slope angles at channel constrictions. Both the mean depth of erosion (approximately 1.0 m) and mean depth of deposition (0.67 m) were greater than for hillslope flows.

The two intermediate events mapped deposited at slope angles similar to hillslope flows (mean of 19.7°), but showed similar confinement to torrent events— the mean flow width/depth ratio through transport reaches was 1.7. It may be that the increased confinement aids flow mobility through the channelized section of the path, but that higher solids concentrations hamper mobility during unconfined runout phase of motion.

9.4. Modelling the travel distance of the documented flows

In order to suggest input parameters which may be useful to practitioners and compare the New Zealand data with other debris flows from the literature, Voellmy rheological parameters (friction and turbulent drag coefficients) were back-calculated with the landslide modelling software DAN-W so that the travel distance in each simulation was approximately equal to the travel distance of coarse clastic material observed in the field.

Hillslope flows deposited on higher slope angles, which resulted in higher best-fit Voellmy friction coefficients (μ) between 0.22 to 0.45, with a mean of 0.33. Values of the turbulent drag term (ψ) ranged over two orders of magnitude, from 10 ms^{-2} to over 1000 ms^{-2} . Best-fit values of μ for intermediate events were 0.4 and 0.46, indicating that these events were similar to hillslope flows in terms of mobility.

UBCDflow generally over-predicted the magnitude and travel distance for hillslope and intermediate events, but performed better when all reaches were set to "unconfined". For hillslope flows, a method was presented where UBCDflow can be used to estimate the depth of erosion in each reach. These erosion depths can be input into DAN-W and used with back-calculated friction coefficients to model a more appropriate travel distance.

Torrent events deposited on lower slope angles and therefore required lower empirical coefficients to predict the actual runout distance than those required for hillslope events. The Voellmy friction coefficients for the torrent events ranged from 0.17 to 0.30 with a mean of 0.23. Values of the turbulent drag term (ψ) ranged over one orders of magnitude, from 10 ms^{-2} to 100 ms^{-2}. For torrent events, UBCDflow can be used to predict travel distance and event volume. These values can then be used to calibrate frictional parameters in DAN-W. While this method

is not appropriate for design purposes on its own, it may be useful to estimate potential flow velocities and explore the effect of different boundary conditions on flow model behaviour.

9.5. Comparison of the events documented with others in the debris flow literature

While the back-calculated friction coefficients for the New Zealand events in this data-set were much higher than for larger, torrent type events in the literature, they were within the range of values cited for smaller torrent and hillslope flows (Brideau et al., 2006; Brideau, 2009). When the friction coefficient values were plotted against the upslope area contributing to the debris flow, a weak correlation became apparent. This is because upslope area increases with decreasing slope angle. In theory, the water availability also increases downslope, which may result in lower solids concentrations and higher mobility.

When world-wide friction coefficient values were plotted against event volume, a weak correlation between volume and mobility was found. This, too, was a reflection of the depositional slope at which large events come to rest. The scatter in friction coefficients at smaller event volumes was thought to be related to increased susceptibility to small changes in confinement and channel roughness.

In Chapter 8, the runout distances of NZ debris flows were modelled using the Takahashi/Hungr momentum equation. The results show that the S_f (friction slope) term for the hillslope events is also higher than for the torrent events, although the values of the empirical coefficient f are slightly smaller. The values of f also fall within the range of values back-calculated for debris flow events in Japan, Italy, and in the Swiss Alps (Okuda and Suwa, 1984; Rickenmann, 2005).

These analyses suggest that using empirical friction coefficients from other small, torrent or hillslope flows in DAN-W, careful analysis with UBCDflow, and the use of the Takahashi/Hungr momentum equation are all appropriate tools to use in New Zealand, at least for preliminary hazard evaluation. These results will assist hazard forecasters concerned with debris flows in the field areas studied. For example, a simple analysis of terrain steepness and stream orders would provide guideance on what type of debris flow (torrent or hillslope, or both) that could be expected for a catchment. The modelling approach adopted here could then provide first-order estimates of travel distances and velocities. This information could then guide the prioritization of site-specific assessments of hazard.

9.6. Better understanding of the mechanics of small debris flows

The results of 18 debris flow tests using a geotechnical centrifuge, described in Chapter 7, show that such tests are able to model many important processes observed in field-scale flows. A clear Perspex wall on one side of the flume allowed a high-speed camera to observe a cross-sectional view of the flow as it passed during each test. This, along with pore-pressure transducers installed in the base of the flume, allowed the velocity of the flows to be observed. After each test, the runout and depth of each deposit was measured.

Thirteen fixed bed (unerodable substrate) tests were designed to investigate the influence of moisture content, volume, and pore-fluid rheology on flow velocity and runout. All tests were conducted at a rotational velocity which produced an acceleration field of 40g in the flow runout zone. Three different pore-fluids were used to test the effect of pore fluid rheology on flow behaviour; water (Newtonian), Glycerine (Newtonian, used to increase viscosity), and methyl cellulose (shear-thinning, used to increase viscosity).

Increases in both volume and moisture content resulted in an increase in peak velocity during down-slope movement. However, the effect of increasing the moisture content of the flow was found to be much more pronounced than than the effect of increasing the flow volume.

Pore fluid rheology also affected the flow velocity observed at the high-speed camera position. The flows using methyl cellulose as a pore-fluid accelerated to peak velocities which were generally twice as fast as the equivalent glycerine flow. This was related to the shear thinning behaviour of the pore fluid and the resulting decreased viscous drag between particles and the interstitial fluid.

The peak momentum (defined by the product of velocity at the high-speed camera position and the mass of the flow) controlled the runout of the flows, but different relationships were found for the three pore-fluid types. Methyl cellulose flows ran out less for a given peak momentum than an otherwise equivalent glycerine flow. The shear-thinning, methyl cellulose flows were more mobile (faster) as a consequence of a lower pore fluid viscosity at high shear rates, despite the drop in viscosity also potentially leading to an increased rate of consolidation. Conversely, the glycerine flows were made relatively slower by greater viscous shearing or drag during the acceleration phase.

While the methyl cellulose flows accelerated faster, they also decelerated faster than the glycerine flows. This could be explained by either increasing viscosity and viscous drag as the flow decelerated and shear rates dropped, increased consolidation rate, or increased frictional

resistance at the front due to greater segregation, or some combination of these processes.

Two tests conducted with a finer PSD and water as a pore-fluid (but supposedly equivalent in terms of consolidation behaviour to the coarser material using glycerine) demonstrated that the viscosity of the pore-fluid must be scaled with the g-level. The flows were thinner and faster than the equivalent glycerine test because they were less viscous.

In addition to the 13 fixed bed tests, 5 tests were run with an erodible bed to explore the effect of entrainment on flow behaviour. Flow velocities and runouts were similar to the equivalent fixed bed test using the same moisture content and material volume. The main mechanism of erosion was single particle scour by the watery tail and knickpoint retreat. Erosion caused by undrained loading and the impact pressure of the bouldery front, which is known to be important in some field-scale events (Iverson et al., 2011; Berger and Schlunegger, 2011) was not observed in the centrifuge experiments. This may be due to the fact that the flows are too viscous (not collisional enough) to produce high granular temperatures and resulting pressure fluctuations which seem to be associated with debris flow erosion in the field.

9.7. Determining whether small-scale experiments are able to adequately model the mobility of larger scale flows

Dimensional analyses of the centrifuge flows indicated that while the centrifuge was able to increase prototype stress levels and thereby increase frictional shear stress, overall, the flows in this set of tests were more dominated by viscous stresses than are field scale granular debris flows. The introduction of a viscous pore fluid increases viscous stresses, as shown by low values of N_R and N_B. These may be especially important while the flow is accelerating down the flume, as high fluid pressures will decrease frictional resistance and hence viscous stresses begin to have a greater influence on flow velocity. The major shear stresses acting on the particles will then be controlled by the viscosity of the interstitial fluid.

The centrifuge, however, does have some useful advantages over small scale, 1-g flume testing. The increased g-level causes increased frictional shear stress, which decreased values of N_S to values which are closer to field scale debris flow events. The centrifuge is also able to replicate lower values of N_P, meaning that elevated pore-pressures will persist over the length of the test.

Chapter 8 showed that the range of back-calculated friction slope values in a set of small-scale, 1-g flume experiments was similar to the range observed in field events. This result suggests that laboratory flows are able to adequately reproduce the mobility of larger

scale granular type flows during the runout phase of movement. This implies that the scaling limitations supposedly inherent in small scale flume testing may not be as insurmountable as previously suggested (Iverson and Denlinger, 2001). If segregation is achieved, the laboratory flow is able to simulate the relationship between the tail and front of the flow, and thus able to model many of the processes and morphological features observed in larger scale flows (Bowman and Sanvitale, 2009). Since the runout in granular debris flows is controlled by interactions between a finer body and tail and a dryer, more frictional front, it makes sense to apply a scaling analysis to both finer and coarser grain sizes, rather than to the average grain size of the entire flow. This analysis mitigated some of these scaling problems associated with small scale experiments, especially for the bouldery front part of the flows.

Further, the small scale experiments demonstrate that the friction slope is not simply a product of solids concentration and dynamic friction angle, but must also take into account the variance in grain size and fluid viscosity. Experimental flows which use a single particle size, therefore, may be limited in their ability to simulate important processes of granular debris flows.

9.8. Recommendations for future research

9.8.1. Field studies

While the field methodology described in this study worked well to characterize volumes eroded and deposited and travel distance of small debris flow events, the method could be improved in future field studies. More time could be spent characterizing the debris flow material, as this would allow some insight into the physical parameters which influence the rheology of flow. Measurements could be made on the particle size distribution, type of fines, and amount of organics present. It would also be useful to pay particular attention to the maximum particle size present, especially in reaches in which particle clogging caused deposition.

Some details recorded in this study, however, could be dispensed with in future field work. The complex confinement categorization described in Chapter 3 was found to be largely irrelevant to flow behaviour. Confined in gully and confined in channel reaches could simply be considered confined, while partially confined reaches could be considered unconfined.

The problem of error quantification in debris flow studies deserves more research attention. The main source of error in estimating erosion and deposition is uncertainty of the pre-event channel and fan morphology. This uncertainty limits the confidence and power of

empirical observations of yield/lag rates and erosive depths such as those given in Chapter 5 and other debris flow studies.

To obtain more certain estimates of eroded and deposited volume, a very detailed series of before and after observations of channel morphology are needed, such those done at the Illgraben catchment in Switzerland (Berger et al., 2010; McCoy et al., 2010; Schlunegger et al., 2009). Although these detailed studies allow some generalizations to be made for other sites with similar geology and climate (i.e. the Swiss Alps), erosion and runout behaviour are likely to be substantially different in New Zealand. Therefore, repeated, detailed topographic surveys of typical debris flow paths in New Zealand, using more sophisticated methods such as terrestrial laser scanning or photogrammetry, would be beneficial to understanding site-specific processes. This work could also be compared to manual mapping methods, such as the one presented in Chapter 3, to help quantify the error involved in field mapping.

Further, the lack of a congruent landslide taxonomy and nationwide database hampers debris flow research in New Zealand. Robust empirical modelling of debris flows requires large amounts of debris flow observations. At present, debris flows are noticed by employees of various government agencies, such as the Department of Conservation or the NZ Transport Agency, but little, if any, data are collected. Many flows are labeled simply as slips and cleared away. A project to educate employees of various agencies in how to classify various landslide types and collect rudimentary data (i.e. runout and volumes deposited) would enhance landslide science in the country.

While many studies have been conducted on torrent events, less research has been conducted on hillslope debris flows. This is partly due to confusing terminology; hillslope flows are often referred to by various names in the literature such as debris avalanches, slides, slips, open-slope flows. The extent of saturation and confinement of these flows often left undiscussed.

While many empirical and analytical models exist for torrent type flows, few exist for hillslope flows. Empirical models of hillslope debris flow travel distance and runout would be useful to practitioners estimating the hazard or designing infrastructure on or adjacent to hill-sides prone to these type of flows.

In some ways, future research into hillslope flows will be easier than for torrent events, as their higher frequency provides ample opportunities to study new events. Such studies will benefit from frequent high-resolution observations now available with new terrestrial laser scanning or photogrammetry techniques. The area around Cass may be ideal for this, as the hillsides are almost completely devoid of vegetation and access is relatively easy. Higher resolution models of the topography would also enable the use of more advanced 2-D runout

models. This is a promising avenue for future research.

The relationships between small hillslope flows, moderate sized torrent events, and even larger, catastrophic debris flows remain poorly understood. To what extent are large, catastrophic debris flows produced by the coalescence of many smaller hillslope flows? What is the dominant process of entrainment in such events? These questions are avenues for future research.

Similarly, the debris flow magnitude-frequency relationships in the field areas studied deserve more attention. Based on aerial photography, satellite imagery, and the succession of vegetation after disturbance, all of the flows mapped in this study were estimated to be under five years old. However, more precise estimates of the recurrence interval of debris flows would be useful to quantify the hazard and better understand the roll of the flows in the geomorphic system. In Europe and North America, numerous studies have used dendrochronology to constrain ages of debris flow events and even link them with changes in climate. Similar studies would be useful in New Zealand.

Debris flow research in New Zealand is, in many ways, still catching up to the state of the art in North America and Europe. While the country's low population density in alpine areas has spared it from the fatalities suffered in other parts of the world, fatalities and significant property damage are almost certain in the future. Debris flow data is a sparse commodity in New Zealand, which makes calibration of empirical models challenging. Even analytical models require knowledge of relevant debris flow parameters observed in past events.

Calibrated models provide useful decision support tools which can inform, check, and justify the judgement of the investigator. This dissertation has begun to provide the data needed to calibrate these tools and create New Zealand specific models and guidelines. It is hoped that it is also part of a continued research effort in New Zealand to collect data and classify debris flows as they occur.

9.8.2. Physical modelling

It is clear from the set of centrifuge experiments described here, as well as from Bowman et al. (2010), that in "models of models", testing the viscosity of the interstitial pore fluid needed to be scaled with the g-level, at least when using fine material and viscous pore fluids. This is an important lesson for future centrifuge flume studies. Further modelling of models is needed to determine which parameters are most important to match between model and prototype.

The effect of the boundary conditions of the experiment, in particular the diameter of the feeder tube, should also be investigated. This could be done by using less volume of

material in each test or restricting the diameter of the feeder tube and observing the effect on flow height. Using less material would also speed the preparation and clean up time for each test. If less material is used, however, the width of the flume might need to be further reduced, perhaps to 40 mm, to enable reasonable flow heights and confinement.

The instrumentation could also be improved. Specifically, a high-speed camera installed in the centrifuge to give an overhead view of the entire runout zone would be very helpful in assessing surface flow velocity and how the material is deposited. It would also be useful to observe the erosion behaviour of the flow at a higher slope angle, either by moving the high-speed camera location closer to the head to the flume or by increasing the slope of the flume itself, to see if failure by undrained loading or destabilization by the front occurs.

The centrifuge experiments also showed that the behaviour of the flows that used methyl cellulose is shear rate dependent and thus changes as the flow accelerates or decelerates. Perhaps the most innovative, though complex, experimental set-up would be a conveyer belt apparatus, perhaps a smaller version of the one used by Davies (1988), installed in a larger beam centrifuge. Such an apparatus would allow flow velocity and the g-level to be manipulated independently and thus help clarify the interactions between frictional, viscous, and collisional processes.

More work should be carried out to model the process of debris flow erosion in the centrifuge. In several recent studies (i.e. Berger and Schlunegger 2011; Iverson et al. 2011), major debris flow erosion was associated with significant particle fluctuations produced by the collisional behaviour of the front (Berger and Schlunegger, 2011). If this is the case, a geotechnical centrifuge may present an opportunity to model this mechanism at a higher stress level than possible in 1-g flume apparatus. Using a larger D_{50} would make the flow more collisional and create higher granular temperatures, while the increased g-level may provide larger pressure fluctuations and stress at the bed surface. If erosion was observed using a more collisional flow, it would strongly support the interpretations of Berger and Schlunegger (2011).

The series of experiments described in this dissertation represent the early stages of debris flow centrifuge testing, where the experimental setup, scaling, and experimental limitations are still being developed. The work is, however, an important step in developing centrifuge testing as an accepted method of modelling debris flow processes. The most useful element of the centrifuge is not that it is able to simulate prototype-scale processes perfectly, but that it provides the opportunity to alter the g-level, and therefore the frictional nature of the flows, independent of other variables. By doing so, centrifuge testing compliments the physical modelling techniques in common use.

References

Ancey, C. and Evesque, P. (2000). Frictional-collisional regime for granular suspension flows down an inclined channel. *Physical review. E, Statistical physics, plasmas, fluids, and related interdisciplinary topics*, 62(6 Pt B):8349–60.

Ayotte, D., Evans, N., and Hungr, O. (1999). Runout analysis of debris flows and avalanches in Hong Kong. In *Proceedings of Vancouver Goetechnical Society Symposium Slope Stability and Landslides*, pages 39–46, Vancouver, Canada.

Bagnold, R. A. (1954). Experiments on a gravity-free dispersion of large solid spheres in a Newtonian fluid under shear. *Proceedings of the Royal Society of London. Series A. Mathematical and Physical Sciences*, 225(1160):49.

Bardou, E., Ancey, C., Bonnard, C., and Vuillet, L. (2003). Classification of debris-flow deposits for hazard assessment in alpine areas. In Rickenmann, D. and Chen, L., editors, *Proceedings of the 3rd International Conference on debris flow hazards mitigation*, pages 799–808. MillPress.

Begg, J. G. and McSaveney, M. J. (2005). Wairarapa fault rupture and vertical deformation in 1855 and a history of similar events from Turakirae Head. In *The 1855 Wairarapa Earthquake Symposium*, page 21.

Benda, L. and Dunne, T. (1997). Stochastic forcing of sediment supply to channel networks from landsliding and debris flow. *Water Resources Research*, 33(12):2849–2863.

Benda, L., Hassan, M., Church, M., and May, C. L. (2005). Geomorphology of steepland headwaters: the transition from Hillslopes to channels. *Journal of the American Water Resources Association*, 41(4):835–851.

Benda, L. E. and Cundy, T. W. (1990). Predicting deposition of debris flows in mountain channels. *Canadian Geotechnical Journal*, 27(4):409–417.

Berger, C., McArdell, B. W., Fritschi, B., and Schlunegger, F. (2010). A novel method for measuring the timing of bed erosion during debris flows and floods. *Water Resources Research*, 46(2).

Berger, C., M. B. and Schlunegger, F. (2011). Direct measurement of channel erosion by debris flows, Illgraben, Switzerland. *Journal of Geophysical Research*, 116(January):1–18.

Berti, M. and Simoni, A. (2005). Experimental evidences and numerical modelling of debris flow initiated by channel runoff. *Landslides*, 2(3):171–182.

Bertolo, P. and Wieczorek, G. F. (2005). Calibration of numerical models for small debris flows in Yosemite Valley, California, USA. *Natural Hazards and Earth System Science*, 5(6):993–1001.

Bloomberg, M. and Davies, T. (2012). Do forests reduce erosion? The answer is not as simple as you may think. *New Zealand Journal of Forestry*, 56(4).

Bovis, M. J. and Jakob, M. (1999). The role of debris supply conditions in predicting debris flow activity. *Earth Surface Processes and Landforms*, 24(11):1039–1054.

Bowman, E. T., Imre, B., Laue, J., and Springman, S. M. (2007). Geotechnical centrifuge modelling of debris flows. *4th International Conferences on Debris-Flow Hazards Mitigation: Mechanics, Prediction, and Assessment*, pages 229–240.

Bowman, E. T., Laue, J., Imre, B., and Springman, S. M. (2010). Experimental modelling of debris flow behaviour using a geotechnical centrifuge. *Canadian Geotechnical Journal*, 47(7):742–762.

Bowman, E. T. and Sanvitale, N. (2009). The role of particle size in the flow behaviour of saturated granular materials. In *17th International Conference on Soil Mechanics and Geotechnical Engineering*, Alexandria.

Brardinoni, F., Slaymaker, O., and Hassan, M. A. (2003). Landslide inventory in a rugged forested watershed: a comparison between air-photo and field survey data. *Geomorphology*, 54(3-4):179–196.

Brayshaw, D. and Hassan, M. A. (2009). Geomorphology of debris flow initiation and sediment recharge in gullies. *Geomorphology*, 109(3-4):122–131.

Brideau, M. (2009). Vancouver Island Open Slope Landslide Runout Project. Technical report, Simon Fraser University, Burnaby, BC.

Brideau, M., Stead, D., Millard, T., Ministry, B. C., and Patton, G. (2006). Runout characteristics of open slope landslides in harvested terrain on Vancouver Island: Preliminary results. In *Sea to Sky Geotechnique*, pages 342 – 350.

Brooks, S. M., Crozier, M. J., Glade, T. W., and Anderson, M. G. (2004). Towards Establishing Climatic Thresholds for Slope Stability: Use of a Physically-based Combined Soil Hydrology-slope Stabiltiy Model. *Pure and Applied Geophysics*, 161.

Brummer, C. J. and Montgomery, D. R. (2003). Downstream coarsening in headwater channels. *Water Resources Research*, 39(10):1–14.

Brundall, J. A. (1966). *Recent debris flows and related gullies in the Cass Basin*. Masters, University of Canterbury, Geography, Christchurch.

Busslinger, M. (2010). *Emperical rules for debris flow travel distance: A comparison of field data*. Master of applied science, University of British Columbia, Vancouver, Canada.

Cannon, S. H. and Savage, W. Z. (1988). A mass change model for the estimation of debris flow runout. *J. Geol*, 96:221–227.

Carrara, A., Crosta, G., and Frattini, P. (2008). Comparing models of debris-flow susceptibility in the alpine environment. *Geomorphology*, 94(3-4):353–378.

Carrol, M., Violette, E., and Jackson, P. (2007). Investigating the influence of debris flow when scaling physical models. Honours year project, University of Canterbury, Christchurch.

Chen, J., He, Y. P., and Wei, F. Q. (2005). Debris flow erosion and deposition in Jiangjia Gully, Yunnan, China. *Environmental Geology*, 48(6):771–777.

Chen, N. S., Yue, Z. Q., Cui, P., and Li, Z. L. (2007). A rational method for estimating maximum discharge of a landslide-induced debris flow: A case study from southwestern China. *Geomorphology*, 84(1-2):44–58.

Chien-Yuan, C., Tien-Chien, C., Fan-Chieh, Y., Wen-Hui, Y., and Chun-Chieh, T. (2005). Rainfall duration and debris-flow initiated studies for real-time monitoring. *Environmental Geology*, 47(5):715–724.

Chikatamarla, R., Laue, J., and Springman, S. M. (2006). Centrifuge scaling laws for guided free fall events including rockfalls. *International Journal of Physical Modelling in Geotechnics*, 6(2):15–26.

Christen, M., Kowalski, J., and Bartelt, P. (2010). RAMMS: Numerical simulation of dense snow avalanches in three-dimensional terrain. *Cold Regions Science and Technology*, 63(1):1–14.

Conway, S., Decaulne, a., Balme, M., Murray, J., and Towner, M. (2010). A new approach to estimating hazard posed by debris flows in the Westfjords of Iceland. *Geomorphology*, 114(4):556–572.

Corominas, J. (1996). The angle of reach as a mobility index for small and large landslides. *Canadian Geotechnical Journal*, 33(2):260–271.

Coussot, P. and Meunier, M. (1996). Recognition, classification and mechanical description of debris flows. *Earth Science Reviews*, 40(3-4):209–227.

Craig, W. (1995). Geotechnical centrifuges: past, present, future. In Taylor, R. N., editor, *Geotechnical Centrifuge Technology*, chapter 1, pages 1–16. Taylor and Francis, London, 1 edition.

Crosta, G. (1998). Regionalization of rainfall thresholds-an aid to landslide hazard evaluation. *Environmental Geology*, 35(2-3):131–145.

Crosta, G. B. and Frattini, P. (2008). Rainfall-induced landslides and debris flows. *Hydrological Processes*, 22(4):473.

D'Agostino, V., Cesca, M., and Marchi, L. (2010). Field and laboratory investigations of runout distances of debris flows in the Dolomites Eastern Italian Alps. *Geomorphology*, 115(3-4):294–304.

D'Agostino, V. and Marchi, L. (2001). Debris flow magnitude in the Eastern Italian Alps-data collection and analysis. *Physics and Chemistry of the Earth, Part C: Solar, Terrestrial and Planetary Science*, 26(9):657–663.

D'Agostino, V. and Marchi, L. (2003). Geomorphological estimation of debris flow volumes in alpine basins. *Proceedings 3rd Int Conf on Debris Flow Hazard Mitigation: Mechanics, Prediction, and Assessment, Davos*, 2:1097–1106.

Davies, T. (1986). Large debris flows: a macro-viscous phenomenon. *Acta Mechanica*, 63(1):161–178.

Davies, T. (1997). Large and small debris flows: Occurrence and behaviour. *Recent Developments on Debris Flows*, pages 27–45.

Davies, T. R., Phillips, C. J., Pearce, A. J., and Zhang, X. B. (1992). Debris flow behaviour-an integrated overview. *IAHS Publications*, 209:217–225.

Davies, T. R. H. (1988). Debris flow surges- a laboratory investigation. *Hydrologie und Glaziologie.*

Davies, T. R. H. and Hall, R. J. (1992). A realistic strategy for disaster prevention. In *Proceedings, Interpraevent*, pages 381–390.

de Scally, F., Owens, I., and Louis, J. (2010). Controls on fan depositional processes in the schist ranges of the Southern Alps, New Zealand, and implications for debris-flow hazard assessment. *Geomorphology*, 122(1-2):99–116.

de Scally, F. A. and Owens, I. F. (2005). Depositional processes and particle characteristics on fans in the Southern Alps, New Zealand. *Geomorphology*, 69:46–56.

Degetto, M., Grucil, G., Pimazzoni, A., Masetto, C., and Gregoretti, C. (2011). An estimate of volume entrainable by debris flows along Stobel and South Pezories channels at Fiames (Dolomites, Italy). In *5th International Conference on Debris-Flow Hazards Mitigation: Mechanics, Prediction and Assessment, University of Padova, Italy*, pages 845–853.

Denlinger, R. P. and Iverson, R. M. (2001). Flow of variably fluidized granular masses across three-dimensional terrain 2. Numerical predictions and experimental tests. *Journal of Geophysical Research*, 106(B1):553.

Dewoolkar, M. M., Ko, H. Y., Stadler, A. T., and Astaneh, S. M. F. (1999). A substitute pore fluid for seismic centrifuge modeling. *ASTM geotechnical testing journal*, 22(3):196–210.

Duffy, B. R. and Moffatt, H. K. (1995). Flow of a viscous trickle on a slowly varying incline. *The Chemical Engineering Journal and The Biochemical Engineering Journal*, 60(1-3):141–146.

Fannin, R. J. and Rollerson, T. P. (1993). Debris flows: some physical characteristics and behaviour. *Canadian Geotechnical Journal*, 30(1):71–81.

Fannin, R. J. and Wise, M. P. (2001). An empirical-statistical model for debris flow travel distance. *Canadian Geotechnical Journal*, 38(5):982–994.

Fraccarollo, L. and Papa, M. (2000). Numerical simulation of real debris-flow events. *Physics and Chemistry of the Earth, Part B: Hydrology, Oceans and Atmosphere*, 25(9):757–763.

Gamma, P. (2000). *dfwalk-Ein Murgang-Simulationsprogramm zur Gefahrenzonierung*. Geographisches Institut der Universität Bern.

Garnier, J., Gaudin, C., Springman, S. M., Culligan, P. J., Goodings, D. J., Konig, D., Kutter, B. L., Phillips, R., Randolph, M. F., and Thorel, L. (2007). Catalogue of scaling laws and similitude questions in geotechnical centrifuge modelling. *International Journal of Physical Modelling in Geotechnics*, 7(3):1–23.

Gartner, J. E., Cannon, S. H., Santi, P. M., and Dewolfe, V. G. (2008). Empirical models to predict the volumes of debris flows generated by recently burned basins in the western US. *Geomorphology*, 96(3-4):339–354.

Genevois, R., Berti, M., Ghirotti, M., Simoni, A., and Tecca, P. R. (1999). Debris flow monitoring and analysis in the Dolomitic Region (Upper Boite Valley, Italian Alps). *Thematic report, EC project, ENV4. CT96*, 253.

Glade, T. (2005). Linking debris-flow hazard assessments with geomorphology. *Geomorphology*, 66(1-4):189–213.

Goodings, D. (1984). Relationships for modelling water effects in geotechnical centrifuge models. In *Proceedings of the Symposium of The Application of Centrifuge Modelling to Geotechnical Design*, pages 1–23, Manchester, UK. Balkema, Rotterdam.

Hales, T. C. and Roering, J. J. (2005). Climate-controlled variations in scree production, Southern Alps, New Zealand. *Geology*, 33(9):701.

Hazen, A. (1892). Some physical properties of sands and gravels, with special reference to their use in filtration. *24th Annual Rep Massachusetts State Board of Health*, 34.

Hind, K. and Mcardell, B. W. (2010). Numerical modelling of debris-flows and mitigation structures at Matata, New Zealand. In Williams, A. and Chin, C., editors, *Geologically Active-Proceedings of the 11th Congress of the IAEG*. Taylor and Francis.

Hsu, K. J. (1975). Catastrophic debris streams (sturzstroms) generated by rockfalls. *Bulletin of the Geological Society of America*, 86(1):129.

Hsu, L., Kaitna, R., Dietrich, W. E., and Sklar, L. S. (2011). Boundary shear stress of granular flows. In Genevois, R., Hamilton, D., and Prestininzi, A., editors, *5th International Conference on Debris-Flow Hazards Mitigation: Mechanics, Prediction and Assessment*, page 331, Padua, Italy. Casa Editrice Università La Sapienza.

Hungr, O. (1995). A model for the runout analysis of rapid flow slides, debris flows, and avalanches. *Canadian Geotechnical Journal*, 32(4):610–623.

Hungr, O. (2003). Users manual of DANW Dynamic analysis of landslides.

Hungr, O. (2005). Classification and terminology. In Jakob, M. and Hungr, O., editors, *Debris-flow Hazards and Related Phenomena*, chapter 1. Springer-Praxis.

Hungr, O., Evans, S. G., Bovis, M. J., and Hutchinson, J. N. (2001). A review of the classification of landslides of the flow type. *Environmental and Engineering Geoscience*, 7(3):221.

Hungr, O. and McDougall, S. (2009). Two numerical models for landslide dynamic analysis. *Computers and Geosciences*, 35(5):978–992.

Hungr, O., McDougall, S., and Bovis, M.

Hungr, O., Morgan, G. C., and Kellerhals, P. (1984). Quantitative Analysis of Debris Torrent Hazards for Design of Remedial Measures. *Canadian Geotechnical Journal*, 21(4).

Hungr, O. and Morgenstern, N. R. (1984). Experiments on the flow behaviour of granular materials at high velocity in an open channel. *Geotechnique*, 34(3).

Hürlimann, M., Rickenmann, D., and Graf, C. (2003). Field and monitoring data of debris-flow events in the Swiss Alps. *Geology*, 175:161–175.

Hurlimann, M., Rickenmann, D., Medina, V., and Bateman, a. (2008). Evaluation of approaches to calculate debris-flow parameters for hazard assessment. *Engineering Geology*, 102(3-4):152–163.

Hutchinson, J. N. (1986). A sliding-consolidation model for flow slides. *Canadian Geotechnical Journal*, 23(2):115–126.

Hutchinson, J. N. (2003). The debris-flow rheology myth. In *Debris flow hazard mitigation: mechanics, prediction, and assessment*, pages 303–314. Millhouse.

Hutter, K., Svendsen, B., and Rickenmann, D. (1994). Debris flow modeling: A review. *Continuum Mechanics and Thermodynamics*, 8(1):1–35.

Hutter, K., Wang, Y., and Pudasaini, S. P. (2005). The Savage-Hutter avalanche model: how far can it be pushed? *Philosophical transactions. Series A, Mathematical, physical, and engineering sciences*, 363(1832):1507–28.

Ikeya, H. (1981). A method of designation for area in danger of debris flow. *Erosion and sediment transport in the Pacific Rim Steeplands, IAHS Publ*, 132:576–588.

Iverson, R. M. (1997). The physics of debris flows. *Reviews of Geophysics*, 35(3):245–296.

Iverson, R. M. (2005a). Debris-flow mechanics. In Jakob, M. and Hungr, O., editors, *Debris-flow hazards and related phenomena*, page 105. Springer.

Iverson, R. M. (2005b). Regulation of landslide motion by dilatancy and pore pressure feedback. *Journal of Geophysical Research*, 110(F2):1.

Iverson, R. M. and Denlinger, R. P. (2001). Flow of variably fluidized granular masses across three-dimensional terrain 1. Coulomb mixture theory. *Journal of Geophysical Research*, 106(B1):537.

Iverson, R. M., Reid, M. E., and LaHusen, R. G. (1997). Debris-flow mobilization from landslides 1. *Annual Reviews in Earth and Planetary Sciences*, 25(1):85–138.

Iverson, R. M., Reid, M. E., Logan, M., LaHusen, R. G., Godt, J. W., and Griswold, J. P. (2011). Positive feedback and momentum growth during debris-flow entrainment of wet bed sediment. *Nature Geoscience*, 4(2):116–121.

Jakob, M. (2005). A size classification for debris flows. *Engineering Geology*, 79(3-4):151–161.

Jakob, M., Anderson, D., Fuller, T., Hungr, O., and Ayotte, D. (2000). An unusually large debris flow at Hummingbird Creek, Mara Lake. *British Columbia. Canadian Geotechnical Journal*, 37(5):1109–1125.

Jakob, M., Bovis, M., and Oden, M. (2005). The significance of channel recharge rates for estimating debris-flow magnitude and frequency. *Earth Surface Processes and Landforms*, 30(6):755–766.

Jakob, M., Hungr, O., and Thomson, B. (1997). Two debris flows with anomalously high magnitude. *Proceedings of the 1st International Conference on Debris Flow Hazards Mitigation: Mechanics, Prediction, and Assessment, San Francisco, Calif. Edited by C.-L. Chen. American Society of Civil Engineers (ASCE)*, pages 382–394.

Jakob, M. and Jordan, P. (2001). Design flood estimates in mountain streams: the need for a geomorphic approach. *Canadian Journal of Civil Engineering*, 28(3):425–439.

Johnson, A. (1970). *Physical processes in geology: a method for interpretation of natural phenomena; intrusions in igneous rocks, fractures, and folds, flow of debris and ice.* Freeman, Cooper.

Jordan, P. (1994). *Debris flows in Southern Coast Mountains, British Columbia: Dynamic Behavior and Physical Properties.* Phd, University of British Columbia, Vancouver, Canada.

Kaitna, R., Hsu, L., Rickenmann, D., and Dietrich, W. E. (2011). On the development of an unsaturated front of of debris flows. In Genevois, R., Hamilton, D., and Prestininzi, A., editors, *5th International Conference on Debris-Flow Hazards Mitigation: Mechanics, Prediction and Assessment*, page 351, Padua, Italy. Sapienza University of Rome.

King, J. (1996). Tsing Shan debris flow. Special Report SPR 6/96, Hong Kong Geotechnical Office, Hong Kong.

Kutter, B. L. (1995). Recent advances in centrfuge modeling of seismic shaking. In *3rd International Conference on Recent Adavances in Geotechnical Earthquake Engineering and Soil Dynamics*, pages 927–941, St. Louis. Missouri.

Laigle, D. and Coussot, P. (1997). Numerical modeling of mudflows. *Journal of hydraulic engineering*, 123:617.

Lancaster, S. T., Hayes, S. K., and Grant, G. E. (2003). Effects of wood on debris flow runout in small mountain watersheds. *Water Resources Research*, 39(6):1168.

Leopold, L. B., Wolman, M. G., and Miller, J. P. (1995). *Fluvial processes in geomorphology.* Dover Pubns.

Lopez, J. L., Perez, D., and Garcia, R. (2003). Hydrologic and geomorphologic evaluation of the 1999 debris-flow event in Venezuela. In *Proceedings of the Third International Conference on Debris Flow Hazard Mitigation: Mechanics, Prediction, and Assessment, Davos. Millpress, Rotterdam*, pages 989–1000.

Lowe, D. R. (1976). Grain flow and grain flow deposits. *Journal of Sedimentary Research*, 46(1):188.

Major, J. (2000). Gravity-driven consolidation of granular slurries–Implications for debris-flow deposition and deposit characteristics. *SEPM Journal of Sedimentary Research*, Vol. 70 (2:64–83.

Marchi, L. and DAgostino, V. (2004). Estimation of debris-flow magnitude in the Eastern Italian Alps. *Earth Surface Processes and Landforms*, 29(2):207–220.

May, C. L. and Gresswell, R. E. (2004). Spatial and temporal patterns of debris-flow deposition in the Oregon Coast Range, USA. *Geomorphology*, 57(3-4):135–149.

McArdell, B. W., Zanuttigh, B., Lamberti, A., and Rickenmann, D. (2003). Systematic comparison of debris-flow laws at the Illgraben torrent, Switzerland. In Davos, S., editor, *Proceedings of the 3rd International Conference on debris flow hazards mitigation*, pages 647–657. Rotterdam.

McCoy, S. W., Kean, J. W., Coe, J. a., Staley, D. M., Wasklewicz, T. a., and Tucker, G. E. (2010). Evolution of a natural debris flow: In situ measurements of flow dynamics, video imagery, and terrestrial laser scanning. *Geology*, 38(8):735–738.

Mcdougall, S. (2006). *A new continuum dynamic model for the analysis of extremely rapid landslide motion across complex 3D terrain*. Phd, University of British Columbia, Canada.

Mckinnon, M. (2010). *Landslide Runout-statistical analysis of physical characteristics and model parameters*. Phd, The University of British Columbia.

McSaveney, M. J., Beetham, R. D., and Leonard, G. S. (2005). The 18 May 2005 debris flow disaster at Matata: Causes and mitigation suggestions. *Institute of Geological and Nuclear Sciences (GNS), Lower Hutt, New Zealand*.

McSaveney, M. J. and Davies, T. R. H. (2005). Engineering for debris flows in New Zealand. In Jakob, M. and Hungr, O., editors, *Debris-flow Hazards and Related Phenomena*, chapter 25. Springer-Praxis.

McSaveney, M. J. and Glassey, P. J. (2002). The fatal Cleft Peak debris Flow of 3 January, 2002, Upper Rees Valey, West Otago.

Medina, V., Bateman, a., and Hurlimann, M. (2008). A 2D finite volume model for debris flow and its application to events occurred in the Eastern Pyrenees. *International Journal of Sediment Research*, 23(4):348–360.

Medina, V., Hürlimann, M., and Bateman, A. (2007). Application of FLATModel, a 2D finite volume code, to debris flows in the northeastern part of the Iberian Peninsula. *Landslides*, 5(1):127–142.

Mergili, M., Schneider, D., Worni, R., and Schneider, J. (2011). Glacial lake outburst floods in the Pamir of Tajikistan: challenges in prediction and modelling. In *5th International Conference on Debris-Flow Hazards Mitigation: Mechanics, Prediction and Assessment, University of Padova, Italy*, pages 14–17.

Miyazawa, N. (2001). Intermittent Flow Occurred at Debris Flow Front. In *Proceedings of the Congress-International Association for Hydraulic Research*, pages 344–351.

Munson, B. R., Young, D. F., and Okiishi, T. H. (1998). *Fundamentals of fluid mechanics*, volume 3. Wiley York, NY, USA.

Naef, D., Rickenmann, D., Rutschmann, P., and McArdell, B. W. (2006). Comparison of flow resistance relations for debris flows using a one-dimensional finite element simulation model. *Natural Hazards and Earth System Science*, 6(1):155–165.

Nedderman, R. M. (1992). *Statics and kinematics of granular materials*. Cambridge University Press, Cambridge, U.K.

Okano, K., Suwa, H., and Kanno, T. (2011). Characterization of debris flows by rainstorm condition at a torrent on the Mount Yakedake volcano, Japan. *Geomorphology*.

Okuda, S. and Suwa, H. (1984). Some Relationships Between Debris Flow Motion and Micro-Topography for the Kamikamihori Fan, North Japan Alps. In *Catchment Experiments in Fluvial Geomorphology. Geo Books, Norwich England. 1984. p 447-464, 8 fig, 2 tab, 8 ref.* Geo Books, Norwich England.

Paudel, B. P. and Law, K. T. (2006). Case histories of landslide induced gravitative debris flow.

Petley, D. N. (2012). Landslides and engineered slopes-Protecting society through improved understanding. In Eberhardt, E., F., F., Turner, K., and Leroueil, S., editors, *Proceedings of the 11th International Symposium on Landslides and 2nd North American Symposium on Landslides*, number September 2002, pages 3–13. CRC Press.

Pierson, T. C. (1980). Erosion and deposition by debris flows at Mt. Thomas, North Canterbury, New Zealand. *Earth Surface Processes*, 5:227–247.

Pierson, T. C. (1982). Classification and hydrological characteristics of scree slope deposits in the Northern Craigieburn Range, New Zealand. *Journal of Hydrology (NZ)*, 21(no. 1):34–59.

Pierson, T. C. (1986). Flow behaviour of channelized debris flows, Mount St. Helens, Washington. *Hillslope processes*, (1-4):269–296.

Pierson, T. C. (1995). Flow characteristics of large eruption-triggered debris flows at snow-clad volcanoes: constraints for debris-flow models. *Journal of volcanology and geothermal research*, 66(1-4):283–294.

Pierson, T. C. (2005). Hyperconcentrated flow-transitional process between water flow and debris flow. *Debris-flow Hazards and Related Phenomena*, pages 159–202.

Pierson, T. C. and Scott, K. M. (1985). Debris flow to hyperconcentrated streamflow. *Water resources research*, 21(10):1511–1524.

Pirulli, M. and Sorbino, G. (2008). Assessing potential debris flow runout: a comparison of two simulation models. *Natural Hazards and Earth System Science*, 8(4):961–971.

Poisel, R., Preh, A., and Hungr, O. (2008). Run out of landslides continuum mechanics versus discontinuum mechanics models. *Geomechanik und Tunnelbau*, 1(5):358–366.

Prochaska, a., Santi, P., Higgins, J., and Cannon, S. (2008a). Debris-flow runout predictions based on the average channel slope (ACS). *Engineering Geology*, 98(1-2):29–40.

Prochaska, A. B., Santi, P. M., Higgins, J. D., and Cannon, S. H. (2008b). A study of methods to estimate debris flow velocity. *Landslides*, 5(4):431–444.

Rickenmann, D. (1999). Empirical Relationships for Debris Flows. *Natural Hazards*, (19):47–77.

Rickenmann, D. (2005). Runout prediction methods. In Hungr, O. and Jakob, M., editors, *Debris-flow Hazards and Related Phenomena*, chapter 13, pages 305–324. Springer-Praxis.

Rombi, J., Pooley, E., and Bowman, E. (2006). Factors influencing granular debris flow behaviour: an experimental investigation. In *6th International Conference on Physical Modelling in Geotechnics.*, pages 379–384, Hong Kong.

Santi, P. M., Dewolfe, V. G., Higgins, J. D., Cannon, S. H., and Gartner, J. E. (2008). Sources of debris flow material in burned areas. *Geomorphology*, 96(3-4):310–321.

Santolo, A. S. and Evangelista, A. (2008). Calibration of a rheological model for debris flow hazard mitigation in the Campania region. *Analysis*, pages 913–919.

Sassa, K. (1989). Geotechnical model for the motion of landslides. In *Proc 5th International Symposium on Landslides*, volume 26, pages 37–55, Lausanne. Balkema.

Sassa, K., Fukuoka, H., Wang, G., and Ishikawa, N. (2004). Undrained dynamic-loading ring-shear apparatus and its application to landslide dynamics. *Landslides*, 1(1):7–19.

Sassa, K. and Hui, W. (2005). Mechanism of landslide-triggered debris flows: Liquefaction phenomena due to the undrained loading of torrent deposits. In Hungr, O. and Jakob, M., editors, *Debris-flow Hazards and Related Phenomena*, chapter 5. Springer-Praxis.

Savage, S. B. and Hutter, K. (1989). The motion of a finite mass of granular material down a rough incline. *Journal of Fluid Mechanics*, 199(1):177–215.

Savage, S. B. and Lun, C. K. K. (1988). Particle size segregation in inclined chute flow of dry cohesionless granular solids. *Journal of Fluid Mechanics*, 189(1):311–335.

Schatzmann, M. (2005). *Rheometry for large particle fluids and debris flows*. PhD thesis, Swiss Federal Institute of Technology.

Scheidegger, A. E. (1973). On the prediction of the reach and velocity of catastrophic landslides. *Rock Mechanics and Rock Engineering*, 5(4):231–236.

Scheuner, T. (2007). *Modellierung von Murgangereignissen mit RAMMS und Vergleich durch GIS-basiertes Fliessmodell*. PhD thesis, Institut der Uneversitat Zurich (GIUZ).

Schlunegger, F., Badoux, A., Mcardell, B. W., Gwerder, C., Schnydrig, D., Rieke-zapp, D., and Molnar, P. (2009). Limits of sediment transfer in an alpine debris-flow catchment. *Quaternary Science Reviews*, 28(11-12):1097–1105.

Schofield, A. N. (1980). Cambridge geotechnical centrifuge operations. *Geotechnique*, 30(3):227–268.

Slaymaker, O. (1988). The distinctive attributes of debris torrents. *Hydrological Sciences Journal*, 33(6):567–573.

Springman, S., Laue, J., Boyle, R., White, J., and Zweidler, A. (2001). The ETH Zurich geotechnical drum centrifuge. *International Journal of Physical Modelling in Geotechnics*, 1(1):59–70.

Stead, D., Eberhardt, E., and Coggan, J. S. (2006). Developments in the characterization of complex rock slope deformation and failure using numerical modelling techniques. *Engineering Geology*, 83(1):217–235.

Stewart, D. P., Chen, Y. R., and Kutter, B. L. (1998). Experience with the use of methylcellulose as a viscous pore fluid in centrifuge models. *ASTM geotechnical testing journal*, 21(4):365–369.

Stock, J. and Dietrich, W. E. (2003). Valley incision by debris flows: Evidence of a topographic signature. *Water Resources Research*, 39(4):1089.

Stock, J. D. and Dietrich, W. E. (2006). Erosion of steepland valleys by debris flows. *Bulletin of the Geological Society of America*, 118(9-10):1125.

Takahashi, T. (1978). Mechanical characteristics of debris flow. *Journal of the Hydraulics Division*, 104(8):1153–1169.

Takahashi, T. (1981). Debris Flow. *Annual Reviews in Fluid Mechanics*, 13(1):57–77.

Takahashi, T. (1991). Debris flow: Rotterdam. *Netherlands, Balkema*.

Takahashi, T. (2007). *Debris flow: mechanics, prediction and countermeasures*. Routledge.

Takahashi, T. and Yoshida, H. (1979). Study on the deposition of debris flows. *Annual Report of the Disaster Prevention Institute*, (22):315–328.

Taylor, R. N. (1995). Centrifuges in modelling: principles and scale effects. In Taylor, R. N., editor, *Geotechnical Centrifuge Technology*, chapter 2, pages 19–33. Taylor and Francis, London, 1 edition.

Thompson, C. (2011). HIRDS.V3: High Intensity Rainfall Design System: The method underpinning the development of regional analysis of extreme rainfalls in New Zealand. Technical report, National Institute of Weather and Atmosphere.

Tommasi, P., Campedel, P., Consorti, C., and Ribacchi, R. (2008). A discontinuous approach to the numerical modelling of rock avalanches. *Rock Mechanics and Rock Engineering*, 41(1):37–58.

Vallance, J. W. and Scott, K. M. (1997). The Osceola Mudflow from Mount Rainier- Sedimentology and hazard implications of a huge clay-rich debris flow. *Holocene*, (2):143–163.

Wang, G. and Sassa, K. (2003). Pore-pressure generation and movement of rainfall-induced landslides: effects of grain size and fine-particle content. *Engineering Geology*, 69(1-2):109–125.

Wang, G., Sassa, K., and Fukuoka, H. (2003). Downslope volume enlargement of a debris slideñdebris flow in the 1999 Hiroshima, Japan, rainstorm. *Engineering Geology*, 69(3-4):309–330.

Whitehouse, I. E. and McSaveney, M. J. (1983). Diachronous talus surfaces in the Southern Alps, New Zealand, and their implications to talus accumulation. *Arctic and alpine research*, 15(1):53–64.

Wieczorek, G. F. and Glade, T. (2005). Climatic factors influencing occurrence of debris flows. In Jakob, M. and Hungr, O., editors, *Debris-flow hazards and related phenomena*, pages 325–362. Springer-Praxis.

Williams, P. W. (2004). The evolution of the mountains of New Zealand. *Mountain Geomorphology. London, Arnold*, pages 89–106.

Wilson, R. C. and Wieczorek, G. F. (1995). Rainfall thresholds for the initiation of debris flows at La Honda, California. *Environmental and Engineering Geoscience*, 1(1):11–27.

Wong, H. N., Ho, K. K. S., and Chan, Y. C. (1997). Assessment of consequence of landslides. In *Proceedings of the Workshop on Landslide Risk Assessment*, pages 111–149.

Wood, D. (2005). Centrifuge modelling. In *Geotechnical Modelling*, chapter 6, pages 269–308. Spoon Press, London.

Zhou, G. G. D. and Ng, C. W. W. (2010). Dimensional analysis of natural debris flows. *Canadian Geotechnical Journal*, 47(7):719–729.

Zimmermann, A., Church, M., and Hassan, M. A. (2010). Step-pool stability: Testing the jammed state hypothesis. *Journal of Geophysical Research*, 115(F2):F02008.

Zimmermann, M. (1990). Debris flows 1987 in Switzerland: geomorphological and meteorological aspects. *AHS Hydrology of Mountainous Regions*, 2(194):387–393.

Appendices

A. Additional centrifuge data

Masses left on drum

Table A.1.: Mass of material left in depositional area for centrifuge tests.

Test Code	Mass of material left on drum (g)
T9	416
T10	1101
T7	1573
T12	1023
T22	967
T15	1856*
T14	1142*
T20	2229*
T23	1664*
T11	1343*
T21	no data
T24	662

*Wet weight (glycerine flows could not be oven dried).

Additional velocity profiles

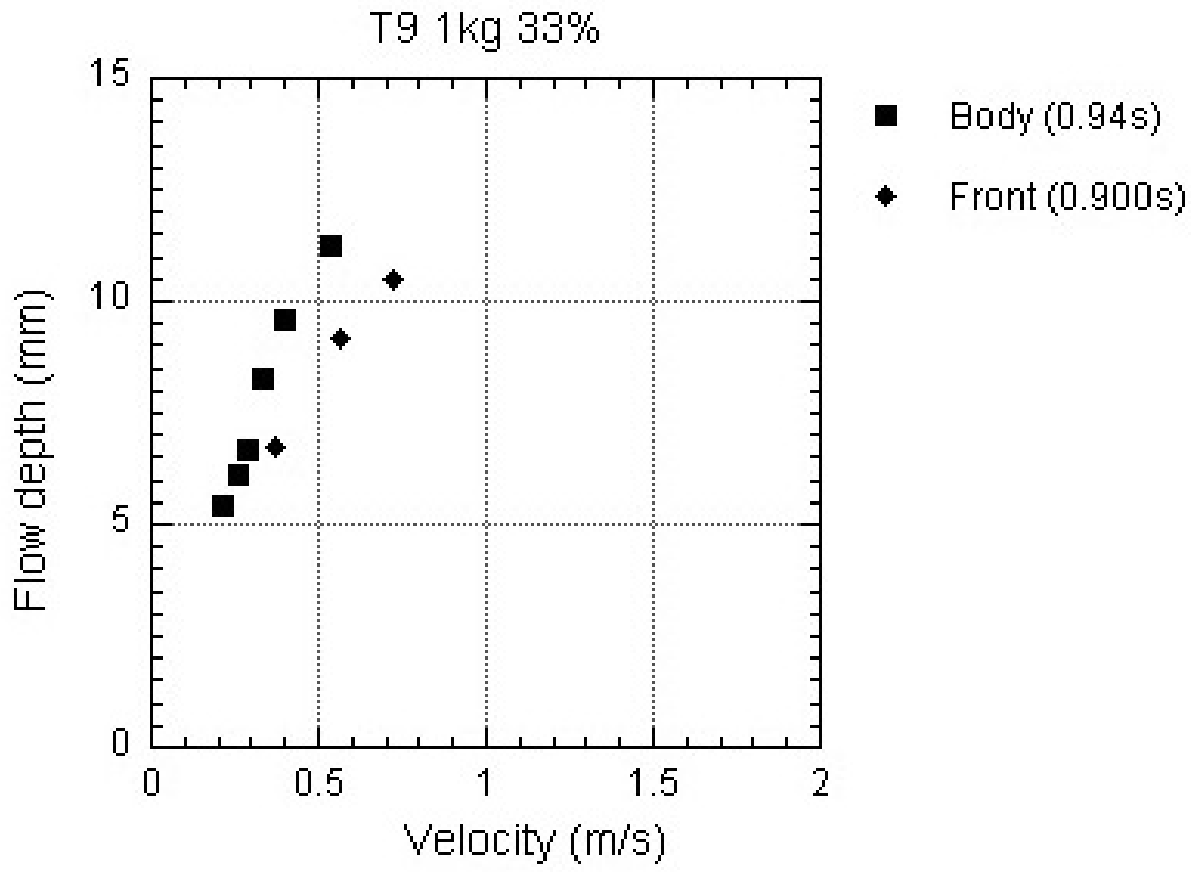

Figure A.1.: Velocity profile for test T9 (1 kg methyl cellulose, 33% moisture content).

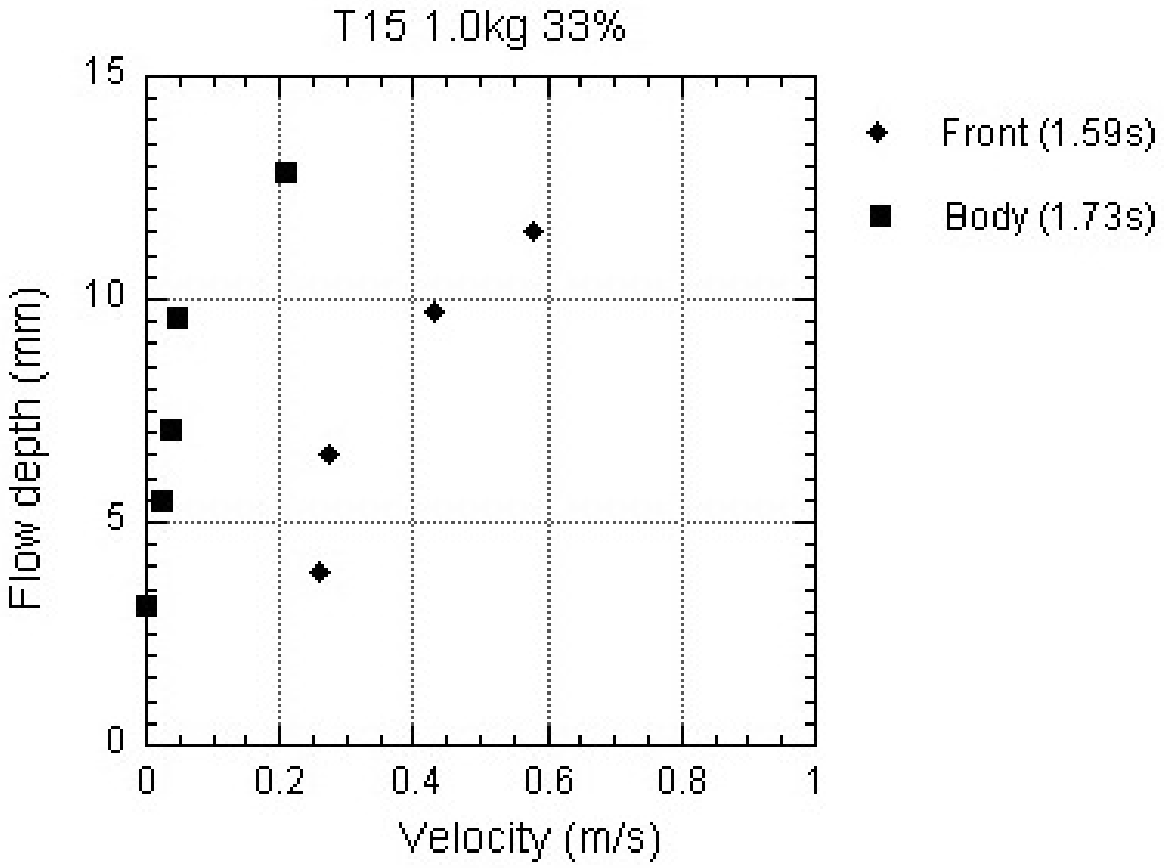

Figure A.2.: Velocity profile for test T15 (1 kg glycerine, 33% moisture content).

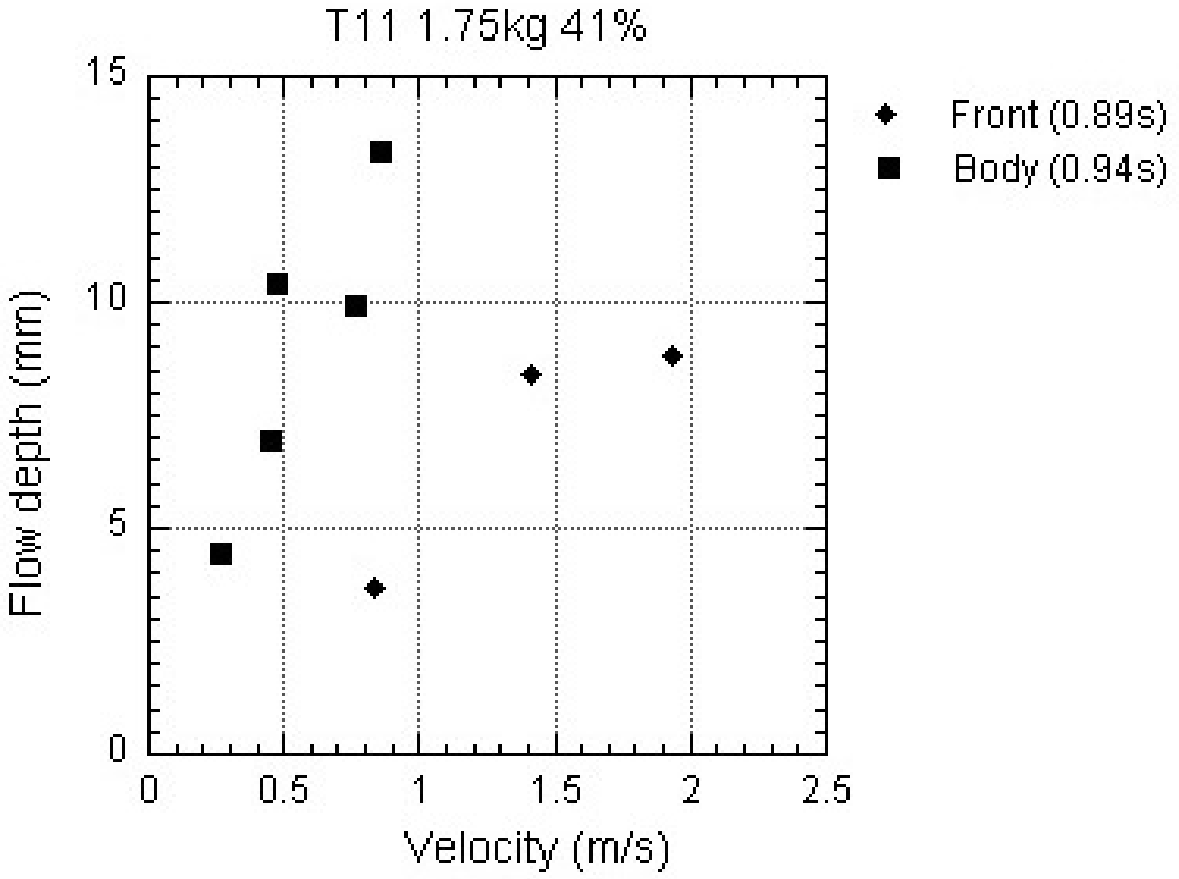

Figure A.3.: Velocity profile for test T11 (1.75 kg glycerine, 41% moisture content)

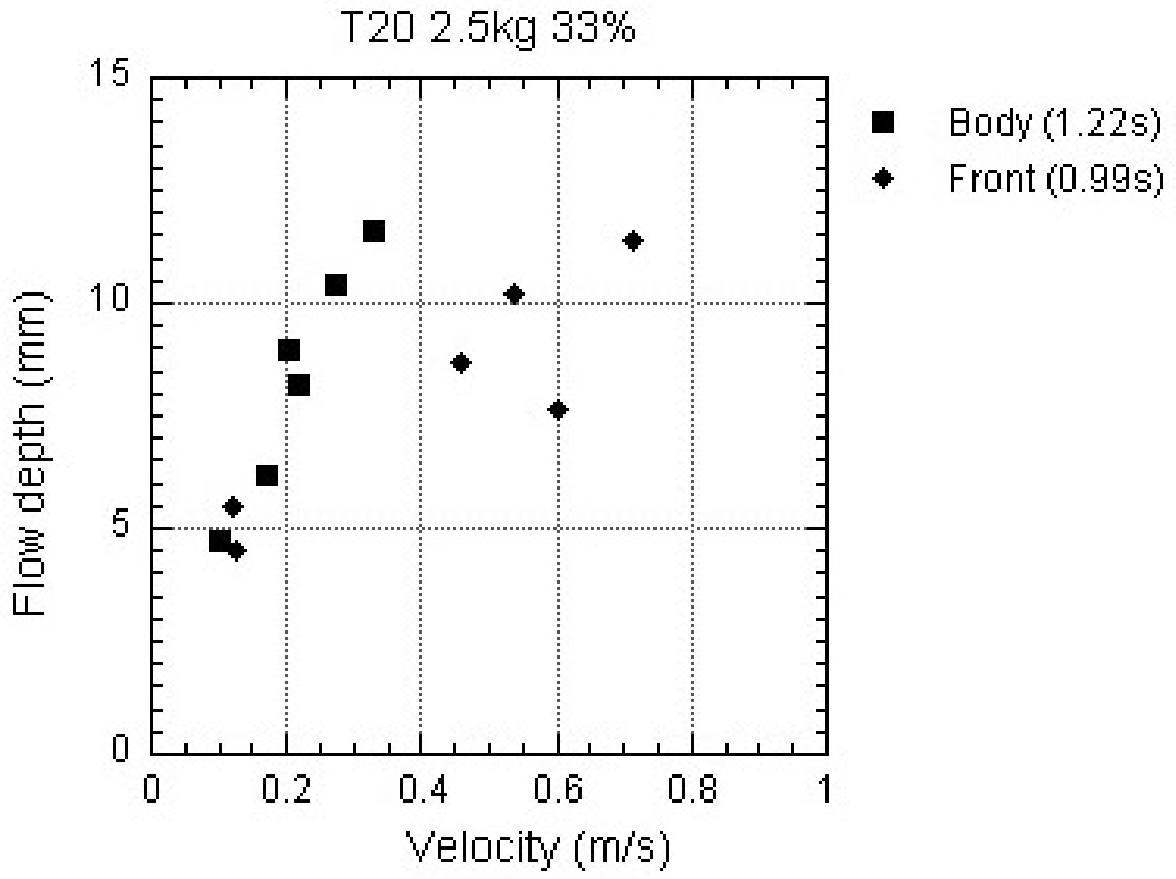

Figure A.4.: Velocity profile for test T20 (2.5 kg glycerine, 33% moisture content).

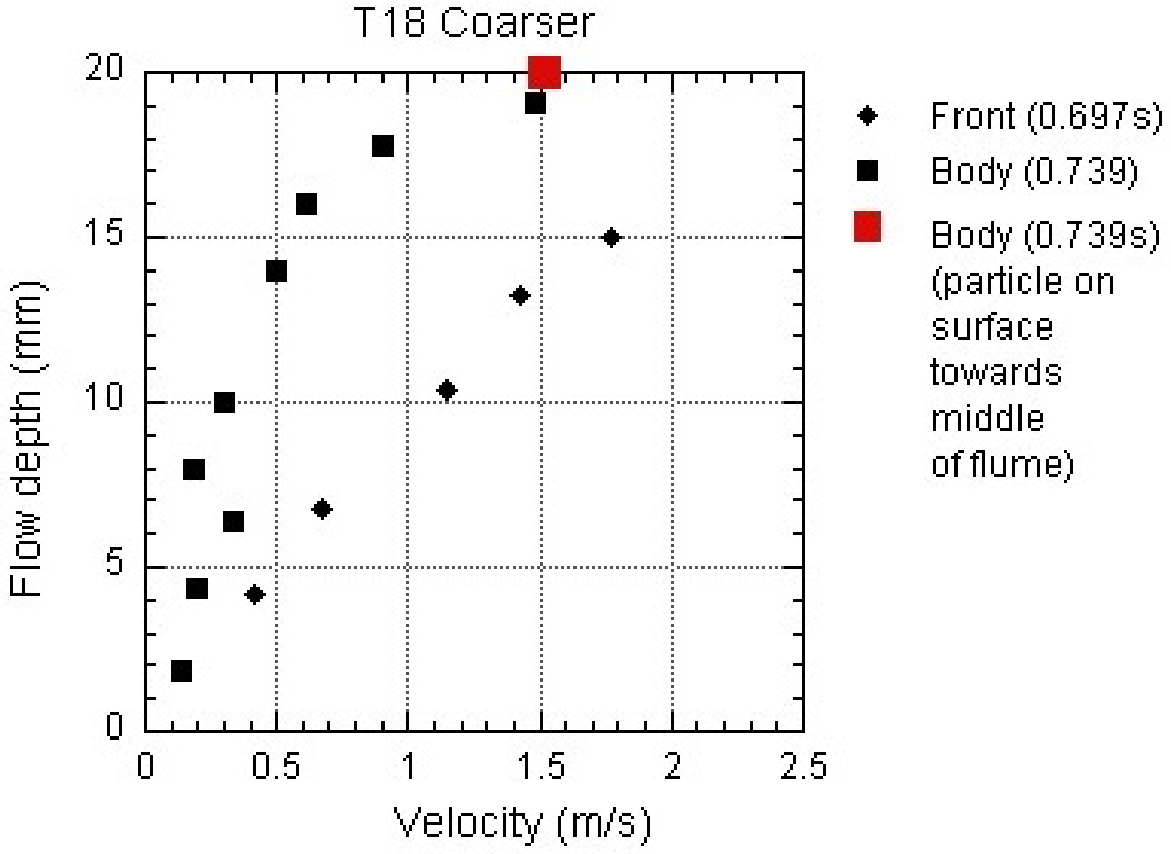

Figure A.5.: Velocity profile for test T18 (erodible bed test with coarser bed).

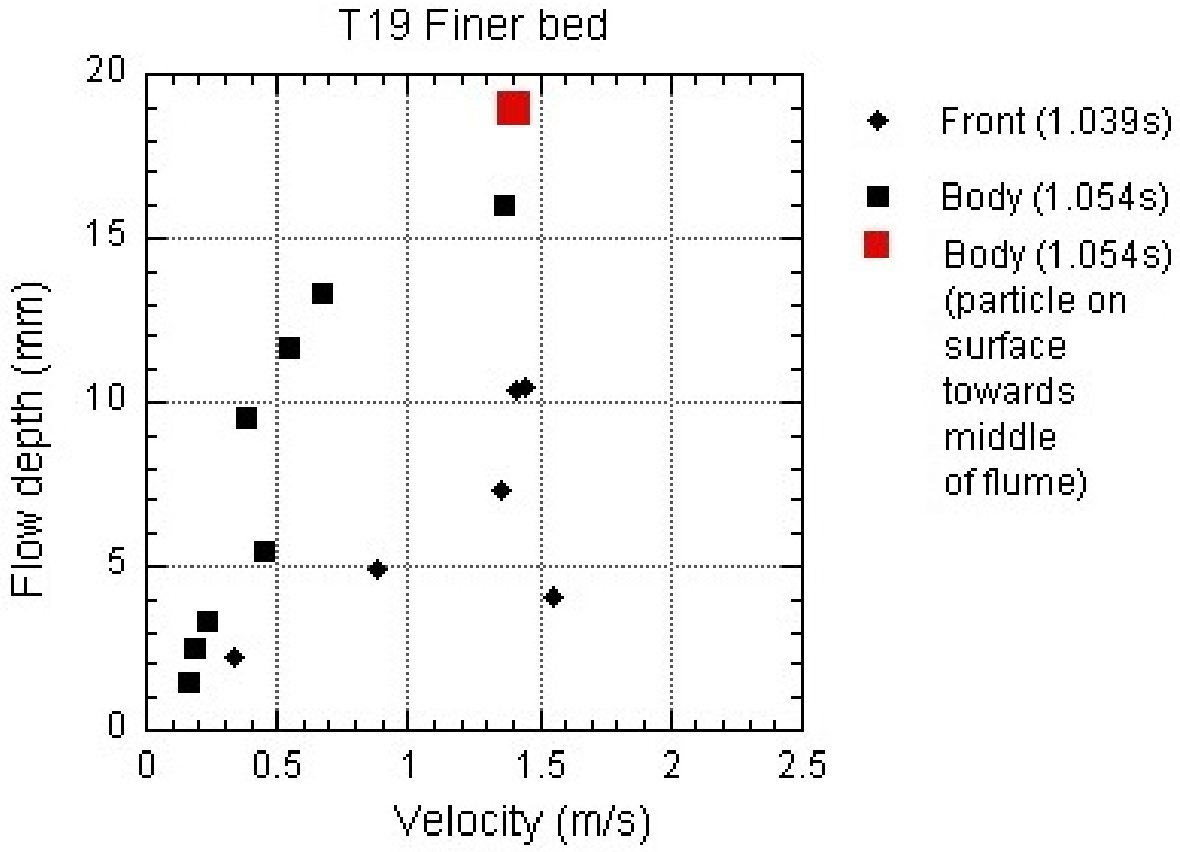

Figure A.6.: Velocity profile for test T19 (erodible bed test with finer bed).

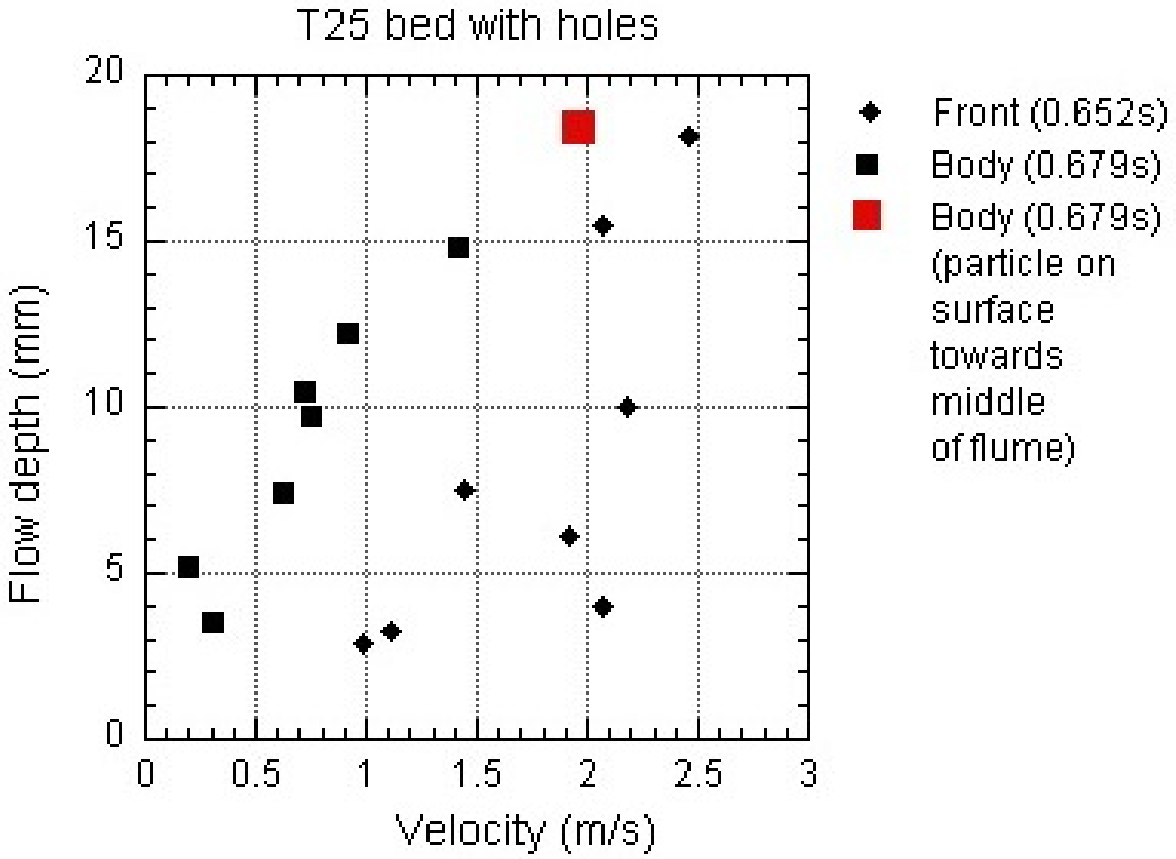

Figure A.7.: Velocity profile for test T25 (erodible bed test with bed prepared with holes).

B. Additional Field data

B.1. Reach Pro-forma

Table B.1.: Reach Proforma used in second field season.

DF Data	DFID		Reach		p.		Name		Date	
Reach data	WP start		Az		Slope		Length		Behavior	
Widths	Gully		Trace		Deposition/type		Erosion		Deposition	
Depths	Channel/scarp		Channelized by?		Original surface		Flow		gully	
eroded depths	total		during event		post-event		comments			
Materials	Dep type		Bed type		availability?		comment			
	% b, c, g, f		% b, c, g, f							
Volumes	Deposition		Lower bound		Upper bound		comments			
Confinement type										
Other factors/ Sketches										
Point sources for sediment	w,d, etc						Pics			

B.2. Additional UBCDflow plots

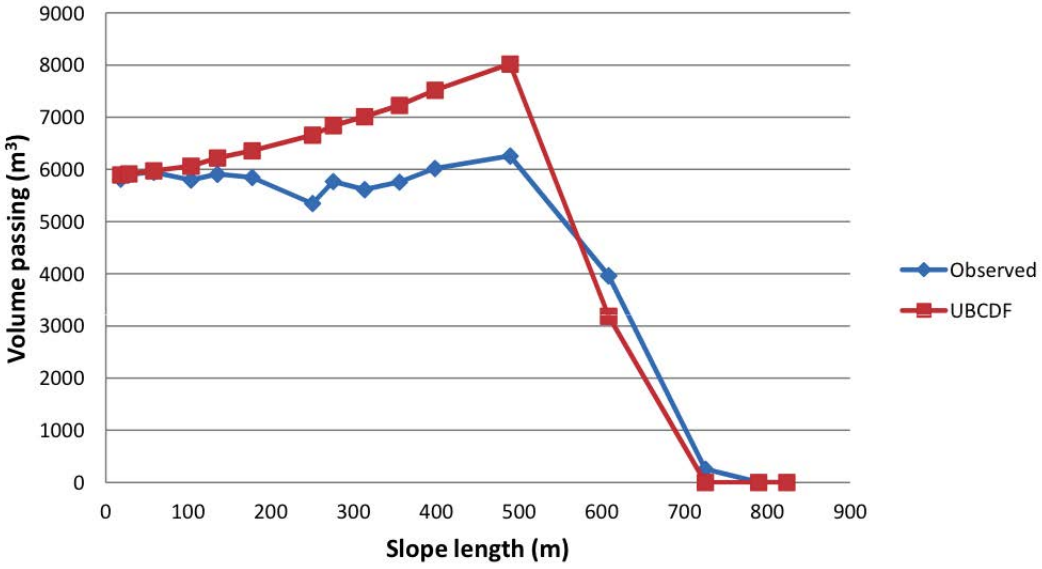

Figure B.1.: Plot of volume passing for OR1. The value for observed is based on the volume passing calculations (discussed in Section 5.4.2).

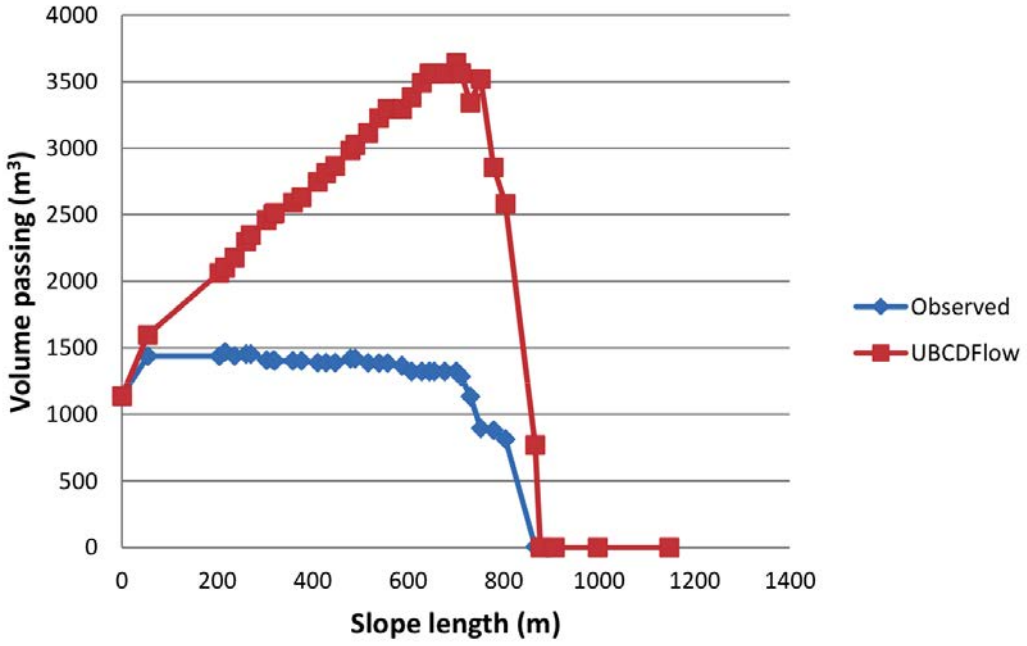

Figure B.2.: Plot of volume passing for OR2. The value for observed is based on the volume passing calculations (discussed in Section 5.4.2).

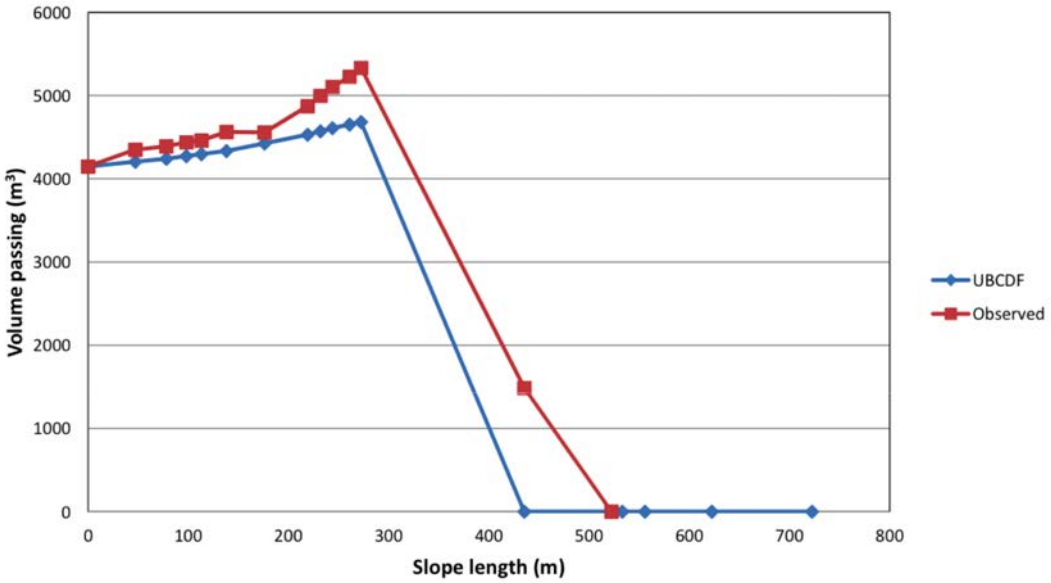

Figure B.3.: Plot of volume passing for OR3. The value for observed is based on the volume passing calculations (discussed in Section 5.4.2).

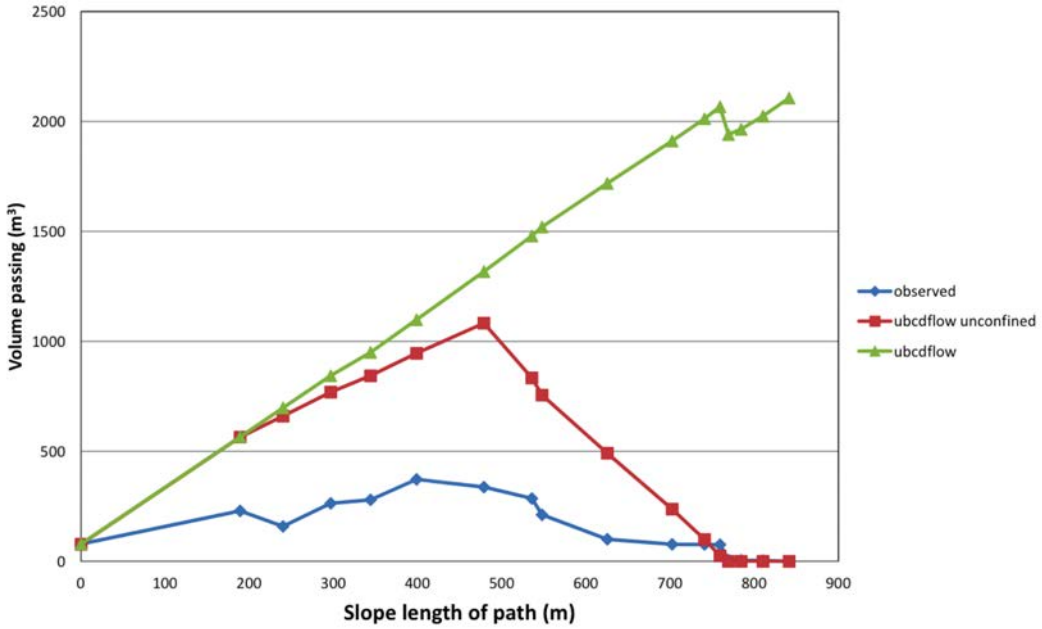

Figure B.4.: Plot of volume passing for C1. The value for observed is based on the volume passing calculations (discussed in Section 5.4.2).

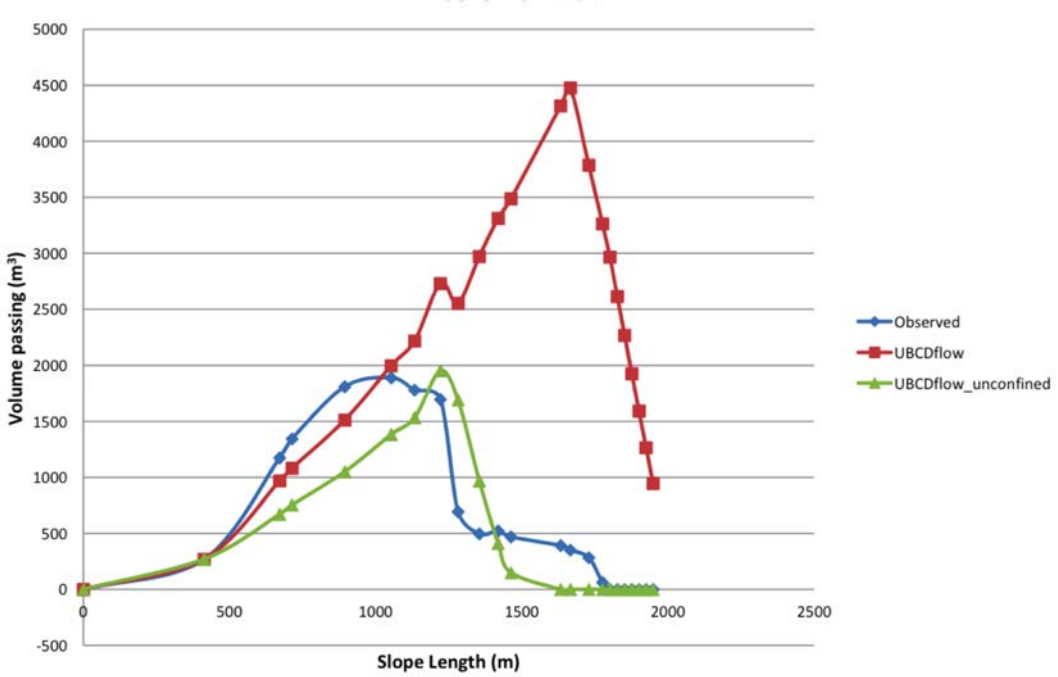

Figure B.5.: Plot of volume passing for C3. The value for observed is based on the volume passing calculations (discussed in Section 5.4.2).

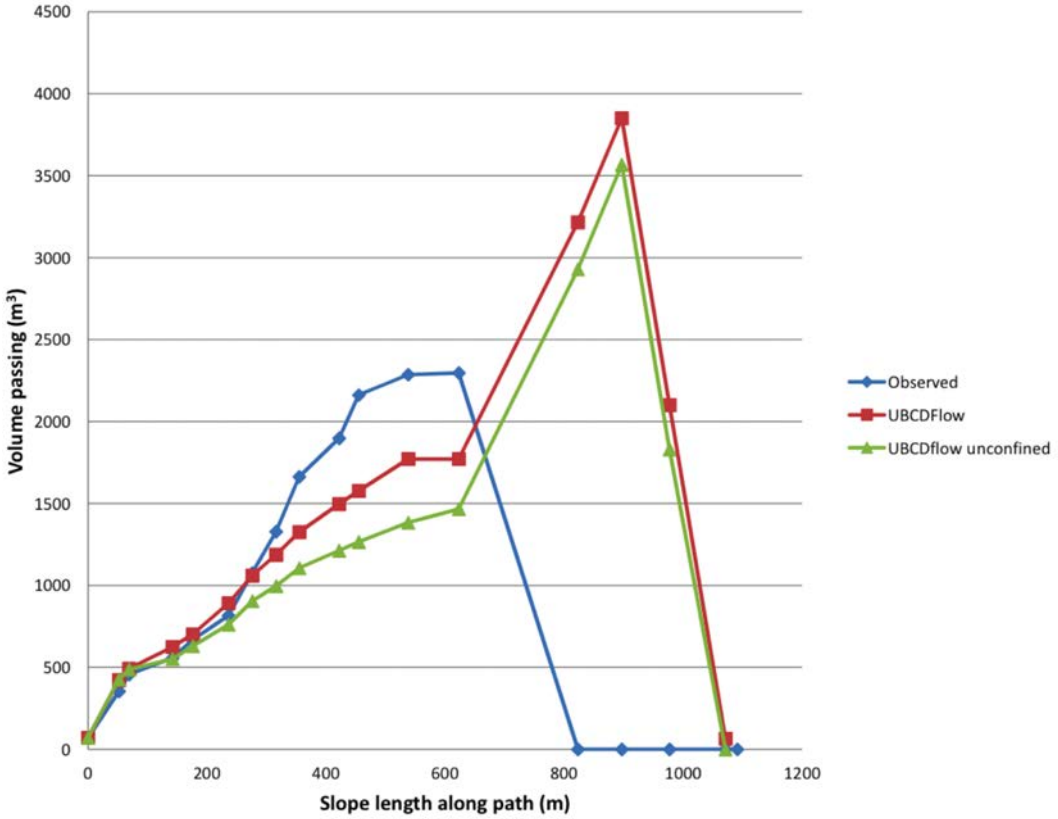

Figure B.6.: Plot of volume passing for C6. The value for observed is based on the volume passing calculations (discussed in Section 5.4.2).

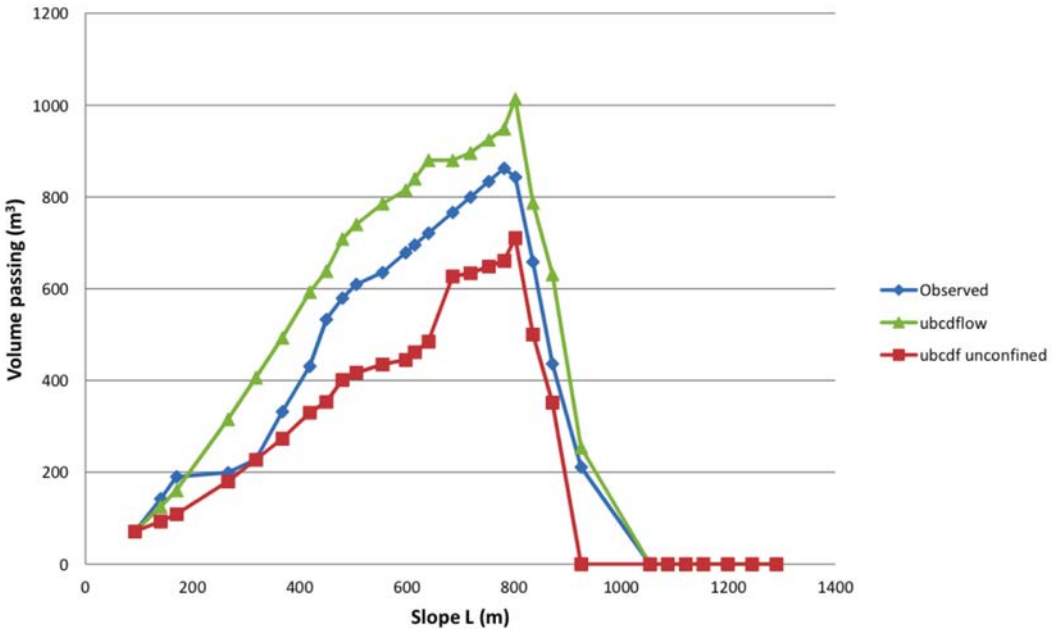

Figure B.7.: Plot of volume passing for C7. The value for observed is based on the volume passing calculations (discussed in Section 5.4.2).

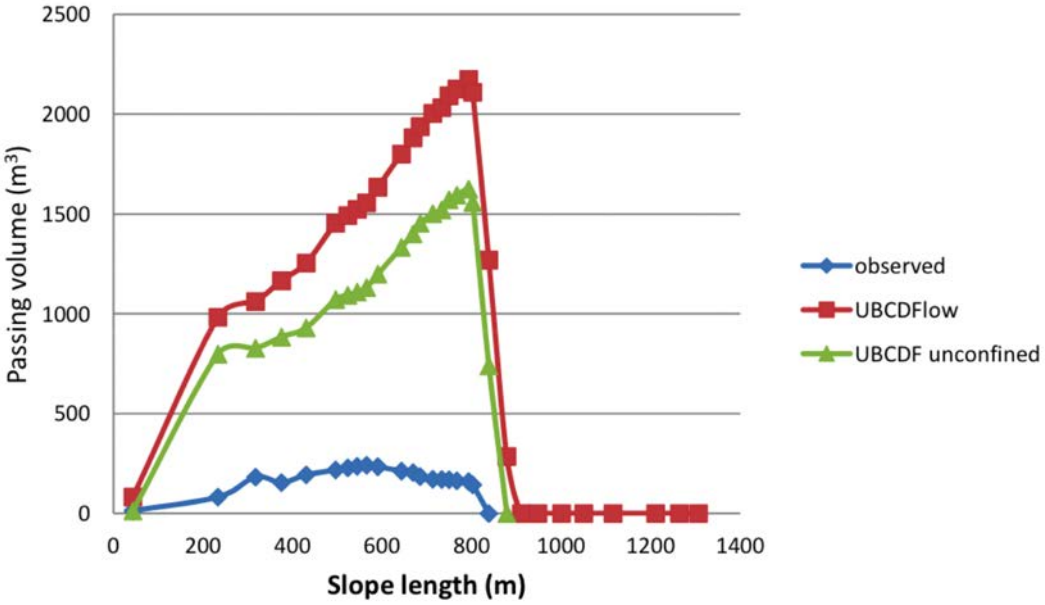

Figure B.8.: Plot of volume passing for C11. The value for observed is based on the volume passing calculations (discussed in Section 5.4.2).

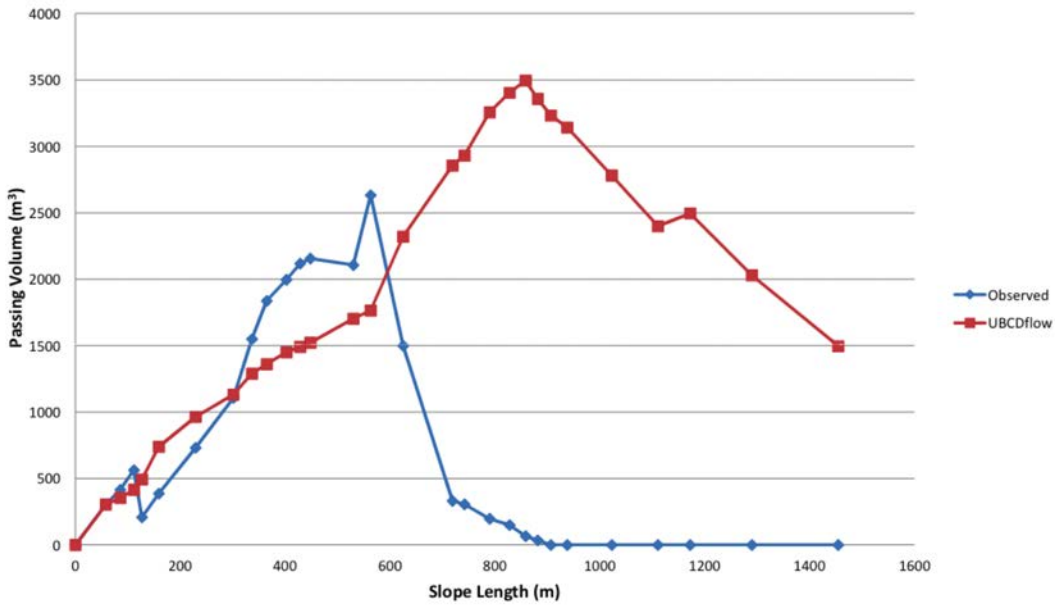

Figure B.9.: Plot of volume passing for C12. The value for observed is based on the volume passing calculations (discussed in Section 5.4.2).

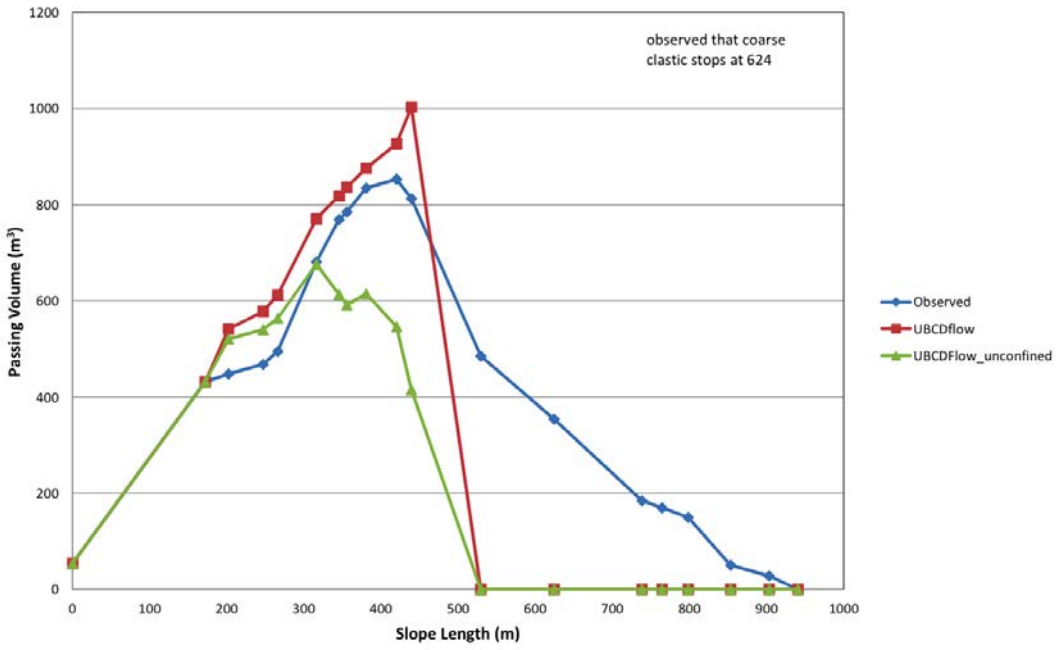

Figure B.10.: Plot of volume passing for C13. The value for observed is based on the volume passing calculations (discussed in Section 5.4.2).

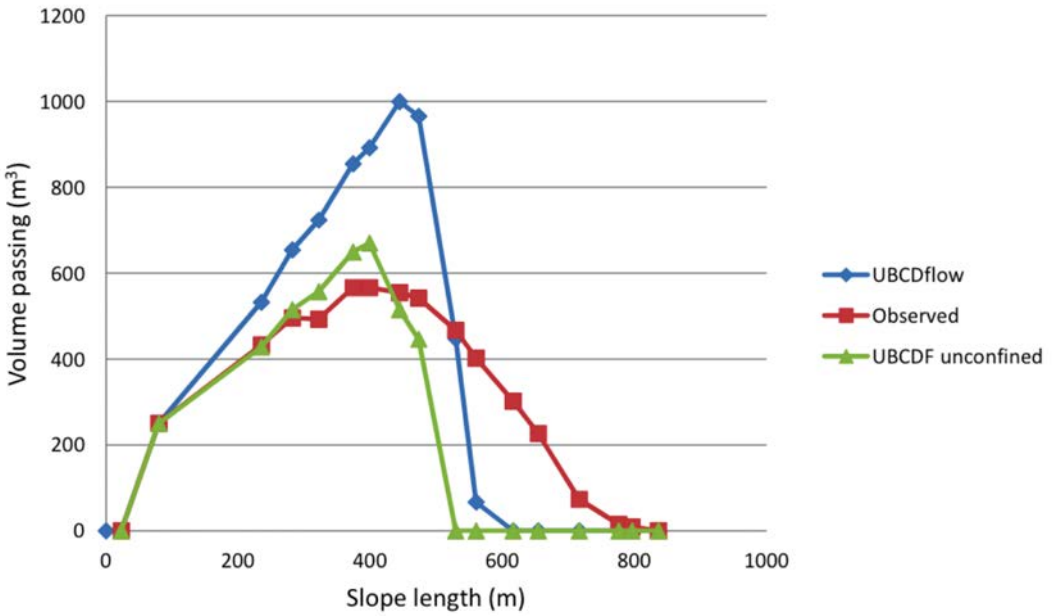

Figure B.11.: Plot of volume passing for C14. The value for observed is based on the volume passing calculations (discussed in Section 5.4.2).

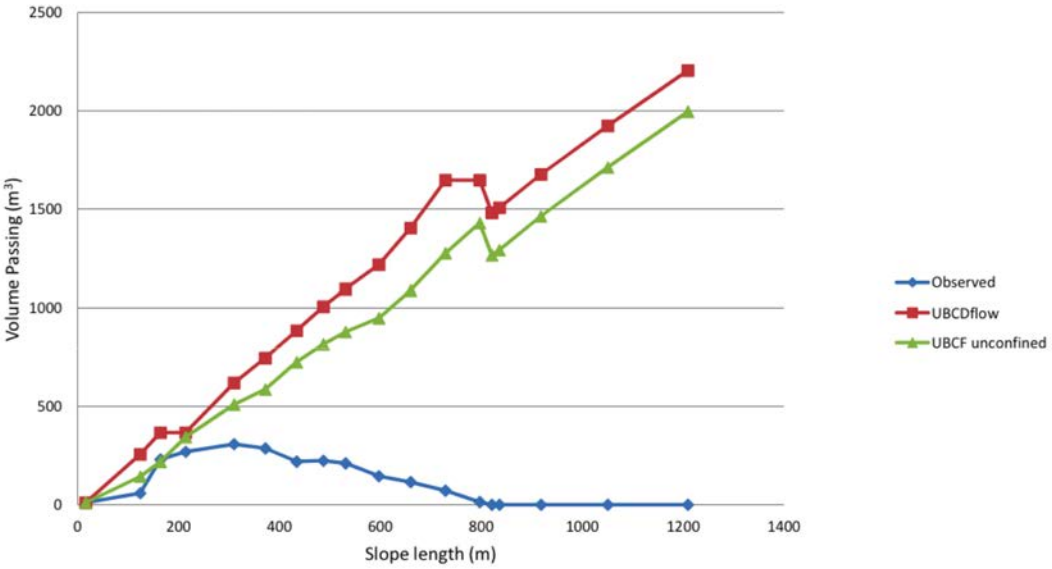

Figure B.12.: Plot of volume passing for BH1. The value for observed is based on the volume passing calculations (discussed in Section 5.4.2).

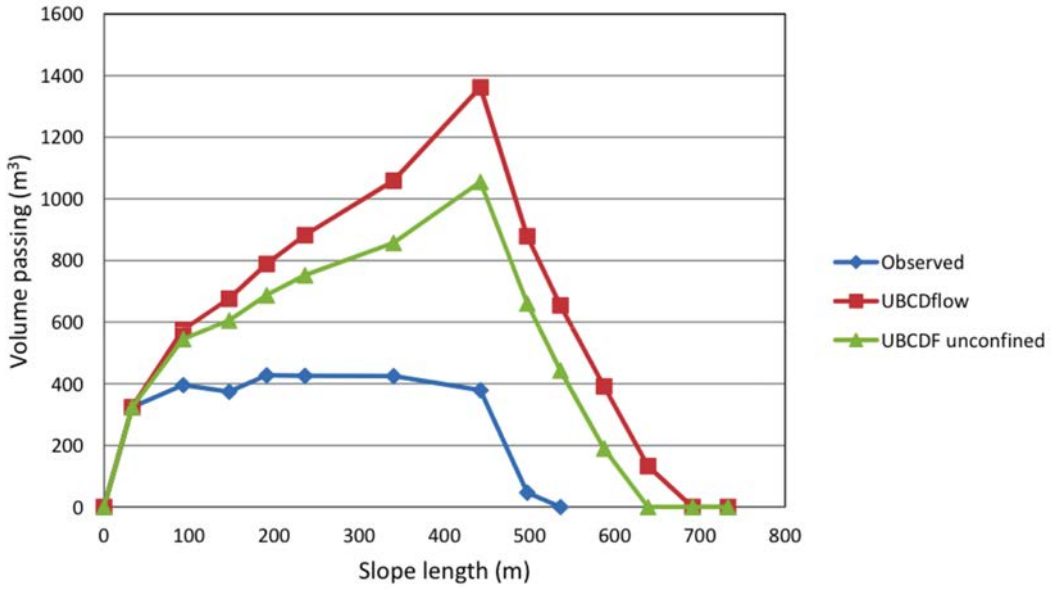

Figure B.13.: Plot of volume passing for BH2. The value for observed is based on the volume passing calculations (discussed in Section 5.4.2).

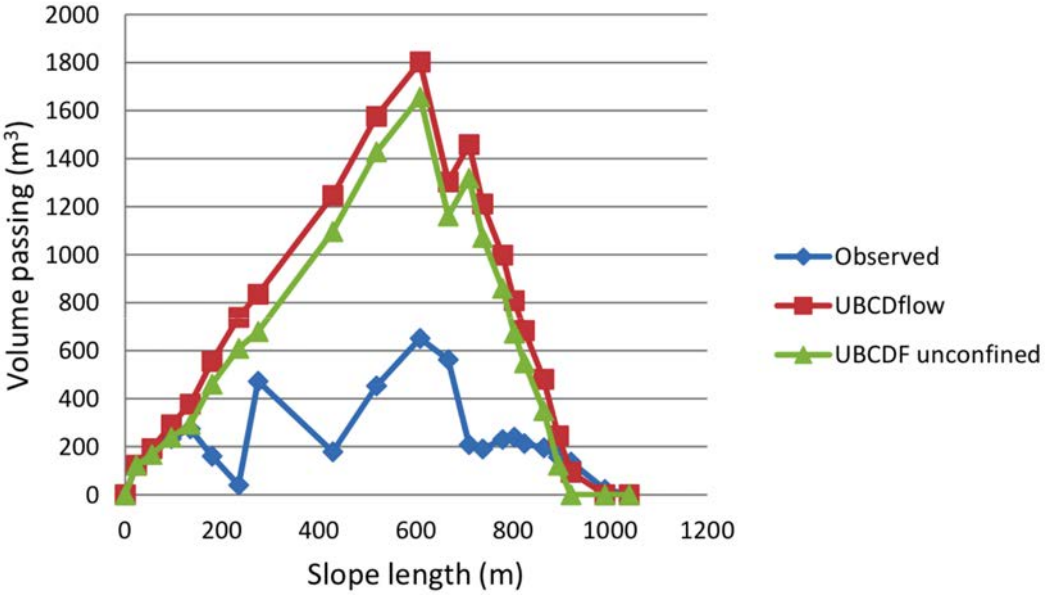

Figure B.14.: Plot of volume passing for BH3. The value for observed is based on the volume passing calculations (discussed in Section 5.4.2).

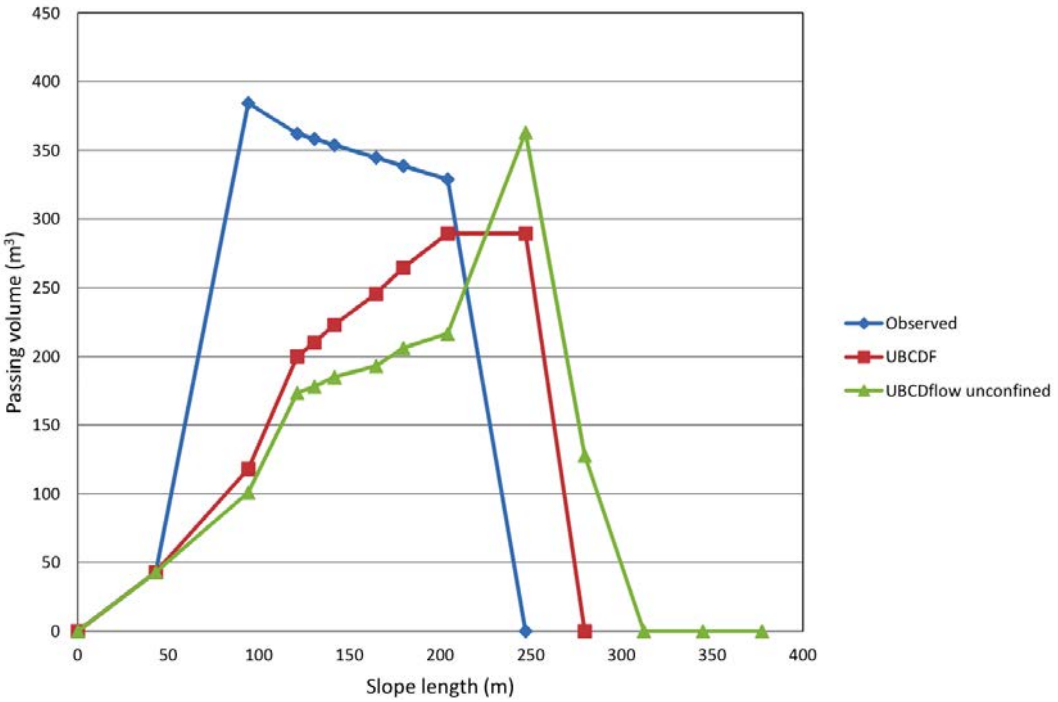

Figure B.15.: Plot of volume passing for BH4. The value for observed is based on the volume passing calculations (discussed in Section 5.4.2).

B.3. Reach data for each flow (see accompanying digital data)

B.3.1. Key

Code	Field Area
1	Orongorongo
2	White Rock Rd.
3	Sugar Loaf
4	Purple Hill
5	Castle Hill
6	Birch Hill
7	Franz Josef

Refer to Chapter 4 a description of each field area.

Code	Behaviour
1	Source
2	Erosion
3	Transport
4	Deposition
5	Reworked
6	Fluvial

Refer to 7.11.3 on page 202 for more information.

Code	Confinement type
1	Confined by gully
2	Confined by channel
3	Partially confined in channel
4	Unconfined in channel
5	Unconfined in gully
6	Unconfined

Refer to 3.4.1.6 on page 38 for more information.

Code	Bed material
1	Bedrock
2	Shallow colluvium (<1m)
3	Deep colluvium (>1m)

Refer to 5.2 on page 95 for more information.

Code	Side slopes (m)
1	<5
2	5-10
3	10-15
4	15-20
5	>20

Refer to 5.2 on page 95 for more information.

Code	Bank Stability
1	Planar
2	Stable slope
3	Meta-stable
4	Active failure observed

Refer to 5.2 on page 95 for more information.

Code	Landscape unit
1	Hillslope
2	Gully
3	Channel
4	Fan